Characterization of cluster-III HIPP proteins targeted to plasmodesmata in *Arabidopsis thaliana*

Inaugural-Dissertation

to obtain the academic degree
Doctor rerum naturalium (Dr. rer. nat.)

submitted to the
Department of Biology, Chemistry, Pharmacy
of Freie Universität Berlin

by

Georgeta Leonte

2020

This work was conducted under supervision of Prof. Dr. Tomáš Werner from June 2015 to September 2020 at the Institute of Biology, Department of Applied Genetics at the Freie Universität Berlin.

1st Reviewer: Prof. Dr. Tomáš Werner (University of Graz)

2nd Reviewer: Prof. Dr. Thomas Schmülling (Freie Universität Berlin)

Date of defense: 03.11.2020

Table of contents

List of figures

List of tables

List of abbreviations

°C	Degree Celsius
ABA	Abscisic acid
ABC	ATP-binding cassette transporter
AHK	ARABIDOPSIS HISTIDINE KINASE
AHP	ARABIDOPSIS HISTIDINE PHOSPHOTRANSFER PROTEIN
AMP	Adenosine monophosphate
Al	Aluminum
ARR	ARABIDOPSIS RESPONSE REGULATOR
ATP	Adenosine triphosphate
ARF	AUXIN RESPONSE FACTORS
AUX	Auxin
BA	N6-Benzyladenine
bHLH	Basic helix-loop-helix
BiFC	Bimolecular fluorescence complementation
bp	Base pair(s)
BP	Biological process (GO category)
BSA	Bovine serum albumin
CALS	Callose synthase
CaMV	Cauliflower mosaic virus
CC	Cellular component (GO category)
CGL1	COMPLEX GLYCAN LESS 1
Cd	Cadmium
cDNA	Complementary deoxyribonucleic acid
CF	Carboxyfluorescein
CFDA	5(6)-carboxyfluorescein diacetate
ChIP	Chromatin immunoprecipitation
CKX	CYTOKININ OXIDASE/DEHYDROGENASE
CLV	*CLAVATA*
CLSM	Confocal laser scanning microscopy
Co-IP	Co-immunoprecipitation
Col-0	Ecotype/accession Columbia-0
CRE1	CYTOKININ RESPONSE 1 (=AHK4)
CRF	CYTOKININ RESPONSE FACTOR
CRISPR/Cas9	Clustered regularly interspaced short palindromic repeats/CRISPR-associated protein 9
CSC	Columella stem cell
Ct	Threshold cycle
CUC	*CUP-SHAPED COTYLEDON*
Cu	Copper
X	

CYP	*CYTOCHROME* P450
*c*Z	*cis*-zeatin
CZ	Central zone
DEG	Differentially expressed gene
ddH_2O	Double deionized water
DMAPP	Dimethylallyl diphosphate
DMSO	Dimethyl sulfoxide
DNA	Deoxyribonucleic acid
DNase	Deoxyribonuclease
dNTP	Deoxyribonucleoside triphosphate
DTT	Dithiothreitol
DZ	Differentiation zone
e.g.	*exempli gratia* (Latin: for example)
EDTA	Ethylenediaminetetraacetic acid
EC1.2	*EGG CELL1.2*
EMS	Ethyl methanesulfonate
ER	Endoplasmic reticulum
ERAD	ER-associated degradation
et al.	*et alii* (Latin: and others)
F	Forward
F1, F2, F3	First, second, third filial generation
FC	Fold change
FDR	False discovery rate
Fe	Iron
FPP	Farnesyl diphosphate
FT	FLOWERING LOCUS T
FTIP1	FT INTERACTING PARTNER 1
FW	Fresh weight
g	Gram
GA	Gibberellic acid
GFP	Green fluorescent protein
GGPP	Geranyl-geranyl diphosphate
GLP	GERMIN-LIKE PROTEIN
GLS	Glucan synthase-like
GO	Gene ontology
GOI	Gene of interest
GUS	β-glucuronidase
ICMT	Isoprenyl cysteine methyltransferases
h	Hour
HMA	Heavy metal-associated domain
HIPP	Heavy metal-associated isoprenylated plant protein

IAA	INDOLE-3-ACETIC ACID
i.e.	*id est* (Latin: that is)
iP	Isopentenyl adenine
IPT	Isopentenyltransferase
kb	Kilobase pair(s)
kDa	Kilodalton
KEGG	Kyoto Encyclopedia of Genes and Genomes
KMD	KISS ME DEADLY
L	Liter
LB	Luria and Broth
LD	Long-day light conditions (light/dark: 16 h/8 h)
LOG	LONELY GUY
mA	Miliampere
MEE26	*MATERNAL EFFECT EMBRYO ARREST 26*
MES	2-(N-morpholino)ethanesulfonic acid
MF	Molecular function (GO category)
min	Minute
MP	Movement protein
mPS-PI	Pseudo-Schiff propidium iodide
mRNA	Messenger RNA
Mn	Manganese
MS	Murashige and Skoog
NaKR1	SODIUM POTASSIUM ROOT DEFECTIVE 1
NCBI	National Center for Biotechnology Information
Ni	Nickel
OD	Optical density
p	Probability
P	Phloem
Pb	Lead
PCR	Polymerase chain reaction
PD	Plasmodesmata
PdBG	β-1,3-glucanase
PDCB	Callose-binding protein
PDLP	PD-localized protein
PI	Propidium iodide
PIN	PIN-FORMED
PFT	Farnesyl transferase
PHP	Phosphotransfer protein
PLT	*PLETHORA*
PUP	Purine permease
QC	Quiescent center

qRT-PCR	Quantitative real-time polymerase chain reaction
R	Reverse
RAM	Root apical meristem
RNA	Ribonucleic acid
RNase	Ribonuclease
RNA-Seq	RNA-Sequencing
rpm	Rounds per minute
ROI	Region of interest
RT	Room temperature
RT-PCR	Reverse transcription polymerase chain reaction
sec	Second
SAM	Shoot apical meristem
SAUR	*SMALL AUXIN UPREGULATED RNA*
SC	Stem cell
SCN	Stem cell niche
SCR	*SCARECROW*
SD	Short-day light conditions (light/dark: 8 h/16 h)
SDS	Sodium dodecyl sulfate
SEL	Size exclusion limit
SHR	*SHORT ROOT*
SIGnAL	Salk Institute Genomic Analysis Laboratory
STM	*SHOOT MERISTEMLESS*
SUC2	*SUCROSE-H+ SYMPORTER 2*
T1, T2, T3	First, second, third generation after a transformation
TAE	Tris acetate ethylenediaminetetraacetic acid
TAIR	The *Arabidopsis* Information Resource
TCS	Two-component system
T-DNA	Transfer DNA
TEMED	*N,N,N',N'*-Tetramethylethane-1,2-diamine
Tris	Tris(hydroxymethyl)aminomethane
tRNA	Transfer RNA
*t*Z	*trans*-zeatin
TZ	Transition zone
UBC10	*UBIQUITIN-CONJUGATING ENZYME 10*
UGT	N-glycosyltransferase
WT	Wild type (if not stated otherwise, Col-0)
WOX	*WUSCHEL-RELATED HOMEOBOX*
WUS	*WUSCHEL*
Y2H	Yeast two-hybrid
Zn	Zinc

Summary

The plant hormone cytokinin plays essential regulatory roles in many aspects of plant growth and development. Cellular cytokinin concentrations are controlled by numerous interconnected metabolic reactions, such as hormone biosynthesis, metabolic activation, and inactivation. The irreversible cytokinin degradation is mediated by the cytokinin oxidase/dehydrogenase (CKX) enzymes. Several heavy metal-associated isoprenylated plant proteins (HIPP), which belong to two distinct phylogenetic clusters have been identified to specifically interact with CKX proteins. These plant-unique proteins are defined by the combination of one or two heavy metal-binding domains (HMA) and a C-terminal prenylation site. The physiological function and molecular activity of HIPP proteins are largely unknown, and only few *HIPP* genes have been characterized so far. This work aimed to study the highly homologue *HIPP* genes constituting together the phylogenetic cluster III.

Histochemical analysis of transgenic *Arabidopsis* plants expressing *pHIPP:GUS* chimeric genes demonstrated that the activities of individual *HIPP* promoters were remarkably different, with both discrete and overlapping expression patterns throughout plant development. In good agreement with the *pHIPP:GUS* expression analysis, loss-of-function of cluster-III *HIPP* genes led to multiple phenotypic alterations, pointing to largely redundant functions of *HIPP* genes in a wide variety of developmental processes. Severe pleiotropic defects were particularly pronounced in the *hipp32,33,34* mutant, which for example exhibited impaired reproductive growth, indicating that *HIPP* genes function in processes that govern floral organ development and gametogenesis. Furthermore, the activity of *HIPP* genes is required for pattern formation and maintenance of the shoot and root apical meristems during embryogenesis. For instance, the identity of the quiescent center and columella stem cells was lost in both embryonic and postembryonic *hipp32,33,34* roots, suggesting that *HIPP* genes have crucial roles in cell-fate specification required for proper root patterning.

Consistent with their pleiotropic phenotypes, the transcriptional profiling of *hipp* mutants by RNA-Seq revealed the differential expression of hundreds of genes involved in various processes of plant development. Strikingly, many of these genes are involved in auxin signaling responses, suggesting that HIPP proteins might participate in the crosstalk between components of the auxin signaling and different developmental pathways. Furthermore, the differential expression of several genes is hypothesized to be linked to the presumptive metallochaperone function of HIPP proteins.

Confocal microscopy analysis of GFP-HIPP fusion proteins transiently expressed in *N. benthamiana* leaf epidermal cells revealed that all cluster-III HIPP proteins localize almost exclusively to plasmodesmata (PD), co-localizing with the PD marker PDLP1. The PD-residency was exemplary confirmed for HIPP34 in the transgenic *Arabidopsis* line expressing

35S:GFP-HIPP34. Furthermore, microsomal fractionation and protein analysis revealed that HIPP34 associates with microsomal membranes in a prenylation-dependent manner.

Symplasmic transport assays performed in generated *hipp* mutant plants using the mobile phloem marker *pSUC2:GFP* revealed that the cell-to-cell trafficking is enhanced in the root of distinct *hipp* mutants, suggesting a function of HIPP proteins in restricting PD-mediated macromolecular trafficking. Interestingly, symplasmic trafficking in the root meristem of *hipp* mutants was not affected by iron treatment, suggesting that HIPP proteins are involved in PD regulation in response to iron stress. Furthermore, it was shown that HIPP proteins are also involved in mediating heavy metal homeostasis, as the root growth in *hipp32,33* mutant was insensitive to the toxic concentrations of Cd, Zn and Fe.

Co-IP experiments performed in this study confirmed the interactions between CKX1 and HIPP proteins from cluster III originally identified in yeast. Moreover, BiFC experiments suggested that the CKX1/HIPP protein complex formation likely occurs at HIPP subcellular location sites. The molecular mechanisms underlying the interaction between CKX1 and HIPP proteins remain to be clarified. However, experiments employing the synthetic cytokinin reporter *TCSn:GFP* revealed attenuated cytokinin activity in *hipp* roots, reflecting the redundant function of the *HIPP* genes in positively regulating the cytokinin signaling output. However, the altered *TCSn:GFP* activity in *hipp* mutants cannot entirely be linked to their root phenotypes, indicating that other factors are involved in the *HIPP*-mediated root growth regulation. Nevertheless, transcriptome analysis revealed that 42% to 54% of cytokinin responsive genes failed to respond to exogenous cytokinin in *hipp33* and *hipp32,33,34* mutants, indicating that cluster-III *HIPP* genes are required for the transcriptional response to cytokinin.

Zusammenfassung

Das Pflanzenhormon Cytokinin spielt in vielen Aspekten des Pflanzenwachstums und der Pflanzenentwicklung eine essenzielle regulatorische Rolle. Die zelluläre Konzentration von Cytokinin wird durch zahlreiche miteinander vernetzte Stoffwechselreaktionen, wie Biosynthese, metabolische Aktivierung und Inaktivierung, gesteuert. Der irreversible Abbau von Cytokinin wird durch die Cytokininoxidase/Dehydrogenase (CKX)-Enzyme vermittelt. Mehrere *heavy metal-associated isoprenylated plant proteins* (HIPP-Proteine), die zu zwei unterschiedlichen phylogenetischen Gruppen gehören, wurden identifiziert, spezifisch mit CKX-Proteinen zu interagieren. Diese pflanzenspezifischen Proteine sind durch eine oder zwei Schwermetall-bindende Domänen (HMA) sowie eine C-terminalen Prenylierungsstelle gekennzeichnet. Die physiologische Funktion und die molekulare Aktivität von HIPP-Proteinen sind weitgehend unbekannt, und nur wenige *HIPP*-Gene wurden bisher charakterisiert. Das Ziel dieser Arbeit war, die hochgradig homologen *HIPP*-Gene, die zusammen das phylogenetische Cluster III bilden, zu untersuchen.

Die histochemische Analyse von transgenen *Arabidopsis*-Pflanzen, die chimäre *pHIPP:GUS*-Gene exprimieren, zeigte, dass die Aktivitäten einzelner *HIPP*-Promotoren bemerkenswert unterschiedlich waren, wobei im Verlauf der Pflanzenentwicklung sowohl spezifische als auch überlappende Expressionsmuster auftraten. In Übereinstimmung mit der *pHIPP:GUS*-Expressionsanalyse führte der Funktionsverlust von Cluster-III-*HIPP*-Genen zu vielartigen phänotypischen Veränderungen, was auf weitgehend redundante Funktionen von *HIPP*-Genen in einer Vielzahl von Entwicklungsprozessen hinweist. Starke pleiotrope Defekte waren in der *hipp32,33,34*-Mutante besonders ausgeprägt, die zum Beispiel ein beeinträchtigtes reproduktives Wachstum aufwies. Dies weist darauf hin, dass *HIPP*-Gene funktionell in Prozessen wirken, die die Entwicklung von Blütenorganen und die Gametogenese steuern. Außerdem ist die Aktivität von *HIPP*-Genen für die Zellmusterbildung und Aufrechterhaltung der apikalen Spross- und Wurzelmeristeme während der Embryogenese erforderlich. Beispielsweise zeigte sich ein Verlust der Identität der Zellen des ruhenden Zentrums und der Columella-Stammzellen sowohl in embryonalen als auch in postembryonalen *hipp32,33,34*-Wurzeln. Das deutet darauf hin, dass *HIPP*-Gene eine entscheidende Rolle bei der Spezifikation der Zellidentität spielen, die wiederum für eine korrekte Wurzelentwicklung erforderlich ist.

Übereinstimmend mit den pleiotropen Phänotypen konnte die Genexpressionsanalyse von *hipp*-Mutanten durch RNA-Seq eine Expressionsveränderung von mehreren Hundert Genen nachweisen, die an verschiedenen Prozessen der Pflanzenentwicklung beteiligt sind. Bemerkenswert ist, dass viele dieser Gene an Auxin-Signalantworten beteiligt sind. Das weist wiederum darauf hin, dass HIPP-Proteine an den regulatorischen Netzwerken zwischen der

Auxin-Signalkaskade und verschiedenen Entwicklungswegen beteiligt sein könnten. Des Weiteren wird angenommen, dass zwischen der veränderten Expression zahlreicher Gene und der vermuteten Funktion der HIPP-Proteine, als Metallochaperone zu agieren, ein Zusammenhang besteht.

Die konfokalmikroskopische Analyse von transient in epidermalen *N.-benthamiana*-Blattzellen exprimierten GFP-HIPP-Fusionsproteinen ergab, dass alle HIPP-Proteine aus Cluster III fast ausschließlich an den Plasmodesmen (PD) lokalisieren. HIPP-Proteine wiesen dieselbe Lokalisation wie der PD-Marker PDLP1 auf. Die PD-Lokalisation wurde beispielhaft für HIPP34 in der transgenen *Arabidopsis*-Linie *35S:GFP-HIPP34* bestätigt. Des Weiteren zeigten eine mikrosomale Fraktionierung und Proteinanalyse, dass HIPP34 mit mikrosomalen Membranen assoziiert und dass diese Assoziation von dem Prenylierungsmotiv abhängig ist.

Untersuchungen des symplastischen Transports in den generierten *hipp*-Mutantenpflanzen zeigten unter Verwendung des mobilen Phloem-Markers *pSUC2:GFP* eine erhöhte interzelluläre Kommunikation in der Wurzel bestimmter *hipp*-Mutanten. Dies deutet auf eine Funktion von HIPP-Proteinen bei der Einschränkung des makromolekularen Transports durch PD hin. Interessanterweise hatten Behandlungen von *hipp*-Mutanten mit Eisen keinen Einfluss auf den symplastischen Transport in deren Wurzelmeristemen, was auf die Beteiligung von HIPP-Proteinen an der Regulation von PD als Antwort auf Eisenstressbedingungen hindeutet. Außerdem wurde gezeigt, dass HIPP-Proteine an der Schwermetallhomöostase beteiligt sind, da die *hipp32,33*-Mutante hinsichtlich des Wurzelwachstums unempfindlich gegenüber toxischen Cd-, Zn- und Fe-Konzentrationen war.

In dieser Arbeit durchgeführte Co-IP-Experimente bestätigten die ursprünglich in Hefe identifizierten Interaktionen zwischen CKX1- und HIPP-Proteinen aus Cluster III. Zudem deuteten BiFC-Experimente darauf hin, dass die Bildung von CKX1/HIPP-Proteinkomplexen auf subzellulärer Ebene an HIPP-Lokalisationsstellen erfolgt. Die molekularen Mechanismen, die der Interaktion zwischen CKX1- und HIPP-Proteinen zugrunde liegen, wären noch zu klären. Jedoch zeigten Untersuchungen des synthetischen Cytokinin-Reporters *TCSn:GFP* eine abgeschwächte Cytokinin-Aktivität in Wurzeln von *hipp*-Mutanten, was die redundante Rolle der *HIPP*-Gene in der positiven Regulation des Cytokinin-Signaloutputs widerspiegelt. Die veränderte *TCSn:GFP*-Aktivität in *hipp*-Mutanten kann jedoch nicht vollständig mit ihren Wurzelphänotypen korreliert werden. Dies weist darauf hin, dass andere Faktoren an der *HIPP*-vermittelten Wurzelwachstumsregulation beteiligt sind. Die Transkriptomanalyse ergab jedoch, dass 42% bis 54% der von Cytokinin regulierten Gene auf exogenes Cytokinin in *hipp33*- und *hipp32,33,34*-Mutanten nicht reagierten. Daraus lässt sich schlussfolgern, dass *HIPP*-Gene des Clusters III für die transkriptionelle Antwort auf Cytokinin erforderlich sind.

1. Introduction

The three phylogenetically closely related HIPPs (heavy metal-associated isoprenylated plant proteins) studied in this work were identified to specifically interact with one of the cytokinin-degrading enzymes, CKX1, in a yeast two-hybrid screen. The general function of the *HIPP* genes, which are unique to plants, is largely unknown. Molecular, phenotypic, and functional investigations performed in this study using the generated *hipp* mutant plants revealed that the cluster-III *HIPP* genes regulate various aspects of plant growth, including root and shoot development. Furthermore, the lack of cluster-III *HIPP* genes considerably altered the cytokinin activity in the *hipp* mutant roots. The subcellular localization of the cluster-III HIPP proteins at plasmodesmata was shown to be linked to their function in regulating the symplasmic trafficking. In agreement with the involvement of several known *Arabidopsis* HIPP proteins in heavy metal homeostasis, the lack of distinct *HIPP* genes from cluster-III positively affected *hipp* mutants' tolerance towards exposure to heavy metals. Therefore, the following chapter sections will deal with several diverse topics including a detailed description of HIPP proteins, relevant aspects of cytokinin biology, control of root and shoot development, plasmodesmata and heavy metal homeostasis.

1.1 Heavy metal-associated isoprenylated plant proteins

Proteins containing one or more heavy metal binding domains, known as HMA (heavy metal associated) domains together with a C-terminal isoprenylation motif are plant-specific and were first described by Dykema *et al.* (1999). In addition, most HIPP proteins contain flexible glycine-rich repeats and proline-rich motifs, which are thought to mediate protein-protein interaction (de Abreu-Neto *et al.*, 2013). Figure 1 shows the general structure of a HIPP protein.

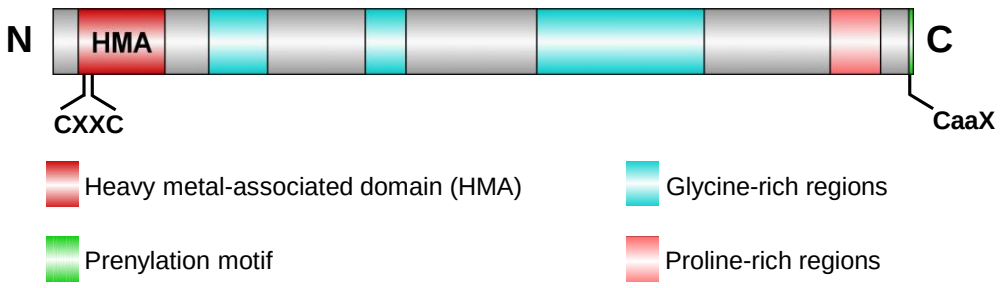

Figure 1. General structure of a heavy metal-associated isoprenylated plant protein (HIPP). Schematic representation of the general structure of a HIPP protein with predicted heavy metal-associated domains (HMA; red box) and prenylation motifs (green box) at the C-terminus. Many HIPPs contain glycine-rich repeats (turquoise boxes) and proline-rich motifs (pink box). The conserved cysteine residues (C) within the HMA domain and the prenylation motif CaaX, as relevant protein features are highlighted (see also sections 1.1.1 and 1.1.2).

In *Arabidopsis thaliana* (*Arabidopsis*), the *HIPP* protein family comprises 45 'true' HIPP proteins and 22 HMA-containing proteins (HPP) which lack the isoprenylation site. These are grouped based on the sequence homologies in seven distinct phylogenetic clusters, I to VII (Figure 2; Tehseen *et al.*, 2010; Guo, 2019).

In the context of this work, HIPP proteins have been identified in Dr. Werner's research group in a genome-wide yeast two-hybrid (Y2H) screen to interact with the cytokinin degrading enzyme CKX1 protein (Guo, 2019). The primary interactions were consequently confirmed and, interestingly, the HIPP proteins identified to interact with CKX1 belong to two phylogenetically distinct clusters: HIPP1, HIPP5, HIPP6 and HIPP7 to cluster I, and HIPP32, HIPP33 and HIPP34 to cluster III (Figure 2). This suggests that the interactions were highly specific and might not have been mediated through the conserved domains of the HIPP proteins. However, the mechanisms underlying the interactions between CKX1 and the HIPP proteins are largely undeciphered and so far, only little is known about their biological function.

1.1.1 HIPP proteins possess HMA domains

The heavy metal ions such as iron, copper or zinc are required as structural components or as enzymatic co-factors of numerous proteins. Although the metallic ions are essential elements, they are toxic for the living cells. Both prokaryotes and eukaryotes have evolved mechanisms that ensure efficient metal homeostasis. This is accomplished by specific delivery proteins – metallochaperones – which are responsible for the site-specific transportation of metallic ions within the cell and their sequestration in subcellular compartments (Huffman and O'Halloran, 2001; Tehseen *et al.*, 2010; Rosenzweig, 2002). The concept of metallochaperones was first studied in *Saccharomyces cerevisiae*, where three copper chaperons known as Atx1, Cox17 and Ccs1 have been shown to deliver copper either to the secretory pathway via Ccc2, a copper-transporting ATPase, or to mitochondria for its incorporation into Cu/Zn superoxide dismutase or into cytochrome c oxidase, respectively (Daviere and Achard, 2017; Sturtz *et al.*, 2001; Wintz and Vulpe, 2002). Meanwhile, functional homologues of copper chaperons have been identified in other organisms, including mammals and plants, for instance the human copper-transporting ATPases, the Menkes and Wilson disease proteins, and the heavy metal P-type ATPases HMA5, HMA6, HMA7 and HMA8 in *Arabidopsis* (Andres-Colas *et al.*, 2006; Solioz and Vulpe, 1996; Barnes *et al.*, 2005). Characteristic for the plant homologs is the presence of a 60-70 amino acid-long HMA domain with a βαββαβ-fold secondary structure containing the highly conserved motif M/L/IXCXXC (M: methionine, L: leucine, I: isoleucine, C: cysteine, X: any amino acid) which is involved in the binding, transport and coordination of metal ions (Dance, 2015; Dykema *et al.*, 1999; Tehseen *et al.*, 2010). The *Arabidopsis* HIPP proteins contain mostly one HMA domain, with exception of the cluster-I proteins, which possess two HMA domains (Figure 1; Tehseen *et al.*, 2010).

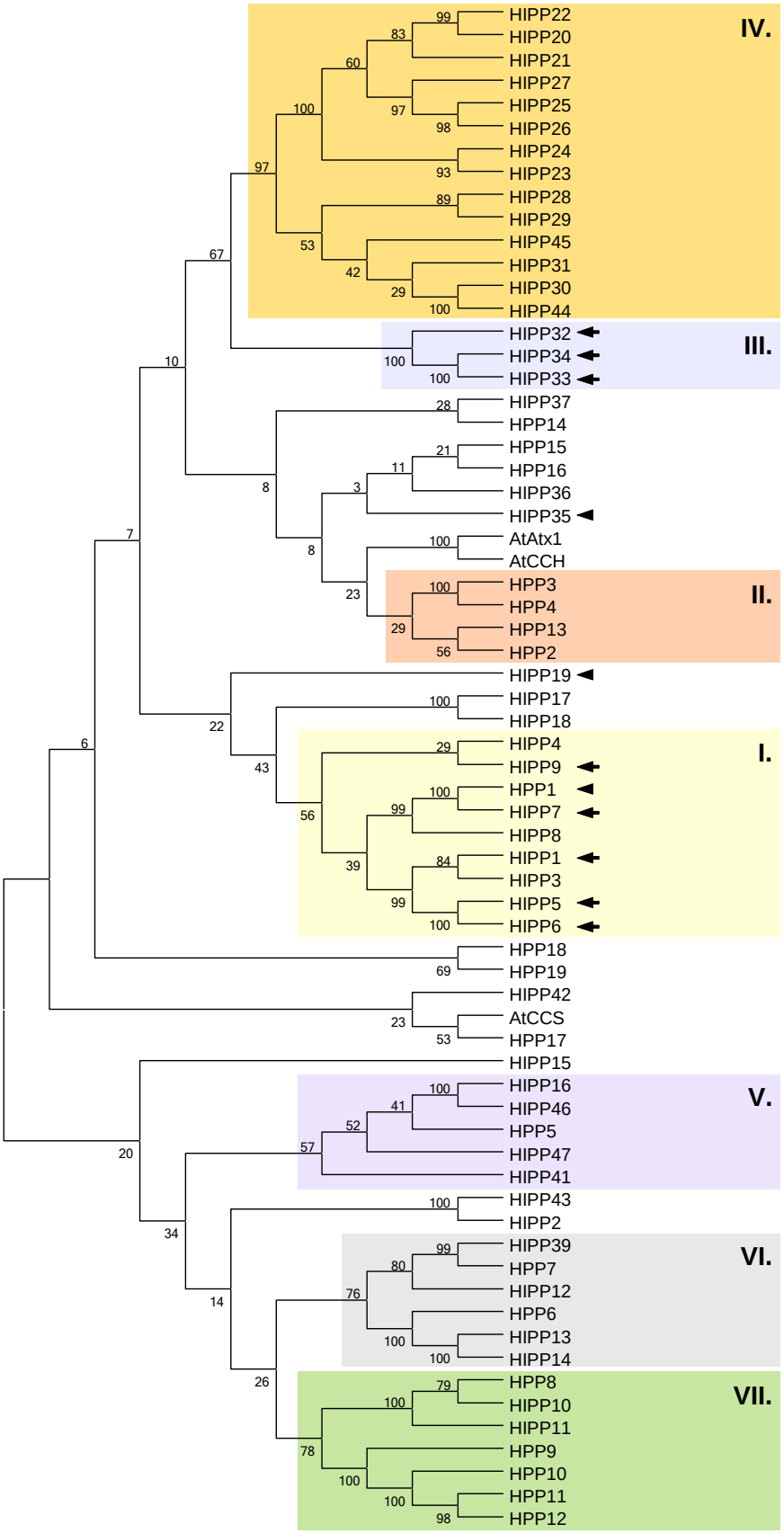

Figure 2. Phylogenetic relationship of HIPP and HPP proteins in *Arabidopsis*.
The nomenclature of HIPP and HPP proteins and the numbering of phylogenetic groups was adopted from Tehseen *et al.* (2010). Arrows and arrowheads indicate proteins interacting and noninteracting with CKX1 in Y2H assays, respectively (Guo, 2019).

Several HIPP proteins from cluster IV and HIPP3 from cluster I have been also shown to bind cadmium and zinc (Tehseen *et al.*, 2010; Zschiesche *et al.*, 2015). Furthermore, studies in *Arabidopsis* have shown that HMA domains are essential for protein-protein interactions. For instance, the interaction between the phloem protein NaKR1/HPP2 and the FLOWERING LOCUS T (FT) required for FT long-distance transport was shown to be mediated by the HMA domain of the NaKR1/HPP2 (Zhu *et al.*, 2016). Similarly, two HIPP family members, HIPP26 and HIPP27, have been shown to interact via the HMA domain with the drought stress-related zinc finger transcription factor ATHB29 and UBIQUITIN-SPECIFIC PROTEASE 16 (Barth *et al.*, 2009; Zhao *et al.*, 2013). In contrast, the interaction between the HIPP26 homologue from *Nicotiana benthamiana* (*N*. *benthamiana*) and the potato mop-top virus movement protein TGB1 was not mediated by the HMA domain (Cowan *et al.*, 2018).

1.1.2 HIPP proteins contain a C-terminal prenylation motif

In addition to the HMA domain, members of the HIPP family contain a C-terminal prenylation motif CaaX (Figure 1; C: cysteine; a: aliphatic amino acid; X: any amino acid, but commonly cysteine, methionine, serine, alanine or glutamine), which is required for the post-translational protein modification by isoprenoid lipids, known as prenylation (Galichet and Gruissem, 2003; Wang and Casey, 2016). The role of prenylation has been extensively studied, as numerous members of the mammalian Ras small GTPases superfamily require prenylation in order to bind to membranes and to mediate signal transduction (Berndt *et al.*, 2011). In *Arabidopsis*, there are 700 proteins predicted to be prenylated (Running, 2014). These proteins are involved in various biological processes including transcriptional regulation, cell cycle regulation, cell wall modification, hormone signaling, metal binding or biotic and abiotic stress responses (Galichet and Gruissem, 2003; Hala and Zarsky, 2019).

Protein prenylation is conserved among eukaryotes and involves the covalent attachment of either a 15-carbon farnesyl or a 20-carbon geranyl-geranyl isoprenoid lipid moiety to the cysteine residue of a target protein via a thioether bond (Zhang and Casey, 1996). The isoprenoid substrates farnesyl diphosphate (FPP) or geranyl-geranyl diphosphate (GGPP) are synthesized by the cellular mevalonate pathway. The enzymatic reaction occurs shortly after translation and is catalyzed by the prenyltransferase enzymes, depending on the last residue in the CaaX motif, farnesyl transferase (PFT, for X: methionine, glutamine, serine, alanine or cysteine) or geranyl-geranyl transferase I (PGGT I, for X: leucine or isoleucine). A second type of geranyl-geranyl transferase – PGGT II, also called Rab-PGGT – exclusively prenylates Rab-GTPase proteins (Crowell, 2000; Crowell and Huizinga, 2009; Resh, 2006). All three enzymes are evolutionarily related, with Rab-PGGT being more distantly related to PGGT I and PFT (Hemsley, 2015). They are heterodimeric enzymes, each of them consisting of an α and β subunit, with PGGT I and PFT sharing a common α subunit. PFT can only use FPP as a

substrate, whereas PGGT I can use both FPP and GGPP. Thus, the substrate and target specificity for these enzymes is granted by the β subunit (Running, 2014). Following prenylation, proteins undergo two additional modifications, collectively referred to as CaaX processing (Figure 3; Sorek *et al.*, 2009). First, the last three amino acids of the protein (aaX) are proteolytically cleaved by specific proteases (Trueblood *et al.*, 2000). Subsequently, the free carboxyl group of the isoprenyl cysteine is reversibly methylated by metyltransferases (Crowell, 2000). In *Arabidopsis*, proteolysis and methylation is achieved by conserved STE24 and RCE1 endoproteases and by two isoprenyl cysteine methyltransferases (ICMTs), respectively, localized at the endoplasmic reticulum membrane (Bracha *et al.*, 2002; Bracha-Drori *et al.*, 2008). The localization of the *Arabidopsis* CaaX-processing enzymes is similar to their homologues in yeast and animal systems, suggesting that following prenylation in the cytoplasm, the prenylated proteins are targeted to the endoplasmic reticulum (Sorek *et al.*, 2009). The fully processed prenylated proteins are then trafficked to their cellular destination. The hydrophobic carboxyl termini of the prenylated proteins confer them an increased capacity to attach to endomembranes and plasma membrane or to operate as peripheral lipid membrane proteins or as a signal for interaction with other proteins (Wang and Casey, 2016).

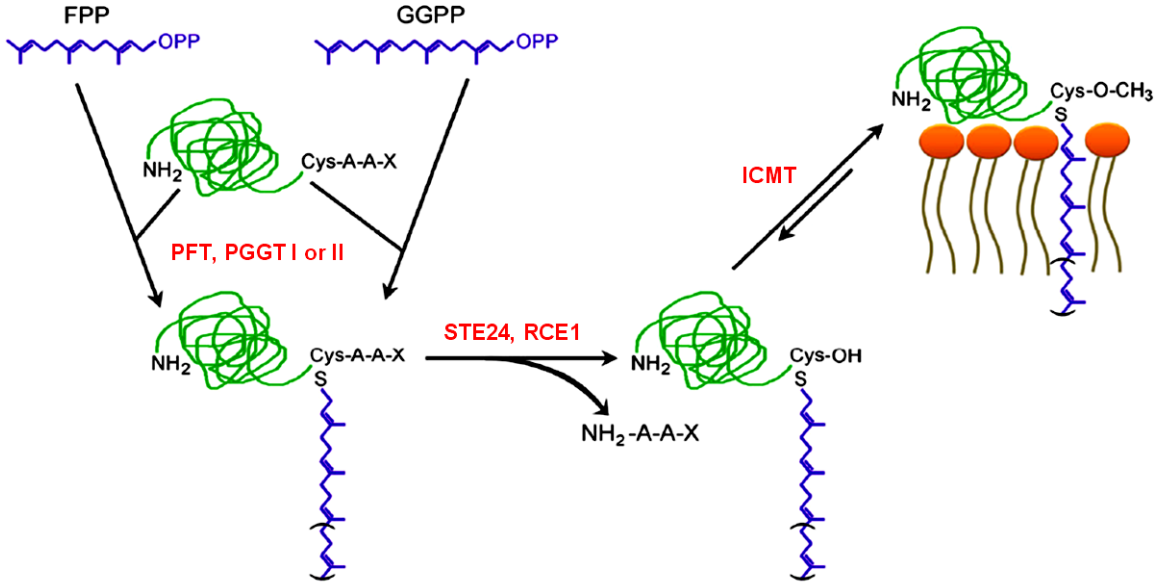

Figure 3. Schematic overview of the post-prenylation processing.
Following prenylation by the prenyltransferase enzymes (PFT, PGGT I or II), the three C-terminal amino acids (aaX) of the prenylated proteins are cleaved by specific endoproteases (STE24 and RCE1) and the terminal cysteine residue is reversibly carboxymethylated by specific methyltransferases (ICMT). FPP: farnesyl diphosphate, GGPP: geranyl-geranyl diphosphate, PFT: farnesyl transferase, PGGT: geranyl-geranyl transferase, ICMT: isoprenyl cysteine methyltransferase. Modified after Xu *et al.* (2015).

Prenylation does not only tend to target proteins from the cytosol to different compartments of the cell, but also affects their functions, such as facilitating specific protein-protein interactions,

organizing the endomembrane trafficking and modulating protein stability (Wang and Casey, 2016; Hala and Zarsky, 2019). Deciphering the role of prenylation has gained extensive attention and several *Arabidopsis* prenylated proteins and their functions have been characterized. For instance, the floral transcription factor APETALA1 (AP1) requires prenylation to modulate its specificity and its regulatory functions during flower development. However, the prenylation did not appear to promote AP1 membrane association (Yalovsky *et al.*, 2000). Several studies have reported that prenylation is necessary for proteins functions. For example, the farnesylation of the cytokinin biosynthesis enzyme IPT3 directs the subcellular localization in the nucleus and cytoplasm, whereas the non-farnesylated protein locates to the plastid. Furthermore, the different subcellular localizations were closely correlated with the biosynthesis of different cytokinin types (Galichet *et al.*, 2008). Similarly, the cytochrome P450, CYP85A2, must be prenylated in order to be targeted to endomembrane compartments and function in the brassinosteroid synthesis pathway. CYP85A2 lacking the CaaX motif was instable and remained in the cytosol (Jamshed *et al.*, 2017). Some prenylated proteins do not use the prenyl group to bind to membranes, but as a targeting signal to interact with other proteins, or to trigger further modifications (Hemsley, 2015).

1.1.3 Biological functions of *HIPP*s

While proteins characterized by the presence of either HMA domains or a prenylation motif are ubiquitously found in both prokaryotes and eukaryotes, HIPP proteins containing both features are present only in vascular plants (Jordan *et al.*, 2001; Zhang and Casey, 1996, de Abreu-Neto *et al.*, 2013). The biological functions of the HIPP proteins are so far largely unknown and only few genes were studied in detail. HIPP proteins were previously identified in the context of heavy metal homeostasis, as metallochaperones able to bind and transit metal ions, such as Cd^{2+}, Cu^{2+}, Ni^{2+} or Zn^{2+} (Dykema *et al.*, 1999; Suzuki *et al.*, 2002). The role of HIPP proteins in heavy metal homeostasis and/or detoxification has been demonstrated by several independent studies. For instance, the overexpression of the *Cdl19/HIPP6* gene conferred tolerance to Cd exposure (Suzuki *et al.*, 2002). Similarly, *Arabidopsis* plants were more tolerant to Cd stress when *HIPP26* was overexpressed, whereas the *hipp20,21,22* triple mutant plants were more sensitive to Cd and accumulated less Cd than the wild type, suggesting a role of HIPP proteins in Cd-detoxification (Gao *et al.*, 2009; Tehseen *et al.*, 2010). Another two *Arabidopsis HIPP* genes from cluster IV, *HIPP22* and *HIPP44*, act downstream of the MYB49 transcription factor to regulate the ABI5-mediated Cd uptake and accumulation (Zhang *et al.*, 2019). Furthermore, HIPP proteins have been identified to be involved in plant responses to biotic and abiotic stress (Barth *et al.*, 2009; de Abreu-Neto *et al.*, 2013; Zschiesche *et al.*, 2015; Cowan *et al.*, 2018; Radakovic *et al.*, 2018). For example, nuclear-localized HIPP26 from *Arabidopsis* was shown to interact via its HMA domain with the drought stress-related zinc

finger transcription factor ATHB29 protein. Moreover, *HIPP26* was induced during cold, salt and drought stress (Barth *et al.*, 2009). The *HIPP41* homologue from *Oryza sativa* is also highly expressed in response to cold and drought stress (de Abreu-Neto *et al.*, 2013). One *Arabidopsis* HIPP family member from cluster I, HIPP3, was described as a zinc-binding protein that functions as an upstream regulator of the salicylate-dependent pathway during pathogen infection, also being involved in abiotic stress responses and seed and flower development (Zschiesche *et al.*, 2015). More recently, HIPP27 was identified as a host susceptibility factor required for beet cyst nematode *Heterodera schachtii* infection and development. The expression of *HIPP27* was specifically and highly upregulated in syncytia induced by *H. schachtii* in A*rabidopsis* roots, whereas the loss of *HIPP27* function reduces plant susceptibility to cyst nematode infection, suggesting thus the role of a HIPP family protein in plant-nematode interactions (Radakovic *et al.*, 2018). The HIPP26 *Arabidopsis* homologue in *N*. *benthamiana* was shown to act as a plasma membrane-to-nucleus signal during abiotic stress by interacting with the potato mop-top virus (PMTV) movement protein, TGB1. TGB1/HIPP26 complex formation leads to NtHIPP26 membrane dissociation. The complex is then redirected via microtubules to the nucleus, thereby activating the drought stress response pathway, which, in turn, facilitates the access of PMTV to the virus long-distance movement via the phloem (Cowan *et al.*, 2018). Several *Arabidopsis* HIPP proteins belonging to different clusters have been identified in transcriptome analysis to be transcriptionally regulated by nitric oxide (NO), a highly reactive free radical with essential cellular regulatory functions involved in a plethora of physiological processes (Hussain *et al.*, 2016).

Several *Arabidopsis* HIPP proteins belonging to the cluster I have been shown to interact with the cytokinin-degrading enzymes CYTOKININ OXIDASE/DEHYDROGENASE (CKXs), and to be involved in CKX regulation via the endoplasmic reticulum-associated degradation (ERAD)-mediated pathway (Guo, 2019). Overexpression of cluster-I HIPP proteins triggered cytokinin-related phenotypic changes, associated with an increased cytokinin activity. Exogenous cytokinin application repressed the expression of these *HIPP* genes, suggesting a regulatory feedback loop between cytokinin and cluster-I *HIPP* genes (Guo, 2019).

Although HIPP proteins are involved in a variety of biological processes, the mechanistic details underlying their roles in these processes remain largely unknown.

1.2 The plant hormone cytokinin

As sessile organisms, plants depend on many environmental and endogenous signals that, together with their intrinsic genetic endowment, determine and control all aspects of plant growth and development. Fundamental to these processes are several growth regulators, collectively known as plant hormones or phytohormones. The phytohormone cytokinin was originally discovered due to its ability to induce cell division (cytokinesis) in cultured plant tissue

(Miller *et al.*, 1955). Since then, cytokinins have been shown to be essential regulators of numerous aspects of growth and development, including cell division, shoot initiation and growth, apical dominance, source sink relationships, leaf senescence, nutrient uptake, phyllotaxis, vascular, gametophyte, and embryonic development, flowering time, as well as biotic and abiotic interactions (Werner and Schmülling, 2009; Cortleven *et al.*, 2019; Hwang *et al.*, 2012; Kieber and Schaller, 2018). The various roles of cytokinins throughout plant life cycle point towards a versatile and complex molecular mechanism of action. Additionally, numerous plant developmental processes are regulated via crosstalk between cytokinin and other plant hormones, such as auxin, gibberellic acid and ethylene (El-Showk *et al.*, 2013).

Chemically, cytokinins are N^6-substituted derivatives of adenine (Sakakibara, 2006). Naturally occurring cytokinins are divided into two groups based on the chemical structure of the N^6-attached side chain – those with isoprene-derived side chains, such as isopentenyladenine (iP) *trans*-zeatin (*t*Z), *cis*-zeatin (*c*Z), and dihydrozeatin (DZ); and those with aromatic side chains, such as benzyladenine (BA; Figure 4). The occurrence of different cytokinin types can vary between different plant species, tissues and developmental stages, being influenced by environmental conditions. The iP- and *t*Z-type cytokinins are the major and most active forms, whereas *c*Z-type cytokinins are thought to be of minor importance in *Arabidopsis* (Osugi and Sakakibara, 2015; Frébort *et al.*, 2011). Natural cytokinins are also present as the corresponding nucleosides, nucleotides, and glycosides or amino acid conjugates (Sakakibara, 2006).

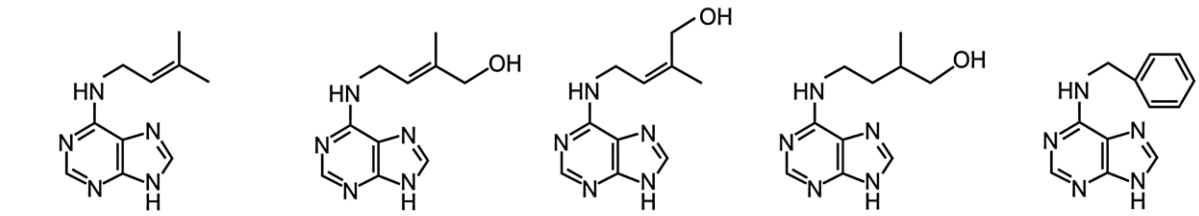

N^6-(Δ^2-isopentenyl)adenine (iP) | ***trans*-zeatin (*t*Z)** | ***cis*-zeatin (*c*Z)** | **dihydrozeatin (DZ)** | **benzyladenine (BA)**

Figure 4. Structures of representative cytokinin species.
Structures of active isoprenoid and aromatic cytokinin forms. The commonly used abbreviations of their trivial names are indicated in parentheses. Modified after Sakakibara (2006).

1.2.1 The biosynthesis and metabolism of cytokinins

The cellular cytokinin homeostasis is mainly determined by two metabolic processes, namely the *de novo* biosynthesis and catabolic degradation (Sakakibara, 2006). The biosynthesis of isoprenoid cytokinins begins with the addition of isoprenoid moiety to adenosine 5'-phosphates (AMP, ADP or ATP) and is catalyzed by the isopentenyltransferase (IPT) enzymes (Figure 5). The major isoprenoid side chain donor is dimethylallyl diphosphate (DMAPP), an isoprenoid

precursor synthesized from the mevalonate pathway (Sakakibara, 2006). The resulting products, iP nucleotides, isopentenyl adenosine 5'-tri-, di-, and/or monophosphates (iPRTP, iPRDP and/or iPRMP), can be subsequently converted to the corresponding *t*Z-nucleotides via hydroxylation of the isoprenoid side chain by the cytochrome P450 monooxygenases CYP735A1/A2 (Figure 5; Takei *et al.*, 2004). The free cytokinin bases iP, *t*Z and their corresponding ribosides are synthesized from cytokinin iP- and *t*Z-nucleotides in a single enzymatic step, which is catalyzed by the cytokinin nucleoside 5'-monophosphate phosphoribohydrolase LONELY GUY (LOG) yielding free cytokinin bases, the active forms of cytokinin (Figure 5; Kurakawa *et al.*, 2007). In some monocot plants, such as maize and rice, *c*Z and its conjugates are the most abundant cytokinin species (Osugi and Sakakibara, 2015). The biosynthesis of *c*Z is not yet elucidated. In *Arabidopsis*, the *c*Z-cytokinins are synthesized by tRNA-IPTs, which catalyze the N^6-prenylation of the an isopentenyladenosine residue at the site adjacent to the anticodon (Figure 5; Kasahara *et al.*, 2004; Sakakibara, 2006).

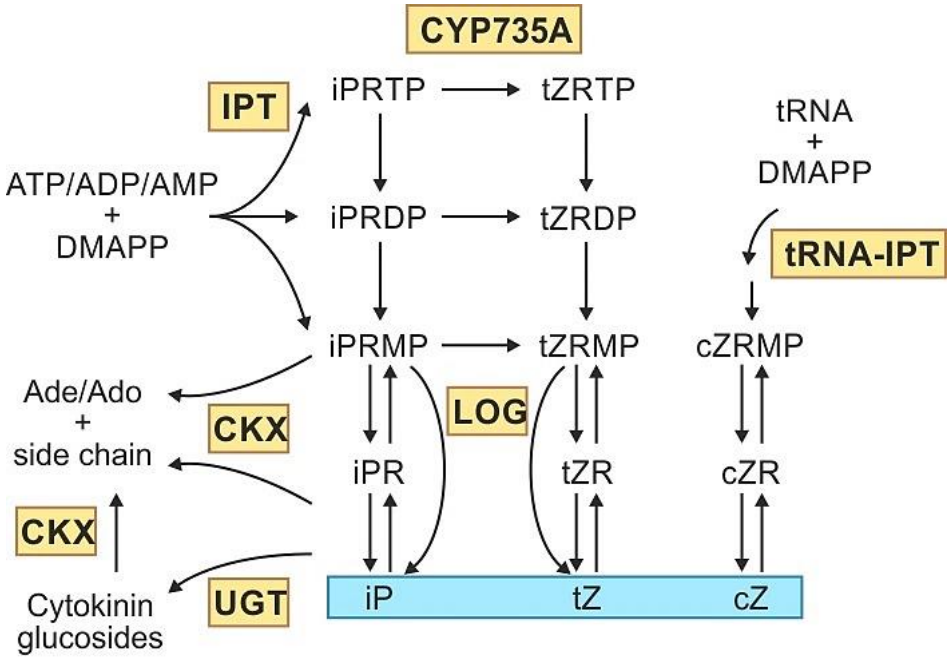

Figure 5. Simplified representation of cytokinin metabolism in *Arabidopsis*.
The biosynthesis of cytokinin ribotides from DMAPP and either adenosine phosphate or tRNA are catalyzed by IPTs. iP ribotides can be converted to *t*Z ribotides by CYP735A enzymes. iP ribotides can be converted to the active free bases in a single- or a two-step process by LOG enzymes. The cytokinin degradation is achieved by CKXs. AMP: adenosine monophosphate; DMAPP: dimethylallyl diphosphate; IPT: isopentenyl transferase; iPRMP: isopentenyladenosine monophosphate; iP: isopentenyl adenine; *t*Z: *trans*-zeatin; *c*Z: *cis*-zeatin; CYP735A: cytochrome P450 monooxygenase. LOG: lonely guy; CKX: cytokinin oxidase/dehydrogenase. UGT: cytokinin *N*-glycosyltransferase. Biologically active cytokinins are highlighted in blue. Adapted from Werner and Schmülling (2009).

Steady-state levels of biologically active cytokinins also depend on the rate of their inactivation by conjugation to sugars, mostly glucose, which is catalyzed by cytokinin glycosyltransferases (UGTs), or by their irreversible degradation by the cytokinin oxidase/dehydrogenases (CKXs),

which oxidatively cleave the unsaturated isoprenyl side chains resulting in the formation of adenine and a side chain-derived aldehyde (Figure 5; McGaw and Horgan, 1983; Werner *et al.*, 2006). CKX is a flavoenzyme, containing a covalently bound flavin adenosine dinucleotide (FAD) as a co-factor that facilitates the catalytic reaction with either molecular oxygen as the oxidant or with other electron acceptors in a dehydrogenase reaction (Galuszka *et al.*, 2007; Frébort *et al.*, 2011). Preferred CKX substrates are iP- and *t*Z-type cytokinin bases and their ribosides (Armstrong, 1994). CKX with high preference for *c*Z and cytokinin *N*-glucosides as substrates has been reported in maize (Smehilova *et al.*, 2009). There are seven homologous *CKX* genes in *Arabidopsis*, encoding isoenzymes with different biochemical characteristics, distinct expression patterns and subcellular locations (Werner *et al.*, 2006; Werner *et al.*, 2003). Thus, it is believed that CKXs control partly different cellular cytokinin pools, depending on their subcellular localizations. For instance, CKX7 are localized to the cytosol, whereas the CKX1 and CKX3 have been shown to localize in the endoplasmic reticulum, endomembrane system and vacuoles (Köllmer *et al.*, 2014; Werner *et al.*, 2003; Niemann *et al.*, 2018). Moreover, it has been demonstrated that CKX1 is a type II integral membrane protein with a short N-terminal cytoplasmic tail, a single transmembrane domain, and a luminally oriented catalytic domain; the protein also localizes predominantly in the endoplasmic reticulum (ER; Niemann *et al.*, 2018). Expression analysis of *Arabidopsis CKX* genes revealed functional diversification during plant development, with the highest activity in the regions or zones of active cell division and growth, such as shoot and root meristems and emerging leaves (Werner *et al.*, 2003). The expression of several *CKX* genes is enhanced by cytokinin, pointing towards a self-regulatory mechanism, which ensures the cellular cytokinin homeostasis (Werner *et al.*, 2006). Environmental cues, such as nitrate and phosphate availability, also regulate the expression of *CKX* and *IPT* genes, thus controlling cellular cytokinin levels (Argueso *et al.*, 2009).

1.2.2 Cytokinin transport, perception and signaling

Cytokinins are synthesized *de novo* in numerous cell types in both roots and shoots and are translocated to target cells by diffusion and/or through active transport mechanisms. Tracer experiments using isotope-labeled cytokinins as well as the detection of both active cytokinin nucleobases and its inactive riboside conjugates in vascular saps demonstrated that cytokinins, as long-distance mobile signals, translocate via xylem and phloem (Osugi and Sakakibara, 2015; Hirose *et al.*, 2008; Kang *et al.*, 2017). *t*Z-type cytokinins have been shown to be more abundant in xylem sap than iP-type, and vice versa in phloem sap (Hirose *et al.*, 2008). Primarily *t*Z-ribosides are transported from roots to shoots via xylem and iP-type cytokinins translocate from shoots to roots via phloem (Hirose *et al.*, 2008). Since the LONELY GUY enzyme, unlike the other cytokinin biosynthesis enzymes, is ubiquitously present, the

inactive cytokinin forms can be activated in most plant tissue (Kuroha *et al.*, 2009). So far, the molecular mechanisms involved in cytokinin transport are not well understood. However, three kinds of membrane transporters have been recognized to be involved in cytokinin distribution and transport. These transporters include a subset of purine permeases (PUPs) and equilibrative nucleoside transporters (ENTs), which act as influx carriers and transport cytokinin nucleobases and respectively nucleosides. Another transporter is the G subfamily ATP-binding cassette transporter, ABCG14, which acts as an efflux pump involved in long-distance acropetal translocation of the root-synthesized cytokinins (Ko *et al.*, 2014)

Cytokinins mainly trigger physiological responses through the regulation of gene expression. The cytokinin signal transduction occurs via a phosphorylation cascade which shares basic similarities with the bacterial two-component system (TCS), where it typically consists of a sensory histidine kinase and response regulator (Osugi and Sakakibara, 2015). In *Arabidopsis*, the phosphorylation cascade is more complex and consists of multistep phosphotransfer events involving several proteins (Figure 6; Kieber and Schaller, 2014).

The cytokinin signal transduction is initiated by the autophosphorylation of histidine kinase receptors (HKs) at a histidine (H) residue in their cytosolic kinase domain in response to cytokinin recognition by the conserved extracytosolic CHASE (cyclases/histidine kinases associated sensing extracellular) domain. The phosphoryl group is intramolecularly transferred to an aspartate residue (D) within the receptor receiver domain (Figure 6). In *Arabidopsis*, the cytokinin receptor family comprises three functionally redundant HKs AHK2, AHK3 and CRE1/AHK4. HKs are mainly localized in the ER, with the CHASE domain oriented into the ER, suggesting that the main site of cytokinin binding *in planta* is the ER lumen (Caesar *et al.*, 2011; Wulfetange *et al.*, 2011; Romanov *et al.*, 2018). After phosphorylation of HKs the phosphate signal is relayed to the downstream histidine phosphotransfer proteins (HPs; El-Showk *et al.*, 2013). In *Arabidopsis*, the phosphorylation is mediated by five true HPs (AHP1 to AHP5), which act in a redundant fashion to forward the signal within the TCS (Hutchison *et al.*, 2006), whereas the pseudo-histidine phosphotransfer protein (PHP) AHP6, which lacks a conserved histidine residue essential for signal transmission, inhibits the phosphoryl group transfer and thus counteracts the cytokinin signaling (Figure 6; Mähönen *et al.*, 2006).

HPs further transmit the signal to the type-B response regulators (RRs) in the nucleus, where these act as transcription factors to modulate the expression of the cytokinin primary response genes. In the *Arabidopsis* genome, there are 11 type-B *ARR* genes, encoding ARR1, ARR2, ARR10 to ARR14 and ARR18 to ARR21 (Heyl and Schmülling, 2003; Kieber and Schaller, 2014). The DNA-binding domains of several type-B ARRs have described so far and they have been shown to bind a common DNA-target sequence, (A/G)GAT(T/C), as found upstream of many cytokinin-regulated genes (Taniguchi *et al.*, 2007; Brenner and Schmülling, 2015). ChIP-Seq experiments have shown that ARR10 bind to their target sites in a cytokinin-dependent

manner (Zubo *et al.*, 2017). The levels of type-B RRs, and thus the cytokinin responses, are partially negatively regulated by degradation, achieved by an E3-ubiquitin ligase complex which includes the KISS ME DEADLY (KMD) F-box proteins (Figure 6; Kim *et al.*, 2013).
Among the main targets of the type-B RRs are the type-A RRs and CYTOKININ RESPONSE FACTOR (CRF) genes, which are strongly and rapidly transcriptionally induced by cytokinin (Figure 6, Brenner *et al.*, 2005; Rashotte *et al.*, 2006). The type-A RRs lack the DNA binding site, but compete with the type-B RRs for the phosphate signal and function thus as negative feedback regulators of the cytokinin signaling (To *et al.*, 2004, Werner and Schmülling, 2009). CRFs, members of the AP2/ERF transcription factor family, make up a side branch of the classical cytokinin TCS signaling, are transcriptionally upregulated by cytokinin and act in tandem with the type-B RRs to activate cytokinin target genes (Rashotte *et al.*, 2006).

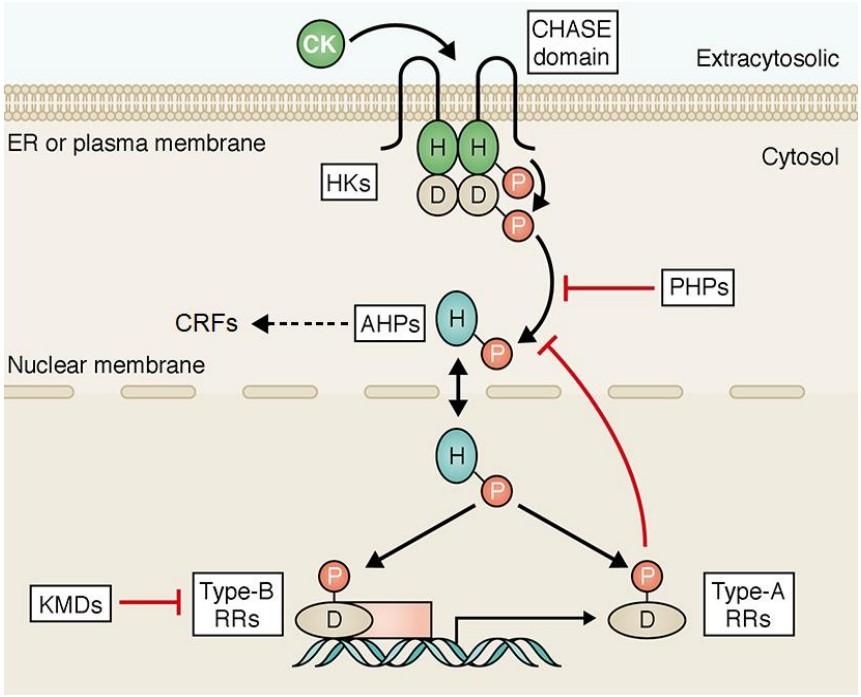

Figure 6. Schematic representation of the cytokinin signaling pathway in *Arabidopsis*.
See text for description. HKs: histidine kinase receptors, consisting of an extracellular CHASE domain, two transmembrane domains and a cytosolic region containing the histidine kinase domain (H) and the receiver domain (D). AHPs: *Arabidopsis* histidine phosphotransfer proteins. RRs: response regulators. KMD: KISS ME DEADLY. PHPs: pseudo-histidine phosphotransfer proteins. CRF: CYTOKININ RESPONSE FACTORS. Adapted from Kieber and Schaller (2018).

In *Arabidopsis*, type-A ARRs are encoded by a gene family comprising ten members *i.e. ARR3 to ARR9, ARR15* to *ARR17*, with partially overlapping and redundant functions in negatively regulating the cytokinin response (To *et al.*, 2004). Cytokinin also controls the levels of type-A ARRs by increasing the protein stability in a phosphorylation-dependent manner (To *et al.*, 2007a). Recently, it has been postulated that type-A ARRs are recruited to autophagosomes

via interaction with the core autophagy protein, ATG8, suggesting that cytokinin signaling can be modulated by selective autophagy (Acheampong *et al.*, 2020).

1.2.3 The transcriptional response to cytokinin

Several studies analyzing the genome-wide transcriptional changes upon treatment of plants with exogenous cytokinin have been conducted in the last years in *Arabidopsis*. Thereby, numerous genes with relevant functions in a plethora of biological processes have been identified to be controlled by cytokinin (Bhargava *et al.*, 2013; Brenner and Schmülling, 2015). Meta-analysis of publicly available microarray and RNA-Sequencing data has established a robust set of cytokinin-regulated genes, which exhibited elevated expression levels following cytokinin treatment (Bhargava *et al.*, 2013). Gene ontology term analyses of type-B ARR targets and cytokinin-regulated genes in the RNA-Seq experiments revealed enrichment for hormonal responses to biotic and abiotic stimuli consistent with previous knowledge about cytokinin action (Bhargava *et al.*, 2013). Additional transcription factors have been shown to act in tandem with type-B ARRs to modulate gene expression. For instance, ARR2 is involved in triggering defense responses by interacting with the salicylic acid-regulated transcription factor TGA3 to activate gene expression in response to pathogens (Choi *et al.*, 2010). Genome-wide binding site analysis has revealed that DELLA proteins, which act as hubs that relay environmental information to multiple transcriptional circuits, are recruited by ARR1 to the promoters of cytokinin-regulated genes, where they act as transcriptional co-activators. It has been shown that the interaction between ARR1 and DELLAs is necessary for proper root meristem maintenance and photomorphogenesis (Marín-de la Rosa *et al.*, 2015). Recent chromatin immunoprecipitation-sequencing (ChIP-Seq) studies have identified targets of predominant type-B ARRs, ARR1, ARR10, and ARR12, and integrated these into the cytokinin-activated transcriptional network. Primary targets of the type-B ARRs are enriched for genes involved in hormonal regulation, emphasizing the extensive crosstalk that occurs between cytokinin and other hormones (Zubo and Schaller, 2020; Mason *et al.*, 2005). Furthermore, assay for transposase accessible chromatin with sequencing (ATAC-Seq) experiments revealed that the type-B ARRs are necessary for the changes in chromatin accessibility in response to cytokinin, thus providing new insights into the dynamics between cytokinin and chromatin to direct transcriptional events and how cytokinin mediates its pleiotropic effects (Potter *et al.*, 2018).

1.2.4 Cytokinin functions in plant growth and development

Cytokinin participates, often in concert with other hormones, in regulating numerous aspects of plant growth and development throughout the life cycle. Most notable is the cytokinin-auxin genetic regulatory network which governs many developmental processes, including the

formation and maintenance of the root apical meristem and cell patterning in growing roots (Bishopp *et al.*, 2011a; Schaller *et al.*, 2015), vascular development (Mähönen *et al.*, 2006), shoot meristem and floral meristem activity (Lee *et al.*, 2019; Besnard *et al.*, 2014), leaf phyllotaxis (Besnard *et al.*, 2014) and shoot branching (Waldie and Leyser, 2018). Another example of hormonal interplay is the counteraction of cytokinin and abscisic acid (ABA) signal transduction pathways that regulate seed germination (Wang *et al.*, 2011). Further plant growth and developmental aspects controlled by cytokinin include the leaf senescence process (Kim *et al.*, 2006), female gametophyte development (Cheng *et al.*, 2013), floral organ size (Bartrina *et al.*, 2011), fruit elongation (Di Marzo *et al.*, 2020), seed size (Riefler *et al.*, 2006) and flowering time and plant longevity (Bartrina *et al.*, 2017). Cytokinin also regulates several responses to abiotic stress, such as light and temperature stress (Cortleven *et al.*, 2019), nutrient availability (Pavlů *et al.*, 2018), heavy metal stress (Bruno *et al.*, 2017) as well as biotic stress, where cytokinin acts as virulence factor during plant-pathogen interactions (Spallek *et al.*, 2018). In the following sections, the molecular mechanisms of four development processes controlled by cytokinin will be elaborated.

1.2.4.1 Role of cytokinin during male and female gametophyte development

Angiosperms as heterosporous plants are characterized by the production of two types of unisexual gametophytes, the megagametophyte (embryo sac) and microgametophyte (pollen). Developments of the female gametophytes occur within the ovule, the male gametophyte within the anther primordia (Berger and Twell, 2011). First evidence for cytokinin phosphorelay affecting the gametogenesis arose as the *cki1* mutant plants displayed female gametophyte lethality, mainly characterized by the abortion or degradation of embryo sacs (Pischke *et al.*, 2002). CKI1 encodes an AHK related to the three cytokinin receptors, but unlike those, the extracellular domain of CKI1 does not bind cytokinin (Hwang *et al.*, 2012). CKI1 can induce a cytokinin response via the AHPs independently of AHK function, as the *ahp1,2,3,4,5* mutant shows defects in female gametophytes development similar to those observed *cki1* (Deng *et al.*, 2010; Zürcher and Müller, 2016). However, only AHP2, AHP3, and AHP5 have been shown to redundantly act downstream of CKI1 to regulate cell type specification and promote female gametophyte development (Cheng *et al.*, 2013; Liu *et al.*, 2017c). Studies using the cytokinin response reporter *TCSn:GFP* revealed that CKI1 is crucial for central cell specification within the embryo sac, whereas its repression is required for synergids and egg cell specification. In *cki1*, the central cell acquires egg cell fate, whereas ectopic expression of *CKI1* confers central cell fate to an egg cell or to the accessory synergid cells (Yuan *et al.*, 2016).

There is some evidence that cytokinins are involved in male gametophyte development as well. For instance, accumulation of CKX in male reproductive tissues of transgenic maize (*Zea mays*) led to male-sterile plants (Huang *et al.*, 2003). Whereas, overexpression of *CKX1* in

transgenic *Arabidopsis* plants lead to a large reduction in pollen formation (Werner *et al.*, 2003). More recent studies indicated that cytokinin receptors are not only required for female gametophyte development and function, but are also important for pollen and pistil formation (Kinoshita-Tsujimura and Kakimoto, 2011).

1.2.4.2 Cytokinin action in the shoot

Classic experiments already demonstrated that cytokinins stimulate the formation of shoot meristems in plant tissue culture (Skoog and Miller, 1957). Since then, numerous studies in *Arabidopsis* and rice have highlighted the importance of cytokinin action in regulating the shoot apical meristem (SAM) establishment and maintenance (Osugi and Sakakibara, 2015). In plants, meristems maintain a pool of totipotent (stem) cells that divide and differentiate, allowing the formation of new plant organs and tissues (Greb and Lohmann, 2016). The dome-shaped SAM is organized in the central zone (CZ) that spans the three cell layers L1, L2 (collectively referred as tunica) and L3 (corpus), which respectively give rise to the distinct cell types of the plant stem: epidermis, ground tissue and vasculature (Gaillochet and Lohmann, 2015). The CZ also contains undifferentiated stem cells (SCs), which divide only rarely and part of their progeny is displaced laterally towards the peripheral zone (PZ), the site of organ primordia initiation, characterized by a much higher cell division rate (Reddy *et al.*, 2004; Gaillochet and Lohmann, 2015; Truskina and Vernoux, 2018). The balance between cell proliferation, to maintain the constant stem cell pool, and cell differentiation, to become organ primordia, is strictly controlled by phytohormonal pathways integrated into local and zone-specific transcriptional networks (Gaillochet and Lohmann, 2015). The molecular patterns associated with the functional SAM zones are established by two master regulator genes: *CLAVATA3 (CLV3)* in the central zone and the homeodomain transcription factor *WUSCHEL (WUS)* in the organizing center (OC), which act in a feedback loop to dynamically maintain the size of the stem cell niche (Mayer *et al.*, 1998; Fletcher *et al.*, 1999; Schoof *et al.*, 2000).
The importance of the role cytokinin plays in cell proliferation in the SAM has been demonstrated by the fact that reduced cytokinin levels resulted in a smaller SAM (Werner *et al.*, 2003). Later studies revealed that the cytokinin signaling domain encompasses the OC and the neighboring cell layers, being indispensable for the positive regulation of *WUS* expression and WUS correct positioning in the SAM, mediated via the AHK4 receptor (Figure 7, Leibfried *et al.*, 2005; Gaillochet and Lohmann, 2015; Pernisova *et al.*, 2018).

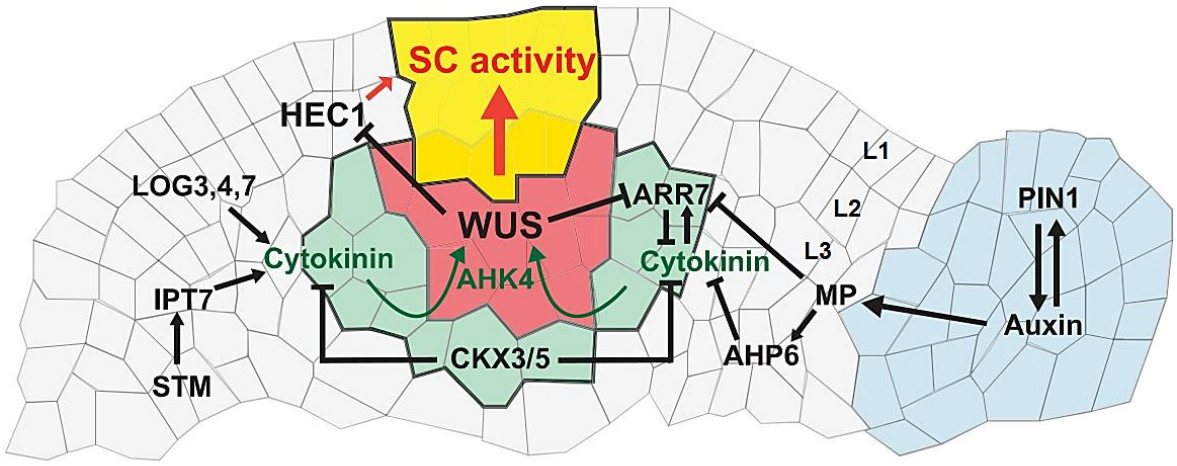

Figure 7. Integration of the cytokinin signaling in the regulation and maintenance of SAM.
The organizing center (OC) is delimited in red. Cytokinin signaling (highlighted in mint and red) controls stem cell (SC) activity together with HECATE1 (HEC1). Cytokinin levels depend on LOG, IPT7 as well as on CKX3 and CKX5 activities. IPT7 acts downstream of SHOOT MERISTEMLESS (STM). WUS facilitates cytokinin signaling by directly repressing the expression of type-A ARRs (ARR7). Auxin also modulates stem cell activity by regulating the type-A ARRs via MONOPTEROS (MP) and determines the sites of primordia initiation, which involves PIN1, MP and AHP6 (Gaillochet and Lohmann, 2015).

Type-B ARRs can also activate the transcription of *WUS* and, in parallel, inhibit auxin accumulation by repressing the expression of *YUCCA*s, which encode key enzymes for auxin biosynthesis, thus indirectly promoting *WUS* induction (Meng *et al.*, 2017). WUS sensitizes the OC to cytokinin by directly repressing the expression of type-A ARRs, which acts as negative regulators of cytokinin signaling contribute to promoting *WUS* expression (Figure 7; Leibfried *et al.*, 2005). Moreover, ARR7 and ARR15 have been shown to be critical for activating *CLV3* expression, thereby restricting *WUS* transcription (Zhao *et al.*, 2010). Cytokinin levels in the SAM are modulated by the activities of LOG enzymes, the loss of which causes severe meristem defects (Kurakawa *et al.*, 2007), and by IPT7, which is activated by the KNOX1 gene *SHOOT MERISTEMLESS* (*STM*), known to suppress cell differentiation throughout the SAM and to promote cell proliferation (Long *et al.*, 1996; Yanai *et al.*, 2005). However, cytokinin levels are restricted by the activity of catabolic enzymes, such as CKX3 and CKX5 (Figure 7). *ckx3,5* mutants, exhibiting increased cytokinin levels, showed elevated *WUS* expression and formed larger SAM (Bartrina *et al.*, 2011). Additionally, the bHLH transcription factor HECATE1 (HEC1), which is a target of WUS, contributes to SAM function by promoting stem cell proliferation, while antagonizing niche cell activity (Figure 7; Schuster *et al.*, 2014). In contrast to cytokinin, auxin signaling guides primordium initiation (Figure 7), leading to the formation of lateral organs, leaves or flowers, mainly involving the intercellular transport of auxin by the PINFORMED1 (PIN1, Gaillochet and Lohmann, 2015). Auxin synergizes with cytokinin to promote SC activity via the AUXIN RESPOSE FACTOR transcription factor MONOPTEROS

(MP), which directly represses the expression of *ARR7* and *ARR15*, thereby enhancing cytokinin signaling output and thus WUS expression (Zhao, 2010). However, MP also promotes the expression of *AHP6*, which interferes with the cytokinin signal transduction pathway and restricts the cytokinin-signaling domain to the center of the SAM, while auxin governs the SAM periphery (Zhao *et al.*, 2010; Besnard *et al.*, 2014).

1.2.4.3 Cytokinin role during flower and fruit development

All the aerial organs of the plant derive from the SAM. This meristem generates leaves, stem and axillary meristems during the vegetative phase, and after the floral transition – in the reproductive phase – transforms into an inflorescence meristem (IM; Benlloch *et al.*, 2007). IM directly initiates floral meristems (FMs) on its flanks. Unlike SAM, which continuously divides to generate new tissues, FMs undergo determinate growth to form flowers, with particular numbers of floral organs of specific size, and subsequently undergo programmed termination (Sablowski, 2007). Cytokinins play a key role during several stages of flower development. For instance, the loss of *LOG* function decreases local levels of active cytokinin, resulting in a reduced number of branches and flowers, and a drastic decline in the number of floral organs (Kurakawa *et al.*, 2007). During floral transition, the emerging FMs require *APETALA1 (AP1)* to specify their floral identities (Liu *et al.*, 2007). Elevation of cytokinin through transgenic expression of *IPT4* under the control of the *AP1* promoter led to alterations of floral development, mainly through AHK2 and AHK3 signaling, leading to increased expression of the boundary identity genes *CUP-SHAPED COTYLEDON2 (CUC2)* and *CUC3* (Liu *et al.*, 2007; Li *et al.*, 2010). Further studies have revealed that ARR1 and ARR10, directly bind to the transcriptional regulatory regions of the carpel identity-defining gene *AGAMOUS (AG)* and induce its expression. The expression of type-B *ARRs* overlapped with that of *AG* in the floral primordia, and defects in these ARRs reduced the carpel number. Altogether, these results suggest that ARR1 and ARR10 regulate carpel initiation and contribute to carpel development via activating *AG* expression (Rong *et al.*, 2018).

There are several studies reporting that, in addition to altering organ number, cytokinins also control fruit morphology, fruit size and yield (Marsch-Martínez *et al.*, 2012). For example, *Arabidopsis ckx3,5* mutants, which contain elevated cytokinin levels, were able to produce increased numbers of ovules and seeds, indicating that cytokinins play an important role in placental formation during gynoecium development (Bartrina *et al.*, 2011). Furthermore, in the *ahk* mutants with severely reduced cytokinin perception, the expression of the auxin efflux facilitator PIN-FORMED 1 (PIN1) is severely reduced, while treatment with exogenous cytokinin alters both auxin distribution and patterning of the ovule, suggesting that cytokinin regulates ovule development through the regulation of PIN1 (Bencivenga *et al.*, 2012). However, this process requires the involvement of two transcription factors BELL1 and

SPOROCYTELESS/NOZZLE, which control ovule pattering and development of the female gametophyte (Bencivenga *et al.*, 2012). A recent study has demonstrated that cytokinins play opposing roles in pistil and fruit growth before and after fertilization (Di Marzo *et al.*, 2020). The positive role of cytokinin in pistil elongation was confirmed in the *ckx3,5* mutants, which exhibited longer pistils than wild type counterparts (Bartrina *et al.*, 2011). After fertilization, the expression of the cytosolic cytokinin-degrading enzyme *CKX7* is induced by SEEDSTICK, a MADS-domain transcription factor crucial for the regulation of ovule integument identity. CKX7 expression contributes to the degradation of the cytosolic cytokinin pool, which positively regulates fruit elongation (Di Marzo *et al.*, 2020; Mizzotti *et al.*, 2012).

1.2.4.4 Cytokinin action in the root

In contrast to their positive role on proliferation of meristematic cells in the shoot, cytokinins negatively regulate root growth. Reducing the endogenous cytokinin levels by overexpressing cytokinin degrading CKX enzymes or by disrupting the *IPT* genes as well as lowering the cytokinin signal output leads to an increase in apical root meristem (RAM) size, whereas increased cytokinin levels or sensitivity cause the opposite (Werner *et al.*, 2003; Dello Ioio *et al.*, 2007; Del Bianco *et al.*, 2013). The post-embryonic RAM is divided into the proximal meristem (PM), the differentiation zone (DZ), and the transition zone (TZ) (Figure 8A; Dello Ioio *et al.*, 2007). The balance between cytokinin and auxin at the TZ controls cell entry into differentiation. Cytokinin promotes cell differentiation by repressing both auxin signaling and transport, whereas auxin sustains root meristem activity by promoting cell division (Di Mambro and Sabatini, 2018). Cytokinin promotes cell differentiation via ARR1, which induces the expression of a negative regulator of auxin responsiveness, the *SHY2* gene (Dello Ioio *et al.*, 2008; Taniguchi *et al.*, 2007; Tian and Reed, 1999). The induction of *SHY2* in turn leads to a negative regulation of the PIN auxin efflux carriers, PIN1, PIN3 and PIN7 (Figure 8A; Blilou *et al.*, 2005). In the PM, auxin acts to mediate the degradation of SHY2, thereby maintaining the expression of PINs in the meristem. Both the polar auxin transport (PAT) and auxin signaling are tightly connected to the activity of *PLETHORA (PLT)* genes, which control the auxin distribution via regulating the expression of PIN1, PIN3 and PIN7 (Blilou *et al.*, 2005). In turn, PLT genes are regulated by tyrosine-sulfated peptides encoded by the ROOT GROWTH FACTOR (RGF) gene family (Figure 8A; Aida *et al.*, 2004).

The quiescent center (QC) is located at the tip of PM and divides only seldom to give rise to the surrounding stem cells, which generate daughter cells that subsequently undergo division in the PM, and as the root grows, start to elongate and differentiate (Su *et al.*, 2011). It is crucial to maintain a balance between the proliferation of the stem cells and the differentiation of the newly formed daughter cells. This is also achieved by the antagonistic interplay between auxin

and cytokinin, which control the root stem cell niche (SCN) specification and maintenance (Gaillochet and Lohmann, 2015).

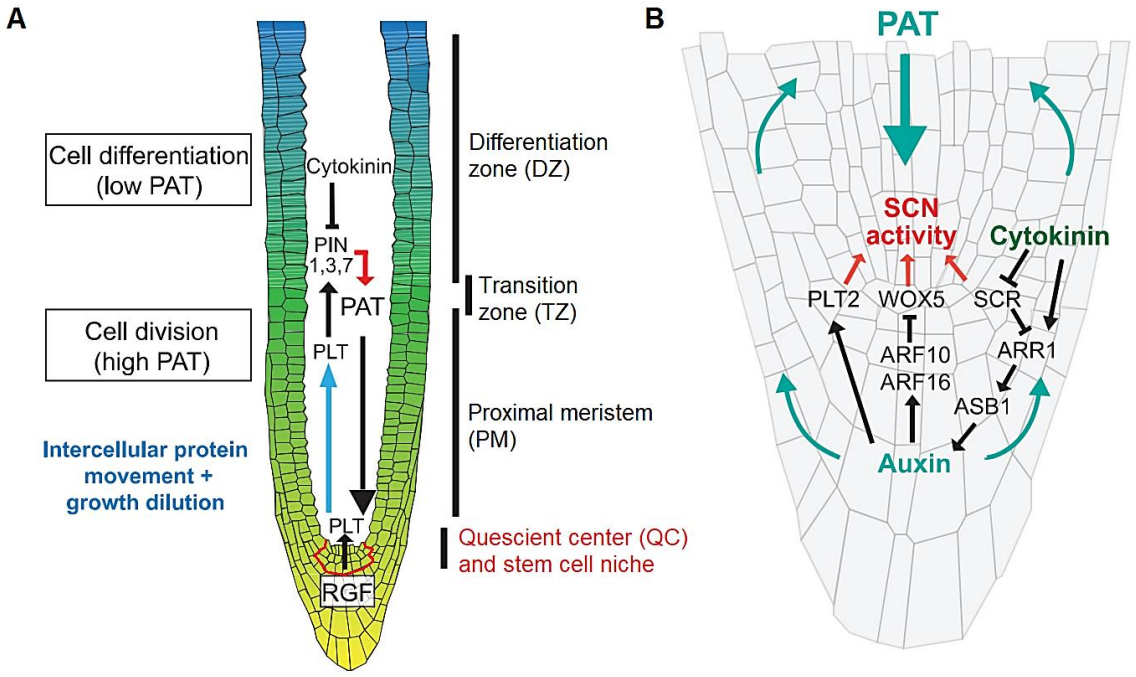

Figure 8. Molecular mechanisms of cytokinin and auxin interaction in the regulation of RAM. **(A)** Overview of the functional domains of the root apical meristem (RAM) and the main events regulating the root meristem growth. **(B)** Schematic representation of root stem cell niche (SCN) activity modulated by the auxin-cytokinin balance. See text for description. Adapted from Gaillochet and Lohmann (2015).

Within the root apex, auxin is distributed in a gradient-like fashion with a maximal concentration at the QC (Eckardt, 2009). This auxin peak promotes the expression of PLT2 which encodes a AP2-domain transcription factor, a key regulator of the SCN activity (Santuari *et al.*, 2016). Auxin also contributes to the establishment of the root SCN, by positively regulating the expression of *AUXIN RESPONSE FACTORS*, *ARF10* and *ARF16*, which repress the expression of *WUSCHEL-RELATED HOMEOBOX 5 (WOX5)* (Figure 8B). *WOX5* is specifically expressed in QC and it is indispensable for the suppression of QC division and differentiation of columella stem cells (CSCs; Sarkar *et al.*, 2007). Cytokinin signaling components function already during embryogenesis, when the QC forms from an asymmetric cell division of a founder cell, the hypophysis (ten Hove *et al.*, 2015). While the apical daughter cell maintains the phosphorelay activity of cytokinin signaling, in the basal daughter cell, the cytokinin signaling is repressed by the auxin-mediated transcriptional activation of type-A *ARR*s, *ARR7* and *ARR15* (Müller and Sheen, 2008). During post-embryonic development, cytokinin instructs cell differentiation by suppressing the expression of *SCARECROW (SCR*) gene, encoding a transcription factor required and sufficient for distal specification of the QC, which in turn regulates stem cell fate of immediately surrounding cells (Figure 8B; Moubayidin *et al.*, 2016). SCR maintains stem cell activities by directly repressing expression of *ARR1* in

the QC, sustaining stem cell activity (Moubayidin *et al.*, 2016). In turn, ARR1 promotes expression of the *ANTRANILATHE SYNTHASE BETA 1* (*ASB1*), encoding an enzyme involved in the first steps of auxin anabolism (Salvi *et al.*, 2018). Another alternative for SCR to sustain the stem cell and meristem activity is by suppressing the cytokinin perception via the cytokinin receptor AHK3 (Moubayidin *et al.*, 2013).

Cytokinins negatively regulate the lateral root formation. Application of exogenous cytokinins inhibits lateral root initiation in both *A. thaliana* and *O. sativa* (Del Bianco *et al.*, 2013). This is consistent with previous studies showing that plants carrying loss-of-function mutations in several type-B *ARR* and *AHK* genes, as well as overexpressing *CKX*, exhibited enhanced lateral root formation, whereas type-A *ARR*s mutants formed less lateral roots (Werner *et al.*, 2003; Riefler *et al.*, 2006; To *et al.*, 2004; Mason *et al.*, 2005). More recently it has been shown that cytokinin signaling functions as a lateral root specific anti-gravitropic component to promote the radial distribution of the root system, and is dependent on the CKX2 local activity (Waidmann *et al.*, 2019).

1.3 Plasmodesmata

In animals and plants, molecular communication occurs via an extracellular (apoplastic) pathway consisting of efflux and influx carriers on the plasma membrane and by means of exocytosis and endocytosis processes (Maule *et al.*, 2012; Yadav *et al.*, 2014). Additionally, the intercellular communication is facilitated by physical structures connecting the cytoplasm of adjacent cells and forming the symplasmic pathway (Maule *et al.*, 2012). In animals, the symplasmic transport of small molecules is mediated by gap junctions and the tunneling nanotubes provide cellular bridges for larger molecules and even organelles (Gerdes and Carvalho, 2008). In plants, the importance and complexity of cell-to-cell communication has an even greater weight due to the existence of rigid cell walls, which act as a physical barrier, thus impeding the direct cell-to-cell contact (Van Norman *et al.*, 2011). To overcome this barrier, plants developed unique cell wall-spanning structures, termed plasmodesmata (PD, Lucas *et al.*, 2009). PD enable the exchange of nutrients, such as ions and sugars, and various non-cell autonomous signals e. g. hormones, RNA, proteins and viruses (Kumar *et al.*, 2015). From a developmental perspective, PD-mediated communication between cells is a crucial step to coordinate the behavior of individual cells, and to establish boundaries within the tissue in order to ensure proper organ formation and tissue patterning, and thus to maintain general plant architecture (Benitez-Alfonso, 2014).

1.3.1 Plasmodesmata function, structure and regulation

The primary formation of PD occurs at cytokinesis, when dividing cells, although separated by the newly formed cell plate, remain connected through the formation of a cytoplasmic bridge

consisting of the ER, which due to the pressure of the cell plate or membrane will be gradually compressed and take the form of a strand, called desmotubules (Brunkard *et al.*, 2013). Structurally, PD appear as concentric cylinders with a diameter between 30 and 50 nm that bridge the walls of adjacent cells and provide the platform for molecular communication between cells, namely the cytoplasmic sleeve (Figure 9; Lucas *et al.*, 2009).

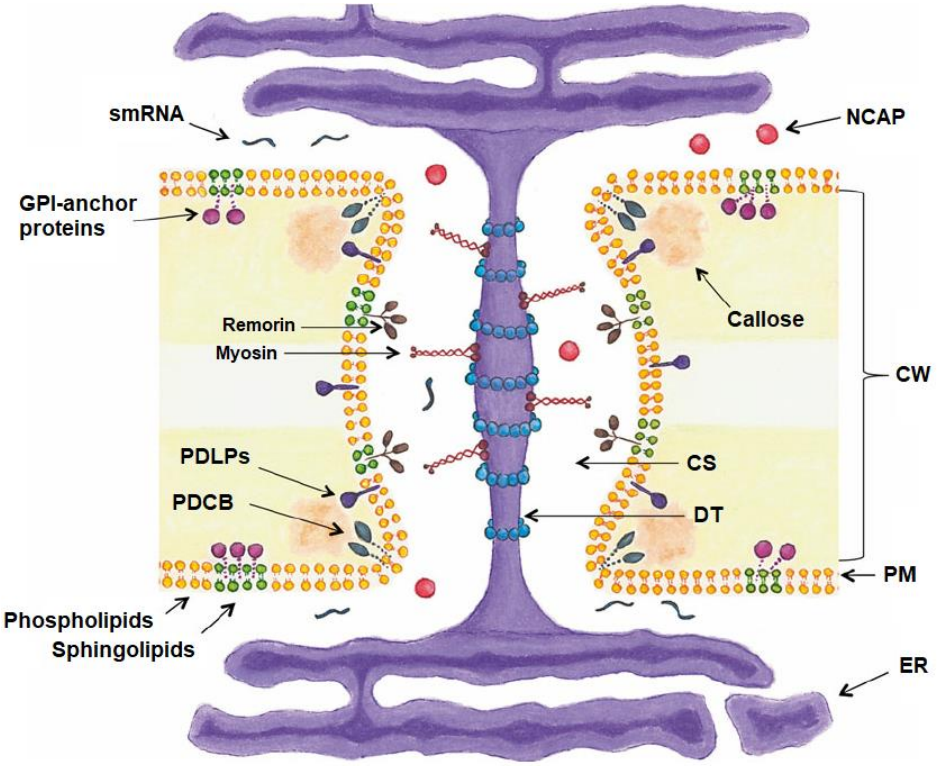

Figure 9. Schematic representation of PD structure.
PD traverse the cell walls and connect the cytoplasms of adjacent cells. The desmotubule (DT) and the cytoplasmic sleeve (CS) form a symplasmic continuum and allows the cell-to-cell movement of molecules, such as non-cell-autonomous proteins (NCAPs) and small RNAs (smRNAs). Callose accumulation and degradation at the apoplastic neck regions are the main regulators of PD aperture. Numerous proteins have been identified to permanently associate with PD and the PM surrounding PD, including remorins, myosin, GPI-anchor proteins, plasmodesmata callose-binding proteins (PDCBs), and plasmodesmata-localized proteins (PDLPs). CW: cell wall, PM: plasma membrane, ER: endoplasmic reticulum. Adapted from Sevilem *et al.* (2015).

Callose, a β-1,3-glucan polymer, accumulates within the cell walls adjacent to the PD neck region and has both structural and regulatory roles in PD function (Maule *et al.*, 2012). Immunolocalization studies revealed that proteins such as actin, myosin, tubulin, and callose-associated proteins constitute further structural components of PD (Han *et al.*, 2019). Moreover, transmembrane receptor-like protein kinases from the family of PD-located proteins (PDLPs) are also associated with the PD. Some PDLPs have been shown to be essential for plant defense responses during pathogen infection (Amari *et al.*, 2010; Caillaud *et al.*, 2014). Studies of PD-enriched membrane fractions indicate that the PD outer membranes may be

composed of different lipids than the plasma membrane (Grison *et al.*, 2015). GPI-anchor proteins and remorins, a family of plant-specific proteins with putative roles in various biotic stress responses, appear to associate with the sphingolipid-rich plasma membrane regions surrounding the PD (Simpson *et al.*, 2009; Raffaele *et al.*, 2009).

PD are dynamic channels whose aperture is defined by their size exclusion limit (SEL), which is the upper size limit of the molecules that can move through PD (Oparka *et al.*, 1999). SEL can vary in different cells and tissues and developmental stage between 27 kDa and greater than 67 kDa (Stadler *et al.*, 2005b).

The most well-known mechanism for regulating PD-mediated trafficking occurs in a SEL-dependent manner and it is mainly achieved by balancing the callose accumulation and degradation at the apoplastic neck of PD (Wu *et al.*, 2018). The callose turnover is tightly controlled by the antagonistic activities of two enzymes located at PD: callose synthase (CALS), also known as glucan synthase-like (GSL), and β-1,3-glucanase (PdBG; Han *et al.*, 2019). Accumulation of callose in the cell wall forms a collar around the PD channel, thereby restricting the molecular passage and thus the transport flux through PD. Various molecular players have been shown to be involved in the regulation of plasmodesmal callose balancing, including several phytohormones, such as auxin, abscisic acid, gibberellin and salicylic acid (Wu *et al.*, 2018). Additionally, the PD aperture can be regulated independently of callose, for instance through the actin and myosin restructuring within the cytoskeleton of the cytoplasmic sleeve, which in turn alters the conformation of the PD channel, and thus the PD-mediated traffic (White and Barton, 2011). Further studies have shown that PD-resident proteins such as the GERMIN-LIKE PROTEIN1 (GLP1), negatively impacts the PD permeability, leading to impaired root growth and development (Ham *et al.*, 2012). Overexpression of another PD-associated protein, NHL26, affects the phloem export and sugar partitioning in *Arabidopsis* (Vilaine *et al.*, 2013). More recently, three PD-resident synaptotagmin proteins have been shown to alter the contact sites between the ER and the plasma membrane around PD, leading thereby to decreased PD aperture (Ishikawa *et al.*, 2019). PD are highly versatile channels and their structure and function vary greatly during the growth and differentiation, and their permeability constantly changes in response to various environmental cues.

1.3.2 Transport via plasmodesmata

In general, there are two mechanisms for molecular movement through PD, non-targeted and targeted. Small molecules, such as sugar, amino acids and ions, phytohormones or soluble proteins whose molecular weight do not exceed the PD SEL, diffuse freely through the cytoplasmic sleeve in a non-targeted (or passive) manner, without requiring interaction with PD or PD-associated proteins. For instance, GFP (~28 kDa) passes freely through PD along its concentration gradient (Crawford and Zambryski, 2001), as does the floral identity protein

LEAFY (LFY), a transcription factor involved in floral meristem formation (Wu *et al.*, 2003). Phytohormones and a wide range of cellular RNAs, such as mRNA transcripts, endogenous small RNAs and defense-related small RNAs have been also reported to move freely from cell-to-cell through PD (Han and Kim, 2016). In contrast, proteins that undergo targeted movement interact with PD and PD-associated components to alter the size of the cytoplasmic sleeve mostly by increasing the SEL, thus facilitating their own passage through PD (Crawford and Zambryski, 2001). A 30-kDa movement protein (MP) of tobacco mosaic virus was the first protein discovered to gate PD, and is required to facilitate cell-to-cell movement of viruses (Wolf *et al.*, 1989). The KNOTTED1 (KN1) homeodomain transcription factor was the first plant protein found to traffic through PD, by comparing the localization of the *KN1* mRNA to the localization of the KN1 protein in the maize SAM. The KN1 protein was found in the L1 layer, although its mRNA was restricted to the L2 and L3 layers (Lucas *et al.*, 1995). Recent studies revealed that chaperonins, which belong to a group of cytosolic chaperones, are essential for the cell-to-cell trafficking of KN1 transcription factor and are responsible for correct protein folding before and after its translocation through PD (Xu *et al.*, 2011). Another example of targeted movement through PD is the translocation of florigen FLOWERING LOCUS T (FT) via the phloem from leaves to apical tissues in order to induce the floral meristem initiation (Corbesier *et al.*, 2007). The FT symplasmic translocation from companion cells to sieve elements requires its interaction with the ER membrane protein FT-INTERACTING PROTEIN (Liu *et al.*, 2012). Alternative translocation methods, such as trafficking of small molecules via the lumen of the ER can also provide a route between cells (Barton *et al.*, 2011).

1.3.3 Plasmodesmata as gateways to molecular translocation through phloem

Besides their essential roles in short-distance transport between adjacent cells, PD are conduits for loading or unloading molecules into the phloem (Brunkard and Zambryski, 2017). In phloem, the enucleated conducting sieve elements (SE) and the accompanying companion cells (CCs) are symplasmically linked by highly specialized asymmetric PD, called plasmodesmata pore units (PPU). Evidently, PD also connects the CC with the surrounding phloem parenchyma cells (PPCs) and other cell types (Turgeon and Wolf, 2009). SE cells within the sieve tube are connected by specialized sieve plate pores (SPPs) derived from PD structures, which mediate the mass flow of phloem content along the sieve tube (Figure 10, Lee and Frank, 2018). Phloem transport begins with the loading of solute and other macromolecules either symplasmically through PD or apoplasmically via membrane transporters (Figure 10B).

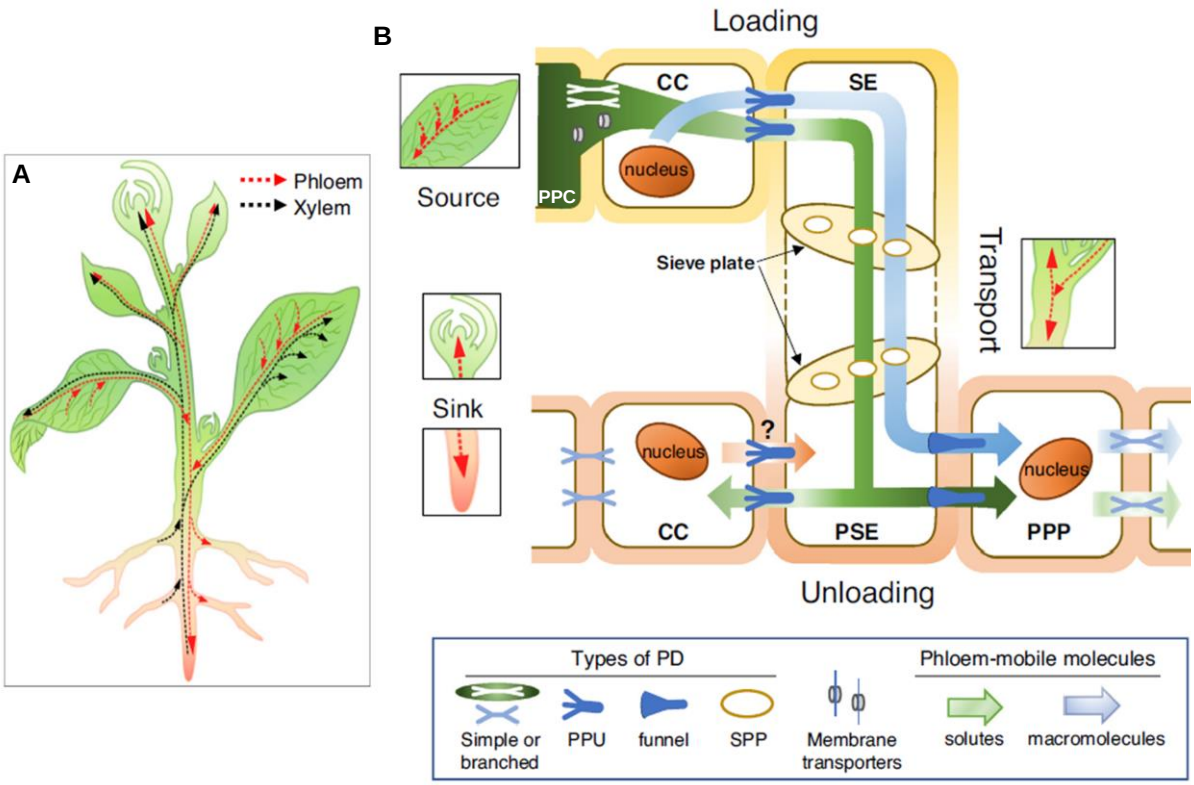

Figure 10. Long-distance transport through phloem is mediated by functionally diverse PD. **(A)** Overview of long-distance transport pathways in angiosperms: phloem (red) and xylem (black). **(B)** Schematic illustration of the phloem loading from source (leaves), translocation through the main veins, and unloading at sink tissues (shoot or root apex). PPC: phloem parenchyma cell; CC: companion cell; PPU: pore-plasmodesmata unit; sieve element (SE); SPP: sieve plate pore; PSE: protophloem sieve element; PPP: phloem pole pericycle. See text for description. Adapted from Lee and Frank (2018).

When apoplastically loaded, prior to active uptake by the phloem, sucrose enters the apoplast between PPCs and CCs via a family of sucrose efflux SWEET transporters (Chen *et al.*, 2012). Sucrose translocation into the CC-SE complex occurs against a concentration gradient and is mediated by secondary active sucrose-H^+ transporters, such as SUC2. In source tissues, solutes and macromolecules that are present in the CCs diffuse freely through PPUs to be then translocated downstream the SEs, following the mass flow and passing through the SPPs (Lee and Frank, 2018). In actively growing shoot or root apices, the protophloem sieve elements (PSE) serve as the phloem terminus and the phloem content is unloaded into the sink cells. During unloading in roots, solutes are diverted into the phloem-pole pericycle (PPP, Figure 10), a tissue connected to the protophloem by a unique class of funnel like-structured PD. Interestingly, solutes are unloaded from PPP without restriction, whereas large proteins remain restricted to PPP and are released in discrete pulses (Ross-Elliott *et al.*, 2017). Small amounts of solutes can also be unloaded into CC through PPUs. It is still unclear whether the PPUs promote also the molecular traffic from CC into PSE (Lee and Frank, 2018). Phloem

loading, transport and unloading patterns are largely determined by the morphology and structure of PD, which in turn influence the macromolecular traffic.

1.3.4 PD roles in biotic and abiotic stress

To adapt to various environmental conditions and challenges, plants are able to constantly modify the extent of molecular trafficking through PD, mainly by dynamically modulating the plasmodesmal permeability (Sager and Lee, 2014). Callose homeostasis at PD is not only essential during plant development, but also plays an important role in response to a plethora of biotic and abiotic stresses (Wu *et al.*, 2018).

Several studies on PD callose regulation in response to abiotic stress exist, including those on chilling stress, wounding, heat and heavy metals (Wu *et al.*, 2018). For instance, in *Zea mays* the photosynthetic efficiency and assimilate export is decreased at low temperature and it is related to decreased PD permeability in leaves. The PD closure is mediated by calreticulin, a calcium-sequestering protein involved in the control of the callose-dependent SEL regulation (Bilska and Sowinski, 2010). Oxidative stress that results in the accumulation of reactive oxygen species (ROS) has also been shown to induce callose deposition at PD (Benitez-Alfonso *et al.*, 2009). Loss of *GFP ARRESTED TRAFFICKING 1* (*GAT1*), which encodes an m-type thioredoxin, induces the PD-localized callose synthesis and structural modification of PDs, accompanied by severe H_2O_2 accumulation in *gat1* mutant roots, leading to seedling lethality (Benitez-Alfonso *et al.*, 2009). Further evidence shows that exposure of *Arabidopsis* roots to heavy metal stress triggers alterations in PD permeability via deposition and breakdown of callose. By limiting the PD permeability, the uptake of metal ions is minimized, thus reducing the metal toxicity throughout the plant (O'Lexy *et al.*, 2018). A more recent study has shown that PD transport is strongly regulated by light and the plant circadian clock: the latter promoting the intercellular trafficking during the day and limiting it at night. Silencing the expression of the core circadian clock gene, *LATE ELONGATED HYPOCOTYL* (*LHY*), promotes PD transport independently of light treatment, during the day or at night, suggesting that the LHY-dependent circadian clock is required to prevent light from inducing higher PD transport rates at night (Brunkard and Zambryski, 2019).

Callose homeostasis at PD is modulated in a similar fashion also in response to diverse biotic stresses. Many viruses have been reported to induce PD callose accumulation, including the tobacco mosaic virus, maize dwarf mosaic virus, potato virus X and tomato bushy stunt virus (Wu *et al.*, 2018). All plant viruses encode one or more specialized MP to facilitate their own intracellular transport by either interacting with cellular mechanisms to control the SEL of PD or to alter the PD architecture (Amari *et al.*, 2011; Heinlein, 2015). Some viruses spread by diffusion upon undergoing a complex formation with ER-associated MPs and pass as rafts

through the PD, which is strategically regulated by the viral-induced host β-1,3-glucanases (Epel, 2009).

1.4 Metal homeostasis in plants

Heavy metals, such as iron (Fe), zinc (Zn), copper (Cu), and manganese (Mn), have essential roles as trace elements in all living organisms, as almost one third to half of all structurally characterized proteins contain metal ions, either as a structural component or as a catalytic factor (Degtyarenko, 2000; Tehseen *et al.*, 2010). Although absolutely necessary for plant growth, these metal ions are detrimental and toxic when present in excess. Non-essential metals present in contaminated soil, such as cadmium (Cd), aluminium (Al), lead (Pb) or mercury (Hg) are also toxic for plants (Dykema *et al.*, 1999). Plants experience oxidative stress upon exposure to heavy metals that leads to cellular damage, which often can be deduced from the morphological alterations undergone by stressed plants, such as reduced biomass, leaf chlorosis, inhibited root growth or ultimately plant death (Yadav, 2010). Conversely, plants growing on soils with scarce bioavailable micronutrient concentrations can exhibit similar symptoms caused by metal deficiency. Given the ambivalent meaning of the essential metals and the potential toxicity of the non-essential metals, an efficient homeostasis is extremely important and is required in order to maintain the correct concentrations of essential metal ions that need to be absorbed and transported to the right proteins, and to minimize the damage from excess of both essential and non-essential metal ions (Clemens, 2001). Consequently, plants have evolved a suite of complex mechanisms, including a regulated network of metal transport, chelation, trafficking and sequestration activities that function to provide uptake, distribution and detoxification of metal ions (Clemens, 2001).

1.4.1 Uptake, transport and allocation of metal in plants

Metals absorbed from soil are translocated and partitioned either to specific subcellular compartments, such as the nucleus, mitochondria and chloroplasts, where they are required for metalloprotein functions, or they are sequestrated in vacuoles, where they serve as a reservoir to regulate the cellular metal balance (Clemens, 2001; Bashir *et al.*, 2016).
As free metal ions are toxic for the cell, the chelation of metals in the cytosol plays a major role in a basal metal tolerance. For this, plants produce various chelation exudates, such as amino acids, organic acids, phytochelatins and metallothioneins, which bind with high-affinity metal ions to protect the cell from oxidative damage (Bashir *et al.*, 2016; DalCorso *et al.*, 2013). For instance, enhancing the first enzymatic step in the histidine biosynthesis pathway in *Arabidopsis* leads to an increase in the free histidine pool and conferring tolerance to nickel exposure (Wycisk *et al.*, 2004). Similarly, *Arabidopsis* seedlings overexpressing the *PCS1* gene, encoding a phytochelatin synthase, exhibit tolerance towards cadmium directly

correlating with the increased phytochelatin content (Brunetti *et al.*, 2011). Studies conducted in *Arabidopsis*, tobacco and maize have reported that the non-proteinogenic amino acid nicotianamine contributes to an increased plant tolerance to high levels of Fe, Cd, Cu, Mn, Zn and Ni (Zhou *et al.*, 2013; Schuler and Bauer, 2011). Copper chaperones are a novel class of proteins described to assist copper intracellular trafficking and its delivery to copper-containing proteins in mitochondria, trans-Golgi network and cytosol (Robinson and Winge, 2010).

Metal transport and allocation represent key components to ensure metal homeostasis, which depends on the operation of a series of transition metal transporters, also called metallochaperones (Krämer *et al.*, 2007; de Abreu-Neto *et al.*, 2013). In *Arabidopsis*, the main families of metal transporters involved in the uptake of heavy metals are CTR/COPT (copper transporter), ZIP (ZTR/IRT-related proteins), and NRAMP (natural resistance-associated macrophage protein; DalCorso *et al.*, 2013). Loss and defects in the transport of essential metal ions lead to severe growth phenotypes. For instance, mutations in either FRO2, the root ferric chelate reductase, or IRT1, the main Fe uptake transporter, cause severe Fe deficiency symptoms in *Arabidopsis* mutant plants (Curie and Briat, 2003). The *Arabidopsis* COPT1 copper transporter was shown to be essential for Cu uptake and targeted distribution, as the *35S:COPT1* antisense transgenic seedlings take up less Cu than wild-type plants and the mature leaf Cu content is lower. Furthermore, *COPT1* antisense plants exhibit root and pollen development defects that are specifically reversed by copper (Sancenón *et al.*, 2004). In plants, NRAMP transporters are expressed in roots and are involved in the Mn, Zn, Cu, Fe, Cd, Ni and Co transport across the plasma membrane and the tonoplast (Krämer *et al.*, 2007). The *Arabidopsis* NRAMP1 transporter, induced by Fe and/or Mn starvation, was shown to be essential for growth under low Fe or Mn conditions. Plants overexpressing *NRAMP1* are more resistant to toxic Fe concentrations than wild type (Cailliatte *et al.*, 2010; DalCorso *et al.*, 2013).

The root-to-shoot transport of metals occurs via xylem and involves several types of translocation proteins, including members of the large P-type ATPases ion transporter family (Rosenzweig, 2002). In *Arabidopsis*, there are eight heavy metal-associated P-type ATPases, also called HMA proteins, which are redundantly involved in the cytosolic efflux and root-to-shoot translocation of a variety of ions, such as Zn, Cd and Cu (DalCorso *et al.*, 2013). Double mutant *Arabidopsis* plants of the Zn transporters HMA2 and HMA4 exhibited pronounced nutritional deficiency phenotype, including chlorosis in leaves of reduced size, impaired inflorescence development and infertility (Hussain *et al.*, 2004). Another two HMA transporters, HMA6 and HMA8, located in the inner chloroplast envelope and in the thylakoid membrane, respectively, have been shown to be required for copper delivery in *Arabidopsis* chloroplasts (Abdel-Ghany *et al.*, 2005).

Metal ions are also translocated through the phloem following the source-to-sink route for redistribution within the shoot and for accumulation in fruits and seeds (DalCorso *et al.*, 2013).

Members of the above-mentioned metal transporter families, together with further described heavy metal transport proteins belonging to the cation diffusion facilitator (CDF) family, the vacuolar iron transporter (VIT) family, and the cation exchange (CAX) family, govern the cellular metal homeostasis, which is achieved by partitioning the heavy metals to chloroplast, mitochondria, vesicles and the Golgi complex and vacuole (Bashir *et al.*, 2016).
It has been reported that the cellular distribution of the metal transporters affects both metal localization and remobilization. For instance, the knockdown of the *VACUOLAR IRON TRANSPORTER 2* (*VIT2*) and *MITOCHONDRIAL IRON TRANSPORTER (MIT)* genes in *Oryza sativa* affected cellular iron trafficking, as deduced from the increased iron accumulation in *vit2* mutant seeds, whereas *mit* knockdown seeds exhibited decreased iron accumulation and elevated *VIT2* expression (Bashir *et al.*, 2013). Another iron remobilization study showed that in *Arabidopsis* seeds, most iron was stored in the vacuoles of cells surrounding the vasculature of the embryo and that NRAMP3 and NRAMP4 function redundantly to retrieve Fe from vacuoles during germination. The development of the *nramp3 nramp4* double mutant is arrested because of impaired iron mobilization, particularly in low-iron growth conditions. However, this phenotype was suppressed by mutations in the *VIT1* gene, encoding an iron vacuolar influx carrier, suggesting a functional link between iron loading in vacuoles by VIT1 and its remobilization by NRAMP3 and NRAMP4 transporters (Mary *et al.*, 2015).

1.4.2 Plant response to heavy metal stress

The production of reactive oxygen species (ROS) is a general response and an important signaling component under many stresses, including heavy metal stress (Dutta *et al.*, 2018). The most common physiological impact of heavy metal stress to plants is growth retardation, accompanied by changes in plant morphology and anatomy and in various physiological processes, ranging from photosynthesis to metabolism (Wani *et al.*, 2018). One of the most accessible traits to analyze plant response to metal stress is however the root system architecture, as many stresses have adverse effects on the primary root growth (Hamim *et al.*, 2018). Although the inhibition of primary root growth is a general response, the mechanistic effects and responses vary at the cellular level. For instance, copper toxicity causes membrane damage as a consequence of cell membrane lipid peroxidation, thus reducing the root activity (Liu *et al.*, 2014). Cadmium toxicity causes reduction in the diameter of the root and changes in cell shape (Lux *et al.*, 2011). It was also showed that cadmium toxicity distorts the structure and function of the cytoskeleton microtubules in the root cells of *Glycine max* (Gzyl *et al.*, 2015). Metal toxicity can also indirectly affect root growth, for instance by disrupting the hormonal balance or inducing changes in the expression of the responsive genes at the transcriptional level (Dutta *et al.*, 2018). Analysis of root growth and organization of *Arabidopsis* seedlings exposed to elevated cadmium levels revealed that the reduction in

root length was related to a misexpression of SCR transcription factor, which is known to modulate the interplay between auxin and cytokinin to control RAM maintenance and activity (Bruno *et al.*, 2017).

Plants have evolved various strategies to alleviate the harmful effects of heavy metal-induced ion toxicity. The most relevant strategy is to restrict the uptake of heavy metals, for instance by association with mycorrhizal fungi, which have the ability to retain heavy metals and thus restrict metal availability and absorption by the host roots (Schutzendübel and Polle, 2002). Another strategy employed is the cellular exclusion of metal ions, as many metal ions have been found in the root apoplastic space, where they also have been shown to undergo complexation with cell wall and root exudates (Viehweger, 2014; Wani *et al.*, 2018; Hall, 2002). Further studies of the root growth responses to heavy metal in excess demonstrated that plants cope with metal toxicity by modulating the symplasmic communication, mainly by decreasing the molecular movement through PD (O'Lexy *et al.*, 2018). However, the closure of PD upon exposure to heavy metal stress is not a universal response, as *Arabidopsi*s seedlings exposed to excess iron and copper display distinct responses. Growth under iron excess inhibits the primary root growth and decreases PD permeability, whereas excess of copper increased movement through PD, but does not alter the cellular integrity and normal root growth (O'Lexy *et al.*, 2018). In a previous study, it has been shown that *Arabidopsis* seedlings grown hydroponically in excess of copper retained copper in the root, whereas the copper accumulation in shoot tissues was reduced (Lequeux *et al.*, 2010), suggesting that there was little copper translocation into the shoot. These findings indicate that sequestration of copper in root tissue may be the major mechanism for detoxification of copper in *Arabidopsis thaliana* (O'Lexy *et al.*, 2018).

There are also plants able to grow on metal-rich soils, including *Arabidopsis helleri*, that possess effective metal acquisition and metal homeostasis systems and accumulate metals to concentrations up to four orders of magnitude higher than "normal" plants (Krämer, 2010). Metal hyperaccumulating is mainly achieved due to an enhanced metal chelator concentration, tissue-specific expression of proteins and overexpression of transport systems required for enhanced sequestration (Viehweger, 2014). Profiling of metal homeostasis gene transcripts indicated that the expression of genes known for their involvement in cellular metal uptake or detoxification is considerably increased in *Arabidopsis halleri* as compared to its close relative, non-accumulator *Arabidopsis thaliana* (Becher *et al.*, 2004).

1.5 Objectives of the thesis

In a previous research, several CKX-interacting proteins have been identified, which belong to two distinct phylogenetic clusters of a largely uncharacterized plant-specific HIPP protein family. Cluster I-HIPP proteins have been studied in detail, demonstrating their function in regulating the CKX1 stability via the ERAD pathway (Guo, 2019).

The aim of the present work was to characterize the CKX-interacting HIPP proteins from cluster III on the molecular and cellular level and to shed light on their biological functions.

In order to investigate the roles of individual *HIPP* genes during plant development, GUS reporter lines were generated, and their expression patterns analyzed. To shed light on the molecular functions of HIPP proteins, the subcellular localization of individual HIPP proteins was investigated and the biochemical properties were explored. Furthermore, the original protein-protein interaction between CKX1 and HIPPs has been tested *in vivo*.

The main focus of this study was the establishment and the molecular characterization of *hipp* loss-of-function *Arabidopsis* mutants. In order to determine if the closely related *HIPP* genes share overlapping functions, double and triple mutants were generated, either by genetic crosses or by employing the CRSIPR/Cas9-based gene editing technique. Single and higher order *hipp* mutants were morphologically analyzed to identify developmental and physiological processes controlled by the *HIPP* genes. Furthermore, to gain insight into the genetic and molecular pathways underlying the function of *HIPP* genes, transcriptional profiling, and differential gene expression analysis in *hipp* mutants by RNA-Seq were performed. Gain-of-function analysis was performed by exemplarily expressing one of the cluster-III members.

To investigate whether cluster-III HIPPs are involved in modulating cytokinin signaling responses and activity, a series of experiments were performed, such as cytokinin sensitivity assays or assessing the cytokinin activity using the synthetic cytokinin reporter *TCSn:GFP* in the *hipp* mutants. In addition, a transcriptomic approach was employed, to determine whether *HIPP* genes play a role in the transcriptional responses to cytokinin.

To dissect the possible biological functions of HIPP proteins in the context of their localization at PD, their influence on the symplasmic transport through PD has been explored, employing different experimental techniques, *e.g.* CFDA loading assays, analysis of the mobile phloem marker *pSUC2:GFP* in *hipp* mutants.

Given the metallochaperone-like features of the HIPP proteins, the possible involvement of the cluster-III HIPP proteins in heavy-metal stress responses was also investigated.

2. Material and methods

2.1 Chemicals and consumables

All laboratory chemicals and solvents used for the analytical procedures within the framework of this doctoral study were purchased, unless otherwise stated, from AppliChem (Darmstadt, DE), Bioline (London, UK), Bio-Rad (Munich, DE), Carl Roth (Karlsruhe, DE) ChromoTek (Planegg-Martinsried, DE), Clontech (California, US), Duchefa (Haarlem, NL), Fluka (Buchs, CH), Merck (Darmstadt, DE), Qiagen (Hilden, DE), Roche (Mannheim, DE), Roth (Karlsruhe, DE), Sarstedt (Nümbrecht, DE) and Sigma-Aldrich (Munich, DE).

2.2 Databases and software

The databases, online tools and software used within the framework of this study are listed in Table 1.

Table 1. Databases, online tools, and software.

Name	Manufacturer and/or reference	Purpose of use
Arabidopsis eFP Browser 2.0	Winter *et al.*, 2007	*In silico* gene expression analysis
AxioVision Rel. 4.6	AxioVision Rel. 4.6	Image acquisition
Bio-Rad CFX Manager 3.1	Bio-Rad Laboratories	qRT-PCR
Chromas 2.6.6	Technelysium Pty Ltd	DNA sequence analysis
ClustalW2	https://www.ebi.ac.uk/Tools/msa/clustalw2/	Multiple sequence alignment
CRISPR-P 1.0	Lei *et al.*, 2014	sgRNA design (CRISPR cloning)
DAVID 6.8	Huang *et al.*, 2009	GO enrichment analysis
DOG2.0	Ren *et al.*, 2009b	Visualisation of protein domain structures
Double Digest Calculator	Thermo Fisher Scientific	Selection of restriction enzymes
EndNote	Thomson Reuters	References management
g:Profiler	Reimand *et al.*, 2007	KEGG pathway analysis
GeneCapture 7.12	VWR	Agarose gel documentation
GIMP 2.10.12	https://gitlab.gnome.org/GNOME/gimp	Image processing
ImageJ	Abràmoff *et al.*, 2004	Image analysis
Inkscape 0.92	https://inkscape.org/es/	Image processing rescaling
JMP Pro 14	SAS Institute	Statistical analysis
LAS AF Lite 2.6.0 LAS AF WPF 4.0	Leica Microsystems	Confocal microscopy and fluorescence quantification
NetPrimer	PREMIER Biosoft	Primer quality assessment
Microsoft Office Package Tools 2010	Microsoft	Generation and processing of text, graphs, and figures
NASC	The European *Arabidopsis* Stock Centre (http://arabidopsis.info/)	Ordering *Arabidopsis* seeds

Table 1. Databases, online tools and software (continued).

Name	Manufacturer and/or reference	Purpose of use
NCBI	The National Center for Biotechnology (http://ncbi.nlm.nih.gov/)	Literature research (PubMed) and primer design (BLAST)
Primer3Plus	Untergasser *et al.*, 2007	Primer design for cloning and genotyping
Restriction mapper	http://www.restrictionmapper.org/	Selection of restriction enzymes
R version 3.6.1	https://www.r-project.org/	RNA-Seq data analysis
Olympus cellSens	Olympus Life Science	Image acquisition
QuantPrime	Arvidsson *et al.*, 2008	Primer design for qRT-PCR
Serial Cloner 2.6.1	Molecular Biology software	*In silico* sequence analysis
SIGnAL	Salk Institute Genomic Analysis Laboratory	Search for *Arabidopsis* T-DNA insertion mutants
TAIR	The *Arabidopsis* Information Resource (http://arabidopsis.org)	Data retrieval
Venny 2.1.0	BioinfoGP Service	Generation of Venn diagrams

2.3 Enzymes, kits, DNA and protein ladders

The enzymes, kits, DNA and protein ladders used in this study are listed in Table 2.

Table 2. Enzymes, kits, DNA and protein ladders.

Name	Manufacturer and Cat. No.	Purpose of use
CloneJET PCR Cloning Kit	Thermo Fisher Scientific, Cat. No. K1231	Cloning
DNase I, RNase-free	Thermo Fisher Scientific, Cat. No. EN0521	DNase digestion during RNA isolation
Gateway® BP Clonase™ enzyme mix	Invitrogen/Thermo Fisher Scientific, Cat. No. 11789013	Cloning
Gateway® LR Clonase™ enzyme mix	Invitrogen/Thermo Fisher Scientific, Cat. No. 11791019	Cloning
GFP-Trap Agarose	ChromoTek, Cat. No. gta-10	Co-immunoprecipitation assay
FastAP Alkaline Phosphatase (1 U/µl)	Thermo Fisher Scientific, Cat. No. EF0651	DNA dephosphorylation
HyperLadder™ I	Bioline, Cat. No. BIO-33026	DNA gel electrophoresis
Immolase™ DNA Polymerase	Bioline, Cat. No. BIO-21047	qRT-PCR
T4 DNA Ligase (1 U/µL)	Thermo Fisher Scientific, Cat. No. 15224017	Ligation of DNA fragments
NucleoSpin Gel and PCR Clean-up	Machery-Nagel, Cat. No. 740609.250	DNA extraction from agarose gel or PCR
NucleoSpin Plasmid EasyPure	Machery-Nagel, Cat. No. 740727.250	Plasmid isolation from *E. coli*
Pierce™ BCA Protein Assay Kit	Pierce Biotechnology, Cat. No. 23225	BCA protein assay

Table 2. Enzymes, kits, DNA and protein ladders (continued).

Name	Manufacturer and Cat. No.	Purpose of use
Phusion High-Fidelity DNA Polymerase	Thermo Fisher Scientific, Cat. No. F530S	PCR (cloning)
PageRuler™ Prestained Protein Ladder	Thermo Fisher Scientific, Cat. No. 26616	SDS-PAGE electrophoresis
QuikChange™ Site-Directed Mutagenesis	Stratagene, Cat. No. 200518	Site-directed mutagenesis
Restriction enzymes	Thermo Fisher Scientific	Restriction digestion for cloning and genotyping
RNase-Free DNase Set	Qiagen, Cat. No. 79254	DNase digestion during RNA isolation
RNeasy Plant Mini Kit	Qiagen, Cat. No. 74904	RNA extraction
SuperScript® III Reverse Transcriptase	Invitrogen/Thermo Fisher Scientific, Cat. No. 18080-044	cDNA synthesis
SuperSignal™ West Pico PLUS Chemiluminescent Substrate	Thermo Fisher Scientific, Cat. No. 34577	Immunodetection of proteins
Taq DNA Polymerase	AG Schuster, Institute of Biology/Applied Genetics, FU Berlin	PCR (genotyping, sequencing)
Wizard® Genomic DNA Purification Kit	Promega, Cat. No. A1120	DNA purification during cloning

2.4 Cloning vectors

The cloning vectors used and generated in this work are listed in Table 3.

Table 3. List of plasmids.

Name	Selection marker in bacteria	Selection marker in plants	References
pB7FW2.0-PDLP1-RFP	$Spec^R$	$Basta^R$	Thomas *et al.*, 2008
pCB308-pHIPP34:GUS	Kan^R	$Basta^R$	Dr. H. Weber (unpublished)
pDOE-08-CKX1	Kan^R	$Basta^R$	Niemann *et al.*, 2018
pDOE-08-CKX1/HIPP32	Kan^R	$Basta^R$	This study
pDOE-08-CKX1/HIPP34	Kan^R	$Basta^R$	This study
pDONR™221	Kan^R, Cm^R	-	Invitrogen/Thermo Fisher Scientific
pDONR™221-HIPP34	Kan^R	-	Dr. H. Weber (unpublished)
pDONR™222	Kan^R, Cm^R	-	Invitrogen/Thermo Fisher Scientific
pDONR™222-pHIPP32	Kan^R, Cm^R	-	This study
pDONR™222-pHIPP33	Kan^R, Cm^R	-	This study
pBGWFS7	$Spec^R$, Cm^R	$Basta^R$	Karimi *et al.*, 2002
pBGWFS7-pHIPP32:GUS	$Spec^R$	$Basta^R$	This study
pBGWFS7-pHIPP33:GUS	$Spec^R$	$Basta^R$	This study
pB7FWG2	$Spec^R$, Cm^R	$Basta^R$	Karimi *et al.*, 2002
pB7FWG2-GFP-HIPP32	$Spec^R$, Cm^R	$Basta^R$	This study
pB7FWG2-GFP-HIPP33	$Spec^R$, Cm^R	$Basta^R$	This study
pGPTVII-CGL1-OFP	Kan^R	Hyg^R	Frank *et al.*, 2008

Table 3 List of plasmids (continued).

Name	Selection marker in bacteria	Selection marker in plants	References
pGWB18-myc-CKX1	Kan^R, Hyg^R	Kan^R, Hyg^R	Niemann *et al.*, 2015
pHEE401E	Kan^R, $Spec^R$	Hyg^R	Wang *et al.*, 2015
pHEE401E-sg32 (HIPP32)	Kan^R	Hyg^R	This study
pHEE401E-sg71 (HIPP32)	Kan^R	Hyg^R	This study
pJET	Amp^R	-	Invitrogen/Thermo Fisher Scientific
pJET-HIPP33	Amp^R	-	This study
pK7FWG2-GFP-HIPP34	$Spec^R$, Cm^R	Kan^R	Dr. H. Weber (unpublished)
pK7FWG2-GFP-HIPP34^{hma}	$Spec^R$, Cm^R	$Basta^R$	This study
pK7FWG2-GFP-HIPP34^{prenyl}	$Spec^R$, Cm^R	$Basta^R$	This study

2.5 Bacteria strains

The bacteria strains used in this work are listed in Table 4.

Table 4. Bacteria strains.

Specie	Strain	Genetic marker	References
Agrobacterium tumefaciens	C58C1 (pCH32)	pBin61-P19; Rif^R, Tet^R	Voinnet *et al.*, 2003
Agrobacterium tumefaciens	GV3101	pMP90 (pTiC58ΔT-DNA); Rif^R, $Gent^R$	Koncz and Schell, 1986
Escherichia coli	DB3.1	F^- *gyrA462 endA1 glnV44* Δ(*sr1-recA*) *mcrB mrr hsdS20*(r_B^-, m_B^-) *ara14 galK2 lacY1 proA2 rpsL20*(Sm^r) *xyl5* Δ*leu mtl1*	Bernard and Couturier, 1992
Escherichia coli	DH5α	F^- Φ80d*lacZ*ΔM15 Δ(*lacZYA-argF*)-U169 *endA1 recA1 glnV44 thi-1 relA1 gyrA96 deoR nupG hsdR17* (r_K^-, m_K^+) λ^-	Grant *et al.*, 1990
Escherichia coli	TOP10	F^- *mcr*A Δ(*mrr-hsd*RMS-*mcr*BC) φ80*lac*ZΔM15 Δ*lac*X74 *rec*A1 *ara*D139 Δ(*ara-leu*)7697 *gal*U *gal*K λ^- *rps*L(Str^R) *end*A1 *nup*G	Invitrogen/Thermo Fisher Scientific

The *Escherichia coli* strains DH5α and TOP10 were used for the replication of most vectors during cloning, with the exception of the Gateway® empty vectors, which required the use of the DB3.1 strain due to the toxicity of the ccdB gene product. The *Agrobacterium tumefaciens* strain GV3101 was used for stable transformation of *Arabidopsis thaliana* and for the transient protein expression in *Nicotiana benthamiana*. The strain C58C1 (pCH32) was also used for the transient expression in *N. benthamiana* leaves in order to express the p19 protein, a suppressor of gene-silencing (Voinnet *et al.*, 2003).

2.6 Growth conditions for bacteria

E. coli and *A. tumefaciens* strains were grown in liquid or on solid Luria Broth (LB) media (10 g/L tryptone, 5 g/L yeast extract, 5 g/L NaCl and 15 g/L agar for solid LB-medium, pH 7.5; Bertani, 1951), supplemented with the adequate antibiotics.

SOC medium (20 g/L tryptone, 5 g/L yeast extract, 10 mM NaCl, 2.5 mM KCl, 10 mM MgCl2, 10 mM MgSO4, and 20 mM glucose) was used for growth of *E. coli* and *A. tumefaciens* immediately after transformation.

For the propagation of *A. tumefaciens* cells used for *Arabidopsis* transformation liquid YEBS medium (1 g/L yeast extract, 5 g/L beef extract, 5 g/L sucrose, 5 g/L bacto peptone, 0.5 g/L MgSO4, pH 7.0; Davis *et al.*, 2009) was used.

E. coli strains were grown overnight at 37 °C and *A. tumefaciens* at 28 °C for 2 days.

The antibiotics used for the selection of transformed bacterial cells and the concentration used in the medium are listed in Table 5.

Table 5. Antibiotics used for selection of bacterial cells.

Antibiotic	Stock solution	Final concentration in medium
Ampicillin (Amp)*	100 mg/ml; in ddH_2O	100 µg/ml
Carbenicillin (Carb)*	50 mg/ml; in ddH_2O	50 µg/ml
Chloramphenicol (Cm)	34 mg/ml; in 100 % EtOH	34 µg/ml
Gentamycin (Gent)*	25 mg/ml; in ddH_2O	25 µg/ml
Kanamycin (Kan)*	50 mg/ml; in ddH_2O	50 µg/ml
Rifampicin (Rif)	50 mg/ml; in DMSO	50µg/ml
Spectinomycin (Spec)*	50 mg/ml; in ddH_2O	50 µg/ml

The antibiotic stock solutions were filter-sterilized or remained unsterile, and stored at - 20 °C. The antibiotics were added to the sterile autoclaved medium before use, at the concentrations indicated in Table 5.

2.7 Preparation of cryo-conserved bacterial cultures

To prepare cryo-conserved cultures of *E. coli* or *A. tumefaciens* for a long-term storage of plasmids, a 10 ml culture (LB medium with appropriate antibiotics) was inoculated with a colony and incubated overnight at 37 °C or 28 °C respectively with shaking. 1 ml of this culture was mixed with 600 µl 70 % (w/v) glycerol, snap-frozen in liquid nitrogen and stored at -80 °C.

2.8 Plants

Within the framework of this study, *N. benthamiana* wild-type plants were used for transient protein expression assays. If not stated otherwise *Arabidopsis thaliana* ecotype Columbia-0 (Col-0) was used as the wild type in this study. In Table 6 are listed all mutant and transgenic *Arabidopsis* plants that were used throughout this work.

Table 6. Mutant and transgenic *Arabidopsis* plants.

Name[1)]	NASC identification number	Reference
35S:At5g24010-RFP	-	Fernandez-Calvino *et al.*, 2011
35S:At5g24010-RFP 35S:GFP-HIPP34	-	This study
35S:GFP-HIPP34[3)]	-	Dr. H. Weber/This study
hipp32-1	SALK_017337	This study
hipp32-2 (hipp32) [2)]	SAIL_273_B10	This study
hipp32-3	-	This study
hipp33-1	SAIL_1235_G02	This study
hipp33-2 (hipp33) [2)]	SAIL_899_D10C1	This study
hipp34-1	SALK_079319C	This study
hipp34-2 (hipp34) [2)]	WiscDsLox248H10	This study
hipp32-2,hipp33-2 (hipp32,33)	-	This study
hipp32-3,hipp34-2 (hipp32,34)	-	This study
hipp32-3,hipp33-2, hipp34-2 (hipp32,33,34)	-	This study
hipp33-2,hipp34-2 (hipp33,34)	-	This study
pHIPP32:GUS	-	This study
pHIPP33:GUS	-	This study
pHIPP34:GUS[4)]	-	Dr. H. Weber
pSUC2:GFP	-	Truernit and Sauer, 1995
pSUC2:GFP hipp32	-	This study
pSUC2:GFP hipp33	-	This study
pSUC2:GFP hipp34	-	This study
pSUC2:GFP hipp32,33	-	This study
pSUC2:GFP hipp33,34	-	This study
pSUC2:GFP hipp32,34	-	This study
TCSn:GFP	-	Zürcher *et al.*, 2013
TCSn:GFP hipp32	-	This study
TCSn:GFP hipp33	-	This study
TCSn:GFP hipp34	-	This study
TCSn:GFP hipp32,33	-	This study
TCSn:GFP hipp33,34	-	This study
TCSn:GFP hipp32,34	-	This study
TCSn:GFP hipp32,33,34	-	This study

[1)] In parentheses are mentioned the names used throughout this thesis.
[2)] These lines were used for crosses with *TCSn:GFP* and *pSUC2:GFP* lines
[3)] The transformation of *Arabidopsis* with *35S:GFP-HIPP34* was conducted by Dr. H. Weber. The selection of *35S:GFP-HIPP34* homozygous lines was part of this study.
[4)] The selection of *pHIPP43:GUS* homozygous lines was conducted by Dr. H. Weber.

2.9 Growth conditions for plants

For most of the, *Arabidopsis* plants were grown under standard, long day (LD) conditions (light/dark:16 h/8 h)*, in vitro* cultures or on soil, in the greenhouse. For flowering experiments, *Arabidopsis* plants were grown on soil under short day (SD) conditions (light/dark:8 h/16 h) in a phytochamber at 22 °C and light intensities of 120 - 170 µmol m^{-2} s^{-1}.

N. benthamiana plants were grown in the greenhouse at 24 °C (light/dark:14 h/10 h).

2.9.1 *In vitro* culture

For growth of *Arabidopsi*s seedlings *in vitro* cultures, seeds were surface-sterilized by soaking and shaking for 5 min in 70% ethanol containing 0.01% (v/v) Triton X-100. Afterwards, seeds were rinsed twice with 70% ethanol under clean bench (semi-sterile) and finally transferred by pipetting onto a sterile filter paper in a Petri dish. Using sterile toothpicks, the dried seeds were transferred onto solid Murashige and Skoog (MS) medium (4.3 g/L MS basal salt mixture, 0.5 g/L MES, 1 g/L sucrose and 10 g/L agar for solid medium, pH 5.7; Murashige and Skoog, 1962). After stratification for two days in dark at 4 °C, the Petri plates were transferred to a climate chamber and cultivated under long day conditions (see also section 2.9).
The antibiotics used for the selection of *Arabidopsis* plants and the concentration used in the medium are listed in Table 7.

Table 7. Antibiotics used for selection of bacterial cells.

Antibiotic	Stock solution	Final concentration in medium
Hygromycin (Hyg)	50 mg/ml; in ddH_2O	15 µg/ml
Kanamycin (Kan)	50 mg/ml; in ddH_2O	30 µg/ml
Phosphinothricin (PPT)	10 mg/ml; in 100 % EtOH	10 µg/ml

The antibiotic stock solutions were filter-sterilised or remained unsterile and stored at -20 °C. The antibiotics were added to the sterile autoclaved medium before use, at the concentrations indicated in Table 7.

2.9.2 Growth on soil

Arabidopsis seeds were sown on thoroughly watered “sowing soil” (2:2:1, soil type P:soil type T:sand), stratified at 4 °C for two days, and then transferred to the greenhouse (LD) or the phytochamber (SD). For the first two days the plant trays were covered with a clear plastic hood to protect seeds and germinating seedlings from desiccation. 10 to 12 days after germination, seedlings were singled onto ‘growing’ soil (2:2:1, soil type P:soil type T: Perligran G) and were further grown in LD or SD light conditions (see also section 2.9).
The selection of *Arabidopsis* plants on soil was carried out by spraying the seedlings with 0.1 % (v/v) Basta (Bayer, Leverkusen, DE).

2.10 Genetic crosses

To perform crosses between *Arabidopsis* plants, the female parent was prepared under the binocular one day in advance. Two to three flower buds were selected, in which the tips of the petals were barely visible and before the anthers began to release pollen. Siliques, leaves, younger flower buds, and open flowers in the immediate proximity as well as all six stamens on the selected flower buds were removed using a small pair of scissors and precision

clamping tweezers, respectively. It was ensured that no pollen has been deposited on the stigma and that the pistil was fully intact. The following day, the male flowers were selected with anthers that were dehiscent. The complete flower was removed by squeezing near the pedicel with a pair of tweezers. The female parent was pollinated by taking the fully open flower of the male parent and brushing the anthers over the bare stigma of the female parent. It was ensured that the stigma was covered with pollen. Crosses were successful when siliques started elongating after two to three days. Seeds from the respective siliques were harvested and used for propagation and for assessing gamete fertility.

2.11 Transformation techniques

2.11.1 Bacteria transformation

For transformation of *E. coli* cells with plasmid DNA, chemically competent cells were used. 50 - 200 ng plasmid DNA was mixed with 200 µl of competent cells (previously thawed on ice) and incubated for 20 minutes on ice. After incubation, cells were heat-shocked in at 42 °C thermo mixer for 30 sec and then kept on ice for 2 min. Afterwards, 800 µl of SOC medium (see section 2.6) was added to the cell suspension and this was incubated at 37 °C for 45 min with shaking at 225 - 250 rpm. The cell suspension was spread on LB agar plates containing the appropriate antibiotic and incubated overnight at 37 °C.

Transformation of *A. tumefaciens* cells with plasmid DNA was performed by electroporation. For this, 50 µl of electrocompetent cells were gently mixed with 50 - 150 ng of plasmid DNA (1 - 2 µl) and incubated on ice for 2 min. After incubation, the mixture was transferred into a pre-cooled electroporation cuvette and an electric pulse (200 Ω, 1.8 kV, 2.5 to 5 ms) was applied using the Genepulser II (Bio-Rad, Munich, DE). Immediately after the electroporation, 900 µl of SOC medium (see section 2.6) was added to the cell suspension. The mixture was transferred into a 1.5 ml reaction tube, incubated at 28 °C on a shaker for 2 h and subsequently plated on selection medium and incubated at 28 °C for two days.

2.11.2 Stable transformation of *Arabidopsis thaliana*

Transgenic *Arabidopsis* plants were obtained by *Agrobacterium*-mediated transformation using the floral dip method (Clough and Bent, 1998). A single colony of *A. tumefaciens* carrying the desired binary vector was inoculated into 4 ml of LB medium containing selective antibiotics and grown as starting culture at 28 °C for two days. 1 ml of this culture was then added into 250 ml LB selection media and grown for another 24 h at 28 °C with shaking. Bacteria were centrifuged at 5,500 × g for 20 min at RT and resuspended in 250 ml infiltration medium (50 g/L sucrose, 2.19 g/L MS salts, 50 µl/L Silwet 77). Inflorescences of 4-week-old plants were dipped into the *A. tumefaciens* suspension for 30 seconds, under gentle agitation. Dipped plants were then sealed in a plastic bag for 24 hours to maintain high humidity and then

transferred to the greenhouse. Primary transformants were selected using appropriate antibiotics or herbicides.

2.11.3 Agroinfiltration of *N. benthamiana* for transient expression of proteins

For the transient expression of proteins in *N. benthamiana* leaves, the *Agrobacterium*-mediated infiltration technique was used (Sparkes *et al.*, 2006). A single colony of *A. tumefaciens* harboring the desired expression vector was inoculated into 2 ml LB medium containing the corresponding antibiotics and grown overnight at 37 °C with shaking. The culture was centrifuged at 835 g for 10 min and the cell pellet was resuspended in 1 ml freshly prepared infiltration buffer (0.5% glucose, 50 mM MES, 10 mM $MgCl_2$, 100 µM acetosyringone (in DMSO). The cells were centrifuged again for 10 minutes to wash away the remaining antibiotics and resuspended in 1 ml of infiltration buffer. The constructs that were to be co-transformed were diluted together in infiltration medium to a final OD_{600} of 0.1 for each construct. Additionally, agrobacteria carrying the 35S:p19 construct was permanently co-infiltrated, in order to suppress the post-transcriptional gene silencing (Voinnet *et al.*, 2003). Infiltration was performed using 6-week-old *N. benthamiana* plants. The abaxial leaf side was slightly injured with a yellow pipette tip and the agrobacteria suspension was pressed into the leaf with a syringe. The plants were placed in the greenhouse until further analysis.

2.12 General nucleic acid methods

2.12.1 Extraction of plasmid DNA from bacteria

For the isolation of plasmid DNA from *E. coli* cells, 4 ml LB liquid medium containing the appropriate antibiotics (Table 7) was inoculated with a bacterial colony and incubated overnight at 37 °C with shaking (180 rpm). The plasmid isolation was performed according to the manufacturer's instructions, using the NucleoSpin Plasmid EasyPure kit (Machery-Nagel). Plasmid DNA concentration was determined using a spectrophotometer (NanoDrop ND-1000, PEQLAB, Erlangen, DE) at 260 nm, where $E_{260} = 1$ corresponds to an amount of 50 ng dsDNA per µl.

2.12.2 Extraction of genomic DNA from *Arabidopsis*

Plant material was snap-frozen in liquid nitrogen in 1.5 ml microcentrifuge tubes containing two steel beads and ground in adapters using a Retsch mill (Retsch Mixer Mill MM2000). 400 µL of the extraction buffer (200 mM Tris/HCl pH 7.5, 250 mM NaCl, 25 mM EDTA, 0.5 % SDS) was added to the plant powder and the mixture was vigorously vortexed. The sample was centrifuged in a microcentrifuge for 3 min at 13,000 rpm and 300 µl of the supernatant was transferred into a fresh 1.5 mL-microcentrifuge tube. 300 µl of isopropyl alcohol were added, the sample was vortexed, incubated at RT for at least 2 min, and then centrifuged again (5 min; 10,000 rpm). The supernatant was discarded and the pellet washed with 300 µl 70 %

ethanol. After another centrifugation step (5 min; 10,000 rpm) the supernatant was discarded and the pellet dried at 50 °C. 100 µl ddH_2O were added to the dried pellet, vigorously vortexed and incubated for 10 min at RT. The samples were kept overnight at 4 °C and then used for PCR analysis.

2.12.3 Isolation and purification of total RNA from *Arabidopsis*

The total RNA was extracted from plant tissue using a modified TRIzol method (Chomczynski and Sacchi, 1987). Approximately 200 mg of plant material was collected in a 2-ml microcentrifuge tube containing two steel beads and snap-frozen in liquid nitrogen. The plant material was ground using a Retsch mill (Retsch Mixer Mill MM2000). Afterwards, 1 ml of TRIzol reagent (38% phenol, 800 mM guanidinium thiocyanate, 400 mM ammonium thiocyanate, 100 mM sodium acetate pH 5, 5% glycerol) was added and the sample was vortexed until it thawed and homogenized. The cell debris was centrifuged at 13,200 rpm and 4 °C for five minutes and the supernatant was transferred to a new 2-ml microcentrifuge tube. Then 400 µl chloroform/isoamyl alcohol (24:1) was added and the sample was vortexed, incubated for five minutes at room temperature and finally centrifuged for 15 minutes at 13,200 rpm and 4 °C. After centrifugation, 700 µl of the upper aqueous phase were transferred to a new 1.5-ml microcentrifuge tube and the RNA was precipitated at room temperature for ten minutes by adding 350 µl isopropanol and 350 µl high salt solution (1.2 M sodium chloride, 800 mM sodium citrate). The samples were centrifuged for ten minutes at 13,200 rpm and 4 °C. The pellet was washed with 900 ul 70% ethanol, centrifuged for five minutes at 13,200 rpm and 4 °C and dried. The RNA was dissolved in 100 µl RNase-free ddH_2O at 60 °C for 5 min.
In order to determine the quality of the isolated RNA, 1 µl of the RNA solution was separated by gel electrophoresis in a 1% agarose gel and analyzed for the presence of distinct rRNA bands.
For the RNA-sequencing experiments (section 2.17.8), the total RNA was isolated according to the manufacturer's instructions, using the RNeasy Plant Mini Kit (Qiagen) and RNase-Free DNase Set (Qiagen). Total RNA concentration was determined using a spectrophotometer (NanoDrop ND-1000, PEQLAB, Erlangen, DE) at 260 nm, where $E_{260} = 1$ corresponds to an amount of 40 ng RNA per µl.

2.12.4 Standard polymerase chain reactions (PCR)

Standard PCR (Mullis and Faloona, 1987) was performed to genotype *Arabidopsis* plants, to amplify DNA fragments during cloning or sequencing, and to analyze bacterial colonies.
For genotyping, colony PCR and sequencing, a *Taq* polymerase (Table 2) and a 10x *Taq* PCR reaction buffer (160 mM $(NH_4)_2SO_4$, 0.1% (v/v) Tween 20, 20 mM $MgCl_2$, 670 mM Tris/HCl pH 8.8, in ddH_2O) were used. The composition of a typical *Taq* PCR reaction mixture (20 µl) is shown in Table 8.

Table 8. *Taq*-PCR reaction mixture.

Component	Volume (µl)	Final concentration
10x *Taq* PCR buffer	2	1x
20 mM dNTPs	0.5	0.5 mM
10 µM 5'-Primer	1	5 µM
10 µM 3'-Primer	1	5 µM
Taq polymerase	0.5	
Template-DNA*	0.5 - 2	
ddH_2O	to 20 µl	

* For colony PCR, a single colony was picked with a toothpick and dissolved in 5 µl ddH_20, from this 2 µl were used for the PCR reaction mixture. For PCR based on the supernatant of a bacterial culture, 2 µl of the supernatant was used as PCR template.

For DNA amplification for cloning purposes, the *Phusion* high-fidelity DNA polymerase (Thermo Fisher Scientific) with proofreading activity (3 '→ 5' exonuclease activity) was used. The composition of a typical *Phusion* PCR reaction mixture (20 µl) is shown in Table 9.

Table 9. *Phusion*-PCR reaction mixture.

Component	Volume (µl)	Final concentration
5x *Phusion* HF-Puffer	4	1x
50 mM $MgCl_2$	0.2	0.5 mM
20 mM dNTPs	0.4	0.4 mM
10 µM 5'-Primer	0.5	2.5 µM
10 µM 3'-Primer	0.5	2.5 µM
Phusion polymerase	0.2	0.02 U/µl
Template-DNA	0.5 - 2	
ddH_2O	to 20 µl	

PCR reactions were carried out in the Thermocycler T-Gradient, T1, T3 or T Professional from Biometra (Göttingen, DE). PCR programs were adapted to the respective reactions, taking into consideration primer annealing temperature (optimal temperature for the attachment of the oligonucleotides to the DNA), elongation time and number of cycles. The typical PCR programs for *Taq* and *Phusion* PCR reaction are listed in Table 10.

Table 10. Standard PCR program.

PCR step[1)]	***Taq* PCR**	***Phusion* PCR**
1. Initial denaturation	95 °C, 2 min[2)]	95 °C, 1 min
2. Denaturation	95 °C, 30 sec	98 °C, 10 sec
3. Primer annealing	55 - 58 °C, 30 sec	5 - 60 °C, 30 sec
4. Elongation	72 °C, 1 kB/min	72 °C, 2 kB/min
5. Final elongation	72 °C, ~5 min[3)]	72 °C, 5 min
Pause	16 °C	16 °C

1) The steps 1 and 5 were completed only once, whereas the steps 2 to 4 were cyclically repeated between 30 to 34 times.

2) 10 min for colony and bacterial culture PCR reactions.

3) Double the time required for the amplicon elongation.

2.12.5 DNase I treatment

In order to remove DNA residues from the RNA solution, prior the reverse transcription (see 2.12.6), the isolated RNA (see 2.12.3) was treated with DNase I (Thermo Fisher Scientific), according to the manufacturer's instructions (Table 2)

2.12.6 Reverse transcription (cDNA synthesis)

The reverse transcription (RT) of RNA into cDNA (cDNA synthesis) was performed using the enzyme kit SuperScript® III Reverse Transcriptase (Table 2) enzyme kit. First, 1 µg of purified total RNA was mixed with 2 µl dNTPs (5 mM), 1 µl oligo(dT) primers (50 µM), 1.8 µl random hexamers (50 µM) and ddH_2O added to 14.5 µl and incubated for 5 min at 65 °C and then cooled down on ice (5 min). Afterwards, the 4 µl of 5x first strand buffer (50 mM Tris-Cl pH 8.3, 75 mM KCl, 3 mM $MgCl_2$), 1 µl DTT (0.1 M) and 0.5 µl SuperScript® III (200 U/µl) were added to the reaction mixture. The total volume of the reaction (20 µl) was adjusted with ddH_2O. The reaction was incubated for 5 min at 25 °C for primer attachment, 60 min at 50 °C for reverse transcription and 15 minutes at 70 °C for the deactivation of the enzyme. After the reaction was completed, the cDNA was diluted 1:10 and stored at -20 °C.

2.12.7 Semi-quantitative RT-PCR

The semi-quantitative RT-PCR was used to investigate whether in the isolated T-DNA insertion lines transcripts of the respective genes were formed. Standard *Taq* PCR reaction was performed (Table 8), using as template 2 µl cDNA reverse transcribed from RNA extracted from inflorescence and leaf tissues, and gene-specific primers spanning the T-DNA insertion sites, listed in Table 11. Per PCR reaction 25, 30 and 35 cycles were completed. The amplification of the housekeeping gene *ACTIN7* was included as control.

Table 11. Primer sequences for RT-PCR.

T-DNA insertion line*	Gene name and AGI number	Forward (F) and reverse (R) primer sequences (5'- 3')
hipp32-1, SALK_017337	*HIPP32*, AT3G05220	F-AATAAAGGTGGGGGCAAAAC R-TCCTCCTCCTTTGCTGTGTT
hipp32-2, SAIL_273_B10	*HIPP32,* AT3G05220	F-GTGGACCTAAGGGTCCCAAT R-CCAGCGCTCTTCTTCTCATC
hipp33-1, SAIL_1235_G02	*HIPP33,* AT5G19090	F-AGCTCCCAAGGGAGGATCTA R-AACTGCTGCATCTGTTGTGG
hipp33-2, SAIL_899_D10C1	*HIPP33,* AT5G19090	F-AGCTCCCAAGGGAGGATCTA R-AACTGCTGCATCTGTTGTGG
hipp34-1, SALK_079319C	*HIPP34,* AT3G06130	F-GGTGCACCACAGGGTTATTT R-TCGCAGCTTGATGTGTTCTC
hipp34-2, WiscDsLox248H10	*HIPP34,* AT3G06130	F-TCAAGAAGCTCGCCAAATCT R-AAGCTGCTGCAAATGTTGTG
PCR amplification control	*ACTIN7,* AT5G09810	F-TACAACGAGCTTCGTGTTGC R-TCCACATCTGTTGGAAGGTG

* Quantitative RT-PCR in each T-DNA insertion line was performed in comparison to wild-type as control.

2.12.8 Quantitative real-time PCR (qRT-PCR)

qRT-PCR analysis was performed with the Bio-Rad CFX96 REAL-TIME PCR Machine, using SYBR green I as DNA-binding dye and Immolase (Table 2) as hot-start DNA polymerase. The composition of one reaction mixture is listed in Table 12 and the program for qRT-PCR is showed in Table 13.

The primer pairs used for qRT-PCR were designed using the QuantPrime online tool (Table 1), considering an optimum Tm of 60 °C, GC content between 20 % and 80 % and an amplicon size of 60-150 bp. The primer specificity and quality were tested using BLASTN (TAIR) and NetPrimer (Table 1), respectively. Before being used in qRT-PCR reaction, the primer efficiency of the designed primer pairs was tested. For that, a cDNA mix (1:10 diluted) originating from wild-type plant RNA was prepared in 4 sequential dilution steps (1:2, 1:4, 1:8 and 1:16). These cDNA samples, along with the original sample (not diluted) were used in technical triplicates as template to test the primer efficiency using the standard qRT-PCR program (Table 12). Primer efficiency (E in %) was calculated as $E = 10^{-1/slope} \times 100$ plotting the logarithm of the dilutions on the X axis and the Ct values on the Y axis using the Bio-Rad CFX Manager software (Table 1). Primers were defined as suitable if the efficiency between 84 % and 110%. The qRT-PCR results were evaluated according to Vandesompele *et al.* (2002). Two housekeeping genes, *TFAII15* and *UBC10*, were used as reference genes for the normalization of the relative transcript abundance of each gene of interest (Vandesompele *et al.*, 2002). Primers used for qRT-PCR are listed in Table 14.

Table 12. Reaction mixture for qRT-PCR.

Component	Volume (µl)	Final concentration
10x Immolase buffer	2	1x
50 mM MgCl2	0.8	2 mM
5 mM dNTPs	0.4	100 µM
10x SYBR Green I	0.2	0.1x
50 µM forward primer	0.12	300 nM
50 µM reverse primer	0.12	300 nM
Immolase (5 U/µL)	0.04	0.01 U
cDNA (1:10)*	2	1:200
ddH_2O	to 20 µl	

* ddH_2O was used as no template control.

Table 13. qRT-PCR reaction program.

qRT-PCR step*	Run information
1. DNA polymerase heat activation	95 °C, 15 min
2. Denaturation	95 °C, 5 sec
3. Primer annealing	55 °C, 15 sec
4. Elongation	72 °C, 10 sec
5. Melt curve generation	60 °C to 95 °C, increment 0.5 °C

* The steps 1 and 5 were completed only once, whereas the steps 2 to 4 were cyclically repeated between 40 times.

Table 14. Primer sequences for qRT-PCR.

Target gene	AGI number	Forward (F) and reverse (R) primer sequences (5'- 3')
ARR5	AT3G48100	F-CTACTCGCAGCTAAAACGC R-GCCGAAAGAATCAGGACA
ARR6	AT5G62920	F-GAGCTCTCCGATGCAAAT R-GAAAAAGGCCATAGGGGT
ARR7	AT1G19050	F-CTTGGAACCAATCTGCTCTC R-ATCATCGACGGCAAGAAC
ARR15	AT1G74890	F-GAGAGGTGGTGAAGCTGAA R-GATGGAGTGTCGTCATCAAG
ARR16	AT2G40670	F-CCTGTAACGTTATGAAGGTGAGT R-GACTCCTTCACTTTCTTGAGTAG
HIPP32	AT3G05220	F-AGCTGTAGCTCATGGTGGCTAT R-TAAGGCCGAGCGTACATCATCG
HIPP33	AT5G19090	F-AAACGAACGGTTCCAGCCGATG R-TGCGGTTGTGGTGGCATATAGTTG
HIPP34	AT3G06130	F-ATGATGTACGCAAGGCCACCAC R-TCGGATATTGGTGCGGGTTTGG
TFAII15	AT4G31720	F-GAATCACGGCCAACAATC R-ACTCTTAGCCAAGTAGTGCTCC
UBC10	AT5G53300	F-CCATGGGCTAAATGGAAA R-TTCATTTGGTCCTGTCTTCAG

2.12.9 Agarose gel electrophoresis

Agarose gel electrophoresis was performed in order to separate DNA fragments by size, assess the quality of the extracted RNA (see section 2.13.3), purify of PCR products (see section 2.12.10), evaluate restriction digestion (see section 2.12.10), estimate the DNA concentration of gel-purified DNA fragments or plasmids during cloning. Prior to electrophoresis, the samples were mixed with 10x gel loading buffer (30 % glycerol, 0.25 % bromophenol blue, 0.25 % xylene cyanol) to reach 1x. Depending on the expected DNA size 0.8 - 2.0 % agarose dissolved in 1x TAE electrophoresis buffer, consisting of 40 mM Tris, 20 mM acetic acid, and 1 mM EDTA pH 8 was used. HyperLadder™ I (Table 2) was mostly used as molecular weight marker for DNA size determination. Depending on the gel size, the electrophoresis ran at 80 to 115 V, using a Bio-Rad basic power supply. For DNA or RNA visualization, ethidium bromide (0.3 µg/ml gel) was added to the gel prior solidification. The evaluation and documentation of the electrophoresis were performed using an ultraviolet (UV) transilluminator and the GeneCapture software (Table 1).

2.12.10 Purification of DNA fragments

Extraction of DNA fragments from agarose gel was performed using the NucleoSpin Gel and PCR Clean-up kit (Table 2), following the manufacturer's instructions. DNA concentration was

estimated from the band strength after the electrophoretic separation of 5 µl DNA solution on a 1% agarose gel, along with 2.5 µl HyperLadder™ I (Table 2), used as a quantitative standard.

2.12.11 Restriction digest

The online tool Restriction Mapper (Table 1) was used to find suitable enzymes for a desired restriction digestion reaction. In the case of restriction digests with several enzymes, the online tool Double Digest Calculator (Thermo Scientific) (Table 1) was consulted to determine the optimal conditions for a given reaction. The restriction enzymes were acquired from Thermo Scientific and the reactions were performed following the manufacturer's instructions. Serial Cloner (Table 1) was used to perform virtual digestion reactions. In case of a following ligation reaction (see section 2.12.13) the restriction digestion reaction was purified using the Wizard® Genomic DNA Purification kit (Table 2).

2.12.12 DNA dephosphorylation

To avoid self-ligation of DNA molecules purified for cloning purposes, either the insert or the backbone vector was dephosphorylated before ligation (see 2.12.13). The 5'-phosphate group was enzymatically cleaved by incubating the DNA mixture after the restriction digest with 1 µl FastAP Thermosensitive Alkaline Phosphatase (1 U/µl) for 10 minutes at 37 °C. The FastAP enzyme was deactivated by incubation at 75 °C for 5 minutes.

2.12.13 Ligation of DNA fragments

For the cloning of DNA constructs, DNA molecules were covalently linked in 20 µl ligation reaction using 1 µl of the enzyme T4 ligase (Table 2), 20 - 50 ng vector and 3- to 10-fold molar excess of insert. The ligation reaction was incubated overnight at room temperature.

2.12.14 Genotyping of plants

Mutant plants carrying T-DNA insertions were genotyped via PCR using two primer pairs. To amplify the mutant allele, the primer pair comprised of a gene- and a T-DNA-specific primer, binding to the left border of the T-DNA. To amplify the wild-type allele gene-specific primers flanking the insertion site were used. In Table 15 are listed all T-DNA insertion-specific primers used for PCR-genotyping. Table 16 contains all gene-specific primer pairs and further information about the primer pair combination used for detecting the respective mutant allele. For genotyping standard *Taq* PCR were performed (see section 2.12.4) with an annealing temperature of 56 °C.

Table 15. T-DNA insertion-specific primers used for PCR-genotyping.

Name*	Primer sequences (5'- 3')
SALK LBb1.3 (SALK)	ATTTTGCCGATTTCGGAAC
SAIL IT-LB1 (SAIL)	GCCTTTTCAGAAATGGATAAATAGCCTTGCTTCC
WiscDsLox p745 (Wisc)	AACGTCCGCAATGTGTTATTAAGTTGTC

* In parentheses are mentioned the names used in Table 16.

Table 16. Primer sequences for genotyping of T-DNA insertional mutants.

Mutant	Forward (F) and reverse (R) wild-type* primer sequences (5'- 3')	Wild-type product size (bp)	Primer combination to detect the mutant allele and product size
hipp32-1	F-TCTCAACATGGGTGGAAACA (P_32_a) R-CTTGAACCGCTGGGTAAGAG (P_32_b) R_2- TCACATAATACTACAACTAC (P_32_c)**	1166	SALK + R_2 (ca. 850 bp)
hipp32-2	F-TCTCAACATGGGTGGAAACA (P_32_a) R-CTTGAACCGCTGGGTAAGAG (P_32_b)	1166	F + SAIL (ca. 500 bp)
hipp33-1	F-TTCATTGTGATGGTTGTAAGCAG (P_33_a) R-CGCCCATTTTTCCATCTAAC (P_33_b)	1118	F + SAIL (ca. 900 bp)
hipp33-2	F-TTCATTGTGATGGTTGTAAGCAG (P_33_a) R-CGCCCATTTTTCCATCTAAC (P_33_b)	1118	SAIL + R (ca. 400 bp)
hipp34-1	F-ATGAGTAAAGAAGAGTTC (P_34_a) R-TCACATAATATCGCAGC (P_34_b)	1626	F + SALK (ca. 1735 bp)
hipp34-2	F-GTGAACATACACTGTGATGGCTG (P_34_c) R-TGCCTCCACCTTGGTTTTGA (P_34_d)	950	Wisc + R (ca. 1000 bp)

* In parentheses are mentioned the names used in Figure 19, section 3.3.1.
** R_2 primer was used only in combination with T-DNA specific-primer to detect the *hipp32-1* mutant allele.

The genotyping of the *HIPP32* CRISPR locus (*hipp32-3*) was performed by sequencing (see section 2.12.5) or by performing the loss of the restriction site assay (Belhaj *et al.*, 2015, see section 2.13.5). Both CRISPR loci, sgRNA32 and sgRNA71, were amplified by standard *Taq* PCR using the following primer pair (at an annealing temperature of 55 °C):

HIPP32_CRISPR_163 F-CACTGTGAAGGGTGTAAGCA
HIPP32_CRISPR_2271 R-ATTGGTGGAGGGTGAGCATA

The genotyping of sgRNA32 locus was carried out by sequencing (Table 17). To genotype the sgRNA71 locus, the 2128-bp-long PCR product was purified (see section 2.12.10) and digested with *BglII* overnight at 37 °C and the analyzed on a 1% agarose gel.

For genotyping of F2 or F3 generations resulted from genetic crosses PCR-based genotyping and additional genotyping based on selection marker, *e.g.* Kan resistance of *pSUC2:GFP* line or segregation analysis via microscopy, in the case of crosses with the *TCSn:GFP* line.

2.12.15 Sequencing of DNA

DNA sequencing was performed mostly by the GATC Biotech company (Konstanz, DE) and partially by GENEWIZ® company (Prague, CZ). The sequences of the primers used for sequencing are listed in Table 17.

Table 17. Sequences of primers used for sequencing.

Name	Primer sequences (5'- 3')	Purpose of use
AT1G07340 _255	CCCACACGTGTACGAGAAGA	Cas9 off-target analysis
AT1G29000_1294	GCGACAAGCATTAGGGTTTT	Cas9 off-target analysis
AT3G06130_1036	ATTCCCAGGACCACCCTTAG	Cas9 off-target analysis
AT5G19090_142	TTCATTGTGATGGTTGTAAGCAG	Cas9 off-target analysis
HIPP32_523	GTCCTCCATTTATGTCAATTTCCCA	Sequencing of CRISPR loci
M13_forward	GTAAAACGACGGCCAG	Gateway, CRISPR cloning
M13_reverse	CACAGGAAACAGCTATGAC	Gateway cloning
NOSt_R	ATTACATGCTTAACGTAATTCAACAG	MCS3 sequencing (BiFC cloning)
pDOE_mcs3bF	GGACACGCCTCAGGTACAGAGCATA	MCS3 sequencing (BiFC cloning)
pJET1.2_forward	CGACTCACTATAGGGAGAGCGGC	pJET cloning
pJET1.2_reverse	AAGAACATCGATTTTCCATGGCAG	pJET cloning

2.13 Cloning and DNA editing techniques

2.13.1 Gateway® recombination

The Gateway® cloning technology (Thermo Fisher Scientific, Table 2) was used to generate the promoter GUS reporter vectors (see section 2.13.2), the *HIPP32* and *HIPP33* overexpression vectors (see section 2.13.3) and to generate HMA and prenylation mutant variants of HIPP34 (see section 2.13.6).

The entry clones were obtained by performing the BP recombination reaction using the donor vectors pDONR™221 and pDONR™222 and *attB*-flanked PCR products, amplified in a second PCR reaction, using the following primer pair:

attB1 F-GGGGACAAGTTTGTACAAAAAAGCAGGCTTCACC
attB2 R-GGGGACCACTTTGTACAAGAAAGCTGGGTG

The BP reaction consisting of 50 ng pDONR, 20 - 50 ng *attB*-PCR product, 1 µl BP buffer and 1 µl BP Clonase™ enzyme mix (5 µl 1x TE buffer, pH 8) and incubated overnight at 25 °C. To stop the reaction, 1 µl of Proteinase K solution was added to the reaction and incubated for 10 minutes at 37 °C.
The expression vectors were obtained by performing the LR recombination reaction consisting of 50 - 100 ng purified entry clone (resulted from the BP reaction), 50 ng destination vector (pB7FWG2 or pBGWFS7), 1 µl LR buffer and 1 µl LR Clonase™ enzyme mix (5 µl 1x TE buffer, pH 8) and incubated overnight at 25 °C. 1 µl of Proteinase K solution was added to the reaction and incubated for 10 minutes at 37 °C.

2.13.2 Generation of *pHIPP:GUS* reporter constructs

The *HIPP32* promoter sequence (-2113 to -2 bp upstream of the start codon) was amplified from *Arabidopsis* Col-0 genomic DNA using *attB*-adapter sequence (small letters) integrated in the promoter-specific primer sequence used for amplification:

attB1-pHIPP32 F-aaaaagcaggcttcacctGGTCTAGCCTTTGTTTTTAGCT
attB2-pHIPP32 R-agaaagctgggtgCTTCTCTTAGATTTGTGTGTTTTCA

Similarly, the *HIPP33* promoter sequence (-2196 to -59 bp upstream of ATG) was amplified using the following primer pair:

attB1-pHIPP33 F-aaaaagcaggcttcaccAAAACGAGCCATGCGTGATATG
attB2-pHIPP33 R-agaaagctgggtgCAACTCCGCTGGTTCTTGAAAG

The PCR product was used as template for the second PCR reaction, in which the attachment site primer pair *attB1* and *attB2* (see 2.13.1) was used. The *attB*-flanked PCR products obtained were then used to perform the BP reaction (see 2.13.1) to obtain the entry vectors pDONR™222-pHIPP32 and pDONR™222-pHIPP33. The amplified PCR-product were tested by sequencing using the M13 forward und reverse primers. Positive entry clone was used to perform the LR reaction, using the pBGWS7 destination vector (see 2.13.1). The obtained expression vectors pBGWFS7-pHIPP32:GUS and pBGWFS7-pHIPP33:GUS were then used for *Arabidopsis* transformation (see section 2.11.2).

2.13.3 Generation of *HIPP*-overexpression constructs

HIPP32 and *HIPP33* are expressed in *Arabidopsis* at very low levels, thus their amplification from *Arabidopsis* Col-0 cDNA was not possible. Hence, for cloning of the overexpression vector, the genomic sequence of *HIPP32* was amplified, using the following primer pairs (small letters indicate *attB*-adapter sequences):

attB1-HIPP32	F-aaaaagcaggcttcaccATGAATAAACAAGATGTTATG
attB2-HIPP32	R-agaaagctgggtgTCACATAATACTACAACTACCTGGA

The amplification of *HIPP33* genomic sequence using the *attB*-adapter primers was not directly possible, therefore a modified version of nested PCR was adapted. First, primers situated within the intron region upstream of 5'-UTR and within the 3'-UTR sequence regions were designed and used for PCR:

HIPP33 (-262 bp upstream of ATG)	F-TTCATTCAAGTAAGTCTCTGATTTG
HIPP33 (+12 bp downstream of TGA)	R-CGGACACAAACTATGGAAAGTTT

The amplified 2268-bp-long sequence was cloned into pJET vector using the ClonepJET PCR Cloning kit (Table 2) and according to the user guide provided by manufacturer. The amplification was analyzed by sequencing, using the pJET1.2 primers (see 2.12.15).

The pJET-HIPP33 vector was then used as template to amplify *HIP*P33 using following primers (small letters indicate attB-adapter sequences):

attB1-HIPP33	F-aaaaagcaggcttcaccATGAGTAAAGAAGAGTTTATG
attB2-HIPP33	R-agaaagctgggtgTCACATAATATTGCAGCTTGAT

In a second PCR reaction, using the attachment site primer pair *attB1* and *attB2* (see section 2.13.1) the *attB*-flanked PCR products for *HIPP32* and *HIPP33* genomic sequence were obtained. BP reactions were performed (see section 2.13.1) to obtain the entry vectors pDONR^{TM}-pHIPP32 and pDONR^{TM}-pHIPP33. These were individually used to perform LR reaction with the destination vector pB7FWG2, to generate the N-terminal GFP fusion constructs overexpressing *HIPP32* and *HIPP33* under the control of the cauliflower mosaic virus (CaMV) 35S promoter, pB7FWG2-35S:GFP-HIPP32 and pB7FWG2-35S:GFP-HIPP33 respectively.

2.13.4 Generation of BiFC constructs

The cloning of BiFC constructs, pDOE-08-CKX1/HIPP32 and pDOE-08-CKX1/HIPP34, was based on the pDOE-08-CKX1 parent vector expressing CKX1 N-terminally tagged with the N-terminal fragment of monomeric Venus split at residue 210 (NVen-CKX1) and unfused C-

terminal Venus (CVen) fragment (Niemann *et al.*, 2018; Gookin and Assmann, 2014). This vector was used as a negative control during microscopy analysis (see section 3.2.3).
The genomic *HIPP32* sequence and *HIPP34* cDNA sequences were amplified from the pDONR^{TM}222-pHIPP32 and pDONR^{TM}221-pHIPP34 (see also section 2.13.3), using the following primer pairs (*Aat*II and *Kfl*I restriction sites are underlined):

BiFC_HIPP32	F-GACGTCATGAATAAACAAGATGTTAT
BiFC_HIPP32	R-GACGTCTCACATAATACTACAACTAC
BiFC_HIPP34	F-GGGTCCCCGAGTAAAGAAGAGTTC
BiFC_HIPP34	R-GGGACCCTCACATAATATCGCAGC

In the next step, the amplified HIPP32 and HIPP34 fragments were individually subcloned into the MCS3 *Aat*II and *Kfl*I site of the pDOE-08-CKX1 parent vector respectively, resulting in pDOE-08 BiFC vectors expressing NVen-CKX1/CVen-HIPP32 (pDOE-08-CKX1/HIPP32) and NVen-CKX1/CVen-HIPP34 (pDOE-08-CKX1/HIPP34) respectively.

2.13.5 CRISPR/Cas9 genome editing approach

To CRISPR/Cas9 genome editing approach was used in order to generate the *hipp32-3* mutant line in genetic background of *hipp34-2* T-DNA insertional mutant, thus resulting in the double mutant line *hipp32-3,hipp34-2* (*hipp32,34*) (see also Table 6). For this purpose, an optimized CRISPR/Cas9 system was used, in which the *Cas9* expression is driven by the egg cell-specific promoter *EC1.2* (Wang *et al.*, 2015).

2.13.5.1 Designing the sgRNA

Two single guides RNA (sgRNAs) for *HIPP32* locus (At3g05220.1) were designed using the CRISPR-P 1.0 (Lei *et al.*, 2014) web tool with 99% efficiency score. The sequences are listed below, with the NGG sequence highlighted in bold and with the *Bgl*II recognition site underlined:

sgRNA32 (+765 bp downstream of ATG):	AAGTGAACGTACACTGTGAA**GGG**
sgRNA71 (+831 bp downstream of ATG):	GGCAAACATGCCGAGATCTT**AGG**

2.13.5.2 Generation of the CRISPR/Cas9-sgRNA constructs

The plasmid pHEE401E published in Wang *et al.* (2015) was used to generate the CRISPR/Cas9-sgRNA constructs. For each sgRNA, forward and reverse oligonucleotides were designed:

sgRNA32	F-ATTGCAGGGGAGAGTTACTGTTAC
sgRNA32	R-GTCCCCTCTCAATGACAATGCAAA

sgRNA71 F-ATTGGGCAAACATGCCGAGATCTT
sgRNA71 R-CCGTTTGTACGGCTCTAGAACAAA

Forward and reverse oligonucleotides (2 µM of each in 50 µl ddH_2O) were incubated at 95 °C for 5 min and subsequently cooled at room temperature for 20 min, enabling their annealing. Meanwhile, the pHEE401E binary vector was digested for 2 hours, at 37 °C, using the type IIs restriction enzyme *Bsa*I, resulting in non-palindromic overhangs complementary to the 4-nucleotide overhangs flanking the protospacer.
Next, 10 µl of the annealed oligonucleotides and 50 ng pHEE401E (linearized and purified) were used to carry out the DNA ligation (see section 2.12.13). The ligation success was tested by sequencing using the M13 forward primer (see section 2.12.15). The positive clones were used for *Agrobacterium*-mediated transformation of *hipp34-2 Arabidopsis* plants.

2.13.5.3 Loss of enzyme recognition site assay

The loss of enzyme recognition site assay described in Belhaj *et al.* (2015) relies on the *Bgl*II recognition site within the sgRNA71 protospacer (see section 2.13.5.1) and it was used to genotype T1, as described in section 2.12.14. Additional sequencing was performed to identify the nature of the genetic events occurred (Table 17).

2.13.5.4 Cas9 outsegregation and Cas9 off-targets analysis

T2 plants homozygous for the CRISPR genetic event occurred at sgRNA71 locus were investigated by PCR for outsegregation of the Cas9, using the following primer pair (at an annealing temperature of 55 °C):

zCas9 F-ACGGTTAAGCAGCTCAAGGA
zCas9 R-CCTGGTGAGGACCTTGTTGT

For the amplification of the predicted off-target site loci, following primer pairs were used:

AT5G19090_142 F-TTCATTGTGATGGTTGTAAGCAG
AT5G19090_1240 R-CGCCCATTTTTCCATCTAAC

AT1G29000_893 F-CGATACAAAGGCGCAAACTC
AT1G29000_1294 R-GCGACAAGCATTAGGGTTTT

AT1G07340 _255 F-CCCACACGTGTACGAGAAGA
AT1G07340 _1300 R-GTAGCGGTCATCTGGAGAGC

AT3G06130_385 F-TCAAGAAGCTCGCCAAATCT
AT3G06130_1036 R-ATTCCCAGGACCACCCTTAG

For each off-target one of the primers was used for sequencing (Table 17).

2.13.6 Site-directed mutagenesis

Variants of HIPP34 containing point mutations either within the HMA domain (^{20,23}C→G, HIPP34^{hma}) or the prenylation site (^{470}C→G, HIPP34^{prenyl}) were generated following the one-step site-directed mutagenesis protocol described in Zheng *et al.*, 2004 and using the QuikChange™ Site-Directed Mutagenesis kit (Table 2). pDONR^{TM}221-pHIPP34 served as PCR template, using the following primer pairs:

HIPP34_HMA	F-GTGAACATACACGGTGATGGCGGTAAGCAGAAAG
HIPP34_HMA	R-CTTTCTGCTTACCGCCATCACCGTGTATGTTCAC

HIPP34_prenyl	F-GAACACATCAAGCGGCGATATTATGTG
HIPP34_prenyl	R-CACATAATATCGCCGCTTGATGTGTTC

The obtained pDONR^{TM}221-pHIPP34^{hma} and respectively pDONR^{TM}221-pHIPP34^{prenyl} were sequenced using the M13 primers. Positive clones were subsequently used in Gateway LR recombination reaction with the destination vector pK7FWG2 to generate N-terminally fused GFP-HIPP34^{hma} to generate pK7FWG2-GFP-HIPP34^{hma}, and GFP-HIPP34^{prenyl} to generate pK7FWG2-GFP-HIPP34^{prenyl}, overexpressed under the control of 35S promoter.

2.14 Protein methods

2.14.1 Protein isolation

For the extraction of the total protein from *Arabidopsis* and *N. benthamiana*, 0.3 mg to 1 g plant material was snap-frozen in liquid nitrogen and, in the frozen state, either shredded using steel beads in precooled adapters and the Retsch mill (Retsch Mixer Mill MM2000) or crashed into a fine powder by using a precooled mortar and pestle. Protein extraction buffer at a ratio of 1:3 (w/v) was added to the homogenized leaf material. The buffer consisted of 100 mM Tris/HCl pH 7.5, 150 mM NaCl pH 7, 0.3 % - 1 % Triton X-100 and protease inhibitor cocktail without EDTA (1 tablet/10 ml extraction buffer, Roche, Cat. No. 11836170001). The samples were thoroughly vortexed and incubated for 30 min under constant shaking at 4 °C. Afterwards, the extracted proteins were separated from the cell debris by a 10-minute centrifugation at 6,000 x g at 4 °C. The supernatants were used to measure the protein concentration and, subsequently, for protein blot analysis or co-immunoprecipitation assays.

2.14.2 Determination of protein concentration

The protein concentration in the protein extract was determined using the bicinchoninic acid (BCA) method (Smith *et al.*, 1985). This method combines the biuret reaction, the reduction of Cu^{+2} ions to Cu^{+1} by proteins in an alkaline medium with complexation of the latter with bicinchoninic acid, visible by the purple color formation. The measurement was carried out in a microplate, using the Pierce BCA protein assay kit (Table 2). BSA (bovine serum albumin)

dilution series (2, 1, 0.75, 0.5, 0.25, 0.125 and 0 mg/ml) were used to prepare a standard curve. BSA standards, proteins samples (previously diluted 1:5 and 1:10), and blanks (extraction buffer) were measured in triplicates. 200 µl of detection reagent was added to 10 µl of BSA standard, blank and protein sample and the microplate was incubated at 37 °C for 30 min in the Synergy 2 Microplate Reader (Biotek). The absorbance was subsequently measured at 562 nm. The protein concentration of unknown samples was determined by interpolating into the BSA standard curve using linear regression.

2.14.3 Membrane-association studies

Microsomal membranes from *Arabidopsis* were isolated using the microcentrifuge-based method (Abas and Luschnig, 2010). Briefly, proteins were extracted from 300 mg leaf material shredded to powder (see section 2.14.1). To this, 1 ml of 1.5x extraction buffer (100 mM Tris-HCl, pH 7.5, 300 mM NaCl, 25% (w/v) sucrose, 5% (v/v) glycerol and protease inhibitor cocktail without EDTA (1 tablet/10 ml extraction buffer, Roche, Cat. No. 11836170001) was added and vigorously vortexed. The homogenate was incubated on ice for 30 min (vortexed every 10 min). The homogenous lysate was centrifuged at 600 g for 3 min. After an additional 30 min of incubation on ice, the supernatant was diluted with 1 volume of water, divided into 200 µl-aliquots in 1.5-ml tubes, and centrifuged at 22,000g for 2.5 h at 4 °C. 30 µl volume from the supernatants was kept for protein blot analysis, the rest was discarded. The pellet was dissolved in 200 µl of 0.65x extraction buffer and used for protein blot analysis.
Microsomal membranes from *N. benthamiana* were isolated using the ultracentrifuge-based protocol. For this, snap-frozen leaf material (1 g) was homogenized using a precooled mortar and pestle. To this 3 ml of homogenization buffer (25 mM Tris-HCl, pH 7.5, 250 mM sucrose, and complete protease inhibitor cocktail without EDTA (see also section 2.14.1) was added. The homogenate was passed through a 60-µm gaze (Miracloth, Calbiochem) and collected in a 50-ml falcon tube. Further 3 ml of the homogenization buffer was added. To remove cell debris, the homogenate was split into 2-ml tubes and centrifuged at 6,000 g for 3.5 min (4 °C). The supernatants (6 ml) were transferred into BECKMAN tubes, from which 30 µl was taken prior ultracentrifugation for protein blot analysis (total protein). The microsomal membrane fraction was pelleted by ultracentrifugation at 100,000g for 90 min at 4 °C. After this, 30 µl of the supernatant was kept for SDS blot analysis (see 2.14.5) and the rest was discarded. The pellet was resuspended in 600 µl of homogenization buffer, from which 30 µl were used for SDS blot analysis.

2.14.4 Co-immunoprecipitation assays

For co-immunoprecipitation (Co-IP) assays, GFP and myc fusion proteins were co-expressed in *N. benthamiana* leaves, which were ground in liquid nitrogen and homogenized in extraction

buffer (50 mM Tris-HCl, pH 7.5,150 mM NaCl, 0.3% Triton X-100, 0.2% Igepal and complete protease inhibitor cocktail (see section 2.14.1). The homogenate was centrifuged at 6,000 g for 10 min. 15 µl of the supernatant was kept for protein blot analysis and the rest transferred to a new 1.5-ml tube. Protein concentration was estimated by BCA assay (see 2.14.2). 3 mg of total protein in 1.4 ml extraction buffer were incubated in 1.5-ml tubes with 35 µl GFP-Trap-A beads (Chromotek) for 240 min at 4 °C, with gentle agitation. Beads were washed five times with the extraction buffer (1 min centrifugation at 1,000 g). The last centrifugation step was performed for 2 min at 2,500 g. After this step, the supernatant was discarded and the pellet was mixed with 20 µL of 2x SDS-PAGE sample buffer (see section 2.14.5), incubated for 5 min at 95 °C and cleared by centrifugation (2 min at 2,500 g). The proteins were subjected to SDS-PAGE and immunoblot analysis using anti-myc antibody (see section 2.14.6).

2.14.5 SDS polyacrylamide gel electrophoresis (SDS-PAGE)

For protein blot analysis, proteins were separated according to their size using denaturing discontinuous SDS-PAGE (Laemmli, 1970). For this purpose, SDS polyacrylamide gels consisting of two layers were prepared using the Hoefer™ Mighty Small II System. The upper layer (stacking gel) contained 4 % acrylamide and the lower layer (separating gel) contained 10 % acrylamide (Table 18).

Table 18. Composition of one SDS polyacrylamide gel.

Component	Stacking gel	Separating gel
Tris/HCl pH 8	-	375 mM
Tris/HCl pH 6.8	125 mM	-
Acrylamid/Bis-Acrylamid (19:1)	4 %	10 %
SDS (sodium dodecyl sulfate)	0.075 %	0.1 %
APS (ammonium persulfate)	0.0375 %	0.05 %
TEMED (*N,N,N′,N′*-tetramethylethane-1,2-diamine)	0.06 %	0.05 %

The 1x electrophoresis buffer was prepared based on a 10x stock solution, which consisted of 1.92 M glycine, 0.25 M, Tris, and 1 % SDS. Prior electrophoresis, the protein samples (15 or 30 µg) were mixed down to 1x with the adequate amount of 4x loading buffer (250 mM Tris/HCl pH 6.8, 8 % SDS, 10 % β-mercaptoethanol, 40 % glycerol and 0.01 % bromphenol blue) and incubated for 10 min at 95 °C. As protein molecular weight marker, 3 µl of PageRuler Prestained Protein Ladder (Table 2) was used. The electrophoresis was carried out at a constant current of 20 mA per gel in a Bio-Rad running chamber.

2.14.6 Protein blotting and immunodetection

Myc or GFP fusion proteins were detected by immunoblot analysis. The proteins, previously separated by SDS-PAGE electrophoresis were, transferred (blotted) on a PVDF membrane (Immobilon-P Membrane, Cat. No. IPVH00010, pore size 0.45 µm, EMD Millipore) using the

Trans-Blot Electrophoretic Transfer Cell System (Bio-Rad). Prior blotting, the SDS-gels were equilibrated for 15 min in blotting buffer (192 mM glycine, 25 mM Tris). During this time PVDF membrane was activated with methanol (30 sec), rinsed with water (2 min) and equilibrated for 5 min in the blotting buffer. Two foam pads and 2 Whatman papers were also pre-soaked in the blotting buffer. The blotting cassette was built as follows: cathode, foam pad, Whatman paper layer, gel, PVDF membrane, Whatman paper layer, foam pad, anode. The cassette was inserted into the blotting module and blotting was carried out at constant current of 30 V, for 16 hours at 4 °C.

After successful blotting, indicated by the presence of the protein marker on the membrane, the membrane was briefly rinsed with ddH_2O. In order to minimize the unspecific binding of proteins, the membrane was incubated for one hour with 6 % skim milk dissolved in PBS-T (137 mM NaCl, 2.7 mM KCl, 10 mM Na_2HPO_4, 1.8 mM KH_2PO_4, 0.1 % Tween-20) under gentle rotation. The membrane was then incubated for 2 hours with the respective primary antibody in 6 % skim milk in PBS-T. A mouse monoclonal anti-myc antibody (clone 4A6; Millipore; dilution 1:1,000) was used to detect the myc epitope and the mouse anti-GFP antibody (clone JL-8; Clontech; dilution 1:2,500) was used for GFP detection. Unbound antibody was washed away with PBS-T (3 times for 5minutes each). Afterwards, the membrane was incubated with the secondary antibody in 6 % skim milk in PBS-T, followed by 3 washing steps as described above. The goat anti-mouse antibody coupled to horseradish peroxidase (sc-2005; Santa-Cruz; dilution 1:2,000) was used as secondary antibody. The bound antibodies were detected by chemiluminescence assay according to the manufacturer's instructions, using the SuperSignal West Pico Chemiluminescent Substrate Kit (Table 2). After incubation with the ECL substrate, the chemiluminescence was detected on a CL-XPosure™ film (Thermo Fisher Scientific). The exposure time varied between 5 sec and 15 min.

2.14.7 Coomassie staining

To check whether equal amounts of protein were loaded, the PVDF membrane was stained with Coomassie blue. First, the membrane was washed twice for 5 min with PBS-T. Then, it was incubated for ca. 3 min with 0.1 % Coomassie R-350 in methanol/H_2O (1:1) under gentle shaking. The excessive staining was removed by incubating the membrane in acetic acid/ethanol//H_2O (1:5:4) for 20 min. Finally, the membrane was washed with H_2O, air-dried and scanned.

2.15 Histological and histochemical analyses

2.15.1 GUS staining

The β-glucuronidase (GUS) enzyme activity in transgenic *Arabidopsis* plants was detected by histological staining upon conversion of the substrate 5-bromo-4-chloro-3-indolyl-β-D-

glucoronide (X-Gluc) into a blue dye (Jefferson *et al.*, 1987). The tissue to be examined was fixed in 90 % acetone for at least hour at -20 °C. Then the acetone was removed by washing twice with 50 mM sodium phosphate buffer (pH 7). The tissue was incubated with GUS staining solution (50 mM sodium phosphate buffer pH 7.5, 5 mM potassium ferrocyanide, 5 mM potassium ferricyanide, 0.2 % Triton X-100 and 1 mM X-Gluc) overnight at 37 °C. After staining, the plant material was washed with 50 mM sodium phosphate buffer (pH 7.0). To remove the excessive staining, the plant material was washed several times with 70% ethanol at 37 °C. For microscopic analysis, any remaining dyes were washed out by incubation for 15 to 30 minutes in 0.24 M HCl in 20 % ethanol at 57 °C and subsequent incubation for 15 to 30 minutes in 7 % NaOH in 60 % ethanol at room temperature (Malamy and Benfey, 1997). The plant tissue was then rehydrated by subsequently washing with 40 %, 20% and 10 % ethanol (5 min each), at room temperature. Finally, the plant tissue was transferred to a solution of 25% glycerol and 5 % ethanol for microscopy. For root analysis, the seedlings were cleared by incubation in clearing solution consisting of chloral hydrate solution (8 g chloral hydrate, 1 ml glycerol and 2 ml water). The light microscopic analysis was carried out with the Axioskop2 plus microscope (Zeiss) and with a light stereomicroscope (SZX12, Olympus).

2.15.2 Staining with propidium iodide (PI)

To visualize cell organization in seedling roots, tissue was stained with 0.1 mg/ml propidium iodide (PI) by mounting the roots in PI solution instead of water during microscopy analysis.

2.15.3 *ClearSee*-based clearing and staining technique

The fluorescence microscopy analysis of transgene *Arabidopsis* plants expressing *35S:GFP-HIPP34* (line #5-1) was performed in collaboration with Matthieu Bourdon (Sainsbury Laboratory University of Cambridge). The seedlings were fixed in 4 % formaldehyde, cleared using the *ClearSee* protocol (Kurihara *et al.*, 2015) and then stained for cell visualization with Direct Red 23 (Ursache *et al.*, 2018).

2.15.4 mPS-PI technique

The modified pseudo-Schiff propidium iodide (mPS-PI) staining technique described in Truernit *et al.*, 2008 was used for the microscopy analysis of *Arabidopsis* embryos and for the visualization of starch formation within the columella root cells. Embryos or whole seedlings were fixed in fixative (50 % methanol and 10 % acetic acid) at 48 °C for at least 12 h. The tissue was then transferred to 80 % ethanol and incubated at 80 °C for 5 min. Tissue was transferred back to fixative and incubated for another hour. Next, tissue was rinsed with water and incubated in 1 % periodic acid at room temperature for 40 min. Afterwards, the tissue was rinsed again with water and incubated for 2 h in Schiff reagent with propidium iodide (100 mM sodium metabisulphite and 0.15 M HCl and propidium iodide to a final concentration of 100

mg/ml was freshly added). The samples were then transferred onto microscope slides and covered with a chloral hydrate solution (4 g chloral hydrate, 1 ml glycerol and 2 ml water), stored at 4 °C overnight (or at longest 3 days) before microscopy analysis.

2.16 Confocal laser scanning microscopy (CLSM)

Confocal imaging analyses were mainly performed using a Leica TCS SP5 confocal laser scanning microscope (CLSM). Table 19 shows an overview of the fluorescent proteins and fluorescence dyes used in this study, including the excitation wavelength and the wavelength interval in which the fluorescence emission was detected.

The quantification of the fluorescence intensity was performed using the LAS AF Lite software (Table 1). Briefly, a region of interest (ROI) was selected and the histogram function of the quantification tool was used, measuring the mean gray values (intensity per pixel as unit area) of the ROI.

Table 19. Fluorescent proteins and fluorescence dyes used for CSLM analysis.

Fluorescent protein/dye	Excitation (nm)	Emission (nm)
CF (6-carboxyfluorescein)	488	500 - 551
Direct Red 23	561	580 - 615
GFP (green fluorescent protein)	488	498 - 538
mPS-PI (modified pseudo-Schiff propidium iodide)	488	528 - 693
mTurqouise2	458	461 - 504
OFP (orange fluorescent protein)	561	577 - 600
PI (propidium iodide)	561	650 - 700
RFP (red fluorescent protein)	561	590 - 650

2.17 Plant experiments

2.17.1 Germination assay

For germination assay, 100 *Arabidopsis* seeds per genotype and biological replicate were sterilized, sawed out and treated with cold as describe in section 2.9.1. Four days after transferring the plates to light, the germinated seeds with green cotyledons were counted and the percentage of the germination rate was determined.

2.17.2 Isolation of *Arabidopsis* embryos

Arabidopsis mature embryos were isolated from ripened seeds. For this, the seeds were imbibed in water for 4 hours and the embryos were dissected out of the seed coat using a needle and a pair of forceps under a light stereomicroscope (SZX12, Olympus).

2.17.3 Hormone treatment

For analysis of root growth responses to exogenous cytokinin, *Arabidopsis* seedlings germinated and grown on ½ MS medium (see section 2.9.1), containing 20, 30 and 40 nM 6-Benzylaminopurine (BA, dissolved in 100 % DMSO). 20, 30 and 40 nM BA, and 0.001 % DMSO as control were used. The root growth parameter (see section 2.17.5) were monitored 12 days after germination (see also section 2.17.7).

For monitoring the *TCSn:GFP* expression in root tissues, *Arabidopsis* seedlings were grown for 5 days on ½ MS medium (see section 2.9.1) and then 30 seedlings were transferred for 16 hours to petri dishes containing 10 ml of liquid ½ MS medium supplemented with either 1 µM BA or 0.001 % DMSO as control.

To measure the expression of cluster-III *HIPP* genes in response to cytokinin, cDNA from 12-day-old *Arabidopsis* wild-type seedlings treated with 0.001 % DMSO (control) or with 1 µM BA was used. Briefly, seedlings were grown either in short day, in which case the RNA samples were taken 1 h, 2 h and 6 h after induction, or in long day conditions, with RNA sampling at 30 min and 120 min after induction.

For the RNA-Seq analysis (see section 2.12.16), *Arabidopsis* seedlings were grown for 5 days on ½ MS medium (see section 2.9.1). Approximately 10 seedlings per genotype and per sample were transferred to a 6-well plate containing 2 ml of liquid ½ MS medium supplemented with either 5 µM BA or 0.001 % DMSO as control. The 6-well plate was then placed in a speed vacuum concentrator and 2 series of vacuum of 30 sec each was applied. The plate was then placed in the growth chamber for 1 hour. Then seedlings were frozen in liquid nitrogen and kept at -80° C until RNA isolation (see section 2.12.3).

2.17.4 Cytokinin content measurement

To analyze the cytokinin metabolites, the plants were grown *in vitro* under long day conditions (see section 2.9.1). Approximately 20 mg of material from ten-day-old seedlings was combined, frozen in liquid nitrogen and kept at -80 °C until processing stored. The measurements were carried out by Dr. Ondrej Novàk (Palacký University, Olomouc, CZ). Four biological replicates per genotype were analyzed.

2.17.5 Analysis of growth and developmental parameters

The rosette size was determined by measuring the widest rosette diameter of 3.5-week-old plants. The area of the seventh rosette leaf were measured using *ImageJ* (area measurement function) at bolting. Bolting or flowering starting point was considered when the inflorescence stem had reached 5 mm.

The height of the inflorescence stem was measured closed to the end of the life cycle, when 5 to 10 white flower buds were visible. The diameter of the inflorescence stem was measured 1

cm above the rosette level using a light stereomicroscope, based on 4-week-old plants. The term of axillary rosette branch refers to the primary rosette-leaf branch (Aguilar-Martinez *et al.*, 2007) and its number was determined at the end of the reproductive growth phase.

The silique rate formation was determined by counting the total siliques of the main stem at three different time points during the linear growth phase. The total number of siliques was measured at the very end of the reproductive growth phase, when flower buds stopped to form.

Seed area was determined using *ImageJ* (area measurement function).

Embryo size determined by measuring the length of the embryonic axis and the length of the cotyledons using *ImageJ*, based on embryos stained with mPS-PI (see 2.15.4) and imaged using a confocal microscope (see section 2.16).

The root growth was analyzed 12 days after germination. The primary root elongation was determined using *ImageJ*, while the lateral roots were counted using a binocular. For synchronized root growth, the root length was marked 3 days after germination. Thus, the root elongation and the lateral root number was determined between 3 and 12 days after germination.

The root meristem size was determined by counting the number of cortex cells in a file extending from the quiescent center (Perilli and Sabatini, 2010) based on 6-day-old roots stained with PI (see 2.15.2) and imaged using a confocal microscope (see section 2.16).

2.17.6 Measuring PD conductivity

2.17.6.1 CFDA-loading and transport assay

To assess phloem unloading in the root meristem, *Arabidopsis* seedlings were grown on vertical culture plates for 4 days. Then, they were placed horizontally for further 2 days to facilitate the carboxyfluorescein diacetate (CFDA) application. 0.3 µl of 1 mM CFDA (dissolved in 1440 ml acetonitrile and 650 ml ddH_2O) was applied to one cotyledon, which was previously gently crimped with a pair of forceps. The dye was then allowed to translocate and the carboxyfluorescein (CF) unloading into the root meristem was analyzed by confocal microscopy 1 h after CFDA application.

To assess symplastic transport in the root meristem, root tips of 5-day-old seedlings were dipped into 1 mM CFDA solution for 15 sec and rinsed in water before microscopy. CF diffusion into the root meristem was monitored at 5, 20 and 60 min after CFDA exposure.

2.17.6.2 SUC2:GFP diffusion measurements

To quantify movement of GFP from the phloem into the meristem, the ratio between the GFP fluorescence in a defined ROI above the QC relative to an ROI within the phloem in the stele was built (QC:P) (see section 2.16).

2.17.7 Heavy metal stress experiments

For analysis of root growth in response to heavy metal stress, *Arabidopsis* seedlings were germinated and grown on standard ½ MS medium (see section 2.9.1), containing excessive concentrations of heavy metals or lacking iron. For plates containing excess heavy metals, the following metal concentrations were added to ½ MS medium: 25 µM $CdCl_2$, 300 µM $ZnSO_4 \cdot 7H_2O$ and 250 µM $FeSO_4$ (Remy and Duque, 2016). The primary root elongation and the lateral root formation were determined 10 days after germination using *ImageJ* and a binocular (see section 2.17.5).To prepare ½ MS medium without iron, 50 µM NaFeEDTA (Murashige and Skoog, 1962) was omitted and a100 µM Ferrozine, an iron chelator to chelate residual iron from the agar, was added (O'Lexy *et al.*, 2018).

To analyze the effect of excessive iron on the movement of GFP from the phloem into the root meristem, *Arabidopsis* seedlings were grown on standard ½ MS medium for 5 days and then were transferred for 48 hours on ½ MS plates supplemented with 1 mM NaFeEDTA and control plates respectively. GFP movement was assessed as described in section 2.17.6.2.

To determine the root elongation in the presence of excessive iron, 5-day-old seedlings were transferred onto ½ MS plates supplemented with 1 mM NaFeEDTA and control plates. To synchronize growth, root length was marked after the transfer and the root elongation was measured 48 hours later, using *ImageJ*.

2.17.8 RNA-Sequencing analysis

Within the frame of this study, two RNA-Sequencing (RNA-Seq) experiments were performed. The first RNA-Seq experiment aimed to compare the ‘steady-state’ transcriptome between *hipp* single and *hipp* triple mutants to the wild type. The second RNA-Seq experiment was performed to analyze the transcriptional changes in selected *hipp* mutants and wild-type seedlings treated with cytokinin (see section 2.17.3). For both experiments, samples were collected from 5-day-old seedling grown *in vitro* (see section 2.9.1). For RNA extraction, 3 biological replicates per genotype and treatment were used, whereby each biological replicate (sample) contained approximately 10 seedlings.

Total isolated RNA of concentration between 100 and 180 ng/µl was submitted to BGI Genomics (Hong Kong, China) for mRNA enrichment, library preparation and sequencing using the DNBSEQ-G50 platform with 20M clean reads per sample.

The sequencing generated in total about 387 million reads. The sequencing reads were filtered by BGI using the internal software *SOAPnuke* v1.5.2. Low quality reads with base quality <10, reads with adaptors and reads with unknown bases were filtered out to obtain the ‘clean reads’ which were stored in FASTQ format. A total of 372,099,461 reads passed the quality filter and were mapped to the reference (*Arabidopsis* Col-0 genome assembly, TAIR10), using *Bowtie2* v2.2.5 (Kim *et al.*, 2015). On average, 90.5% of the clean reads were mapped uniquely to only

one location and 81.89% could be assigned to a single annotated TAIR10 gene. The genome mapping results for each sample were provided by BGI in BAM format. *RSEM* (v1.2.12) was used to determine the gene expression level, calculated as fragments per kilobase of exon model per million mapped fragments (FPKM) of each transcript in each sample. FPKM values determined for all the samples were provided by BGI. The differential gene expression analysis between samples and/or treatment and control samples was performed based on the negative binomial distribution using DEseq2 method/R package (Love *et al.*, 2014). The false discovery rate (FDR) for differentially expressed genes was set to 5% using the Benjamini and Hochberg method (Benjamini and Hochberg, 1995).

Genes with an adjustment of p-value for FDR < 0.05 and a minimum of 1.5-fold up- or downregulation (log2 fold change ≥ 0.584 or ≤ -0.585) in *hipp* mutants compared to wild type (section 3.5) were considered differentially expressed genes. No cut off for log2 fold change was applied when determining the differentially expressed genes after cytokinin treatment compared to control (section 3.7.5). The overlapping genes were analyzed with *Venny 2.0* software (Table 1). The gene ontology (GO) enrichment analysis was conducted using DAVID 6.8 (Table 1). GO enrichments were considered statistically significant with an enrichment p-value < 0.05. The Kyoto Encyclopedia of Genes and Genomes (KEGG) pathway analysis was performed with the *g:Profiler* web-based tool, with an enrichment p-value < 0.05. Hierarchical cluster analysis was applied to all genes showing expression differences (FDR < 0.05) after cytokinin treatment at least in one genotype, using the *dendextend* package in R (Table 1). Density plots and heat maps were generated using the R *hexbin* package and *heatmap* R function, respectively (Table 1).

2.18 Contributions

The following material used in the framework of this study was previously generated by Dr. Henriette Weber (Applied Genetics, FU Berlin, DE): the vectors pDONR^{TM}221-HIPP34 and pK7FWG2-GFP-HIPP34, T0 *Arabidopsis* seeds expressing *pK7FWG2-GFP-HIPP34* and several T2 homozygous transgenic *Arabidopsis* lines expressing *pCB308-pHIPP34:GUS*. Dr. Henriette Weber also identified the *hipp32-1* and *hipp34-1* T-DNA insertion lines (Table 16), ordered seeds and designed primers for the PCR-based genotyping for these lines.

Segregation analysis of the transgenic *pHIPP32:GUS* and *pHIPP33:GUS* lines, and the cloning of the BiFC vector pDOE-08-CKX1/HIPP34 were performed by Jennifer Kümmele as part of her bachelor thesis.

The BiFC control vector pDOE-08-CKX1/empty was generated by Dr. Michael Niemann (Applied Genetics, FU Berlin, DE).

The CRISPR/Cas9 vector was obtained from The Gregor Mendel Institute of Molecular Plant Biology (Austria, AT), courtesy of Michael Nodine.

The fluorescence microscopy analysis of *35S:GFP-HIPP34* (line #5-1) was performed by Matthieu Bourdon from Sainsbury Laboratory University of Cambridge (Cambridge, UK).
The cytokinin content measurements and analysis were performed by Dr. Ondrej Novàk (Palacký University, Olomouc, CZ).
cDNA used to investigate the expression of cluster-III *HIPP* genes in response to cytokinin was courtesy of Dr. Sören Werner (Applied Genetics, FU Berlin, DE).
pSUC2:GFP Arabidopsis seeds and CFDA were provided by Andrea Paterlini from Sainsbury Laboratory University of Cambridge (Cambridge, UK).
TCSn:GFP Arabidopsis seeds were available in the laboratory seed collection, originally courtesy of Dr. Bruno Müller, University of Zurich (Zurich, CH).

3. Results

3.1 Expression analysis of *HIPP* genes from cluster III

In *Arabidopsis*, the metallochaperone-like genes are grouped in a large family of 67 members, from which 45 genes encode for HIPP proteins (Tehseen *et al.*, 2010). The functions of the HIPP proteins are largely unknown and only few genes were studied in detail. Based on their high sequence homology, HIPP32, HIPP33 and HIPP34 (hereinafter collectively referred to as HIPPs) are the only members of cluster III (see phylogenetic tree; Figure 2). Despite their high sequence homology, HIPP proteins might play different roles or might be involved in different biological processes.

To investigate the roles of individual *HIPP* genes during plant development, their expression patterns were analyzed using the β-Glucuronidase (GUS) reporter system. The GUS system is a versatile tool in plant molecular biology frequently used to study temporal and spatial expression patterns of unknown genes. The method is based on the detection of the enzymatic activity of GUS in cells and tissues of transformed plants using histochemical assays (Jefferson *et al.*, 1987). For this purpose, GUS reporter lines were generated, in which the *GUS* gene (*uidA*) is controlled by the endogenous *HIPP* promoters. Concretely, a region of 2,113 bp long for *HIPP32* promoter (*pHIPP32*) and of 2,196 bp long for *HIPP33* promoter (*pHIPP33*) situated directly upstream of the translational start sites were transcriptionally fused to *GUS* in pBGWS7 vector (Karimi *et al.*, 2002). The *HIPP34* promoter, an approximately 2-kb promoter region upstream of the start codon, was fused to *GUS* in pCB308 (Dr. H. Weber, unpublished). The generated constructs were transformed in *Arabidopsis thaliana* to produce *pHIPP32:GUS*, *pHIPP33:GUS* and *pHIPP34:GUS* transgenic lines. 20 *pHIPP32:GUS* and 12 *pHIPP33:GUS* independent lines were analyzed in T1 via GUS histochemical staining. 8 *pHIPP32:GUS* lines and 6 *pHIPP33:GUS* lines showed similar *GUS* expression patterns in root, leaves and floral organs. For *pHIPP34:GUS,* 8 transgenic lines showing similar expression pattern were available (Dr. H. Weber, unpublished). Based on the segregation analysis of the selectable marker of the T2 transgenic progenies, two representative lines for each reporter line carrying the construct for a single T-DNA insertion were selected for detailed histochemical analysis.

The *HIPP32* promoter showed GUS activity in various tissues and organs at different developmental stages (Figure 11). In mature embryos, *pHIPP32:GUS* was exclusively expressed in the radicle and colette regions of the root meristem (Figure 11A; Bassel *et al.*, 2014). Later, in 5-day-old seedlings, the *pHIPP32:GUS* expression was localized in the shoot apex at the base of emerging leaves, at the root-hypocotyl junction, within the differentiated root vascular tissues and in the root apical meristem (Figure 11B). In the roots, *pHIPP32:GUS* was strongly active in the root apical meristem (Figure 11C), in the root vasculature and in

emerging lateral roots (Figure 11D). In young leaves, *pHIPP32:GUS* was restricted to the leaf margins (Figure 11E), whereas in mature rosette leaf GUS activity was present in the vasculature and in the stomata (Figure 11F). In adult plants, GUS activity driven by the *HIPP32* promoter was detectable in the stem vascular tissue (Figure 11G) and throughout the inflorescence organs such as flower stalks (Figure 11H), carpel walls of the gynoecium (Figure 11I) and vascular bundle of the anthers (Figure 11J). At the fruit stage, *pHIPP32:GUS* expression was restricted to the silique septum (Figure 11K).

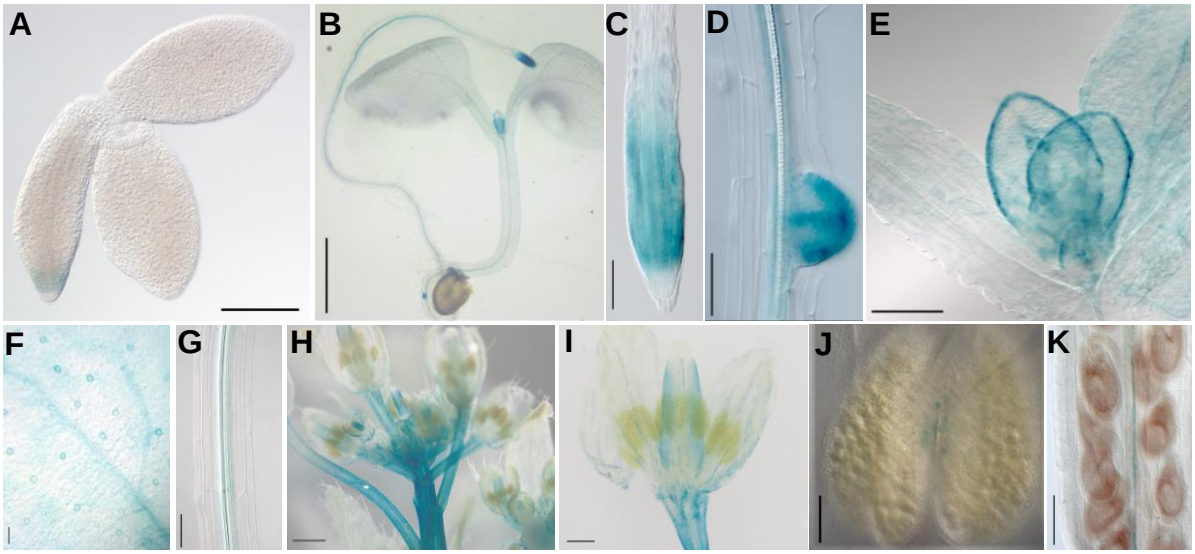

Figure 11. Spatiotemporal expression pattern of *pHIPP32:GUS*.
pHIPP32:GUS is expressed in the radicle and colette regions of mature embryo **(A)**, in the shoot apex at the base of young leaves, at the root-hypocotyl junction, within the differentiated root vascular tissues and in the root apical meristem of a 5-day-old seedling **(B)**. In 7-day-old seedlings, the *pHIPP32:GUS* activity remains present in the root meristem **(C)**, in the root vasculature, and appears high in the emerging lateral root **(D)** and at the margins of the young leaves **(E)**. Later, *pHIPP32:GUS* activity is observed in the vasculature and stomata of rosette leaf **(F)** and in the stem vascular tissue **(G)**. In flowers, strong expression is detected in the flower stalks **(H)**, in the carpel walls of the gynoecium **(I)** and in the vascular bundle of the anthers **(J)**. In the fruit, *GUS* expression appears exclusively at the silique septum **(K)**. Scale bars = 100 µm; exceptions: **B, I** = 1 mm and **H** = 3 mm.

Compared to the broad expression pattern of *pHIPP32:GUS* reporter line, the *pHIPP33:GUS* expression was restricted only to a few tissues during plant growth (Figure 12). In 5-day-old seedlings, GUS activity driven by the *HIPP33* promoter was detected in the stipules of arising leaves (Figure 12A), in the quiescent center and in the CSCs of the root (Figure 12B). In 7-day-old seedlings, strong *GUS* expression was localized in the stipules of arising leaves and in the shoot apical meristem (Figure 12C) as well as in the vasculature of the hypocotyl (Figure 12D). In flowers, *pHIPP33:GUS* expression was detectable in the gynoecium at different stages: in replum at stage 10 (Figure 12F), in ovules at stage 11-12 (Figure 12G) and post-anthesis in the funiculus at stage 14 (Figure 12H) as well as in the funiculus and in the micropyle at stage 17 (Figure 12I; Ferrandiz *et al.*, 1999).

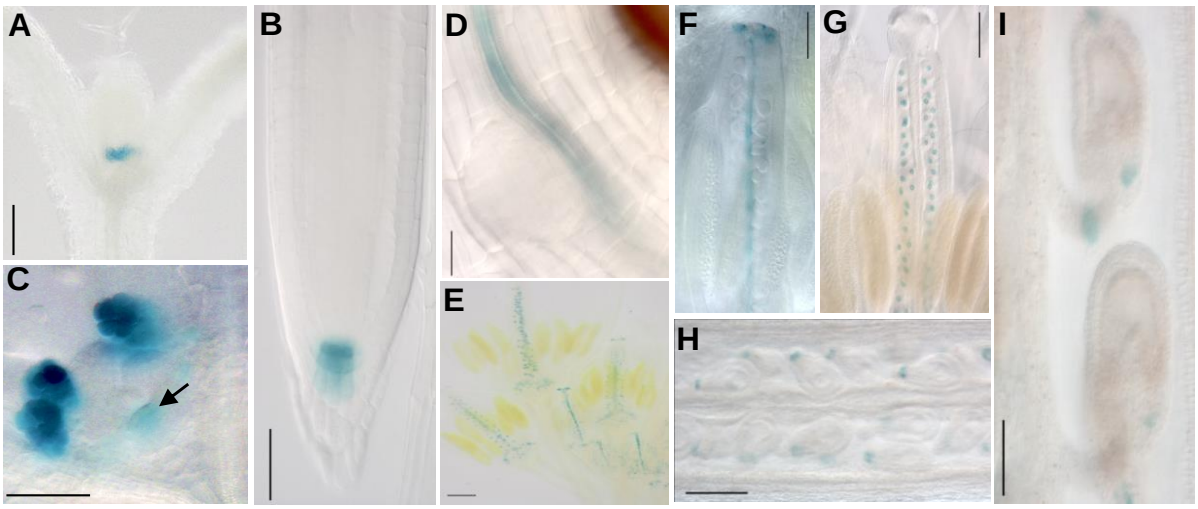

Figure 12. Spatiotemporal expression pattern of *pHIPP33:GUS*.
5-day-old seedlings, *pHIPP33:GUS* expression is localized in the stipules of arising leaves **(A)** and in the quiescent center cells and in the columella stem cells of the root **(B).** Seven days after germination, strong *pHIPP33:GUS* activity is detectable in the stipules, in the shoot apical meristem (arrow) **(C)** and in the vasculature of the hypocotyl **(D)**. In flowers, *pHIPP33:GUS* expression is present in the gynoecium of different stages (**E - I**). Scale bars = 100 µm; exceptions: **A, E** = 1 mm.

In contrast to its closest relative *HIPP33*, *HIPP34* promoter drove *GUS* expression in several tissues and organs (Figure 13). *pHIPP34:GUS* is expressed throughout the entire mature embryo: in the cotyledons, in the epidermis and in the provasculature of the hypocotyl (Figure 13A). After germination, strong *pHIPP34:GUS* expression was observed in the shoot apex (Figure 13B), in the tissues along the vasculature axis from hypocotyl to the root apical meristem (Figure 13C) and later in the vascular tissues of the emerging lateral root (Figure 13D). *pHIPP34:GUS* expression exhibiting an evident basipetal gradient was observed throughout the young leaves (Figure 13E). In older seedlings, strong *pHIPP34:GUS* expression was exclusive to young leaves (Figure 13F), whereas in rosette leaves, *pHIPP34:GUS* expression was restricted to the vascular tissues (Figure 13G, F) and apparent in the stomatal guard cells (Figure 13H). In inflorescence, *pHIPP34:GUS* was expressed in the gynoecium at stage 12 along its apico-basal axis, with strong expression in the style and the gynophore as well as in the pedicels, petals and the filaments of the anthers. In fully developed siliques *pHIPP34:GUS* activity was confined to the outer integument of the seeds (Figure 13J). The expression of these three *HIPP* genes shows different patterns, implying that they may play distinct roles in plant development or may control different biological processes.

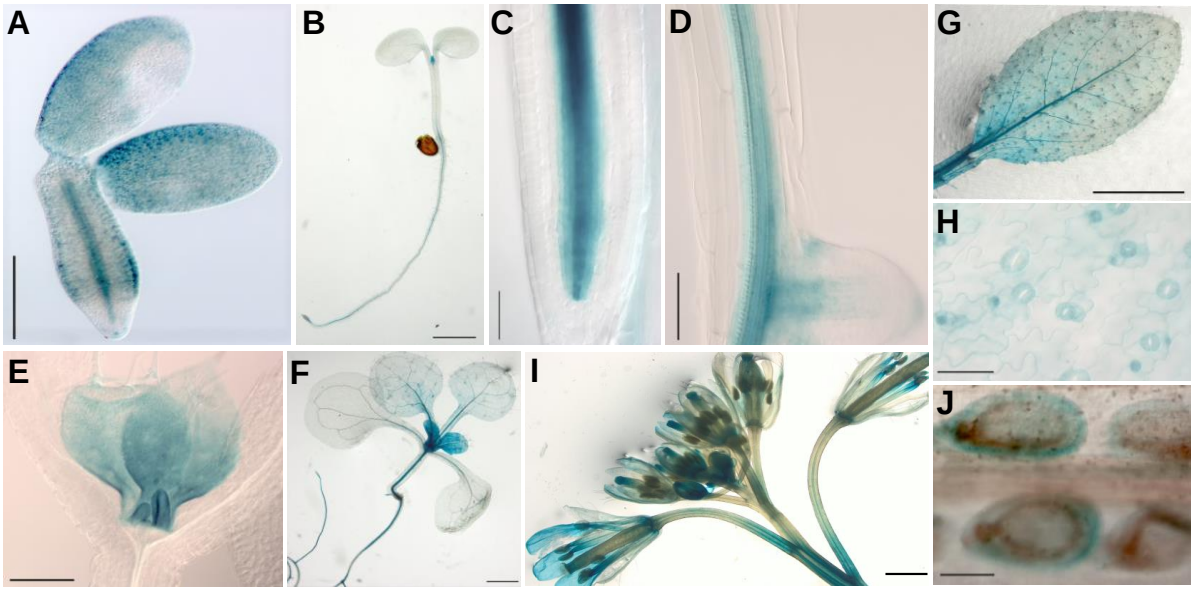

Figure 13. Spatiotemporal expression pattern of *pHIPP34:GUS*.
(A) Mature embryo expressing *pHIPP34:GUS* with strong activity in the cotyledons, epidermis and in hypocotyl provasculature. Strong GUS expression is observed at the shoot apex **(B)** and in tissues along the vasculature axis from hypocotyl to the root apical meristem **(C)** and in the vascular tissue of the emerging lateral root **(D)**. Strong expression in young leaves of 5-day-old **(E)** and 7-day-old seedlings **(F)**. In rosette leaves, *pHIPP34:GUS* is expressed in the vasculature **(G)** and in the guard cells **(H)**. In flowers **(I)**, *pHIPP34:GUS* is expressed in the pedicels, petals, in the style and the gynophore of the gynoecium, as well as in the filaments of the anthers. In siliques, *pHIPP34:GUS* activity is confined to the outer seed integuments **(J)**. Scale bars = 100 µm; exceptions: **B, F, I** = 1 mm and **G** = 5 mm.

3.2 Molecular and cellular characterization of HIPP proteins of cluster III

3.2.1 Subcellular localization of HIPP32, HIPP33 and HIPP34

Knowing the localization of a protein within the cell is an important step in elucidating its biological function. To determine the subcellular localization of here studied HIPP proteins, the individual *HIPP* genomic sequences were fused to the coding region of GFP downstream of the constitutive cauliflower mosaic virus 35S promoter (CaMV 35S) using the *pK7WGF2* destination vector (Karimi *et al.*, 2002), to generate the *35S:GFP-HIPP32* and *35S:GFP-HIPP32*. The similarly generated construct - *35S:GFP-HIPP34* - was available in the laboratory collection. Preliminary results of the *35S:GFP-HIPP34* overexpression in *N. benthamiana* leaf epidermal cells indicated towards a PD-targeted protein (Dr. H. Weber).
The GFP-tagged *HIPP* overexpression constructs were transiently co-expressed in epidermal leaf cells of *N. benthamiana* with the PD marker PLASMODESMATA-LOCATED PROTEIN 1 (PDLP1; Thomas *et al.*, 2008). The confocal microscopy analysis revealed that all three GFP-HIPP fusion proteins showed a fluorescence signal along the periphery of epidermal leaf cells in a punctate pattern, co-localizing with the RFP signal of the PD marker PDLP1 (Figure 14).

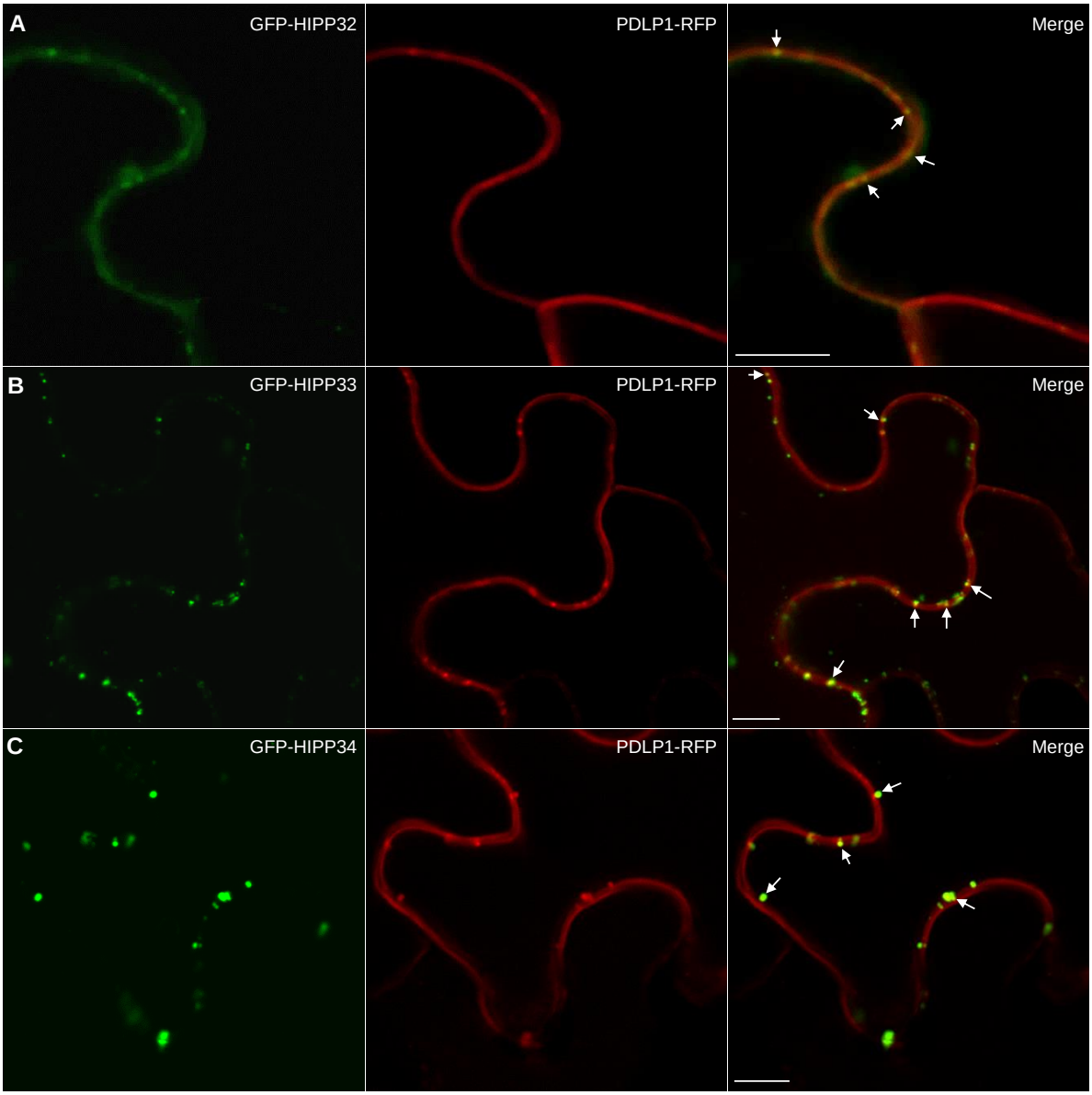

Figure 14. *Arabidopsis* HIPP proteins from cluster III are PD-resident proteins.
Subcellular localization of GFP-HIPP32 **(A)**, GFP-HIPP33 **(B)** and GFP-HIPP34 **(C)** co-expressed with the PD marker PDLP1-RFP in leaves of *N. benthamiana*. Arrows in the merged images exemplify the co-localization of the differently fluorescence-tagged proteins. Scale bars = 10 µm.

The association of HIPP34 with PD observed in transient assays was confirmed in *Arabidopsis* plants stably expressing the 35S:*GFP-HIPP34* transgene. The fluorescence analysis was performed in collaboration with Matthieu Bourdon (Sainsbury Laboratory University of Cambridge) using the *ClearSee*-based clearing and staining technique (Kurihara *et al.*, 2015). In leaf epidermis, GFP-HIPP34 fluorescence was detected integrated in the cell walls (Figure 15A), as inferred from the lack of fluorescence signals emitted by Direct Red 23, a fluorescent dye that enables visualization of cellulose (Anderson *et al.*, 2010). A high density of *GFP-HIPP34* localization was observed at pit fields traversing the longitudinal cell walls of adjacent cells, which became visible due to cell walls being pressed against each other during sample

preparation (magnified inset; Figure 15A; Barnett, 1987; Faulkner *et al.*, 2008). In the roots, strong GFP was detected at the sieve plate and to a less extent throughout the sieve elements of the protophloem (Figure 15B). Taking into account the drawbacks of the transient expression system, the stable *Arabidopsis 35S:GFP-HIPP34* line was used to confirm HIPP34 residency at PD. For this, the *35S:GFP-HIPP34* line was crossed with the *Arabidopsis* line overexpressing the RFP-tagged CrRLK-like protein (At5g24010), a kinase described to localize at PD and plasma membrane (Fernandez-Calvino *et al.*, 2011). Confocal microscope analysis of leaf epidermis from homozygous F2 plants revealed the co-localization of the two differentially tagged proteins (Figure 15C) and confirmed the GFP-HIPP34 residency at PD.

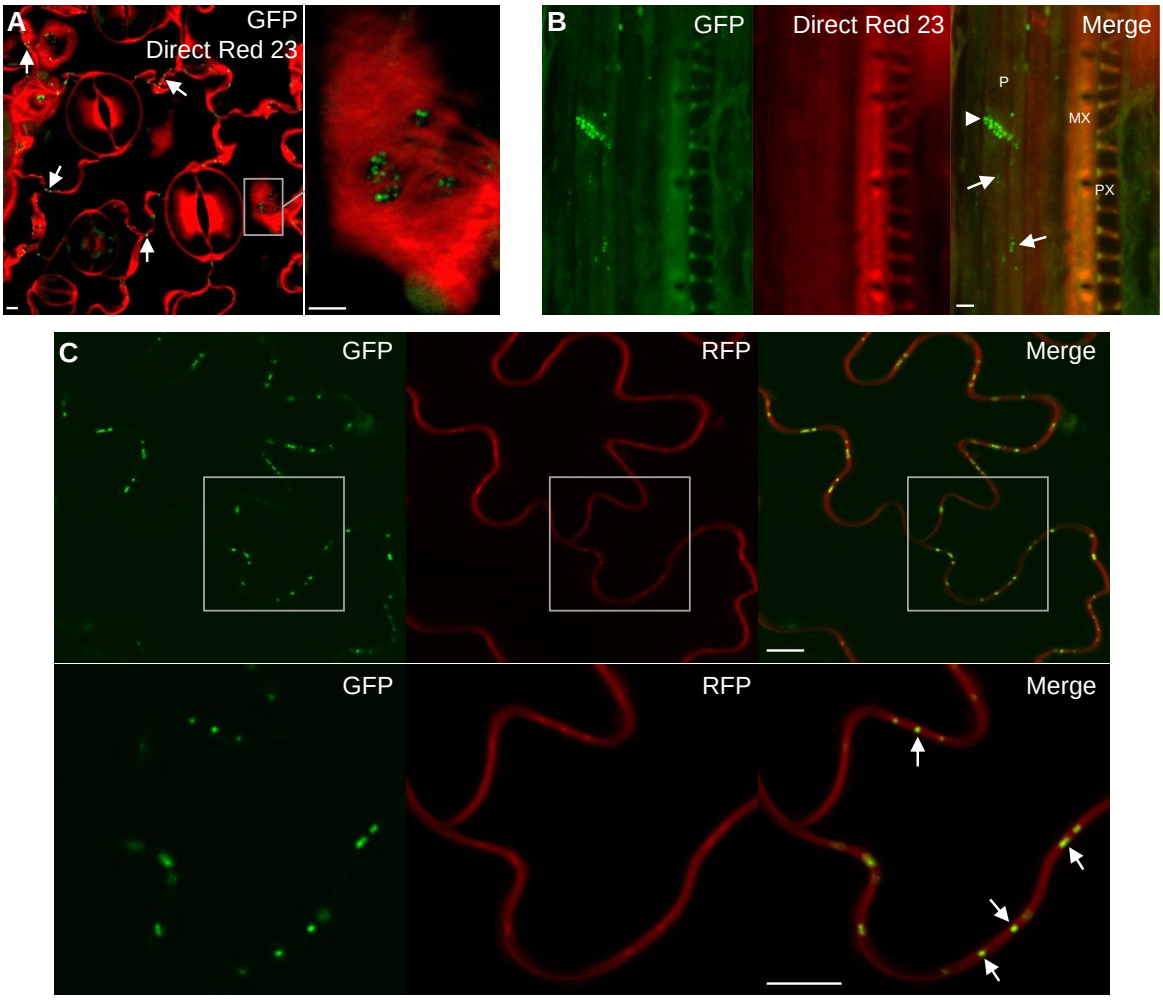

Figure 15. GFP-HIPP34 residency at PD is confirmed in transgenic *Arabidopsis* line.
(A) GFP detection within the cell walls stained with Direct Red 23 (white arrows) and at the PD pit fields (magnified inset) in leaf epidermis cells. Scale bars = 3 µm. **(B)** GFP detection in the sieve elements (white arrows) and at the sieve plate (white arrowhead) of the protophloem (P) in *Arabidopsis* roots. PX: protoxylem; MX: metaxylem. Scale bar = 2.5 µm. **(C)** Confocal images of leaf epidermis cells of *35S:GFP-HIPP34* crossed into PD marker At5g24010-RFP. The gray boxes are shown as magnified images in the lower panel. Co-localization is highlighted with white arrows. Scale bars = 10 µm.

Characteristic for the PD-associated proteins' pattern are the paired fluorescent foci on both sides of the cell walls (Levy *et al.*, 2007), detectable in the *GFP-HIPP33* and *GFP-HIPP34* expressing cells (Figure 14 and 15). However, this punctate GFP fluorescence spanning the walls was rather absent in the tobacco cells expressing *GFP-HIPP32* (Figure 14A), suggesting that HIPP32 PD-association might differ from that of HIPP33 and HIPP34, which also share the highest sequence homology. Furthermore, GFP-HIPP32 fluorescence was observed in intracellular punctate structures throughout entire cells when transiently overexpressed in tobacco leaf epidermal cells (data not shown). Hence the question arose whether HIPP32 associates with other subcellular compartments. Co-expression analyses of *GFP-HIPP32* with several organelle markers containing indicators for the endoplasmic reticulum, peroxisomes and mitochondria were performed (Nelson *et al.*, 2007). However, there were no co-localization of GFP-HIPP32 with any of the tested organelle markers (results not shown). Co-expression analysis with the Golgi marker COMPLEX GLYCAN LESS 1 (CGL1; Frank *et al.*, 2008) revealed co-localization of the two the differently fluorescence-tagged proteins (Figure 16), suggesting the dual subcellular localization of HIPP32, at PD and to the Golgi apparatus.

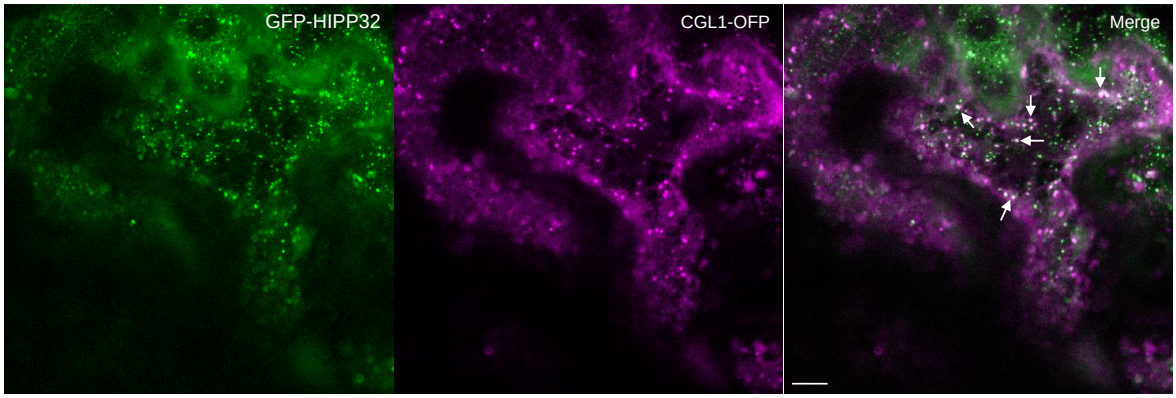

Figure 16. HIPP32 partially resides to the Golgi apparatus in *N. benthamiana.*
Transient expression of *GFP-HIPP32* in tobacco epidermal leaf cells, co-agroinfiltrated with *CGL1-OFP* protein labeling Golgi stacks. Co-localization is highlighted with white arrows in the merged images. Scale bar = 10 µm.

3.2.2 Biochemical properties of HIPP proteins

Sequence analyses revealed that there are 67 metallochaperone-like proteins in *A. thaliana* containing one or two predicted HMA domains (PFAM accession number: PF00403; El-Gebali *et al.*, 2018). 45 proteins contain additional to the HMA domain an isoprenylation site at their C-terminus (Tehseen *et al.*, 2010). The structure of HIPP proteins from cluster III is shown in the Figure 17A. Each of these HIPPs contains one HMA domain which includes the highly conserved CXXC motif (C, cysteine; X, any amino acid; Tehseen *et al.*, 2010) and an isoprenylation CaaX motif (C, cysteine; a, aliphatic amino acid; X, any amino acid) at their C-

termini (Dykema *et al.*, 1999). Additional to the HMA domain and the prenylation motif, HIPP sequences contain regions rich in glycine, glutamine, and proline (Figure 17A).

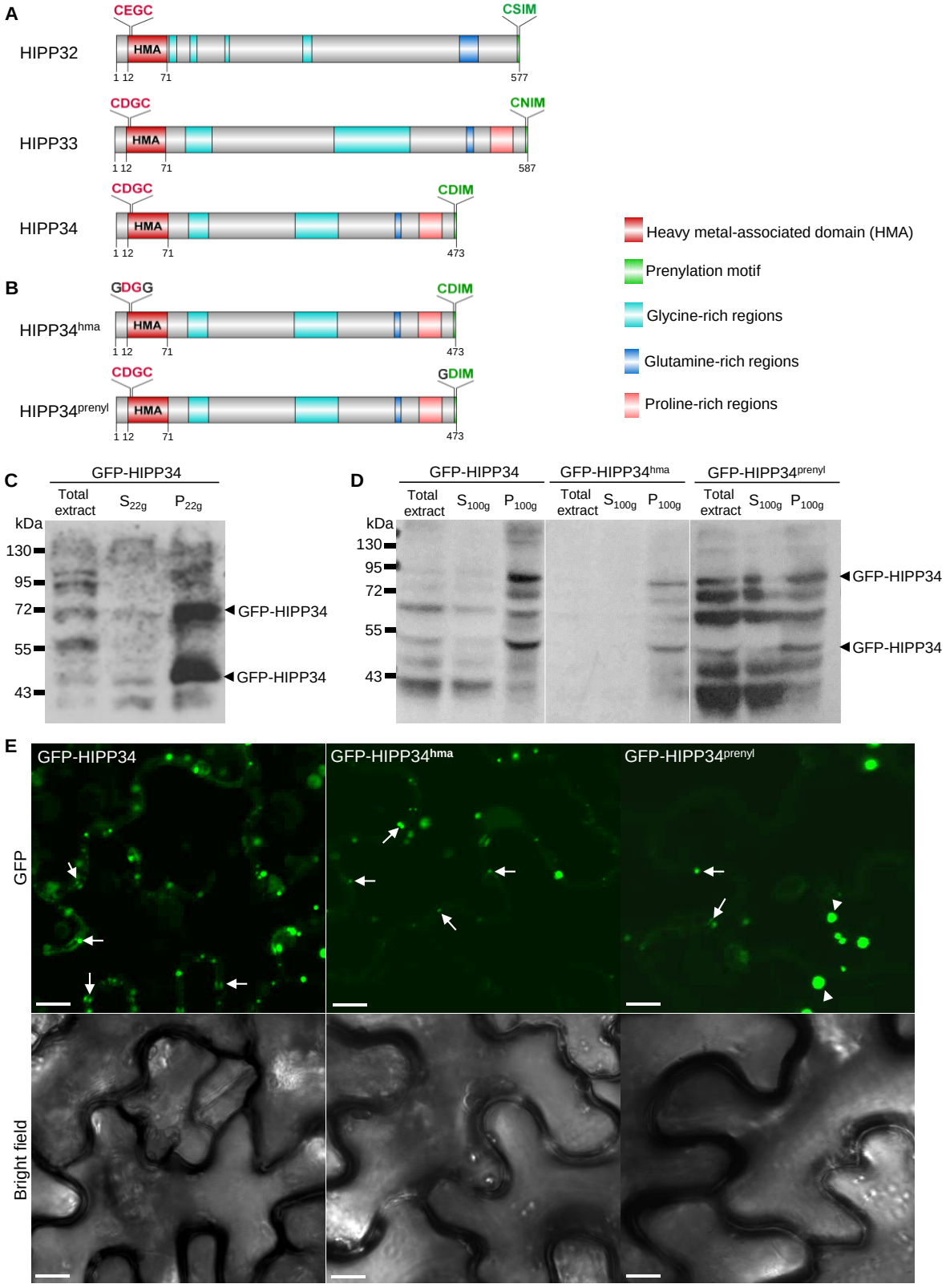

Figure 17. HIPP34 associates with the membrane in a prenylation-dependent manner.

Figure 17: Continued.
(A) Schematic representation of the cluster-III protein structures with predicted heavy metal-associated domains (HMA, red boxes) and prenylation motif (green boxes) at the C-terminus. HIPP protein sequences contain further regions rich in glycine, glutamine, and proline. **(B)** Variants of HIPP34 containing either mutated HMA domain (HIPP34^{hma}) or prenylation site (HIPP34^{prenyl}) generated by site-directed mutagenesis. **(C)** GFP-HIPP34 association with the membrane. Total proteins were isolated from *Arabidopsis* leaves constitutively expressing *35S*:*GFP-HIPP34*. Total protein extract, soluble ($S_{22g,}$ supernatant upon centrifugation at 22,000g) and membrane-bound protein fractions (P_{22g}, pellet upon centrifugation at 22,000g) were analyzed by SDS-PAGE and detected by immunoblotting with anti-GFP antibody. **(D)** Membrane association of GFP-HIPP34, GFP-HIPP34^{hma} and GFP-HIPP34^{prenyl} transiently expressed in *N. benthamiana* leaves. Ultracentrifugation was used to separate the soluble proteins (S_{100g}, supernatant upon centrifugation at 100,000g) and the membrane-bound proteins (P_{100g}, pellet upon centrifugation at 100,000g) from the total protein extract. Fractions were analyzed by SDS-PAGE and detected by immunoblotting with anti-GFP antibody. **(E)** Representative confocal images of GFP-fusion HIPP34 protein variants in agroinfiltrated tobacco leaf epidermal cells. Arrows indicate the GFP localization at PD and arrowheads indicate the large protein aggregates predominant in the *GFP-HIPP34*^{prenyl}-expressing leaves. Scale bars = 10 µm.

Multiple alignment of HIPP protein sequences performed using DNAMAN software (Lynnon Biosoft) revealed an overall identity of 56.41%. At the amino acid level, the highest homology of 76% exists between HIPP33 and HIPP34; 44% of the HIPP32 sequence is homologous to those of HIPP33 and HIPP34.

In order to study the function of the HMA domain and prenylation, mutant variants of HIPP34 were generated by using the site-directed mutagenesis. The HMA domain was mutated by exchanging the two conserved cysteine residues at the position 20 and 23 within the CXXC motif to glycine to generate the HMA-mutated HIPP34 variant, HIPP34^{hma} (Figure 17B). The prenylation site was mutated by exchanging the cysteine residue at the position 470 to glycine, to generate the prenylation-mutated HIPP34 variant, HIPP34^{prenyl} (Figure 17B).

To study the association of HIPP to the membrane, membrane-association experiments performed using the *Arabidopsis* line overexpressing *35S:GFP-HIPP34*, line #5-1 (see section 3.6). Western blot analysis revealed that GFP-HIPP34 – detected as two bands of different molecular weights – was present in the microsomal pellet fraction but not in the supernatant (Figure 17C). This indicates that HIPP34 is associated either with the plasma membrane or with microsomal membranes. In plants, the microsomal fraction consists of the plasma membrane and organelles such endoplasmic reticulum, Golgi apparatus and various endosomal vesicles and compartments (Abas and Luschnig, 2010). The analysis of the HIPP34 sequence using the *TMpred* tool (ExPASy) did not predict any transmembrane domain (result not shown). This suggests that GFP-HIPP34 association with the plasma membrane or the endosomal membranes might occur in a prenylation-dependent manner, as it has been known that prenylation promotes protein-membrane interactions due to its hydrophobic character conferred by lipids involved in the prenylation process (Zhang and Casey, 1996).

To test this hypothesis, the membrane association of both HIPP34 mutant variants was studied. For this purpose, the constructs *35S:GFP-HIPP34*, *35S:GFP-HIPP34^{hma}* and *35S:GFP-HIPP34^{prenyl}* were transiently expressed in *N. benthamiana* leaves and microsomal membrane protein fractions were separated from the soluble proteins by ultracentrifugation. Similar *GFP-HIPP34* expressed in *Arabidopsis*, GFP-HIPP34 was enriched in the microsomal fraction but it was also present in the supernatant (Figure 17D). Similar distribution was observed for the GFP-HIPP34^{hma} protein, however GFP-HIPP34^{hma} levels were extremely low, since no protein could be detected in the total extract (Figure 17D). In contrast, GFP-HIPP34^{prenyl} was abundantly detected in both the total extract and the supernatant fraction, but relatively less enriched in the microsomal fraction (Figure 17D), suggesting that membrane-association of GFP-HIPP34^{prenyl} was in part mediated by the protein prenylation.

To investigate whether the mutation of the HMA domain and the prenylation site affect the subcellular localization of HIPP34, confocal microscopy analysis of *N. benthamiana* epidermal leaf cells expressing *GFP-HIPP34*, *GFP-HIPP34^{hma}* and *GFP-HIPP34^{prenyl}* were performed (Figure 17E). GFP-HIPP34^{hma} signals were observed in PD-specific punctate pattern at the plasma membrane, however they appear, due to the low GFP-HIPP34^{hma} expression, weaker and were less frequent than those of GFP-HIPP34 (Figure 17D). Consistent with the high protein abundancy detected in the soluble GFP-HIPP34^{prenyl} protein fraction, only scarce GFP-HIPP34^{prenyl} fluorescence was observed at PD, whereas accumulations of large cytosolic protein aggregates of high fluorescence intensity were rather prominent (Figure 17E). These results indicate that the prenylation is not only required for HIPP34 localization at PD, probably via plasma membrane-association, but it is also essential for its functional significance.

3.2.3 HIPP proteins of cluster III interact with cytokinin-degrading enzyme CKX1

Six members of the HIPP protein family were identified to interact with the cytokinin degrading enzyme CYTOKININ OXIDASE/DEHYDROGENASE 1 (CKX1) in a yeast two-hybrid screening (Y2H) screen performed in Werner's laboratory (Guo, 2019). Interestingly, the identified HIPPs belong to two phylogenetically distinct clusters: HIPP5, HIPP6 and HIPP7 belong to cluster I, whereas HIPP32, HIPP33 and HIPP34 belong to cluster III (Tehseen *et al.*, 2010).

One objective of this doctoral work was to confirm the interactions between CKX1 and HIPP proteins from cluster III identified in yeast. To address this question, GFP-tagged HIPPs and myc-CKX1 fusion proteins were transiently co-expressed in *N. benthamiana* leaves, and total protein extracts were used for co-immunoprecipitation (Co-IP) using anti-GFP antibody. Figure 18A shows an immunoblot where an anti-myc antibody was used to detect myc-CKX1 in the immunoprecipitated fraction: myc-CKX1 co-immunoprecipitated with all GFP-HIPPs (but not with GFP alone), supporting the idea of CKX1/HIPP complex formation *in vivo.*

To learn more about the CKX1/HIPP complex formation at the cellular level, CKX1/HIPP interaction assays were conducted using the single vector-based bimolecular fluorescence complementation (BiFC) system, which relies on the reconstruction of Venus fragments NVen and CVen split at residue 210 (Gookin and Assmann, 2014).

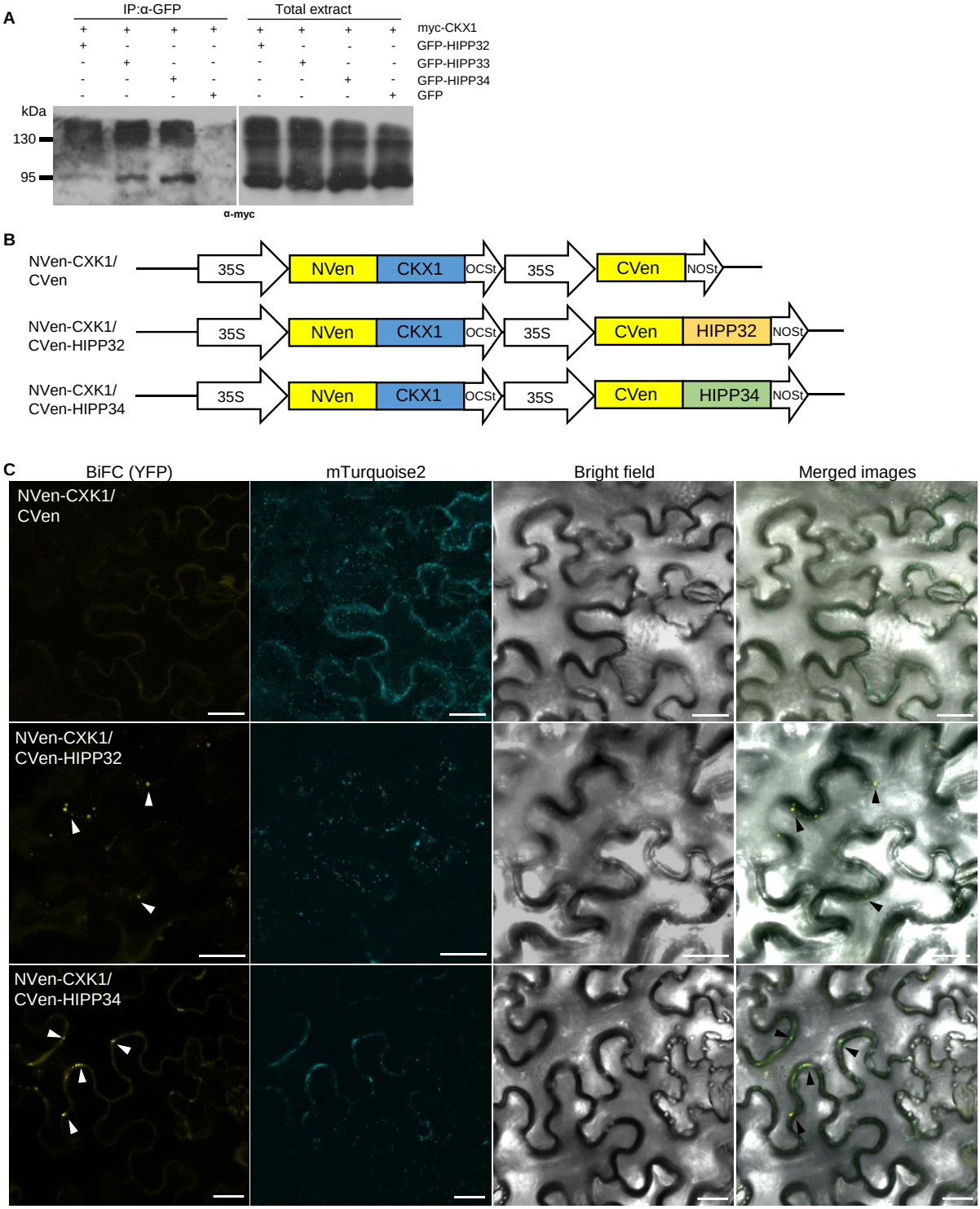

Figure 18. HIPP proteins of cluster III interact with CKX1 *in vivo*.

Figure 18. Continued.
(A) GFP-HIPP32, GFP-HIPP33, GFP-HIPP34 and GFP were transiently co-expressed with myc-CKX1 in *N. benthamiana* and protein extracts were used for co-immunoprecipitations using an anti-GFP antibody. Anti-myc antibodies were used for the immunodetection. The left immunoblot shows the immunoprecipitated fraction (IP:α-GFP) and the right one the input (15 µg of the total extract). **(B)** Schematic representation of the BiFC constructs. **(C)** Confocal images of *N. benthamiana* epidermal leaf cells transiently expressing BiFC constructs, 3 days post infiltration. The control NVen-CKX1/CVen shows a low background BiFC signal, whereas NVen-CKX1/CVen-HIPP32 and NVen-CKX1/CVen-HIPP34 show Venus signals, derived from the reconstitution of the NVen/CVen protein (arrowheads). Successful infiltration is indicated by the mTurquoise2 signals in Golgi. Scale bars = 25 µm.

To generate the BiFC expression vectors, *HIPP32* and *HIPP34* were cloned fused to the C terminus of the Venus protein in the parental vector pDOE-08 containing NVen-fused CKX1 (Niemann *et al.*, 2018). The parental vector with the unfused CVen was used as control to monitor the nonspecific assembly of NVen-CKX1 and CVen. Figure 18B illustrates the structure of the BiFC vectors used. The pDOE-08 vector also contained a Golgi-localized marker (mTurquoise2), which served to identify the transformed tobacco cells. As visible from the mTurquoise2 fluorescence signal, the agrobacterium-based infiltration was successful; however, the transformed cells showed comparatively low Venus fluorescence (Figure 18C). NVen-CKX1/CVen-HIPP32 displayed fluorescence signals in an irregular pattern along the cell periphery, while the NVen-CKX1/CVen-HIPP34 rather weak signals resembled the dot-like pattern specific to PD localization (Figure 18C). Only low diffuse BiFC signal was detected when NVen-CKX1 was co-expressed with the untagged CVen fragment, suggesting that the BiFC signals observed originated from the reconstitution of the NVen/CVen protein.

3.3 Establishment of *HIPP* loss-of-function lines

3.3.1 Selection and molecular characterization of *hipp* T-DNA mutant insertion lines

T-DNA insertional mutagenesis is a powerful tool for functional reverse genetics studies in *Arabidopsis* (Krysan *et al.*, 1990). In order to investigate the functions of individual *HIPP* genes, T-DNA insertion lines were identified in the database collection available on the online platform of the Salk Institute Genome Analysis Laboratory (SIGnAL, Alonso *et al.*, 2003). For each *HIPP* gene from the cluster III, two independent T-DNA insertional mutant alleles were identified. The T-DNA insertions were confirmed by PCR-based genotyping, using T-DNA border primers in combination with gene-specific primers (Figure 19A). The exact locations of the individual T-DNA insertions were subsequently determined by sequencing the border fragments. For all six *hipp* alleles the T-DNA insertion was identified within the largest exons, suggesting that the isolated lines represent functionally null alleles (Wang, 2008).

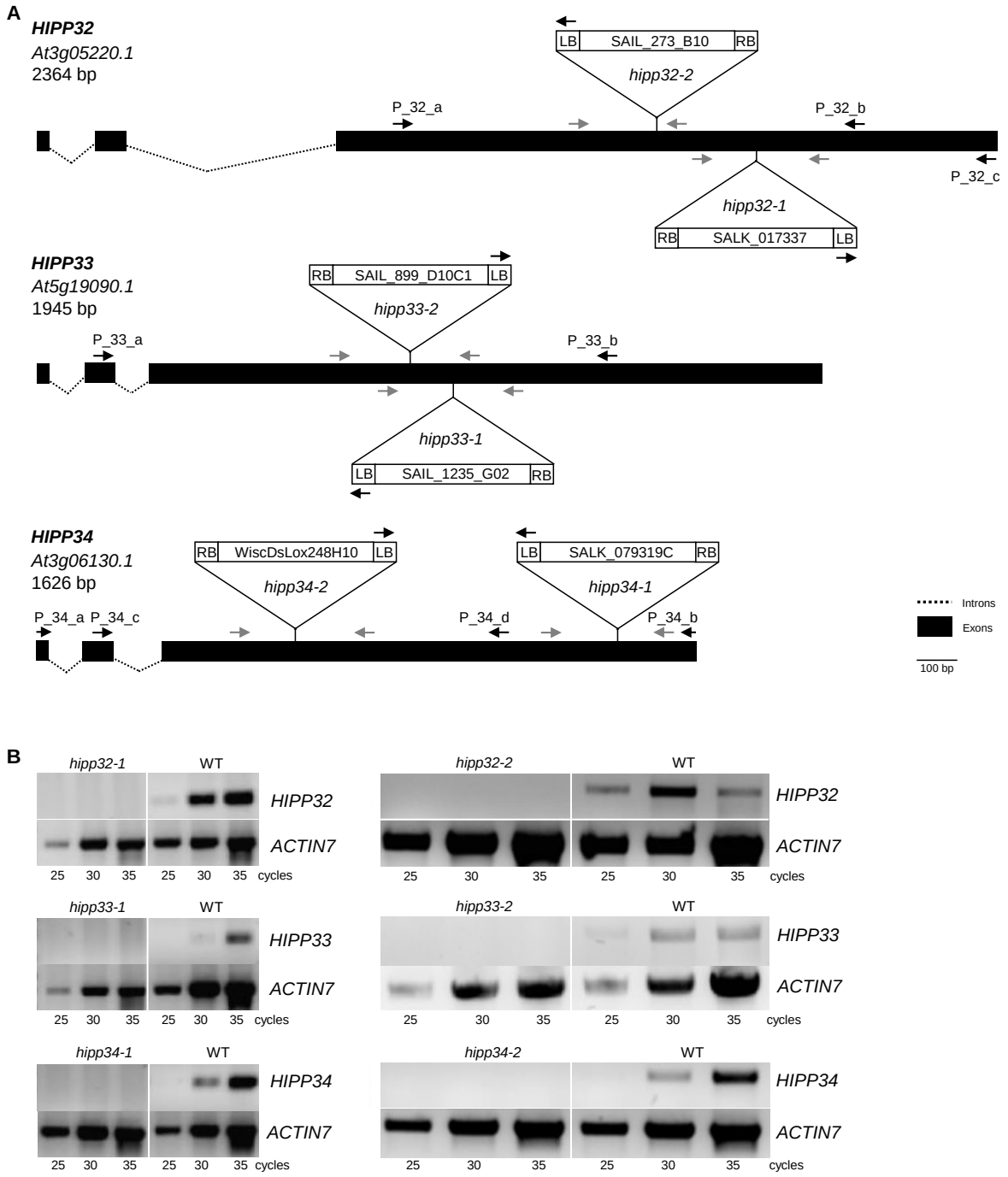

Figure 19. Molecular characterization of *hipp* T-DNA insertion alleles.
(A) Gene structure and positions of T-DNA insertions in the *hipp* mutants. Shown are only the first splicing variants from two (*HIPP32*) or three (*HIPP33* and *HIPP34*) variants annotated by The *Arabidopsis* Information Resource (TAIR; October 2019). Black arrows represent position of gene-specific primers (P) and left border T-DNA-specific primers (LB) used for genotyping. The exact insertion sites were determined by DNA sequencing using the left border primer. T-DNA length not in scale. LB: left border; RB: right border. Gray arrows represent primer pairs used for RT-PCR. **(B)** *HIPP32, HIPP33* and *HIPP34* gene expression in the wild-type *Arabidopsis* (WT) and two different insertional mutants. RNA from 25-day-old plants (leaf and inflorescence) was used as template for the semi-quantitative RT-PCR using primers indicated in **(A)**. 25, 30 and 35 cycles per PCR reaction were performed. *ACTIN7* was included as a control.

To confirm that the isolated *hipp* T-DNA insertion lines represent knock-out mutants, semi-quantitative RT-PCR using gene-specific primers spanning the T-DNA insertion sites were performed based on RNA isolated from homozygous plants. RT-PCR analysis showed that no full-length transcripts were built in all analyzed mutants (Figure 19B), supporting the idea that the T-DNA insertions abolished the expression of the *HIPP* genes (Krysan *et al.*, 1990). The *hipp* insertional mutant lines *hipp32-2*, *hipp33-2* and *hipp34-2* were backcrossed to wild type in order to remove any possible additional mutations. Homozygous lines for each allele were ultimately established. These lines were used for all experiments performed within this doctoral thesis (unless otherwise stated) and will be referred to hereafter as *hipp32*, *hipp33* and *hipp34*. Given the high sequence homology among the analyzed HIPP proteins, it is very probable that the corresponding *HIPP* genes share a high degree of genetic and functional redundancy. Therefore, it was necessary to generate a set of higher-order mutants, including three *hipp* double- and one triple-mutants. For this purpose, crosses between individual *hipp* mutants were performed to generate the *hipp32,33* and *hipp33,34* double mutant lines. Since *HIPP32* and *HIPP34* are genetically linked, being situated only 300 kilobase pairs apart on the same chromosome, generating *hipp32,34* double mutant by crossing *hipp32* and *hipp34* would have been tedious and challenging. Hence another approach was followed to generate this double mutant combination (see section 3.3.2).

3.3.2 CRISPR/Cas9-based gene editing technique to generate *hipp32,34*

CRISPR/Cas9-based genome editing technology has been successfully used in the last years to modify a plethora of target genes in animals and plants. The editing technique relies on the RNA-guided DNA endonuclease's ability to induce DNA double-strand breaks at precise genomic sites specified by the sgRNA (Belhaj *et al.*, 2015). Besides the sgRNA, Cas9 requires a specific protospacer adjacent motif (PAM) consisting of nucleotides NGG (N, any base) situated directly downstream of the target sequence in the genomic DNA (Sternberg *et al.*, 2014). The Cas9-mediated DNA cleavage causes the activation of the endogenous DNA repair system in host cells, primarily via the non-homologous end-joining pathway (Voytas, 2013). However, the repair mechanisms are error-prone, leading to editing events, such as nucleotide deletions or insertions, thus producing mutations at the target genomic locus (Voytas, 2013).
Wang *et al.* (2015) developed an optimized CRISPR/Cas9 system for plants, in which they used the promoter of the egg cell-specific *EC1.2* gene to drive the expression of Cas9. They have shown that the specific expression of CRISPR/Cas9 in egg cells and one-cell stage embryos leads to the creation of homozygous or biallelic mutants in the T1 generation, thus shortening the time required to produce stable homozygous *Arabidopsis* mutants. This CRISPR/Cas9 system was selected to generate the *hipp32,34* double mutant line.

For this purpose, the *hipp34* T-DNA insertional mutant line (*hipp34-2*) was used to target mutations in the *HIPP32* gene. CRSPR-P v1.0 online tool was used to identify sgRNA guides, from which two sgRNAs – sg32 and sg71 – were selected, both having a predicted efficiency score of 99 (out of 100) and 4 potential off-targets (Figure 20A). Five and eight T1 lines transformed with CRISPR/Cas9 construct expressing the sgRNA32 and sgRNA71 respectively were selected. Since sgRNA32 did not contain any recognition site for a restriction enzyme, the targeted *HIPP32* locus in all five T1 plants was sequenced. However, no editing events were identified in the proximity of the Cas9 cleavage site (data not shown), suggesting that this guide RNA did not efficiently target Cas9 to produce DNA strand breaks. The T1 plants carrying the sgRNA71-CRISPR/Cas9 transgene were tested for the loss of recognition site of the *Bgl*II enzyme, which overlapped the Cas9 cleavage site. Four out of eight T1 plants showed partial loss of the *Bgl*II restriction site (Figure 20B), suggesting that these lines were heterozygous for the putative mutations at the *HIPP32* target sequence. However, no homozygous mutation was recovered among the analyzed T1 plants. Gene modifications caused by CRISPR/Cas9 method have been shown to be stably transmitted through the germ line to future generations (Feng *et al.*, 2014). Therefore, the heterozygous sgRNA71 T1 plants were selfed to obtainT2 progenies, from which homozygous T2 individuals were identified by testing for the loss of *Bgl*II recognition site (Figure 20C). The target *HIPP32* targeted locus was sequenced to identify the nature of the editing events (Figure 20D). In the sgRNA71 line #1 an insertion of ten nucleotides upstream and deletion of one nucleotide downstream of the Cas9 cleavage site took place, without leading to any frameshift mutation. In the sgRNA71 line #2 the Cas9-induced double strand breaks caused the excision of two nucleotide downstream of the Cas9 cleavage site, which were replaced by two random nucleotides, thus the reading frame was maintained. The deletion of three bases directly upstream of the PAM sequence identified in the line #5 did not generate any frameshift mutations. Only the insertion of one nucleotide upstream of the Cas9 cleavage site in line #3 led to a frameshift mutation, resulting in an incorrect amino acid sequence and premature termination of *HIPP32* translation (Figure 20E). Hence the sgRNA71 line #3 represented *HIPP32* mutant allele, named hereafter *hipp32-3*.

Several homozygous *hipp32-3* T2 plants were analyzed by means of PCR using *Cas9* specific primer, aiming to screen for Cas9-free plants. One of the identified Cas9-free plants was then backcrossed to wild-type *Arabidopsis*, to clean the genetic background from the possible off-target mutations. F1 plants, heterozygous for *hipp32-3* and *hipp34-2,* were crossed with *hipp33-2* to generate the *hipp* triple mutant plant. Homozygous *hipp32-3*, *hipp34-2* double mutant (hereafter referred to as *hipp32,34*) and *hipp32,33,34* triple mutant plants were isolated in F2 and F3 generation.

Four off-target sites were predicted for the Cas9 when designing the sgRNA71 guide. The off-targets' sequences were predicted to be localized within the exon region of the following genes:

AT5G19090, AT1G29000, AT1G07340 and AT3G06130. To reassure that no off-target mutations had occurred in *hipp32-3*, the corresponding loci were amplified and analyzed by sequencing: no editing events were identified within the predicted off-target genes (results not shown).

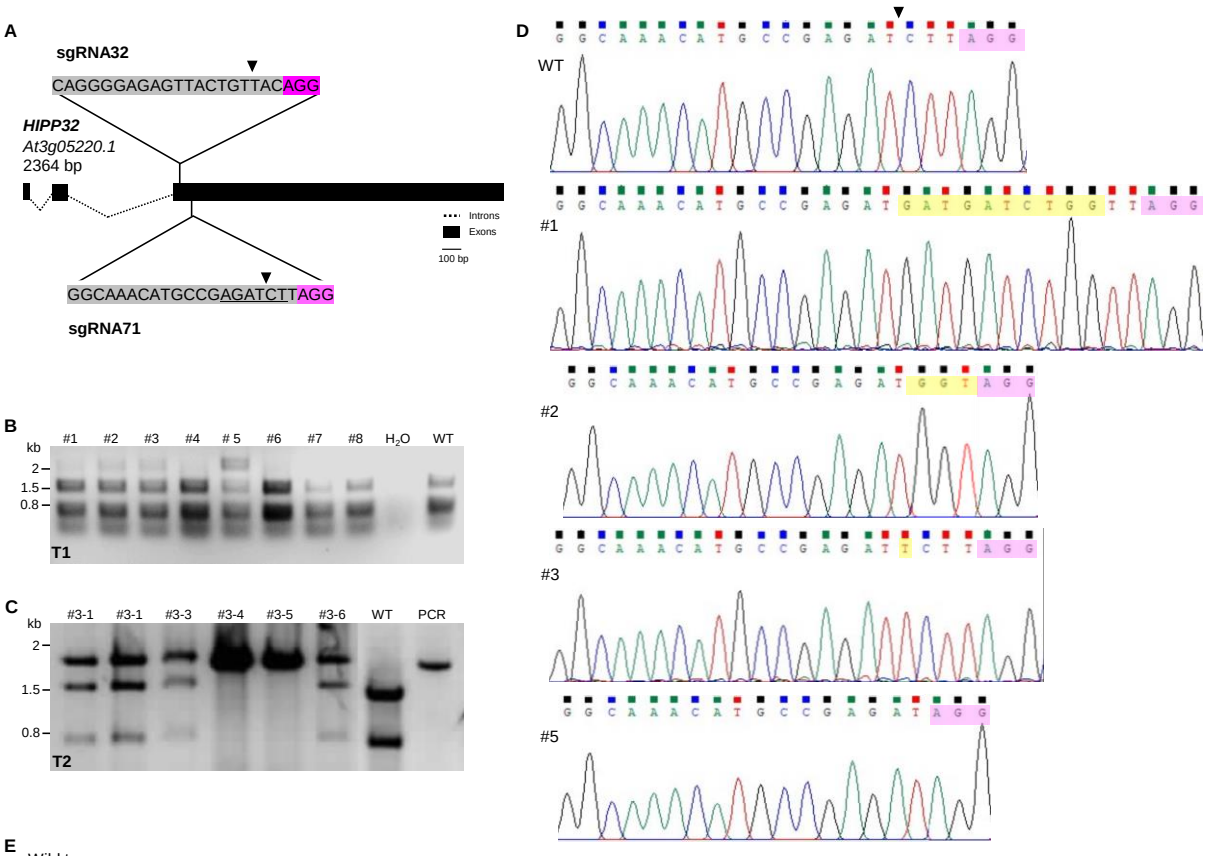

Figure 20. Generation of *hipp32* mutant allele via CRISPR/Cas9 system.
(A) *HIPP32* gene structure showing the sgRNA32 and sgRNA71 target sites. Wild-type sequences of sgRNA target sites are highlighted in gray, along the neighboring protospacer-adjacent motif (PAM), in magenta. The cleavage site of Cas9 is shown as a black triangle. The *Bgl*II recognition site within the sgRNA71 sequence is underlined. **(B)** Restriction enzyme site-loss assay: 4 out of 8 sgRNA71 T1 plants showed partial loss of the restriction site. **(C)** Result of the *Bgl*II digestion assay, exemplified in T2 line #3: #3-4 and #3-5 sgRNA71 plants showed total loss of the restriction site. **(D)** DNA-sequencing chromatograms illustrating the editing events at the sgRNA71 locus. Insertions are highlighted in yellow, PAM in purple. (**E**) The single nucleotide insertion in line #3 leads to a frameshift mutation and premature termination of the translation (highlighted in blue).

3.4 Loss-of-function of cluster-III *HIPP* genes leads to multiple phenotypic and developmental alterations during plant growth

GUS expression analysis showed that the cluster-III *HIPP* genes are differentially expressed, implying that distinct and specific developmental and physiological functions are controlled by each *HIPP* gene. However, the molecular and genetic analyses pointed towards a high level of redundancy among them. In order to shed light on the functional roles the individual HIPPs might fulfil during plant development, all established *hipp* mutant lines – single, double and triple mutant – were morphologically analyzed, aiming to determine the phenotypic changes caused by the loss-of-function of the *HIPP* genes.

3.4.1 Rosette morphology and leaf patterning are differently affected in *hipp* mutants

Leaves can be considered the most important organs for plants since they are indispensable players in the process of photosynthesis and thus enable plant growth. In angiosperm plants, leaf formation originates from the cells flanking the shoot apical meristem (Barton, 2010) and there are a plethora of factors, such as phytohormones and transcriptional regulators, that distinctly influence different stages during leaf development and growth (Bar and Ori, 2014).
In order to find out whether *HIPP* genes are involved in the process of leaf development, the leaf phenotype of the *hipp* mutants was characterized. Figure 21A shows representative images of the rosettes of 3.5-week-old *hipp* plants: *hipp32* and *hipp33* rosettes and leaves were smaller than those of wild-type plants, as determined by measuring the rosette diameter and leaf blade area, whereas the lack of *HIPP34* alone did not affect the leaf development (Figure 21B, C). Further reduction in rosette size was observed in *hipp32,33* in comparison to the respective single mutants and to a greater extent in *hipp32,33,34* (Figure 21A, B). In contrast, both the rosette size and leaf blade area of double mutants *hipp33,34* and *hipp32,34* were not or only little altered, implying thar *HIPP32* and *HIPP33* act redundantly to regulate rosette and leaf size in *Arabidopsis*. The leaf blade area was significantly reduced in *hipp32,33* in comparison to *hipp32* and *hipp33* (Figure 21C). Unlike in the case of rosette size, the reduction was not further enhanced in *hipp32,33,34,* suggesting that *HIPP34* might play opposite role in controlling leaf development than *HIPP32* and *HIPP33*. Furthermore, the lack of *HIPP* genes caused not only changes in leaf size, but also in leaf shape. Particularly *hipp32* and *hipp33* formed leaves with serrated margins (Figure 21A, D). In addition, the leaf blades of *hipp32,33* and *hipp32,33,34* were narrower than those of wild-type plants. These phenotypical traits were more prominent in higher order mutants, suggesting that cluster-III *HIPPs* are redundantly involved in controlling leaf shape.

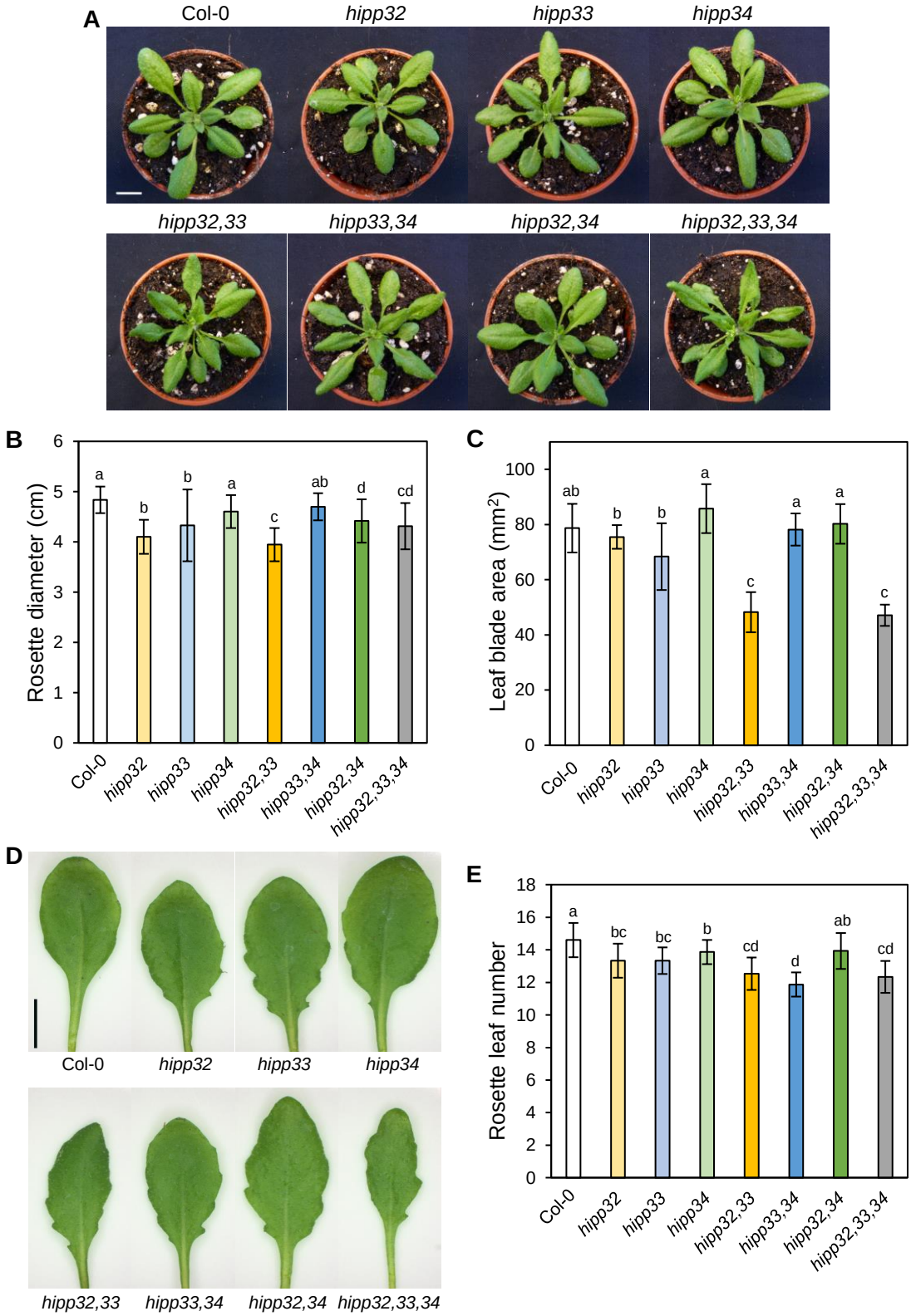

Figure 21. Loss of *HIPP* genes causes changes in rosette leaf development.
(A) Rosettes of *hipp* plants grown under standard conditions. Data show the average rosette diameter of 3.5-week-old plants **(B)**, the surface area of the 7th leaf at bolting **(C)** and the average number of rosette leaves formed during the vegetative growth phase **(E)**. Values represent means ± SD (n = 10-15). Different letters indicate statistically significant differences as evaluated by analysis of variance (one-way ANOVA) followed by Wilcoxon post hoc test ($p < 0.05$). The serration phenotype occurring in *hipp* mutants as compared to wild type is shown based on the 7th rosette leaf **(D)**. Scale bar = 1 cm.

Another morphological alteration observed in the loss-of-function *hipp* plants was the number of rosette leaves formed during the vegetative growth phase (Figure 21E). All single mutant plants formed less rosette leaves than wild type, with an additive effect occurring in the double mutant *hipp33,34*, implying overlapping functions among all three *HIPP* genes, with *HIPP33* being the major player.
Taken together, the rather roughly characterized leaf phenotypes observed in *hipp* mutant plants suggest that the *HIPP* genes might be involved in multiple pathways which control leaf development and morphogenesis.

3.4.2 Distinct double *hipp* mutants and the triple mutant display changes in shoot development

Not only leaves, but all above-ground aerial plant organs are generated by the shoot apical meristem, the activity of which is dynamically controlled by a complex gene regulatory network consisting of signaling molecules, such as plant hormones, and key transcription factors that tightly act together to ensure continuous plant growth and organogenesis (Ha *et al.*, 2010).
Lack of cluster-III *HIPP* genes led to several alterations during the reproductive shoot development of *Arabidopsis* (Figure 22). The loss of individual *HIPP* genes did not affect the plant stature, however the primary inflorescence height was similarly increased in both *hipp33,34* and *hipp32,33,34* (Figure 22A, B), suggesting that *HIPP33* and *HIPP34* function redundantly to regulate shoot height, whereas *HIPP32* appears to not contribute to this trait.
Overlapping functions between *HIPP32* and *HIPP33* can be concluded based the data obtained from analyzing the diameter of the inflorescence stem in *hipp* mutants (Figure 22C, D). The single mutants *hipp32* and *hipp33* developed thinner stems than wild-type plants and an additive effect was observed in *hipp32,33*, which was enhanced in *hipp32,33,34*. These observations suggest that all three *HIPP* genes redundantly function to regulate this particular shoot trait, however the *HIPP34* contribution is apparently slightly weaker.
Furthermore, *HIPP33* and *HIPP34* appeared to function in a redundant fashion to influence the formation of the axillary rosette branches (Figure 22E, F). Single mutant plants exhibited no change in the formation of number of axillary rosette branches. The number of branches remained unchanged also in *hipp32,33* and *hipp32,34*. In contrast, *hipp33,34* mutant plants formed on average 0.8 more branches than wild-type plants, and an enhanced effect was observed in *hipp32,33,34* mutants, which formed on average 1.9 branches more than wild-type plants, and one branch more than *hipp33,34* (Figure 22E). These observations suggest that the cluster-III *HIPP* genes share overlapping functions in negative regulation of the axillary branch formation, with the HIPP33 and HIPP34 being the major players in this regard.

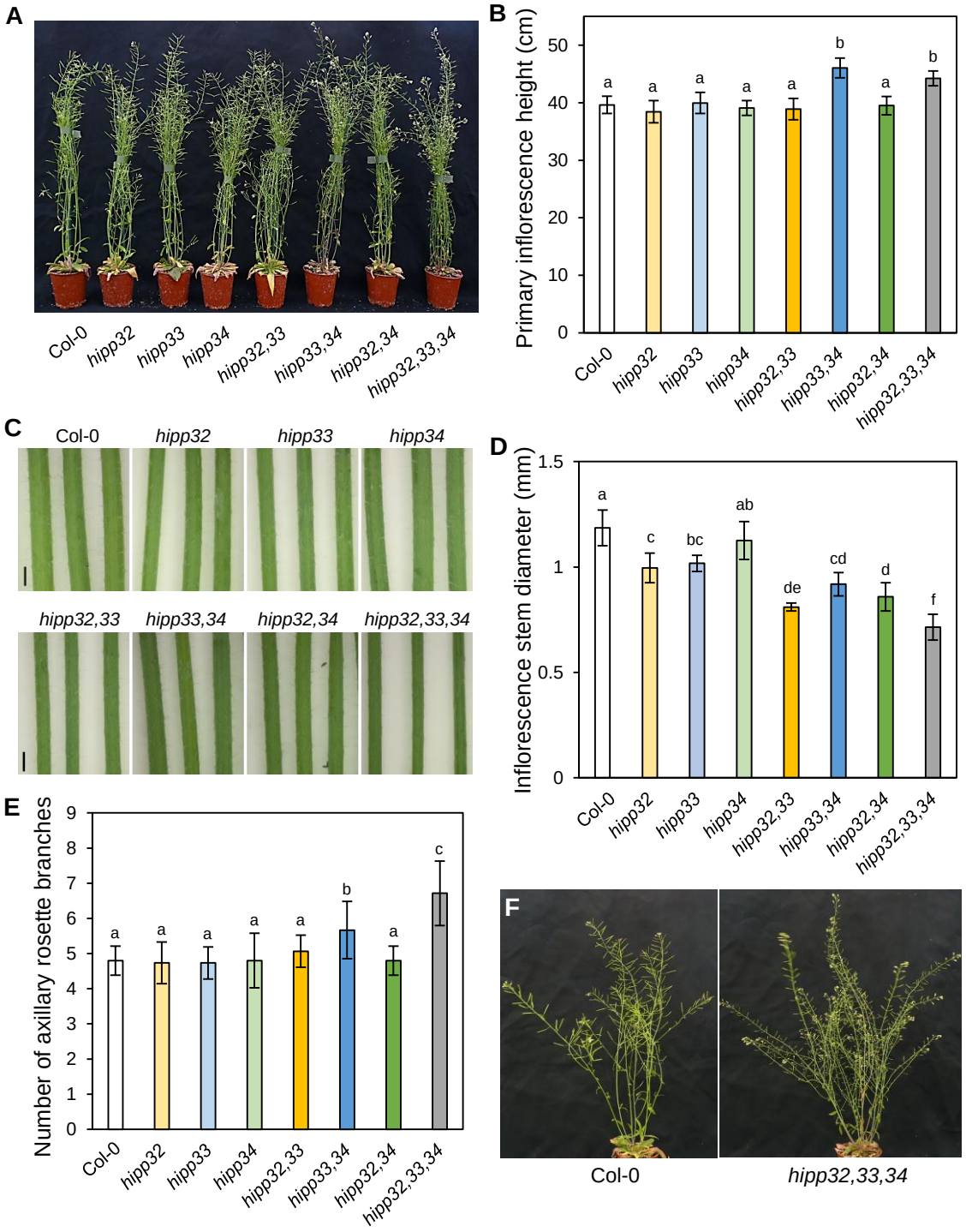

Figure 22. Cluster-III *HIPP* genes share partially overlapping functions during shoot growth. **(A)** 7-week-old wild-type (Col-0) and *hipp* mutant plants grown under standard conditions. **(B)** Data show the height of inflorescence stems of *hipp* mutant plants compared to wild-type plants at the end of the life cycle. Values represent means ± SD (n = 15). **(C)** Inflorescence stem (1 cm above the rosette level) of 4-week-old plants. Scale bars = 1 mm. **(D)** Inflorescence stem diameter measured 1 cm above the rosette level. Values represent means ± SD (n = 5). **(E)** Double mutant *hipp33,34* and triple mutant *hipp32,33,34* plants develop more axillary rosette branches than wild type. Values represent means ± SD (n = 15). **(F)** Representative picture illustrating the increased rosette branching of *hipp32,33,34.* Different letters indicate statistically significant differences as evaluated by analysis of variance (one-way ANOVA) followed by Wilcoxon post hoc test ($p < 0.05$).

3.4.3 Overlapping functions of cluster-III *HIPP* genes during the reproductive growth

After germination, flowering plants undergo two major growth phases during their life cycle: the vegetative phase, in which the photosynthetic capacity is increased, thus enabling the increase in size and mass, and the reproductive phase, in which the vegetative shoot apical meristem undertakes the inflorescence meristem activity to produce flowers, thus allowing the plant to reproduce (Huijser and Schmid, 2011). Molecular aspects controlling the determination of meristem identity and the switch from vegetative to reproductive phase have been intensively investigated in the last decade. The lack of cluster-III *HIPP* genes seems to have several consequences on the reproductive development of *Arabidopsis*, as it can be concluded from the following.

3.4.3.1 *HIPP* genes regulate the flowering time

To investigate whether the loss of *HIPP* genes affects the flowering in *Arabidopsis*, the flowering time was determined for *hipp* mutant plants grown under long-day (LD) and short-day (SD) conditions. Figure 23A illustrates the early flowering phenotype, occurring in most of *hipp* mutants grown under LD conditions. *hipp33* and *hipp34,* flowered on average 1.5 days in advance of wild-type plants (Figure 23B). This phenotype was enhanced in *hipp33,34* double mutant, which started to flower significantly earlier than *hipp33*, but not than *hipp34* (Figure 23B). *hipp32,33* flowered earlier than wild type, but not earlier than *hipp33*, whereas no difference was observed between *hipp32,34* and wild-type plants in this regard (Figure 23B). In contrast, the triple mutant *hipp32,33,34* flowered at the earliest time point, yet the average day to bolting did not significantly differ from that of *hipp33,34* (Figure 23B). These results imply that mainly *HIPP33* and *HIPP34* are involved in the repression of flowering time, whereas *HIPP32* has no or weak influence on this process.

Interestingly, the early flowering phenotype of *hipp* plants was less pronounced under SD conditions (Figure 23C). Neither *hipp33* nor *hipp34* flowered earlier than wild type. Although, the early flowering phenotype of *hipp32,33, hippp33,34* and *hipp32,33,34* tendentially occurred under SD, no statistically significant differences among these genotypes were observed (Figure 23C). This implies that cluster-III *HIPP* genes control flowering initiation depending on the day light period.

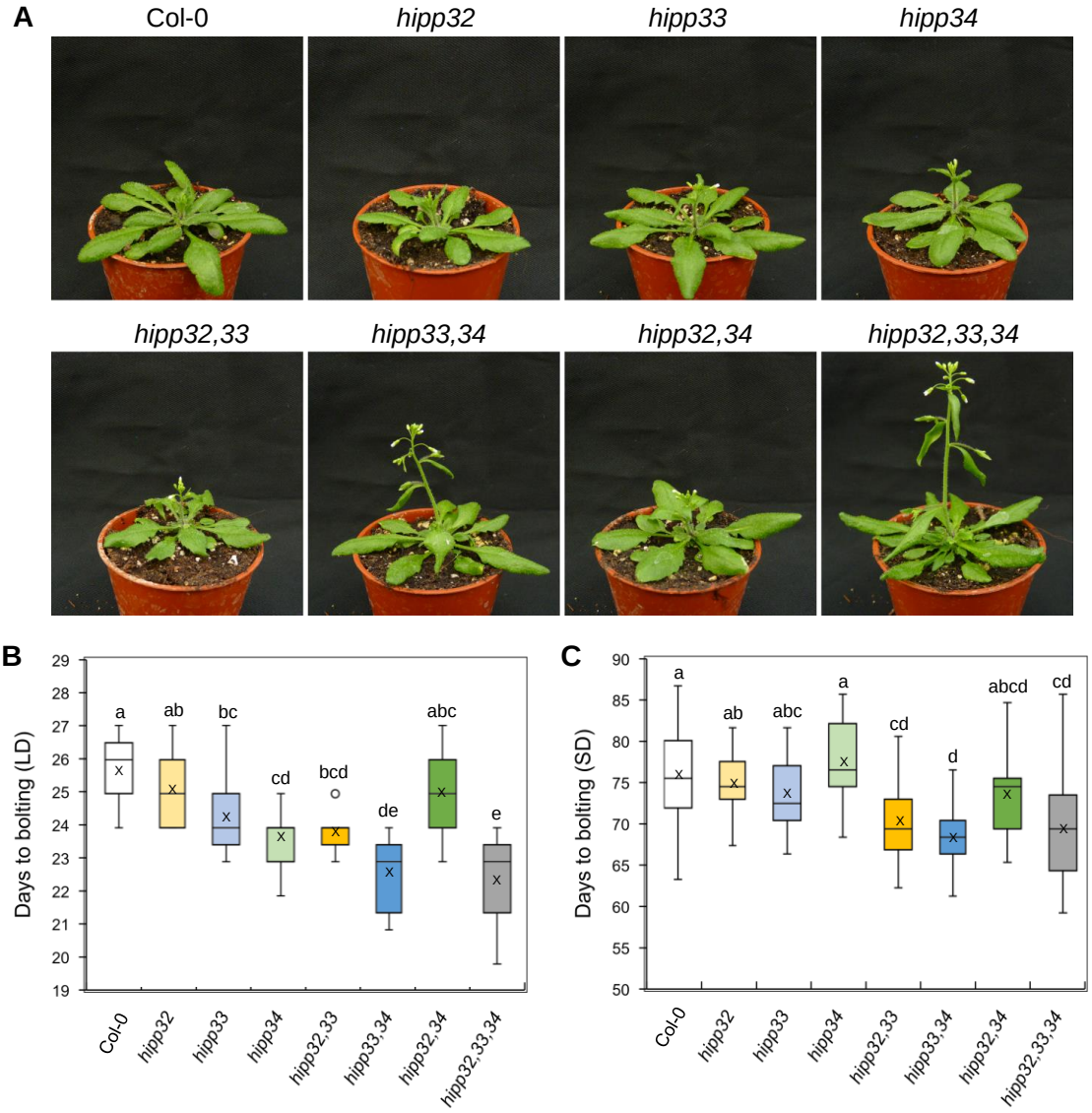

Figure 23. Loss of *HIPP* genes induces early flowering of *Arabidopsis*.
(A) Representative images of 4-week-old wild-type (Col-0) and *hipp* plants grown under LD conditions. Boxplots illustrate the number of days to bolting of wild-type and *hipp* plants grown under LD **(B)** and under SD **(C)** conditions. The segment inside the rectangle shows the median and the cross the mean (n = 15). Different letters indicate significant differences between groups as evaluated by analysis of variance (one-way ANOVA) followed by Wilcoxon post hoc test ($p < 0.05$).

3.4.3.2 Inflorescence meristem activity is altered in *hipp* mutants

After the transition to the reproductive growth phase, the indeterminate inflorescence meristem starts producing flowers, secondary inflorescence meristems and cauline leaves (Wagner *et al.*, 1999). Hence, the number of flowers directly correlates with the activity of the inflorescence meristem, which can be inferred from the number of siliques formed and the rate of formation during the life cycle of a plant.

The inflorescences of *hipp33,34*, *hipp32,34* and *hipp32,33,34* appeared to be larger than those of wild-type plants (Figure 24A). Considering the increased inflorescence sizes, the question arose whether the loss of *HIPP* genes affects the inflorescence meristem activity.

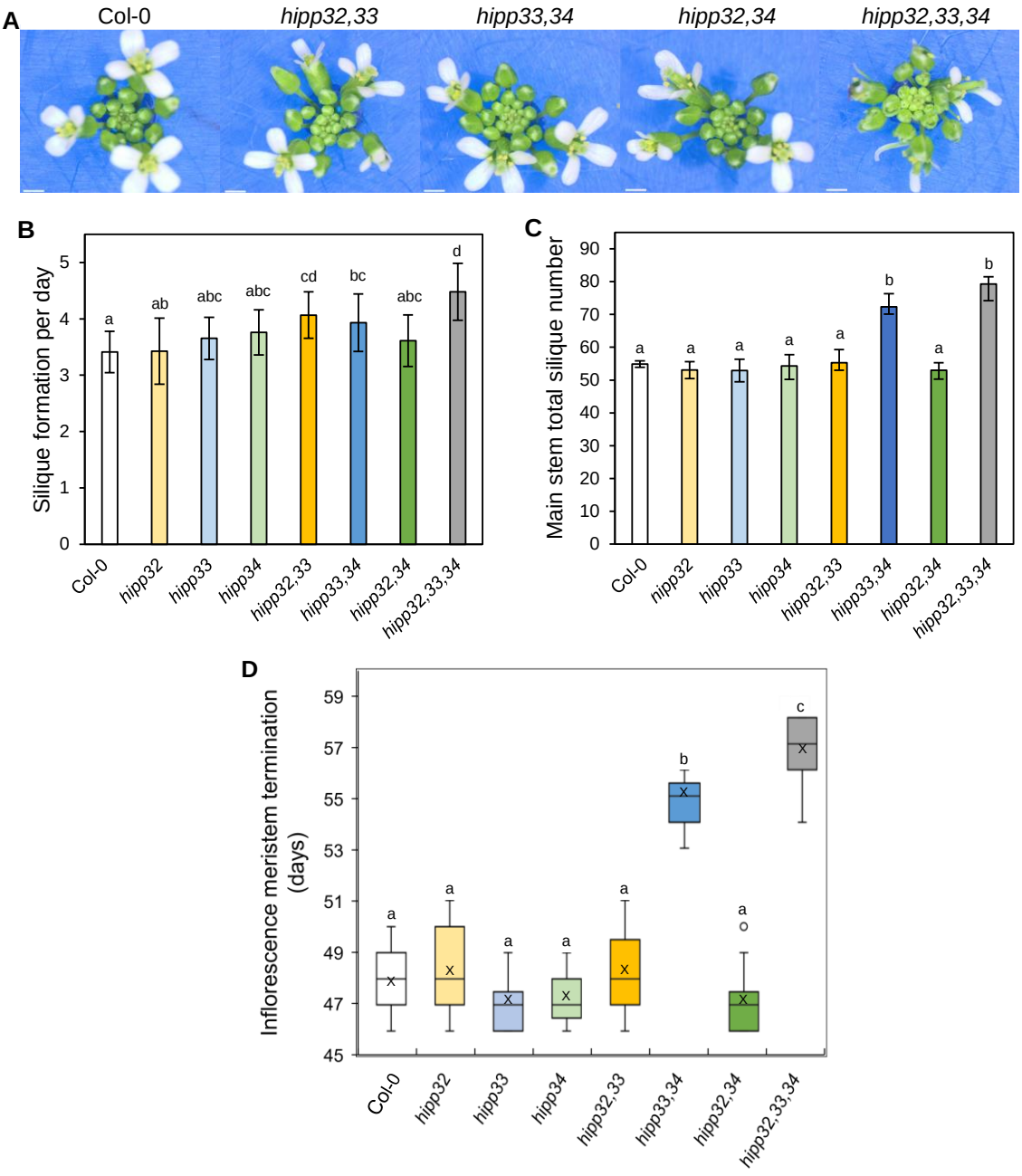

Figure 24. Inflorescence meristem activity is increased in *hipp* mutant plants.
(A) Inflorescences of the 5-week-old wild-type (Col-0) and *hipp* mutant plants. Scale bars = 1 mm. **(B)** Silique formation rate. Values represent means ± SD (n = 15). **(C)** Number of siliques on the main inflorescence stem during one life cycle. Values represent means ± SD (n = 15). **(D)** Time of flowering termination of wild-type and *hipp* plants. The segment inside the rectangle shows the median and the cross the mean (n = 15). Different letters indicate significant differences between groups as evaluated by analysis of variance (one-way ANOVA) followed by Wilcoxon post hoc test ($p < 0.05$).

To investigate the inflorescence meristem activity, the silique rate formation was determined by counting the siliques on the main stem at three different time points during the inflorescence growth. Wild-type plants formed on average 3.5 siliques per day, whereas *hipp32,33* and *hipp33,34* produced up to 0.4 silique more. The most significant increase by 1 silique per day

observed in *hipp32,33,34* mutants (Figure 24B), suggesting functional redundancy among *HIPP* genes, with *HIPP33* having the largest effect in this regard.

Furthermore, the total number of siliques on the inflorescence stem, determined after the formation of the last flower, was increased by ~ 30% in *hipp33,34* and ~ 40% in *hipp32,33,34* mutants (Figure 24C). The other *hipp* mutant plants formed on average as many siliques as wild-type plants. Both the increased rate at which *hipp33,34* and *hipp32,33,34* produce flowers as well as the increased silique number point towards an enhanced activity of the inflorescence meristem of these mutants compared to that of wild-type plants.

In addition to their increased meristematic activity, both *hipp33,34* and *hipp32,33,34* plants were longer reproductively active than wild-type plants (Figure 24D). *hipp33,34* produced flowers for 7, and *hipp32,33,34* for 10 more days, respectively, suggesting that the increase number of formed siliques (Figure 24C) was in part due to longer reproductive growth. Single *hipp* mutant lines and the other combinations of double mutants did not show any increase in their reproductive phase.

Taken together, these results indicate that all cluster-III *HIPPs* redundantly contribute to negatively regulate inflorescence meristem activity. However, *HIPP33* and *HIPP34* have a stronger effect than *HIPP32*.

3.4.3.3 Lack of *HIPP* genes affects floral organ formation, female fertility and seed production

Undifferentiated cells at the floral meristem flanks must properly differentiate in order to generate floral organs (Bowman *et al.*, 2012). No signs of failed differentiation occurred in *hipp* single mutants (images not shown). In contrast, the development of higher order *hipp* mutant flowers was affected. Figure 25A illustrates that flowers of *hipp* double mutants and to a greater extent those of *hipp* triple mutants were smaller compared to wild-type flowers, as evident at developmental stages 12, 13 and 15 (Smyth *et al.*, 1990). *hipp* mutant flowers developed smaller and narrower petals, lacking the paddle-shaped form characteristic for wild-type petals. Particularly the petals of *hipp32,33,34* were small and misshapen, probably due to cell division and patterning defects. Additionally, *hipp32,33,34* flowers exhibited further developmental defects, such as fused sepals and petals, reduced stamen numbers, fused stamens, or stamens with two or three anthers (images not shown).

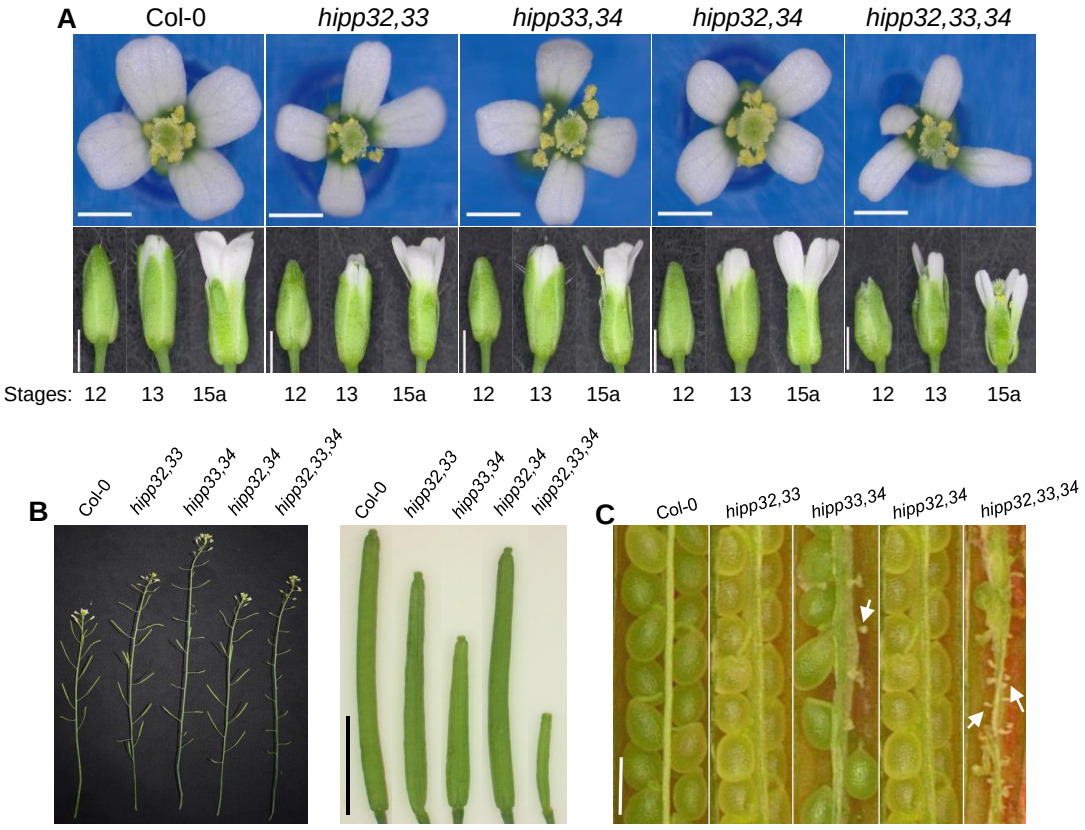

Figure 25. Cluster-III *HIPP* genes influence flower development and fertility in *Arabidopsis*.
(A) Top view of wild-type (Col-0) and *hipp* double and triple mutant flowers (upper row) and flowers at different developmental stages (bottom row). Scale bar = 1 mm. **(B)** Siliques on the inflorescence stem of 5-week-old plants: *hipp33,34* and *hipp32,33,34* siliques are considerably shorter than those of wild type. Scale bar = 0.5 cm. **(C)** Magnified sections of an open silique. White arrows indicate aborted ovules. Scale bar = 1 mm.

The decrease in flower size was reflected by the size of the siliques formed in the *hipp* mutants (Figure 25B). While the siliques in *hipp32,33* were only slightly smaller compared to wild type, the *hipp33,34* silique size was severely affected. An additive effect was observed in *hipp32,33,34* plants, whose siliques reached only about 30% of the will-type silique length.
In addition to the altered silique development, the seed production in *hipp33,34* and particularly in *hipp32,33,34* was significantly affected; the siliques of *hipp33,34* were filled around 60%, whereas those of *hipp32,33,34* rarely contained any seed (Figure 25C). The decreased seed production observed was apparently larger, as a consequence of the high ovule abortion rate occurring in this mutant (Figure 25C). This led to extremely low seed yields – between 20 and 50 seeds per plant were produced.
The ovule abortion observed in *hipp33,34* and *hipp32,33,34* could be the consequence of different developmental defects occurring during the earlier phase of flower development and fertilization. On one hand, the ability of the *hipp* plants to self-pollinate was impaired since the anther filaments fail to sufficiently elongate, and the anther could not reach the stigma at the

time of anthesis (Figure 26A). Particularly *hipp32,33,34* developed short stamen filaments relative to the gynoecium length (Figure 26A). On the other hand, the anthers of *hipp33,34* and to a greater extent of *hipp32,33,34* produced lower amounts of pollen (image not shown). Furthermore, the delayed pollen ripening relative to stigma maturation often observed in *hipp32,33,34* flowers contributed to the extreme low self-pollination rate.

In order to investigate whether the low fertility rate observed in *hipp33,34* and *hipp32,33,34* was caused by male or female infertility, a series of pollination tests were performed. To counteract the low self-pollination rate caused by the reduced stamen length and pollen number, the stigmas were additionally hand-pollinated with sufficient pollen amount of the same genotype. Several days after the hand-pollination, the silique elongation was analyzed (Figure 26B). The siliques of both *hipp33,34* and *hipp32,33,34* failed to expand as compared to wild-type siliques, indicating that either the pollens were defective, or the development of the female gametophyte was impaired.

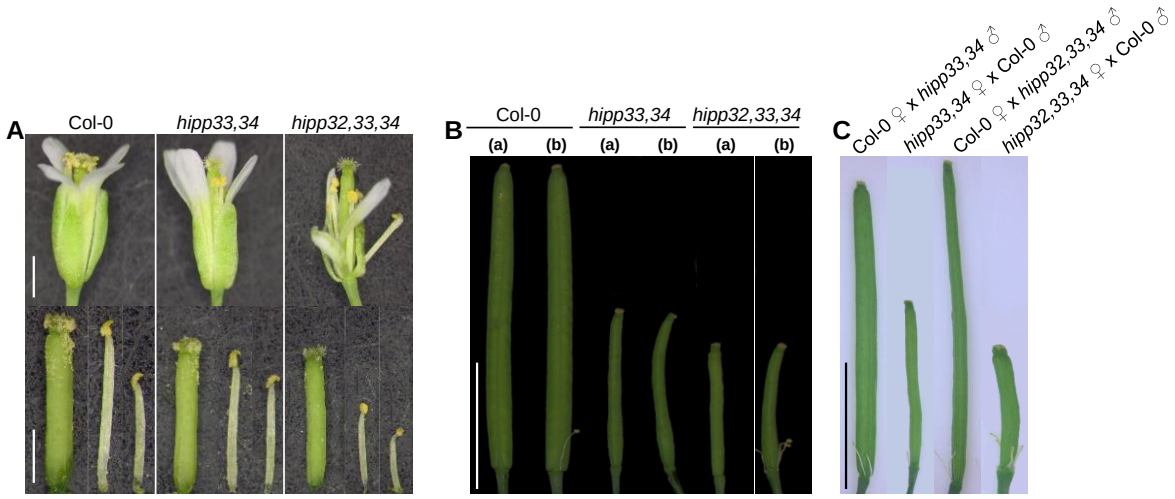

Figure 26. **The development of reproductive organs is affected in *hipp33,34* and *hipp32,33,34*.** **(A)** Side view of individual flowers at the pollination stage (upper row) showing the length differences between pistil and stamens in *hipp* mutant plants compared to wild-type (Col-0). The stamens of *hipp* triple mutants are considerably shorter than the pistil (bottom row). Scale bars = 1 mm. **(B)** *hipp33,34* and *hipp32,33,34* are infertile: the siliques failed to expand when in addition to self-pollination (marked with **a**) the stigmas were hand-pollinated with pollen of the same genotype (marked with **b**). Scale bar = 5 mm. **C)** Crosses between wild-type (Col-0) with *hipp33,34* and *hipp32,33,34* demonstrate the female-specific sterility of *hipp33,34* and *hipp32,33,34* plants. Scale bar = 5 mm.

Cross pollination of *hipp33,34* with wild-type pollen did not rescue the seed development and silique elongation (Figure 26C). In contrast, wild-type siliques developed normally after cross pollination with *hipp33,34* pollen (Figure 26C), suggesting that the *hipp33,34* are female sterile. Similar results were observed after cross pollinations between wild-type and *hipp32,33,34* (Figure 26C), thus supporting the apparent crucial role of *HIPPs* in regulating female gametophyte development.

3.4.3.4 Seed and embryo development are severely affected in *hipp32,33,34* mutants

The morphology of a mature seed is the result of a synchronized and coordinated regulation between the growth of three genetically distinct structures within the seed: the embryo, the endosperm and the seed coat (Orozco-Arroyo *et al.*, 2015).

Inspection of seed morphology revealed two phenotypical alterations occurring in *hipp* mutant seeds. The *hipp33,34* seeds were bigger than wild-type seeds, and those of *hipp32,33,34* exhibited an abnormal morphology, lacking the prolate spheroid shape specific for a normally developed seed (Figure 27A, B; Robert *et al.*, 2008). Neither the seed size nor the seed shape of *hipp* single mutants (data not shown) and the other two double mutants were changed.

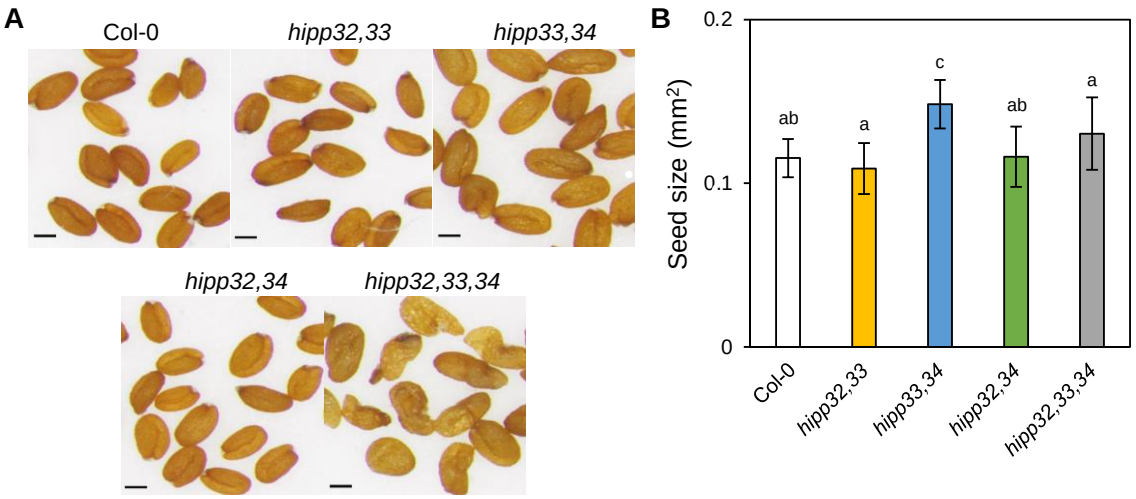

Figure 27. The lack of cluster-III *HIPP* genes affects the seed morphology.
(A) Mature seeds of wild-type (Col-0), *hipp* double and triple mutant plants. Scale bar = 0.2 mm. **(B)** Seed size of mature seeds. Values represent means ± SD (n=15). Different letters indicate significant differences between groups, evaluated by analysis of variance (ANOVA) followed by Tukey honest significant difference (HSD) post hoc test ($p < 0.05$).

To assess whether the altered seed morphology was linked to changes in embryo development, the morphology of mature embryos, dissected from ripe seeds, was analyzed. Confocal microscopy analysis revealed that the increased *hipp33,34* seed size was caused by the increased size of the embryos, determined by measuring the length of the embryonic axis and the length of the cotyledons (Figure 28). As expected, there was no difference between the size of *hipp32,33*, *hipp32,34* and wild-type embryos (Figure 28).

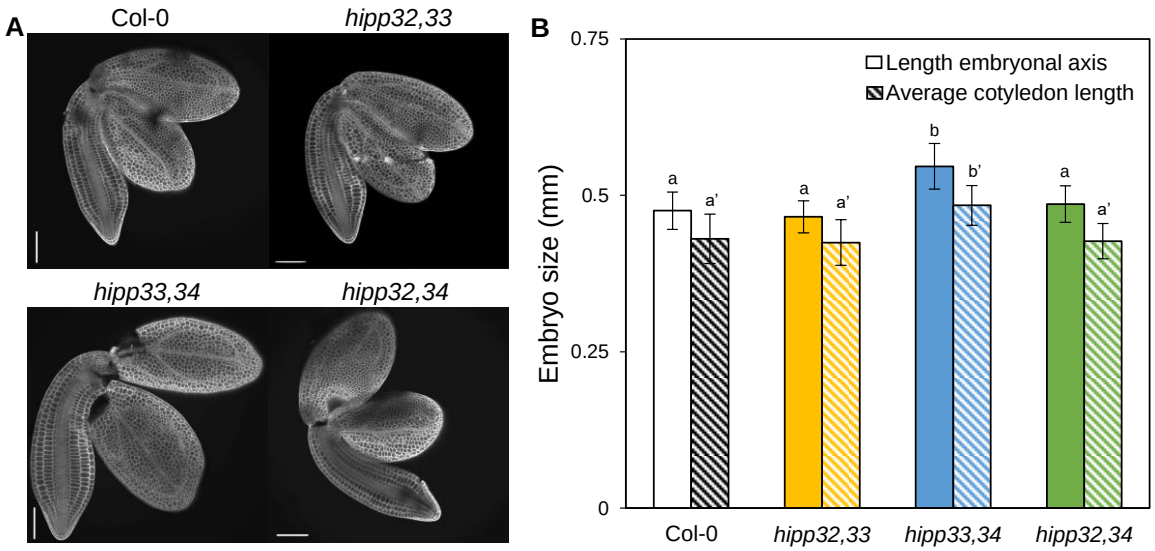

Figure 28. **Overview of embryo morphogenesis in different *hipp* double mutants.**
(A) Mature embryos of wild-type (Col-0) and of *hipp* double mutants stained with pseudo-Schiff propidium iodide (mPS-PI). Scale bars = 100 µm. **(B)** Embryo size determined by measuring the length of the embryonic axis and the length of the cotyledons. Values represent means ± SD (n = 15-22). Different letters indicate significant differences between groups as evaluated by analysis of variance (ANOVA) followed by Tukey honest significant difference (HSD) post hoc test ($p < 0.05$). Non-dashed and dashed letters emphasize the two different parameters statistically evaluated.

In contrast to the unchanged shape of mature embryos of *hipp* double mutants, the embryos of *hipp* triple mutants exhibited various alterations in their shape. Figure 29 illustrates representative phenotypes of *hipp32,33,34* embryos originating from ripe seeds of a single plant (circa 25 seeds were produced and analyzed). Embryos of *hipp32,33,34* exhibited shorter embryonic axis relative to the cotyledon size (Figure 29B), smaller or rudimentary cotyledons, (Figure 29D-H), as well as partially fused cotyledons (Figure 29H). Some of the observed embryonal phenotypes imply that the embryos of *hipp32,33,34* might undergo incomplete or delayed development (Figure 29E, F), since their phenotypes resembled the embryos at the late torpedo stage (Capron *et al.*, 2009). Furthermore, embryos exhibited three cotyledons (Figure 29G) or developed only one cotyledon (Figure 29I), suggesting the relevance of cluster-III *HIPP* genes for cotyledon anlage patterning.

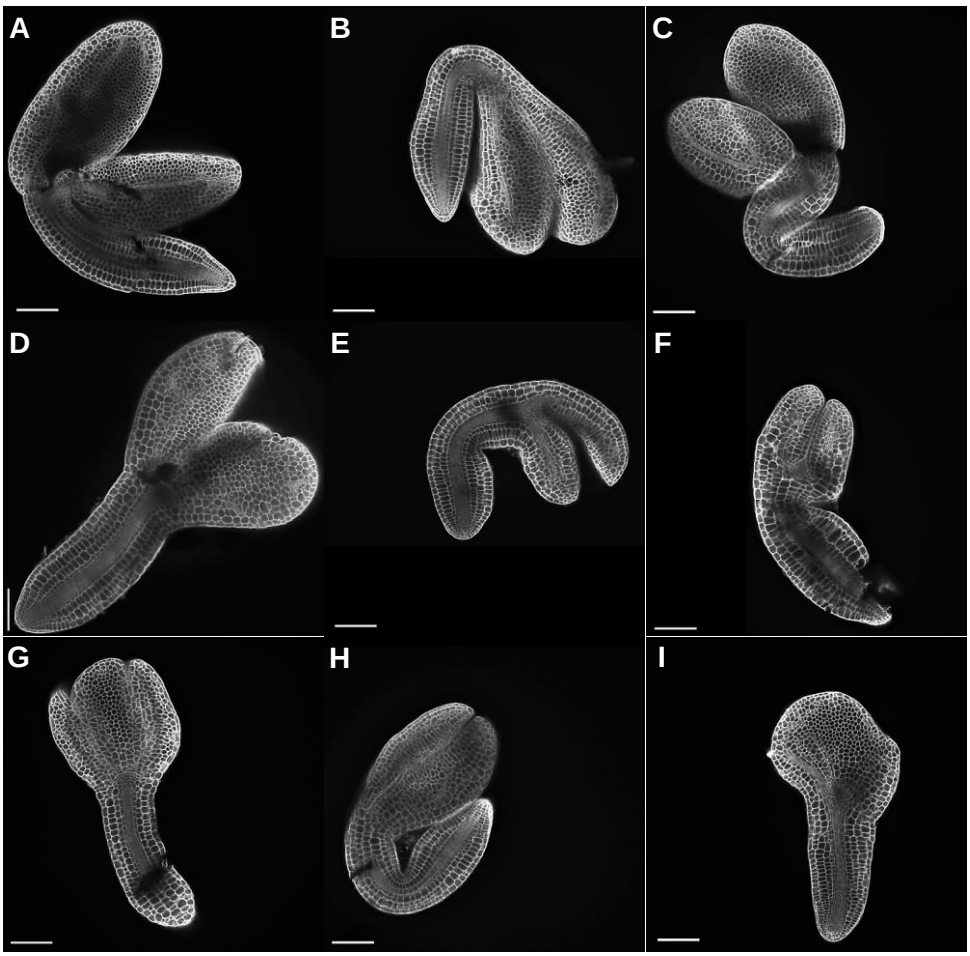

Figure 29. Embryo development is severely affected in *hipp32,33,34* mutants.
Mature embryos of wild-type **(A)** and representative phenotypes of *hipp32,33,34* **(B-I)** stained with pseudo-Schiff propidium iodide (mPS-PI). *hipp32,33,34* mutant embryos show a range of various phenotypes: short embryonic axis **(B)**, twisted embryonic axis **(C),** reduced cotyledon size **(D-H)**, two or three underdeveloped cotyledons **(F, G)**, partially fused cotyledons **(H)** or incompletely developed single cotyledons **(I)**. Scale bars = 100 µm.

A more detailed confocal analysis of the *hipp32,33,34* mature embryos revealed abnormal cell division pattern in both embryonic root and shoot apical meristems (Figure 30). The shoot apical meristem (SAM) of *Arabidopsis* consists of three layers (L1, L2 and L3) that become recognizable in post heart-stage embryos (Barton and Poethig, 1993; Meyerowitz, 1997). In mature embryos the provascular tissue is clearly visible within the cotyledon primordia and the cellular organization of hypocotyl and root meristem is completed. Thus, the complex tissue patterning is achieved. However, the cells in most tissues will complete differentiation after germination (Capron *et al.*, 2009). In comparison to wild-type embryos, the size of embryonic SAM in *hipp* triple mutant was dramatically increased (Figure 30A to 30D). In *hipp32,33,34* embryos with seemingly less overall severe patterning defects (Figure 30B), the SAM region was considerably enlarged: the L1 layer comprised eleven cells and L2 ten, in comparison to the seven- and six-cell L1 and L2 layer, respectively, in wild type (Figure 30A). The size of the

corpus was dramatically increased in this mutant embryo as well (Figure 30B, C). Furthermore, the SAM exhibited a dome-like shape, typical of later post-embryonic development, pointing towards premature cell proliferation. Triple *hipp* mutant embryos developing only one cotyledon exhibited increased SAM size as well (Figure 30D). Despite the rather difficult distinction of SAM and cotyledon primordia borders, it appeared that also in this case the SAM size was increased: up to nine cells made up the L1 and L2 layer (Figure 30D). The embryo depicted in Figure 30E exhibited as well only one cotyledon and its overall shape resembled rather that of an embryo at the bent-cotyledon stage, implying a delayed embryonic development. Furthermore, the organization of the SAM layers was less evident than in other *hipp32,33,34* defective embryos (Figure 30E).

Analogous to SAM, the pattern of the root apical meristem (RAM) is established during embryogenesis and consists of the four cells of the quiescent center (QC), stem cells concentrically surrounding the QC, termed initials, and the central root cap, columella (Capron *et al.*, 2009). The proper RAM establishment and maintenance requires a functional QC, in order to maintain stem cell identity in the surrounding stem cells (Capron *et al.*, 2009). Following germination, the basic radial pattern of RAM is maintained, however the stem cells will asymmetrically divide to produce daughter cells that differentiate in specific tissues with distinct functions (Dolan *et al.*, 1993). The RAM establishment during embryogenesis appeared to be severely affected in the *hipp* triple mutants as compared to wild-type embryos. *hipp32,33,34* embryos had a reduced putative radicle region and exhibited an overall abnormal cell patterning within the RAM, most evident were the disorganized columella initials (Figure 30B to 30E) and the indistinguishable QC cells (Figure 30C to 30E). Moreover, the embryonic RAMs of *hipp32,33,34* mutants were characterized by the abnormal presence of starch granules in the columella initials, distal to the putative QC (Figure 30A to 30E). These starch-containing plastids, called amyloplast, are typically found in differentiated columella root cells (Barlow *et al.*, 1984), implying thus a premature differentiation of the columella initials occurring in the *hipp32,33,34* mutants. Light starch accumulation was observed in the putative QC of *hipp32,33,34* root apex (Figure 30D), suggesting that the QC lost its identity. Interestingly, starch granules were formed in other cell types of the radicle as well (Figure 30E).

To sum up, these observations suggest apparent fundamental role of cluster-III *HIPPs* in regulating embryo pattern formation and development.

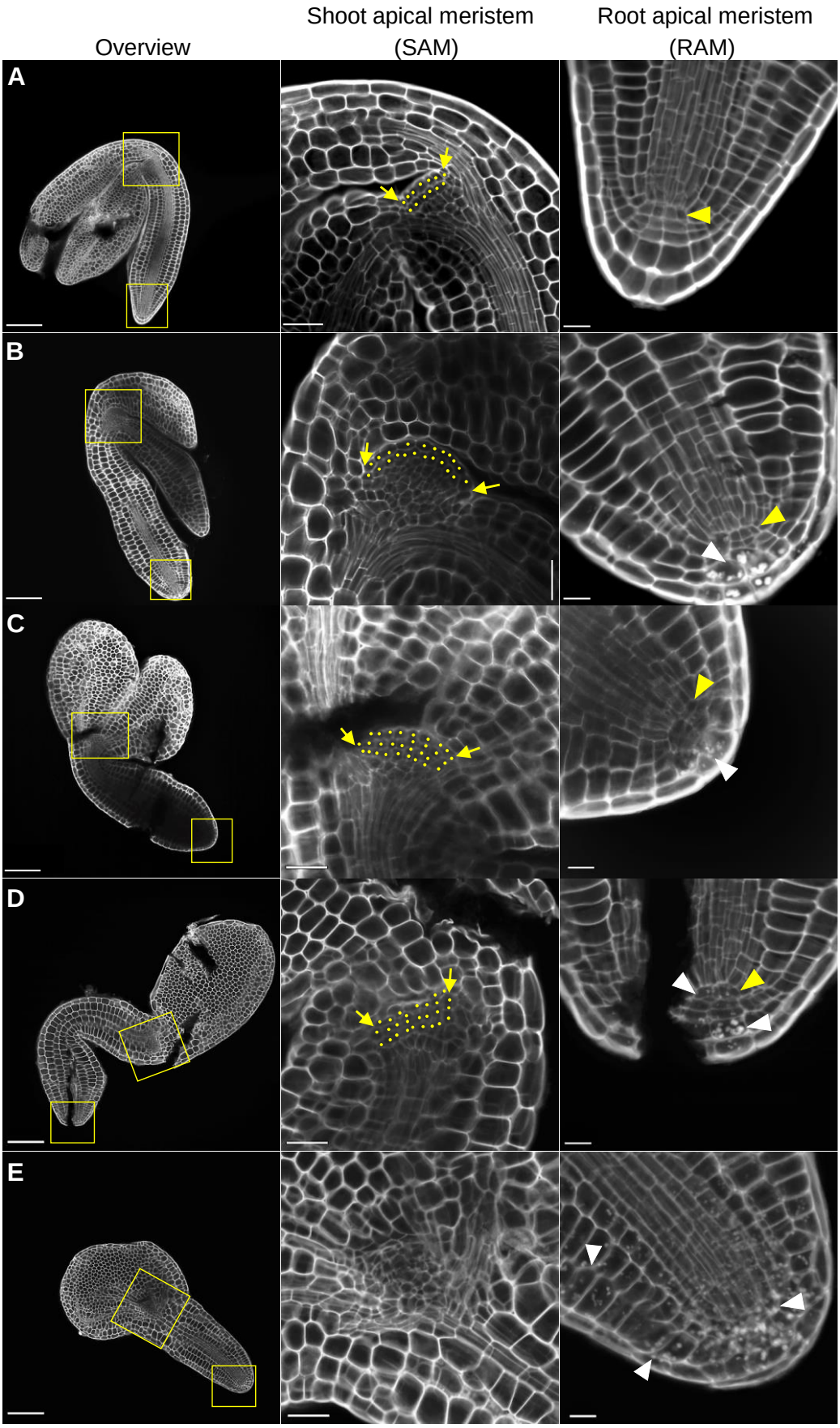

Figure 30. *HIPP* genes influence shoot and root meristem activity during embryogenesis.

Figure 30. Continued.
(A) Mature embryos of wild-type (Col-0) and different phenotypes of *hipp32,33,34* **(B-E)** stained with pseudo-Schiff propidium iodide (mPS-PI) as overview images (left column), magnifications of the shoot meristem (SAM; middle column) and magnifications of the radicle, including the root apical meristem (RAM; right column). Arrows indicate the boundary between cotyledons and SAM **(A-D)**. Yellow arrowheads in the right column indicate the quiescent center cells in wild-type **(A)** or their assumed position in *hipp* triple mutant **(B-D)**. White arrowheads indicate the starch granules in the quiescent center, columella cells **(B-E)** or throughout the entire radicle region **(E)**. Scale bars: overview = 100 µm, SAM = 25 µm and RAM = 10 µm.

3.4.3.5 Seeds of *hipp32,33,34* exhibit low germination ratio

In order to investigate whether the defects occurring during seed and embryo development affect seed germination, germination assays were carried out. Ripe seeds of *hipp* double and triple mutants along with wild type were germinated either on soil or *in vitro*. Prior to light exposure all seeds were stratified two days at 4 °C in the dark. Four days after transfer to light, the germination ratio was determined by counting the germinated seedlings with green cotyledons. No differences were observed between the germination rate of *hipp32,33*, *hipp32,34* and wild type regardless of the growth conditions (Figure 31). In contrast, the germination of *hipp33,34* seeds was reduced compared to wild type by ~10% when germinated on soil and ~20% *in vitro*, respectively. Less than 60% of *hipp32,33,34* seeds germinated on soil and only roughly 20% of seeds germinated on ½ MS medium. It is very probably, that the low germination ratios might be due to the defective embryonic development observed particularly in *hipp32,33,34* (section 3.4.3.4). However, the putative role of *HIPP* genes in redundantly controlling the germination process cannot be excluded.

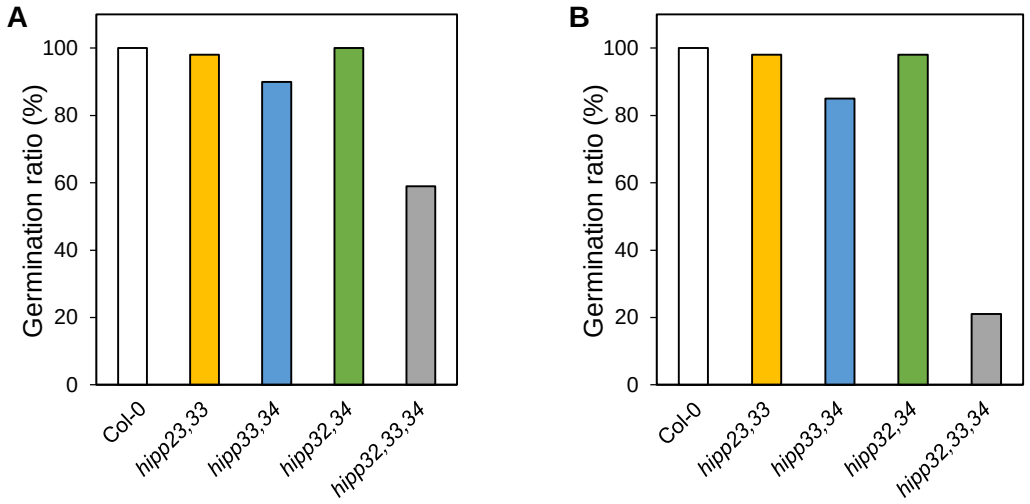

Figure 31. Seed germination is severely affected in *hipp32,33,34* mutants.
For germination assays wild-type (Col-0) and *hipp* seeds germinated on soil **(A)** and on ½ MS medium **(B)**. For each genotype and growth condition 100 seeds were sowed. Seeds were grown for 4 days upon a stratification for 2 days at 4 °C. Germinated seeds with green cotyledons were counted to determine the percentual germination rate.

3.4.4 Cluster-III *HIPP* genes regulate root meristem size and root growth

To assess the possible roles of *HIPP* genes during root growth, *hipp* mutant plants were grown *in vitro* and their root phenotype was analyzed. Figure 32 illustrates representative images of *hipp* single and *hipp* double mutant roots. The lack of *HIPP32* caused a decrease of ~30% in the primary root elongation in comparison to wild type (Figure 32B). Although, the primary root elongation of *hipp33* and *hipp34* was tendentially increased in comparison to wild type, the difference was not statistically significant. The lack of both *HIPP32* and *HIPP33* further decreased the primary root elongation by ~30% and ~50% relative to *hipp32* and to wild type, respectively (Figure 32B). This suggests that *HIPP33* acts synergistically to positively regulate root growth, yet its contribution is smaller as that of *HIPP32*, thus attributing HIPP32 the primary role in positively regulation root growth. The root length of *hipp33,34* was increased by ~15% relative to wild type, but it remained unchanged relative to the length of the respective single mutants, despite the evident tendency to form longer primary roots (Figure 32B). Interestingly, the loss of *HIPP34* suppressed the short root phenotype of *hipp32* as the root length of *hipp32,34* was comparable to wild type (Figure 32B), supporting the idea of *HIPP34* as negative regulator, thus implying an antagonistic interaction between *HIPP32* and *HIPP34* to regulate primary root growth.

Loss of both *HIPP33* and *HIPP34* genes caused a considerable decrease in lateral root (LR) number by ~30% in *hipp33* and *hipp34* in comparison to wild type, whereas the loss of *HIPP32* affected the LR formation to a lesser extent, by only ~13% (Figure 32C). Given that the primary root length of *hipp33* and *hipp34* mutants was comparable to wild type, the LR density was strongly reduced (Figure 32D), suggesting the role of these genes in lateral root primordia formation. In contrast, due to the short root in *hipp32*, the LR density was slightly increased, probably suggesting a negative role of *HIPP32* in LR initiation. The LR formation was further reduced in *hipp32,33*: these mutants formed ~50% fewer LR than wild type and ~25% fewer than the respective single mutants (Figure 32C), suggesting a certain functional redundancy between these genes in this regard. However, loss of *HIPP32* suppressed the reduced LR density caused by *hipp33* and *hipp34* (Figure 32D), thus supporting the idea of *HIPP32* as negative regulator during LR formation. The LR phenotype of *hipp32,34* which resembled that of wild type (Figure 32C) would support this idea regarding this particular root phenotype. However, *hipp32,34* showed an intermediate LR density phenotype (Figure 32D), suggesting antagonistic functions of *HIPP32* and *HIPP34* in regulating LR formation. Intriguingly, in *hipp33,34* double mutant the reduced LR formation observed in the respective single mutants was suppressed, reaching the wild type level (Figure 32C). A partial suppression was also observed regarding the LR density in *hipp33,34* (Figure 32D), implying the existence of a complex genetic compensation in response to the loss of these genes.

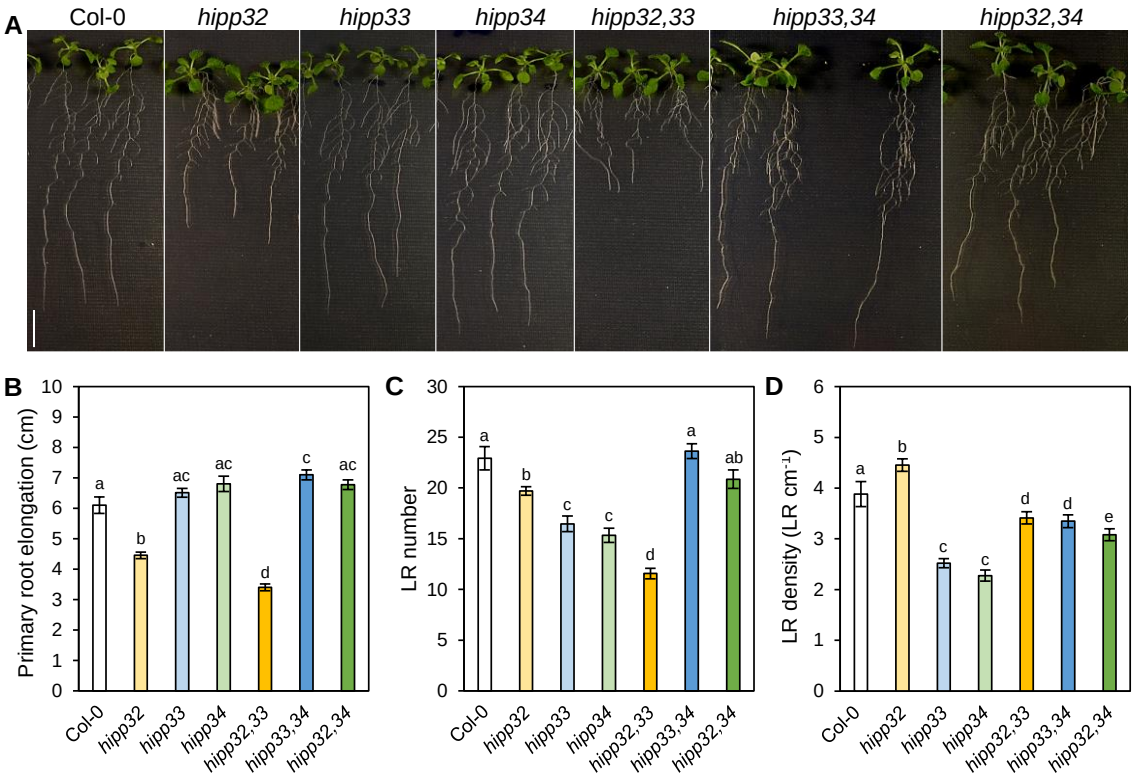

Figure 32. *In vitro* root phenotypes of *hipp* mutants.
(A) Root growth of 12-day-old *hipp* single and double mutants as compared to wild-type (Col-0). Scale bar = 1 cm. **(B)** Primary root elongation between 3 and 12 days after germination (dpg). **(C)** Lateral root (LR) number at 12 dpg. **(D)** LR density as lateral roots cm^{-1} primary root. Values represent means ± SE (n = 15). Different letters indicate significant differences between groups as evaluated by analysis of variance (one-way ANOVA) followed by Wilcoxon post hoc test ($p < 0.05$).

Due to the phenotypical particularities of *hipp* triple mutants, the gross root phenotype of *hipp32,33,34* plants was assessed separately from other *hipp* lines. Loss of all cluster-III *HIPP* genes led to severe alterations during root growth. Up to 20% of the germinated seeds exhibited primary root growth arrest three days after germination (image not shown). The other remaining *hipp32,33,34* seedlings, developed mostly shorter roots and exhibited a bending behavior, suggesting a partial loss of the gravitropic response (Figure 33A). Enhanced wavy root growth was more evident in 7-day-old *hipp32,33,34* mutant seedlings, which showed strongly reduced gravitropic response, as evident from the intensive root banding and formation of coils (Figure 33B). Furthermore, the lack of *HIPP* genes induced premature adventitious root formation in *hipp32,33,34* mutants (Figure 33B). Additional to the wavy and curly root phenotypes, the primary root length of 11-day-old *hipp32,33,34* mutants was dramatically decreased, reaching only ~40% of the wild-type length (Figure 33D), while the LR number increased (Figure 33E). This led to a considerable higher LR density (Figure 33F), thus conferring *hipp32,33,34* mutants a “bushy”-like root phenotype (Figure 33C).

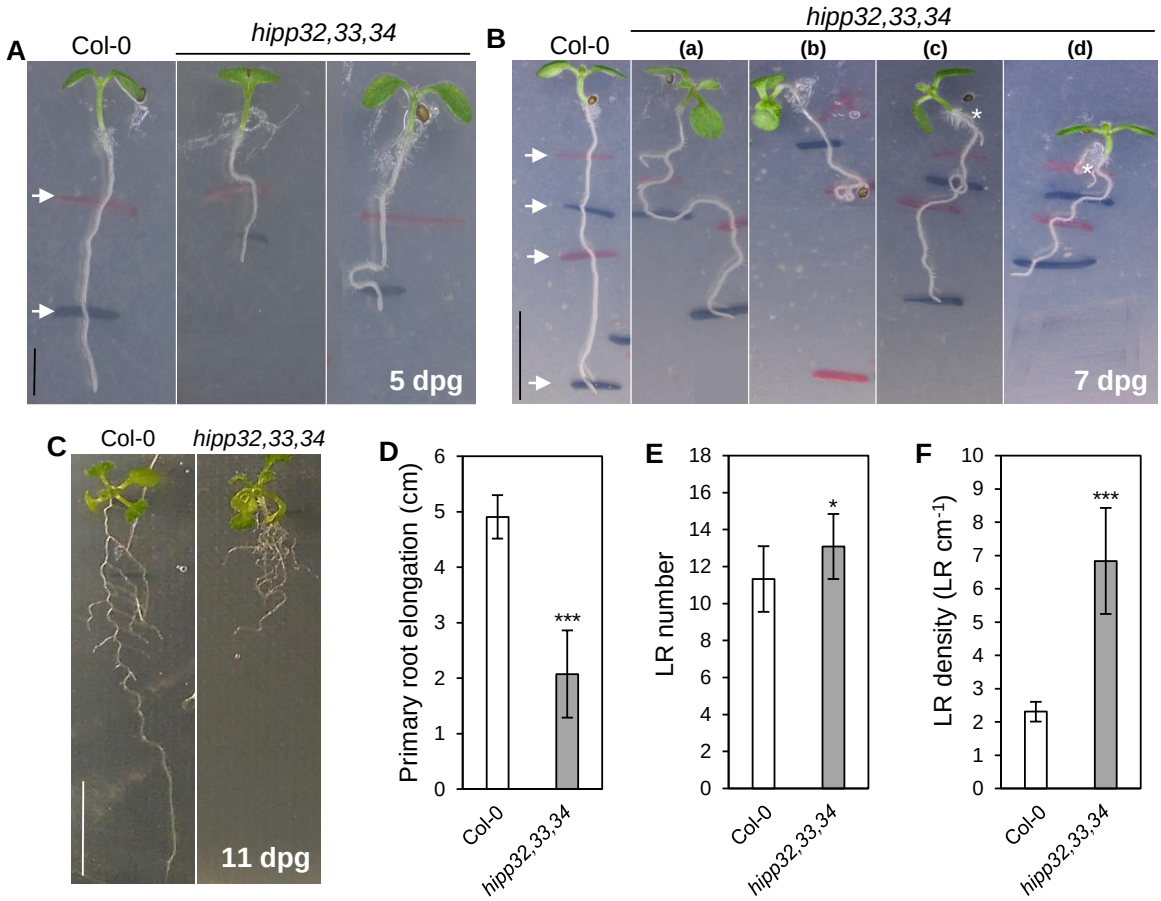

Figure 33. The root system architecture of *hipp32,33,34 is* severely affected.
(A) Phenotypes of 5-day-old seedlings. Compared to wild-type (Col-0), the roots of *hipp32,33,34* are shorter and start to bend. Arrows indicate root length labeled at 3 and at 4 dpg (days post germination). **(B)** 7-day-old *hipp32,33,34* seedlings continue to bend and form partially coiled roots **(b).** Seedlings exhibiting mild bending develop lateral roots earlier than wild type **(a).** *hipp32,33,34* seedlings develop adventitious roots, highlighted with asterisks **(c, d)**. Arrows indicate the root length labeled at 3, 4, 5 and 7 dpg. **(C)** 11-old-day *hipp32,33,34* seedlings display a bushy root phenotype and both primary and lateral roots appear bent and curled. **(D)** Primary root elongation between 3 and 11 dpg. **(E)** *hipp32,33,34* form more lateral roots, leading to a higher lateral root density than in Col-0 **(F)**. Statistically significant differences to wild type were evaluated by using Student's *t-test*: *0.01 < p < 0.05 and ***p < 0.001. Values represent means ± SD (n = 11). Scale bars = 0.2 cm **(A)**, 0.5 cm **(B)** and 1 cm **(C)**.

In order to investigate the causes for the altered root growth of the *hipp* mutant lines, the size of the RAM was determined by counting the number of cortex cells in a file extending from QC to the transition zone (Figure 34A; Perilli and Sabatini, 2010). Loss of either *HIPP32* or *HIPP33* gene resulted in ~18% lower root meristem cell numbers in comparison to wild type (Figure 34B). Loss of *HIPP34* caused tendentially an increase in meristem cell number, albeit the difference to wild type proved to be statistically insignificant (Figure 34A, B). Stronger reduction in the cell meristem number was determined in the short-root mutant *hipp32,33*, which generated ~23% less cells than wild type (Figure 34B), suggesting that *HIPP32* and *HIPP33* synergistically function to positively regulate RAM size. Correlating with the primary root length,

the loss of both *HIPP33* and *HIPP34* resulted in a meristem cell number increase by ~18% compared to wild type (Figure 34A, B). The mutant *hipp32,34* showed an intermediate phenotype: its meristem size was comparable to that of wild type and *hipp32* (Figure 34A, B), supporting the antagonistic activity of *HIPP34* in regulating root growth.

The root meristem size assays proved to be highly reproducible, therefore they were used to investigate the other *hipp* mutant alleles, conforming thus the specificity of the phenotype (see section 3.3.1, Figure 19). Figure 34C displays the average meristem cell number in *hipp* insertional lines: both *hipp32-1* and *hipp33-1* exhibited decreased RAM size in comparison to wild type, thus reproducing the root meristem size of *hipp32* (= *hipp32-2*) and respectively *hipp33* (= *hipp33-2*). No statistically significant difference was observed in the cell meristem number of either *hipp34-1* or *hipp34-2* (= *hipp34-2*) as compared to wild-type, despite the evident tendential increase (Figure 34C). These results support the idea of *HIPP32* and *HIPP33* acting synergistically to positively control RAM development, whereas *HIPP34* might antagonistically contribute to regulate this phenotype.

Additionally, the *hipp32,33* root meristems exhibited aberrant cell patterning, evident from the abnormally shaped stem cell niche - QC and surrounding stem cells - as well as from the perturbed organization of columella root cap cell layers (Figure 34A). Furthermore, CSCs appeared differentiated as evident from the presence of starch granules (Figure 34D). These results confer *HIPP32* and *HIPP33* important roles in stem cells maintenance and differentiation within RAM.

Abnormal patterning was observed in both *hipp33,34 and hipp32,34* root caps, albeit to a lesser extent than in *hipp32,33*. Analysis of the starch granule formation showed that *hipp33,34* and *hipp32,34* developed an overall normal pattern of the differentiated columella cells (Figure 34D), however only four columella cell layers were detected in these mutants, in comparison to wild type containing five columella cell five layers. The most severe developmental abnormalities in the root meristem were observed in *hipp* triple mutants (Figure 34A). *hipp32,33,34* displayed overall an abnormal RAM organization. On one hand, the QC cells were rather indistinguishable; two cells could be assumed to represent a putative QC (Figure 34A, arrowhead). However, abnormal anticlinal division was observed adjacent to the putative QC, indicating aberrant cell specification. Moreover, the overall cell division within the root meristem of *hipp32,33,34* exhibited an irregular pattern. For instance, periclinal cell divisions were observed to occur in cortex and epidermal cells, and the endodermis cell file appeared to be undefined. Furthermore, the stem cell identity appeared to be severely affected in *hipp32,33,34*, marked by the ubiquitous starch granule formation in the cells distal to the putative QC (Figure 34D). These pronounced irregularities impaired the determination of the root meristem size in *hipp32,33,34* and at the same time conferred *HIPP* genes from cluster III crucial roles during cell-fate specification required for proper root patterning.

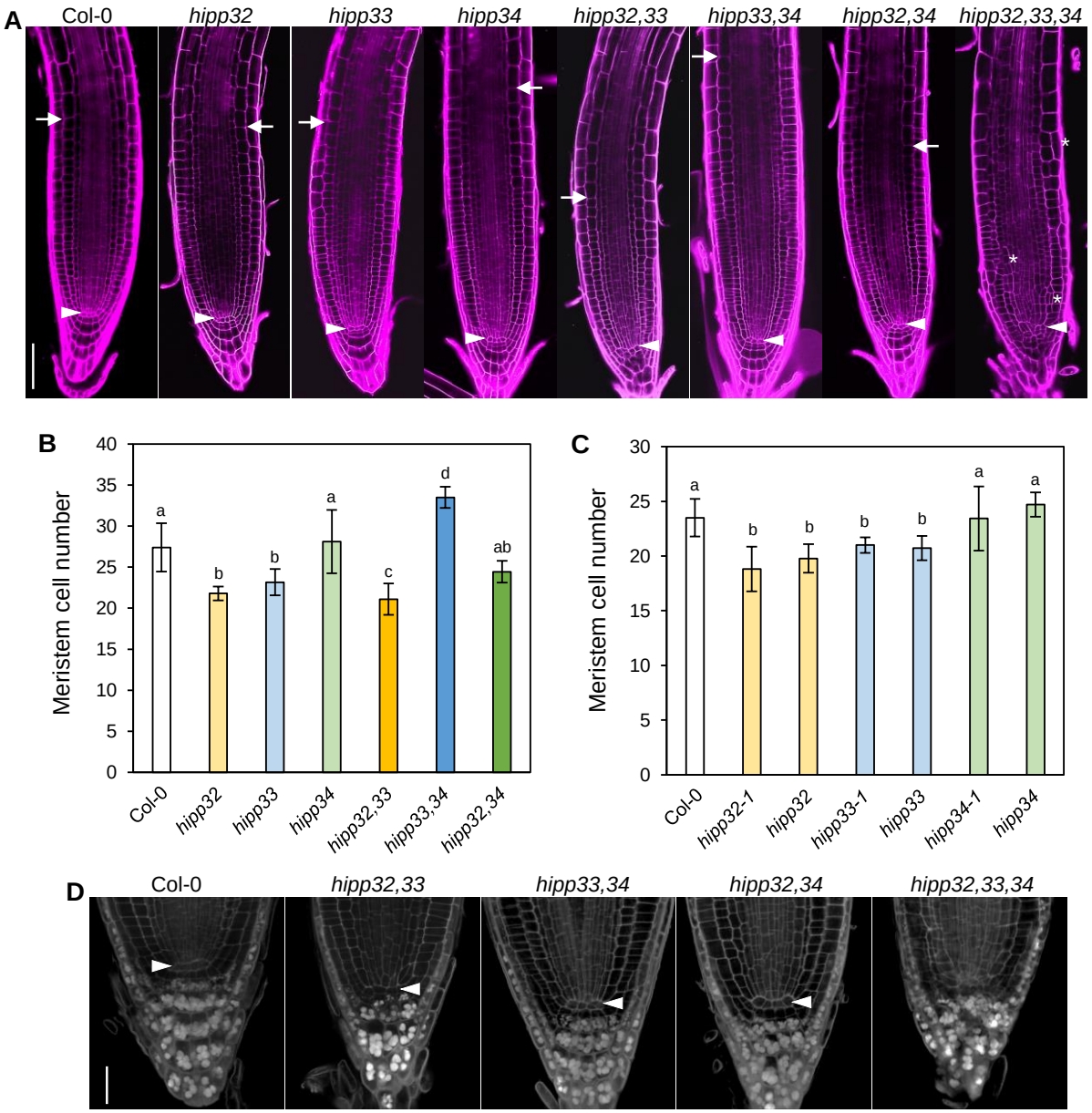

Figure 34. Cluster-III *HIPP* genes differentially regulate the root meristem size and development. **(A)** Confocal images of 6-day-old primary roots stained with propidium iodide (PI) (magenta). Arrows indicate the transition zone (TZ). Arrowheads indicate the position of the QC cells. Root meristem of *hipp32,33,34* appears severely affected, displaying an overall aberrant patterning. Arrowhead indicates the assumed QC. Asterisks in *hipp32,33,34* point to ectopic periclinal cell division. Scale bar = 75 µm. **(B)** Meristem cell number of 6-day-old seedlings, determined by counting the cortex cells along the longitudinal root axis from the QC to the TZ (white arrows). The disorganization of the meristematic cells in *hipp32,33,34* impaired the accurate quantification of the cortex cells. Values represent means ± SD (n = 10). **(C)** The average meristem size measured in 5-day-old seedlings of two independent T-DNA insertional mutant alleles for each *HIPP* gene. Values represent means ± SD (n = 10). Different letters indicate statistically significant differences between groups as evaluated by analysis of variance (ANOVA) followed by Tukey honest significant difference (HSD) post hoc test ($p < 0.05$). **(D)** Confocal images of 5-day-old root tips stained with pseudo-Schiff propidium iodide (mPS-PI) to visualize cell walls and starch granule formation in the columella cells. Arrowheads indicate the position of the QC cells in the root. Scale bar = 25 µm.

3.5 Transcriptional profiling of *hipp* mutants by RNA-Seq

3.5.1 Differential gene expression analysis

Transcriptional profiling using high throughput next-generation sequencing (RNA-Seq) has been intensively used in recent years. In the context of this work, the specific objectives were to identify genetic and molecular pathways underlying the function of the analyzed *HIPP* genes. For this, differentially expressed genes (DEGs) between wild-type seedlings and *hipp* mutants, *hipp*32, *hipp33*, *hipp34* and *hipp32,33,34*, were analyzed. The bioinformatic analysis of the RNA-Seq data was performed by BGI Genomics. The detected DEGs between wild-type and each *hipp* mutant were provided by BGI and were used accordingly for downstream analysis. A threshold for a false discovery rate (FDR) adjusted p-value < 0.05 and a log2 fold change (FC) ± 0.585 used to determine significant differences in gene expression, as compared to wild type (Figure 35). Using these criteria 843 DEGs (442 upregulated and 401 downregulated) were found in *hipp32*, 280 (117 upregulated and 163 downregulated) in *hipp33*, 183 (90 upregulated and 93 downregulated) in *hipp34* and 334 DEGs in *hipp32,33,34*, from which 101 and 233 were upregulated and downregulated, respectively (Figure 35).

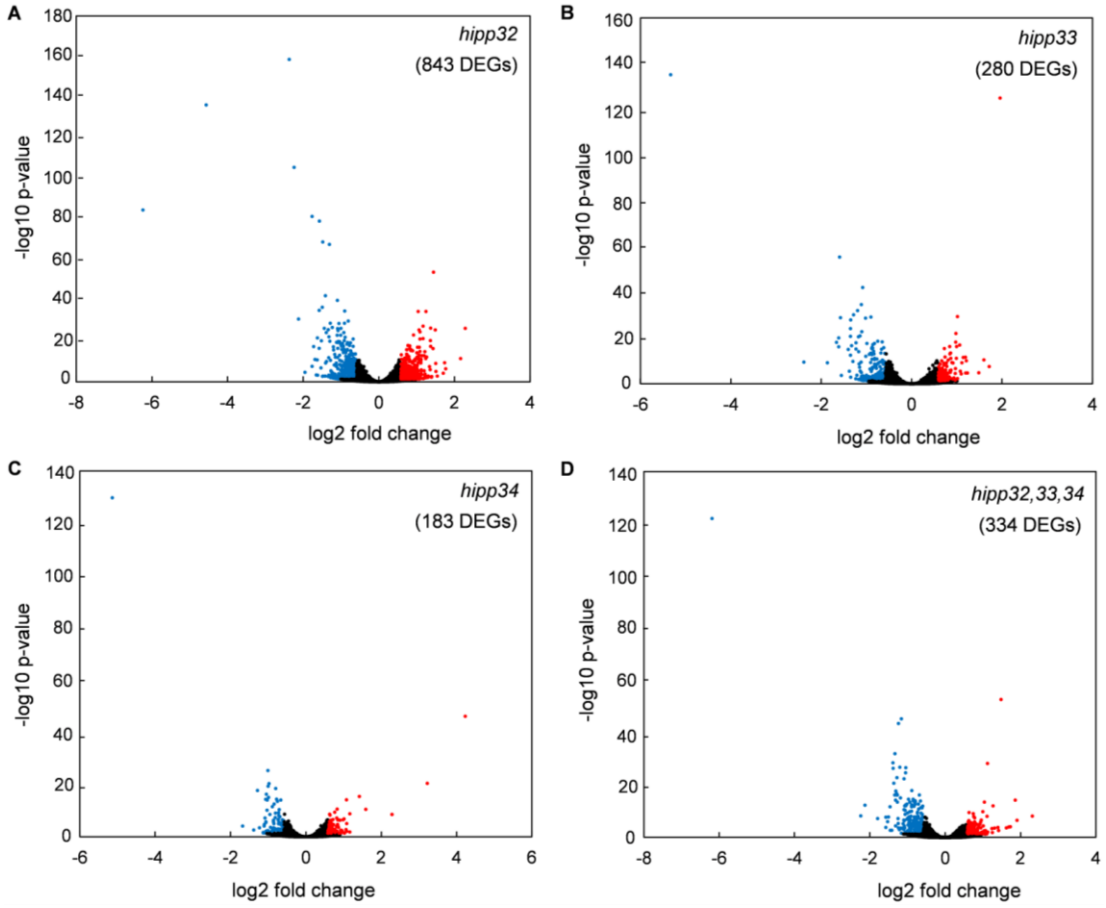

Figure 35. **Differential gene expression in *hipp* mutants.**
Volcano plots showing differentially expressed genes (DEGs) in *hipp32* **(A)**, *hipp33* **(B)**, *hipp34* **(C)** and *hipp32,33,34* **(D)** mutants. Transcripts significantly (false discovery rate < 0.05) downregulated (log2 fold change ≤ 0.585) and upregulated (log2 fold change ≥ 0.585) in comparison to wild type are represented blue and red. The total number of DEGs for each mutant is shown in brackets.

Comparison of the genes that were differentially expressed in each of the *hipp* single mutants showed that there was a large and significant overlap between the DEGs. However, due to the large number of DEGs in *hipp32*, 67% of the total DEGs were unique in this line (Figure 36A). In contrast, only 12% and 20% of the total DEGs were exclusively found in *hipp33* and *hipp34*, respectively (Figure 36A). 99 genes were found to be differentially expressed in all *hipp* single mutants, representing 11%, 35% and 54% of the total DEG number in *hipp32*, *hipp33* and *hipp34*, respectively (Figure 36A). The pairwise comparison of the overlapping DEGs between the *hipp* single mutants revealed that the vast majority of DEGs were regulated in the same direction (data not shown). However, there were two exceptions, namely the *AT5G07010* (*SULFOTRANSFERASE 2A*, *ST2A*) and the *AT1G04180* (*YUCCA9*) genes. *ST2A* was downregulated in *hipp32* and upregulated in *hipp33,* whereas *YUCCA9* was downregulated in *hipp33* and upregulated in *hipp34*. The overlapping 99 DEGs between *hipp* single mutants simultaneously compared showed as well comparable expression levels (data not shown).
Pairwise comparison of the DEGs between each *hipp* single and *hipp* triple mutants revealed that there were many DEGs unique to the *hipp32,33,34* line, particularly when compared to *hipp33* and *hipp34* (Figure 36B). 182 DEGs overlapped between *hipp32* and *hipp32,33,34*, representing ca. 20% of total DEGs in *hipp32* and more than 50% in *hipp32,33,34*. In *hipp33,* the overlap in DEGs number was 131 genes, around 40% of the total DEGs in both lines. 81 DEGs were shared between *hipp34* and *hipp32,33,34*, representing circa 45% of DEGs in *hipp34* and 20% in *hipp32,33,34*.

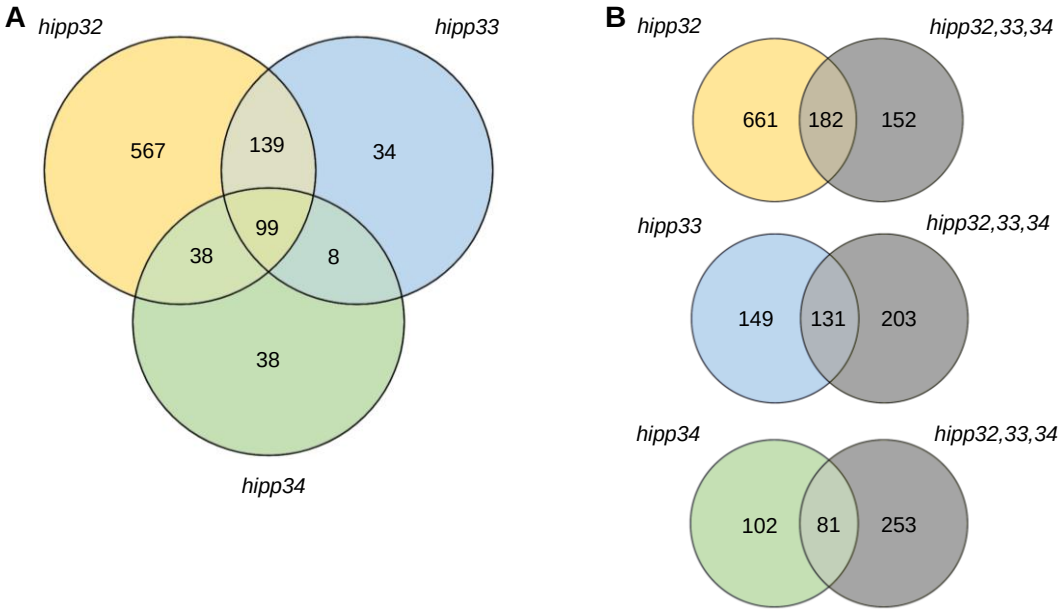

Figure 36. Differential expression analysis in *hipp* mutants by RNA-Seq.
Venn diagrams showing overlap of DEGs between *hipp* single mutants **(A)** and between each *hipp* single and *hipp* triple mutants **(B)**. Analyzed were all genes that were differentially expressed compared to wild type (FDR < 0.05) with a log2 fold change ± 0.585.

Comparison of the differentially expressed genes in all four *hipp* mutants revealed that 64 DEGs were common to all lines. From these DEGs, 24 were upregulated and 40 DEGs downregulated. All overlapping genes among the *hipp* mutants were found to be regulated in the same direction, exhibiting comparable log2 fold change levels (Figure 37).

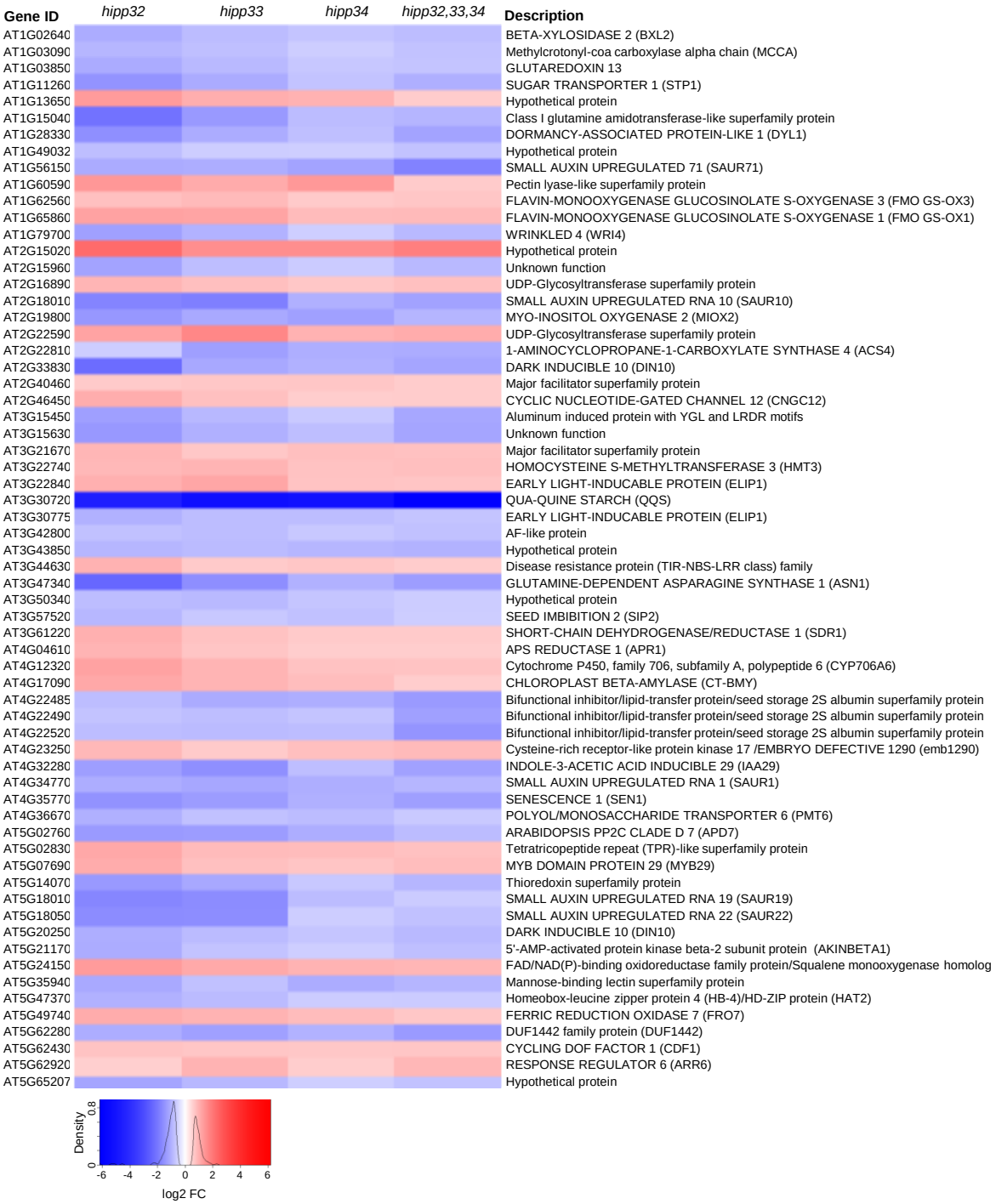

Figure 37. Expression levels of the differentially expressed genes in *hipp* mutants.
The heat map shows the log2 fold change (FC) of 64 DEGs common to all single and triple *hipp* mutants. DEGs with a false discovery rate < 0.05 and a log2 fold change ± 0.585 were statistically significant in comparison to wild type.

To gain further insights into the nature of the deregulated genes in *hipp* mutants, ten of the most upregulated and downregulated genes were identified (Table 20 to 23).

Table 20. Top ten upregulated and downregulated genes in *hipp32*.

Gene ID	log2 FC	FDR	Up/Down	Description
AT2G15020	2.28	5.48E-27	Up	Hypothetical protein
AT3G08700	2.16	3.47E-12	Up	UBIQUITIN-CONJUGATING ENZYME 12 (UBC12)
AT4G13577	1.77	4.00E-07	Up	Hypothetical protein
AT2G29090	1.74	4.28E-10	Up	CYTOCHROME P450, FAMILY 707, SUBFAMILY A, POLYPEPTIDE 2 (CYP707A2)
AT2G20800	1.70	6.65E-05	Up	NAD(P)H DEHYDROGENASE B4 (NDB4)
AT3G54530	1.54	1.56E-03	Up	Hypothetical protein
AT2G18120	1.51	8.78E-06	Up	SHI-RELATED SEQUENCE 4 (SRS4)
AT3G48280	1.51	8.82E-10	Up	CYTOCHROME P450, FAMILY 71, SUBFAMILY A, POLYPEPTIDE 25 (CYP71A25)
AT2G29300	1.49	2.92E-26	Up	NAD(P)-binding Rossmann-fold superfamily protein/Unknown function
AT1G73600	1.44	1.17E-54	Up	N-methyltransferase/(NMT3)
AT3G05230	-6.23	3.64E-85	Down	Signal peptidase subunit/Unknown function
AT3G30720	-4.56	6.81E-137	Down	QUA-QUINE STARCH (QQS)
AT3G47340	-2.37	2.80E-159	Down	GLUTAMINE-DEPENDENT ASPARAGINE SYNTHASE 1 (ASN1)
AT2G33830	-2.24	3.23E-106	Down	DORMANCY ASSOCIATED GENE 2 (DRM2)
AT1G15040	-2.12	1.63E-31	Down	GLUTAMINE AMIDOTRANSFERASE (GAT)
AT3G02000	-1.95	2.50E-05	Down	CC-type glutaredoxin (ROXY) family/(ROXY1)
AT2G18010	-1.76	2.55E-08	Down	SMALL AUXIN UPREGULATED RNA 24 (SAUR24)
AT4G36850	-1.76	5.48E-82	Down	PQ-loop repeat family protein/Unknown function
AT5G18010	-1.72	5.76E-18	Down	SMALL AUXIN UPREGULATED RNA 10 (SAUR10)
AT3G59930	-1.68	1.08E-11	Down	Defensin-like (DEFL) family protein/Unknown function

Table 21. Top ten upregulated and downregulated genes in *hipp33*.

Gene ID	log2 FC	FDR	Up/Down	Description
AT2G22590	1.71	3.17E-08	Up	UDP-Glycosyltransferase superfamily protein/Unknown function
AT2G15020	1.60	3.49E-11	Up	Hypothetical protein
AT3G01345	1.48	1.67E-05	Up	Expressed protein/Unknown function
AT1G80340	1.23	1.90E-05	Up	GIBBERELLIN 3-OXIDASE 2 (GA3OX2)
AT1G65860	1.21	9.12E-11	Up	FLAVIN-MONOOXYGENASE GLUCOSINOLATE S-OXYGENASE 1 (FMO GS-OX1)
AT1G54970	1.19	1.85E-05	Up	PROLINE-RICH PROTEIN 1 (PRP1)
AT3G22840	1.19	2.30E-12	Up	EARLY LIGHT-INDUCABLE PROTEIN (ELIP1)
AT5G24150	1.14	3.03E-12	Up	SQUALENE MONOOXYGENASE 5 (SQE5)
AT1G60590	1.11	7.13E-10	Up	Pectin lyase-like superfamily protein/Unknown function
AT1G69730	1.10	4.58E-05	Up	Wall-associated kinase family protein/Unknown function
AT3G30720	-5.33	7.24E-136	Down	QUA-QUINE STARCH (QQS)
AT3G57787	-2.39	3.38E-10	Down	Hypothetical protein
AT2G18010	-1.87	6.69E-10	Down	SMALL AUXIN UPREGULATED RNA 10 (SAUR10)
AT3G03850	-1.67	8.01E-19	Down	SMALL AUXIN UPREGULATED RNA 26 (SAUR26)
AT5G18010	-1.62	7.28E-17	Down	SMALL AUXIN UPREGULATED RNA 19 (SAUR19)
AT5G18050	-1.61	8.44E-21	Down	SMALL AUXIN UPREGULATED RNA 22 (SAUR22)
AT3G47340	-1.60	3.92E-56	Down	GLUTAMINE-DEPENDENT ASPARAGINE SYNTHASE 1 (ASN1)
AT4G32280	-1.58	1.17E-29	Down	INDOLE-3-ACETIC ACID INDUCIBLE 29 (IAA29)
AT1G08645	-1.56	2.46E-04	Down	Hypothetical protein
AT1G15040	-1.40	1.03E-15	Down	GLUTAMINE AMIDOTRANSFERASE 1_2.1 (GAT1_2.1)

Table 22. Top ten upregulated and downregulated genes in *hipp34*.

Gene ID	log2 FC	FDR	Up/Down	Description
AT1G75945	4.23	7.56E-47	Up	Hypothetical protein
AT1G64795	3.22	3.76E-21	Up	Hypothetical protein
AT1G25025	2.28	3.01E-09	Up	Hypothetical protein
AT1G25112	2.28	3.01E-09	Up	Hypothetical protein
AT2G15020	1.59	3.47E-11	Up	Hypothetical protein
AT1G60590	1.42	3.57E-16	Up	Pectin lyase-like superfamily protein/Unknown function
AT2G35935	1.17	1.41E-02	Up	Hypothetical protein
AT2G29300	1.16	1.57E-09	Up	NAD(P)-binding Rossmann-fold superfamily protein/Unknown function
AT5G25130	1.08	8.32E-06	Up	CYTOCHROME P450, FAMILY 71, SUBFAMILY B, POLYPEPTIDE 12 (CYP71B12)
AT1G06260	1.08	8.69E-03	Up	Cysteine peptidase/Unknown function
AT3G30720	-5.14	1.85E-130	Down	QUA-QUINE STARCH (QQS)
AT4G22710	-1.68	8.31E-05	Down	CYTOCHROME P450, FAMILY 706, SUBFAMILY A, POLYPEPTIDE 2 (CYP706A2)
AT2G30750	-1.39	2.87E-03	Down	CYTOCHROME P450, FAMILY 71, SUBFAMILY A, POLYPEPTIDE 12 (CYP71A12)
AT2G19800	-1.28	2.13E-18	Down	MYO-INOSITOL OXYGENASE 2 (MIOX2)
AT1G56150	-1.23	3.99E-04	Down	SMALL AUXIN UPREGULATED 71 (SAUR71)
AT1G45163	-1.13	3.08E-02	Down	Transmembrane protein
AT1G13609	-1.13	2.16E-02	Down	Defensin-like (DEFL) family protein/Unknown function
AT5G10140	-1.11	8.45E-05	Down	FLOWERING LOCUS C (FLC)
AT3G59930	-1.10	1.93E-05	Down	Defensin-like (DEFL) family protein/Unknown function
AT1G66700	-1.10	3.57E-02	Down	SABATH methyltransferase gene family/PXMT1

Table 23. Top ten upregulated and downregulated genes in *hipp32,33,34*.

Gene ID	log2 FC	FDR	Up/Down	Description
AT2G34870	2.32	7.90E-09	Up	MATERNAL EFFECT EMBRYO ARREST 26 (MEE26)
AT5G44120	1.91	2.89E-07	Up	CRUCIFERINA (CRA1)
AT2G15020	1.86	5.51E-15	Up	Hypothetical protein
AT1G75945	1.73	7.93E-05	Up	Hypothetical protein
AT2G11405	1.69	1.02E-04	Up	Transmembrane protein/Unknown function
AT1G27565	1.63	2.20E-04	Up	Hypothetical protein
AT3G13784	1.42	2.67E-03	Up	CELL WALL INVERTASE 5 (CWINV5)
AT5G54470	1.40	1.58E-04	Up	B-BOX DOMAIN PROTEIN 29 (BBX29)
AT1G54970	1.31	2.86E-04	Up	PROLINE-RICH PROTEIN 1 (PRP1)
AT5G02190	1.27	8.38E-13	Up	PROMOTION OF CELL SURVIVAL 1 (PCS1)
AT3G30720	-6.19	9.05E-123	Down	QUA-QUINE STARCH (QQS)
AT5G46960	-2.24	5.44E-09	Down	INVERTASE INHIBITOR 1 (INVINH1)
AT4G23560	-2.13	4.99E-13	Down	GLYCOSYL HYDROLASE 9B15 (GH9B15)
AT1G56150	-1.79	6.06E-08	Down	SMALL AUXIN UPREGULATED 71 (SAUR71)
AT5G03545	-1.58	1.95E-08	Down	INDUCED BY PI STARVATION 2 (ATIPS2)
ATMG01170	-1.57	1.64E-04	Down	ATPase subunit 6/(ATP6-2)
AT3G29370	-1.53	9.56E-07	Down	bHLH (basic helix-loop-helix) family transcriptional factor/(P1R3)
AT1G75490	-1.51	1.49E-08	Down	FGENESH2_KG.2/Unknown function
AT4G22520	-1.46	2.11E-12	Down	Bifunctional inhibitor/lipid-transfer protein//Unknown function
AT1G29490	-1.45	2.11E-03	Down	SMALL AUXIN UPREGULATED 68 (SAUR68)

Comparison of the top ten most deregulated genes among the *hipp* mutants revealed that both the upregulated and downregulated genes were largely unique to each *hipp* mutant line. Only few genes were shared among *hipp* mutants. For instance, the *AT2G15020* gene, encoding a hypothetical protein, which was upregulated in all *hipp* mutants, exhibiting the strongest upregulation in *hipp32* mutant (Table 20 to 23). The *AT3G30720* (*QUA-QUINE STARCH, QQS*) gene, which encodes a novel protein component of the starch metabolic network (Li *et al.*, 2009), was the strongest downregulated gene in all genotypes (Table 20 to 23). Interestingly, several distinct members of the *SMALL AUXIN UPREGULATED RNA* (*SAUR*)

gene family were identified to be downregulated in *hipp* mutants (Table 20 to 23). 4 of the top ten downregulated genes found in *hipp33* belong to this early auxin-responsive gene family (Table 21; Stortenbeker and Bemer, 2019). The strongest upregulated gene in *hipp32,33,34* was the embryogenesis gene *MATERNAL EMBRYO EFFECT 26* (Table 23) which was shown to be essential for early embryo development (Pagnussat *et al.*, 2005).

3.5.2 Insight into the biological roles of *HIPP* genes based on RNA-Seq data

In order to gain insights into the biological processes that *HIPP* genes might control, the DEGs in *hipp* mutants obtained were functionally categorized by performing a gene ontology (GO) enrichment analysis using DAVID 6.8 (Huang *et al.*, 2009). For functional categorization, the DEGs were assigned to three gene ontology classes: biological process (BP), molecular function (MF) and cellular component (CC).

GO term analysis of DEGs in *hipp32* revealed that genes were enriched in 57 terms in the BP, 35 in the MF category and 10 in the CC category (Figure 38). In the BP category, the highest gene count (74) was identified in ‘oxidation-reduction process’ (GO:0055114), followed by 47 genes annotated in the ‘response to auxin’ GO term (GO:0009733) (Figure 38). In the MF category, the most genes were annotated to the ‘sequence-specific DNA binding transcription factor activity’ term (GO:0003700), followed by ‘heme’ and ‘iron ion binding’ GO terms (Figure 38). In the CC category, the most DEGs were annotated to ‘extracellular region’ (GO:0005576) and to ‘membrane’ (GO:0016020). Approximately 5% of the DEGs in *hipp32* were annotated to ‘plasmodesma’ (GO:0009506) (Figure 38).

GO term analysis of DEGs in *hipp33* resulted in 38 terms categorized in the GO biological process, 27 in the GO molecular function and only one term in the GO cellular component (Figure 39). Within the DEGs involved in biological processes, similar to the GO analysis output in the *hipp32*, ‘response to auxin’ and ‘oxidation-reduction process’ were the most prominent GO terms. The GO terms within the MF category containing the most genes were also remarkably similar to those in *hipp32* (Figure 39). The CC class comprised the ‘intracellular membrane-bounded organelle’ term (GO:0043231), to which 7 of the DEGs in *hipp33* were assigned (Figure 39).

GO term analysis of DEGs in *hipp34* resulted in 22 functional terms in the BP and 15 in the MF category (Figure 40). There were no genes classified into specific GO term within the CC category. In the BP category, the highest gene count (24) was identified in ‘regulation of transcription, DNA-templated’ (GO:0006355), followed by 17 and 16 genes annotated in the GO terms ‘oxidation-reduction process’ and ‘response to auxin’ respectively (Figure 40), similar to the GO functional annotation in *hipp32* and *hipp33*. In the MF category, the most DEGs were annotated to the ‘iron ion binding’ GO term (Figure 40).

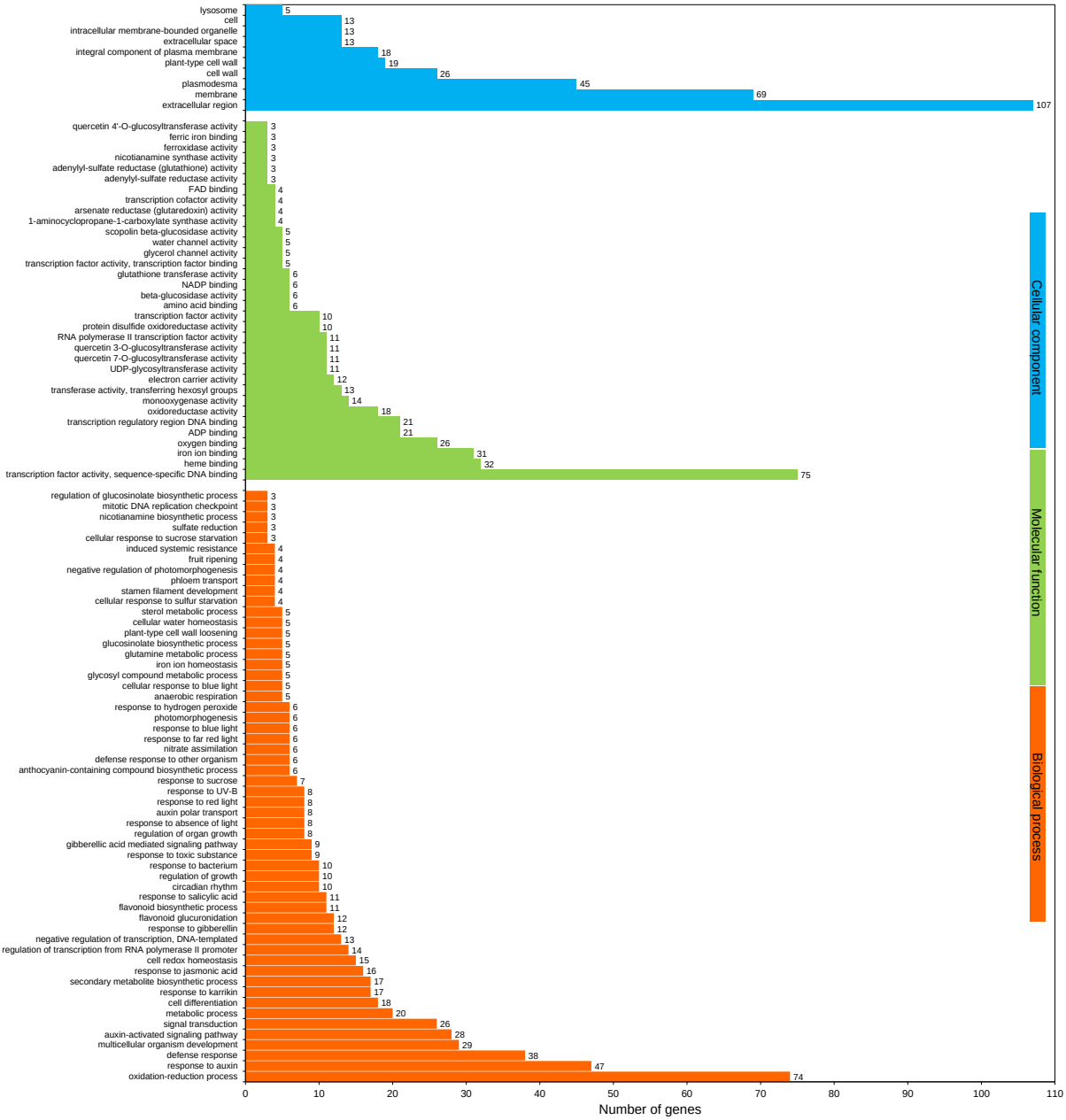

Figure 38. GO term enrichment analysis of DEGs identified in *hipp32*.
Shown are the number of genes enriched in GO terms sorted by' biological process', 'molecular function' and 'cellular component' ontology. Fold enrichment > 1. Fisher Exact modified p-value < 0.05.

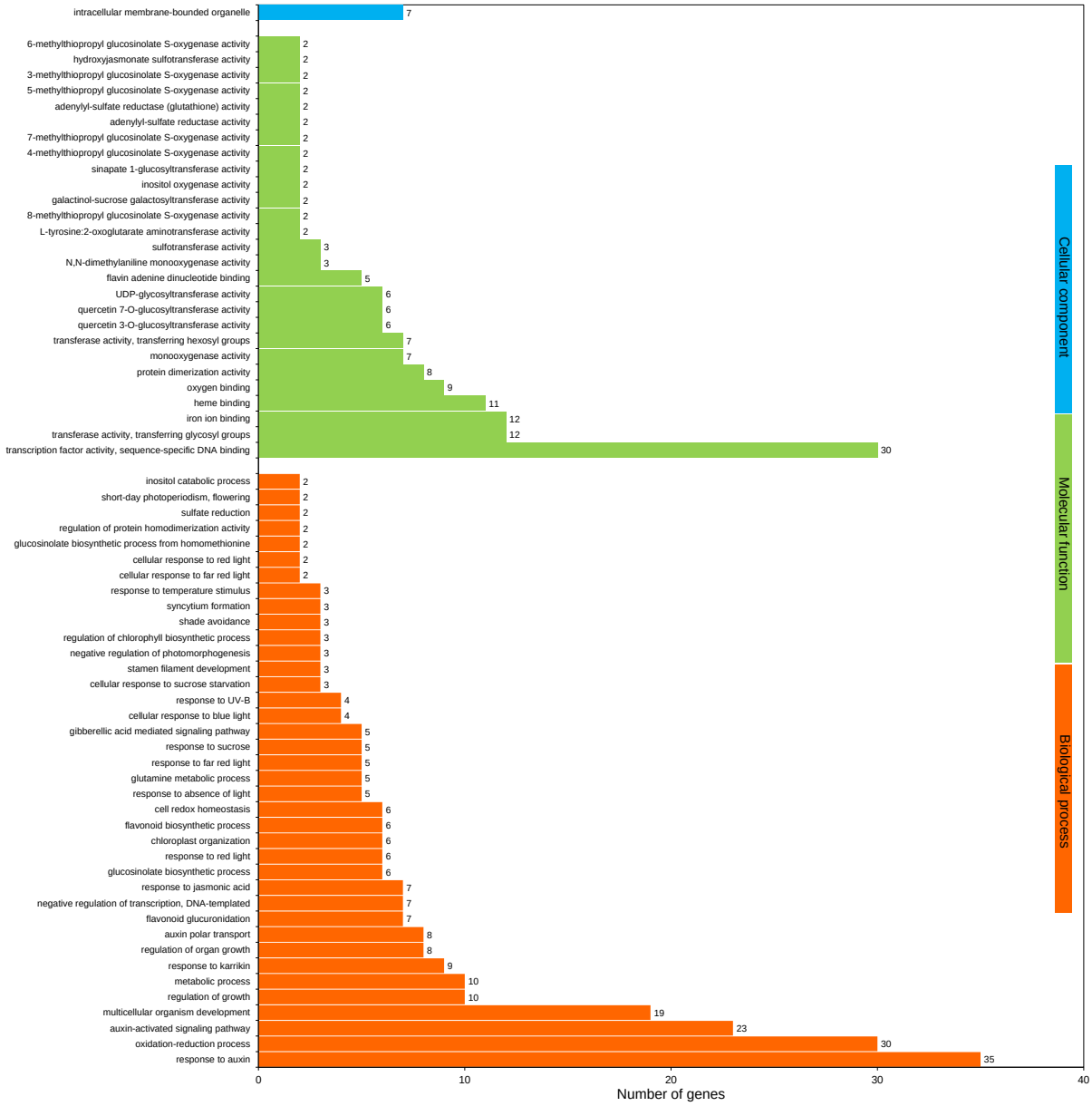

Figure 39. GO term enrichment analysis of DEGs identified in *hipp33*.
Shown are the number of genes enriched in GO terms sorted by 'biological process', 'molecular function' and 'cellular component' ontology. Fold enrichment > 1. Fisher Exact modified < 0.05.

The GO term analysis of the DEGs in *hipp32,33,34* revealed that genes were enriched in 23 terms in the BP ontology category, 21 in the MF category and one GO term, 'extracellular region' was annotated in the CC category (Figure 41). The distribution of gene counts within the GO terms resembled the GO analysis of the *hipp* single mutants, suggesting the functional redundancy among the *HIPP* genes in controlling development via altering the underlying transcriptional programs.

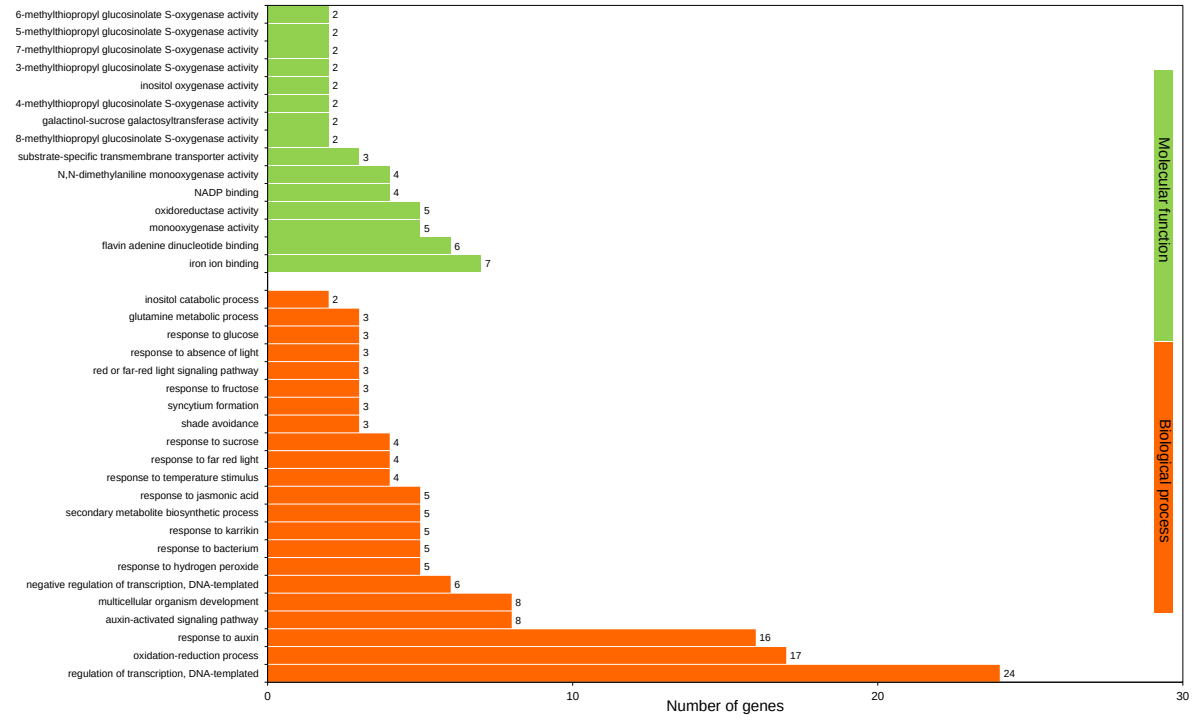

Figure 40. GO term enrichment analysis of DEGs identified in *hipp34*.
Shown are the number of genes enriched in GO terms sorted by 'biological process' and 'molecular function' ontology. Fold enrichment > 1. Fisher Exact modified p-value < 0.05.

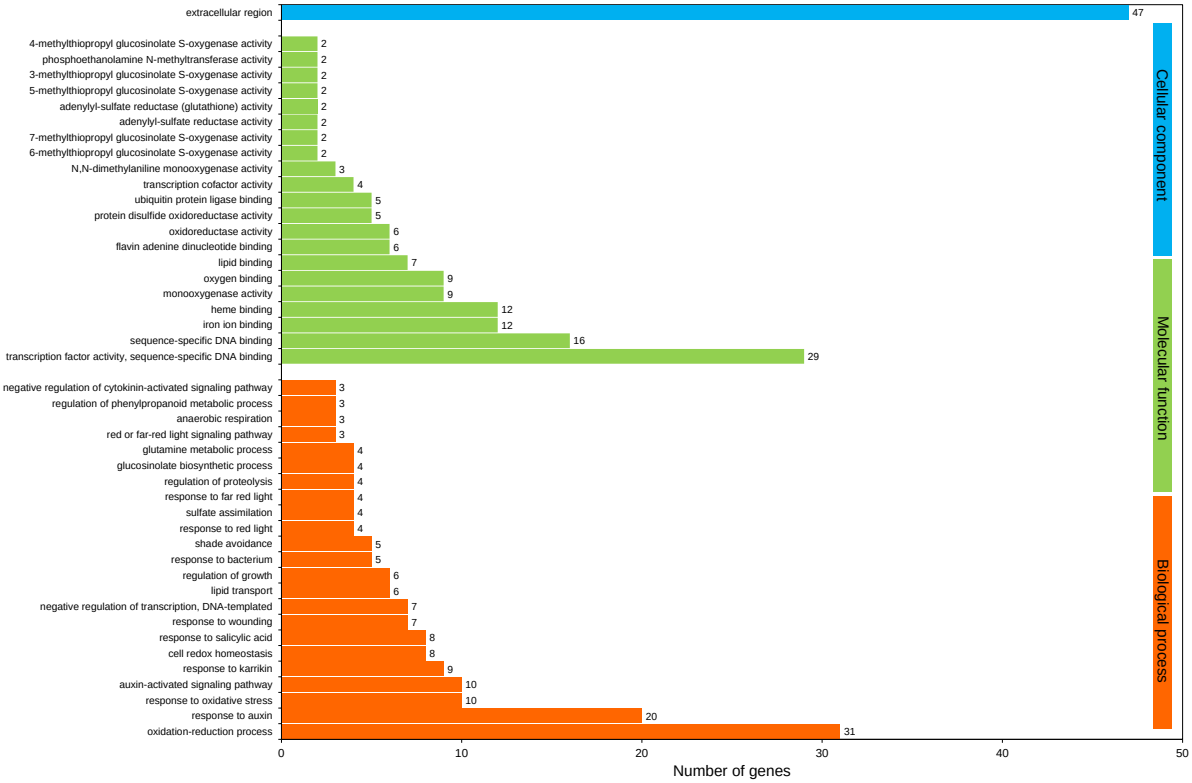

Figure 41. GO term enrichment analysis of DEGs identified in *hipp32,33,34*.
Shown are the number of genes enriched in GO terms sorted by 'biological process', 'molecular function' and 'cellular component' ontology. Fold enrichment > 1. Fisher Exact modified p-value < 0.05.

Biological interpretation of the DEGs identified in *hipp* mutants was also performed using the Kyoto Encyclopedia of Genes and Genomes (KEGG) pathway analysis with the *g:Profiler* web-based tool (Reimand *et al.*, 2007). In total, 7 KEGG pathway terms were significantly enriched, from which the 'plant hormone signal transduction' term contained the highest level of enriched DEGs in all *hipp* mutants (Figure 42), comprising 31 DEGs in *hipp32*, 23 in *hipp33*, 10 in *hipp34* and 15 DEGs in *hipp32,33,34*. Three KEGG pathways, 'flavone and flavonol biosynthesis', 'metabolic pathways' and 'biosynthesis of secondary metabolites', were identified only in *hipp32* and the 'cysteine and methionine metabolism' was unique to *hipp33* line (Figure 42). Five and four genes differentially expressed in *hipp33* and *hipp34*, respectively, were assigned to the 'circadian rhythm' KEGG pathway (Figure 42). The *hipp33* and *hipp32,33,34* mutants had in common the 'glucosinolate biosynthesis' term, where four DEGs were enriched in each line (Figure 42).

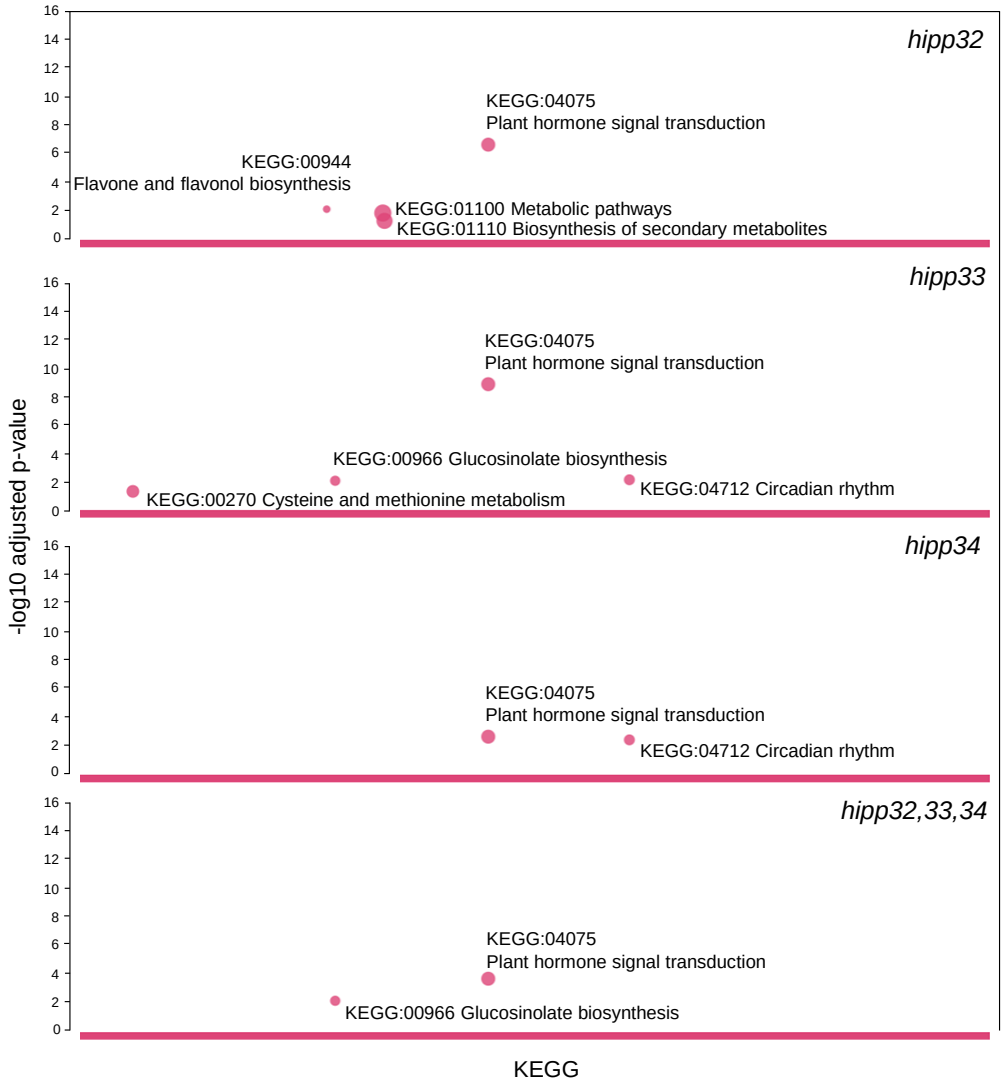

Figure 42. KEGG enrichment pathways of the DEGs identified in *hipp* mutants by RNA-Seq. Seven pathways were significantly enriched in *hipp* mutants. Benjamini-Hochberg-corrected p-value < 0.05. The circle size indicates the number of genes that are associated with that pathway as evaluated in *g:Profiler* database (between 4 and 2193 genes).

The most enriched KEGG pathways were further investigated in order to identify the genes annotated in the respective pathway. In particular, the 'plant hormone signal transduction' was intriguing, since it was enriched in all *hipp* mutants, suggesting altered hormone activity in *hipp* mutants. Moreover, the cytokinin activity and sensitivity was altered during the root development in *hipp* mutants (see section 3.7.4). For this purpose, the genes associated with phytohormone biosynthesis, transport and signal transduction were extracted from KEGG pathway analysis and their expression levels assessed in *hipp* mutants. The vast majority of the genes annotated in the 'plant hormone signal transduction' term was associated with auxin signal transduction pathway, whereas only two genes were associated with cytokinin and gibberellic acid signaling pathway (Figure 43).

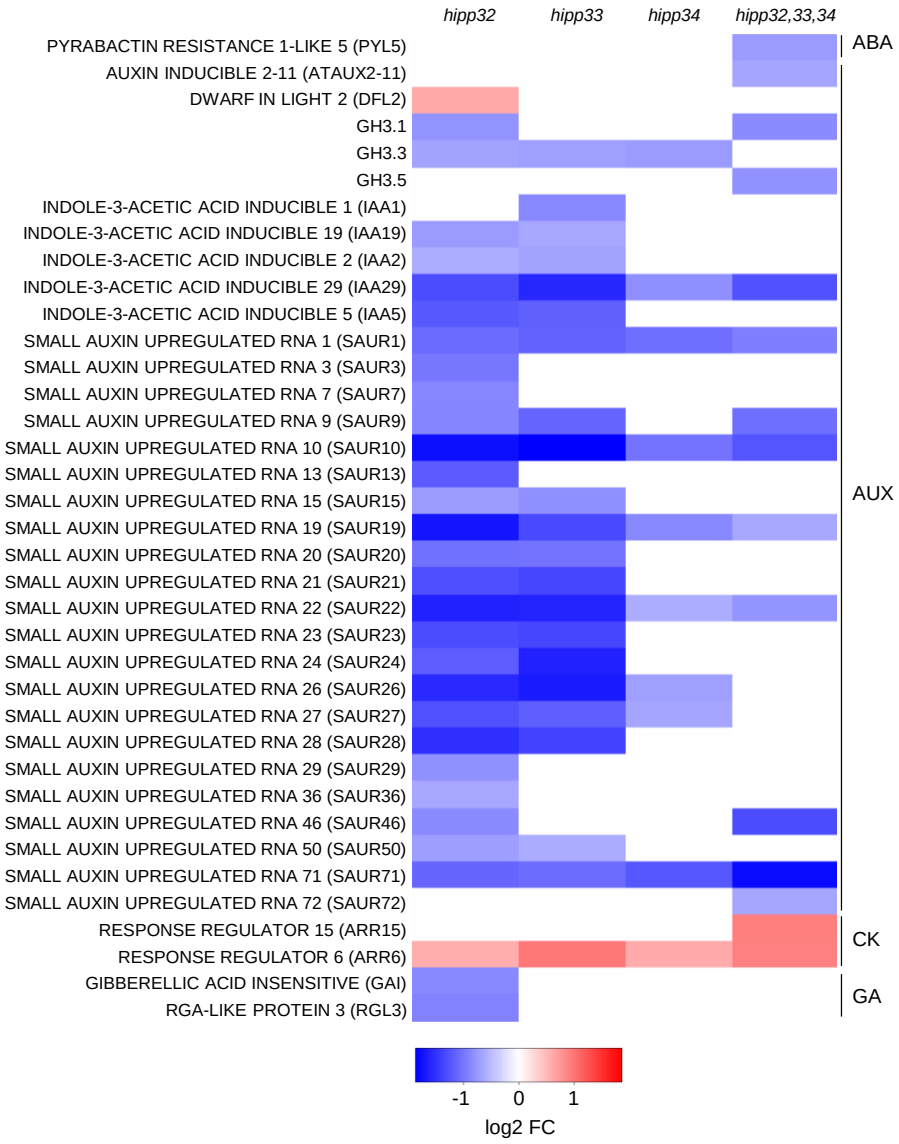

Figure 43. Expression levels of the DEGs in *hipp* mutants related to phytohormone pathway. The heat map shows the log2 fold change (FC) of 37 DEGs identified in the 'plant hormone signal transduction' KEGG pathway. DEGs with a false discovery rate < 0.05 and a log2 fold change ± 0.585 were statistically significant in comparison to wild type. ABA: abscisic acid. AUX: auxin. CK: cytokinin. GA: gibberellic acid.

Several DEGs associating with plant hormones were annotated in the ‘metabolic pathways’ in *hipp32*, for instance the *YUCCA2* and *YUCCA9*, known to mediate auxin biosynthesis in shoot and root, respectively (Mashiguchi *et al.*, 2011; Xu *et al.*, 2017). *ACS8,* which is essential for the early biosynthesis of ethylene was also identified in this enriched pathway (Zhang *et al.*, 2018). Although not enriched in any of the KEGG pathways, two cytokinin-related genes were differentially expressed in *hipp* mutants. The *CYTOKININ-RESPONSIVE GATA FACTOR 1*, a transcription factor that acts downstream of cytokinin to mediate the development of chloroplasts (Chiang *et al.*, 2012), was upregulated in *hipp33* and *CKX4* was upregulated in *hipp32,33,34*.

Taken together, the GO term enrichment analysis revealed that the genes differentially regulated in *hipp* mutants were assigned to various GO terms within the ontology classes. This suggests that the numerous morphological alterations observed in these mutants are the consequence of a complex transcriptional changes, which appears to be mainly controlled by the plant hormone auxin and auxin-related molecular factors.

3.6 Establishment and overall phenotypic characterization of *HIPP34* gain-of-function plants

To gain insight into the physiological function of HIPP proteins, gain-of-function analysis was performed by exemplarily expressing one of the cluster III members, *HIPP34,* N-terminally fused to GFP under the control of the constitutive *CaMV 35S* promoter in stably transformed *Arabidopsis* plants. In T1 generation, circa 40 *35S:GFP-HIPP34* (*HIPP34ox*) primary transformants were analyzed for phenotypic alterations, from which three independent lines were identified and their homozygous progenies were established. *HIPP34ox* lines are distinguished from wild type by their smaller rosettes, decreased shoot height and enhanced leaf senescence (Figure 44A). The transcript levels of *HIPP34* were enhanced in all of three overexpression lines as compared to wild-type plants, with the line #5-1 showing the highest expression of 8-fold increase (Figure 44B). In accordance with this, the immunoblot analysis confirmed that the highest protein level accumulated in the *#5-1 HIPP34ox* (Figure 44C). Furthermore, confocal microscopy analysis revealed that GFP-HIPP34 was expressed along the periphery of epidermal leaf cells in a punctate PD-specific pattern (Figure 44D). In accordance with the *HIPP34* transcript level and immunoblot analysis, the GFP-HIPP34 signal was less frequent in *#20-9* and *#29-3* lines (Figure 44D).

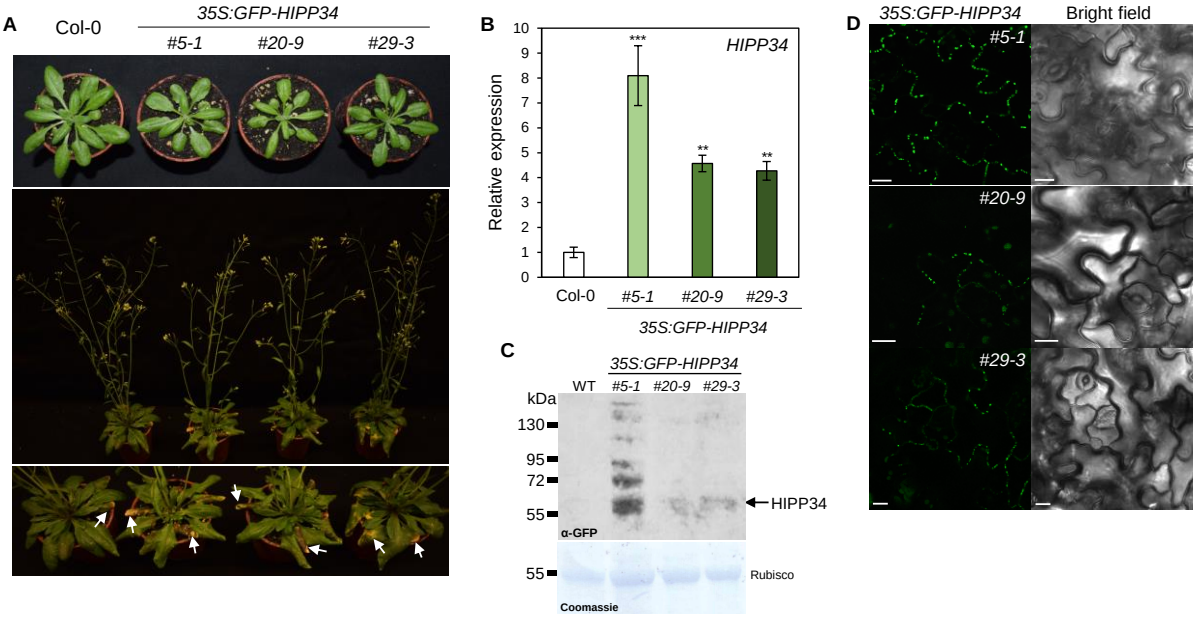

Figure 44. Phenotypic and molecular characterization of *HIPP34*-overexpressing plants.
(A) Rosette and shoot phenotypes of *HIPP34ox* homozygous lines. The bottom image exemplifies the enhanced leaf senescence (white arrows). **(B)** Relative transcript abundances of the *HIPP34* gene in shoots of 15-day-old seedlings expressing *35S:GFP-HIPP34*. Values represent means ± SD (n = 3). Significant differences to Col-0 were evaluated by one-way ANOVA followed by Dunnett post hoc test (*0.01<p<0.05, **0.001<p<0.01 and ***p<0.001. **(C)** Immunoblot showing the GFP-HIPP34 protein levels in the independent *HIPP34ox* homozygous transgenic lines. Rubisco, visualized by staining of the immunoblot with Coomassie, serves as loading control. **D)** Confocal images of leaf epidermal cells of *HIPP34ox* lines. Scale bars = 10 µm.

The expression analysis using the p*HIPP34*:GUS reporter line (see section 3.1) revealed a strong expression within the root vascular tissues from embryonic developmental stages onwards (Figure 13; section 3.1). The loss of function studies suggested a positive function of *HIPP34* during root growth (section 3.4.4). Hence, the question arose whether overexpression of *HIPP34* affects the plant root growth. Two independent *HIPP34ox* lines displayed shorter primary roots compared to wild type (Figure 45A). All three *HIPP34ox* lines formed fewer lateral roots (Figure 45B), while the density of lateral roots remained unchanged (Figure 45C). These results further support the proposed negative role of *HIPP34* in regulation of primary root growth.

Another phenotype investigated in *HIPP34ox* plants was the flowering initiation time, since the lack of *HIPP34* induced early flowering in mutants grown under standard LD conditions, whereas no difference to wild type was observed in SD conditions (section 3.4.3.1). The *HIPP34ox* lines flowered tendentially earlier, but only for one line the difference was statistically significant in LD conditions (Figure 46A). The flowering time of the strongest *HIPP34ox* line *#5-1* was also analyzed under SD conditions. The analysis revealed that *HIPP34ox #5-1*

flowers on average circa 8 days earlier than wild-type plants (Figure 46B), suggesting a link between *HIPP34* and regulation of flowering in response to different light conditions.

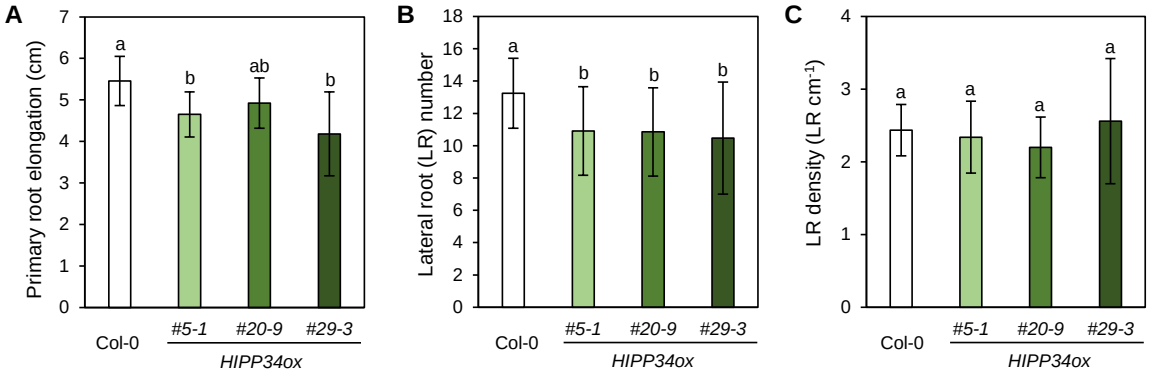

Figure 45. Overexpression of *HIPP34* negatively affects root growth in *Arabidopsis*.
(A) Primary root elongation between 3 and 11 days after germination (dpg). **(B)** Lateral root (LR) formation at 11 dpg. **(C)** Lateral root density as lateral roots cm^{-1} primary root. Values represent means ± SD (n = 7-25). Significant differences were evaluated by analysis of variance (one-way ANOVA) followed by Wilcoxon post hoc test ($p < 0.05$). Different letters indicate significant differences between groups.

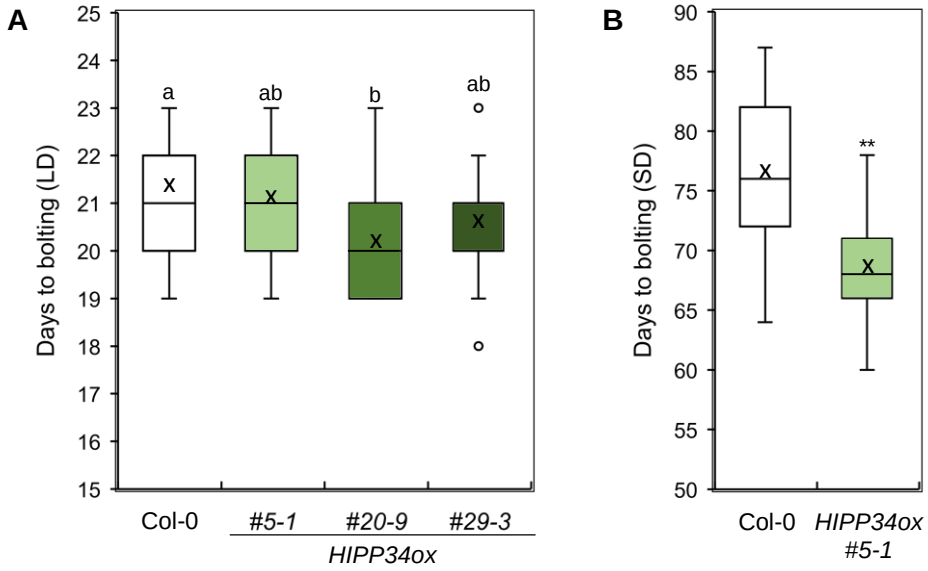

Figure 46. Flowering time analysis in *HIPP34ox* lines.
(A) Number of days to bolting of wild-type (Col-0) and *HIPP34ox* plants grown under long-day (LD) conditions. **(B)** Number of days to bolting of wild-type (Col-0) and *HIPP34ox #5-1* grown under short-day (SD) conditions. The segment inside the rectangle shows the median and the cross the mean (n = 15 - 20). In **A)**, significant differences were evaluated by analysis of variance (one-way ANOVA) followed by Wilcoxon post hoc test ($p < 0.05$). Different letters indicate significant differences between groups. In **B)**, the significant difference to Col-0 was evaluated using Student's *t-test*: $**0.001 < p < 0.01$.

3.7 Analysis of cytokinin signaling responses in *hipp* mutant plants

The phenotypic analyses of *hipp* loss-of-function mutants suggest that the cluster-III *HIPP* genes are involved in various aspects of plant growth, including root development. Considering that HIPP proteins were able to interact with CKX1 and that cytokinin is recognized to play an essential inhibitory role during root growth (Kieber and Schaller, 2014), the question arose whether HIPPs are involved in modulating cytokinin signaling responses and activity. For this purpose, a series of experiments were performed aiming to explore the possible link between HIPP proteins and cytokinin signaling in plants.

3.7.1 *hipp* mutants exhibit overall enhanced sensitivity to cytokinin

To determine whether the lack of functional HIPP affects the cytokinin signaling, cytokinin root response assays were performed, based on the knowledge that exogenous cytokinin inhibits primary root growth and lateral root formation (Cary *et al.*, 1995; Laplaze *et al.*, 2007). Experimentally, *hipp* mutant and wild-type plants were grown *in vitro* on ½ MS-medium supplemented with synthetic cytokinin benzyladenine (BA) and their root responses were quantified 12 days post germination (Figure 47). The elongation of the primary root decreased in all seedlings as the BA concentration increased. It is most evident at 30 nM BA, where wild-type primary root elongation decreased by ~15% and by ~25% in *hipp32* and *hipp33* single mutants, compared to control, indicating that hipp32 and hipp33 are more sensitive to exogenous cytokinin than wild type. The response of *hipp34* was similar to wild type (Figure 47A). On media containing 20 nM BA, only *hipp33* showed a sensitive reaction, whereas no differences were observed in wild type, *hipp32* and *hipp34* (Figure 47A). Similar responses were observed when monitoring the lateral root formation. In the presence of exogenous cytokinin, only *hipp33* was statistically significant more sensitive than wild type (Figure 47B). No difference in lateral root density, no differences were observed between *hipp* single mutants and wild-type seedlings (Figure 47C). Together, these results suggest that *HIPP33* and, to a less extend, *HIPP32* mediate the cytokinin response during the root growth.

In the presence of 20 nM BA, all *hipp* double mutants exhibited enhanced sensitivity to cytokinin compared to wild-type roots, with the strongest response observed in *hipp33,34* primary root elongation (Figure 47D). 40 nM BA dose caused further decrease in primary root elongation, which was yet similar in all genotypes (Figure 47D). Regarding the lateral root formation, *hipp* double mutants responded differently to 20 nM BA (Figure 47E). *hipp32,33* formed 90% fewer lateral roots as compared to control and ~40% fewer than wild type (Figure 47E). *hipp33,34* produced ~55% fewer lateral roots as compared to control and ~5% more than wild type at this concentration (Figure 47E). The reduced sensitivity of *hipp33,34* was also observed at 40 nM BA (Figure 47E). The *hipp32,34* behaved similarly to wild type regardless

of the BA concentration (Figure 47E). Similar responses were observed when determining the density of lateral root formation in *hipp* double mutants (Figure 47F).

In contrast to the hypersensitive double mutants *hipp32,33* and *hipp33,34*, the *hipp* triple mutant appeared to be insensitive to exogenous cytokinin, as the primary root elongation in *hipp32,33*,34 remained unchanged compared to control (Figure 47G). Exogenous cytokinin affected equally the lateral root number in *hipp32,33*,34 and in wild type at 20 nM BA, however the *hipp32,33*,34 sensitivity was slightly reduced at 40 nM BA (Figure 47H). Regarding the lateral root density, *hipp32,33,34* responded more sensitive at 20 nM BA compared to wild type and less sensitive at 40 nM BA (Figure 47I).

These results suggest that HIPPs have partially redundant, mostly negative effects on cytokinin sensitivity in *Arabidopsis* roots.

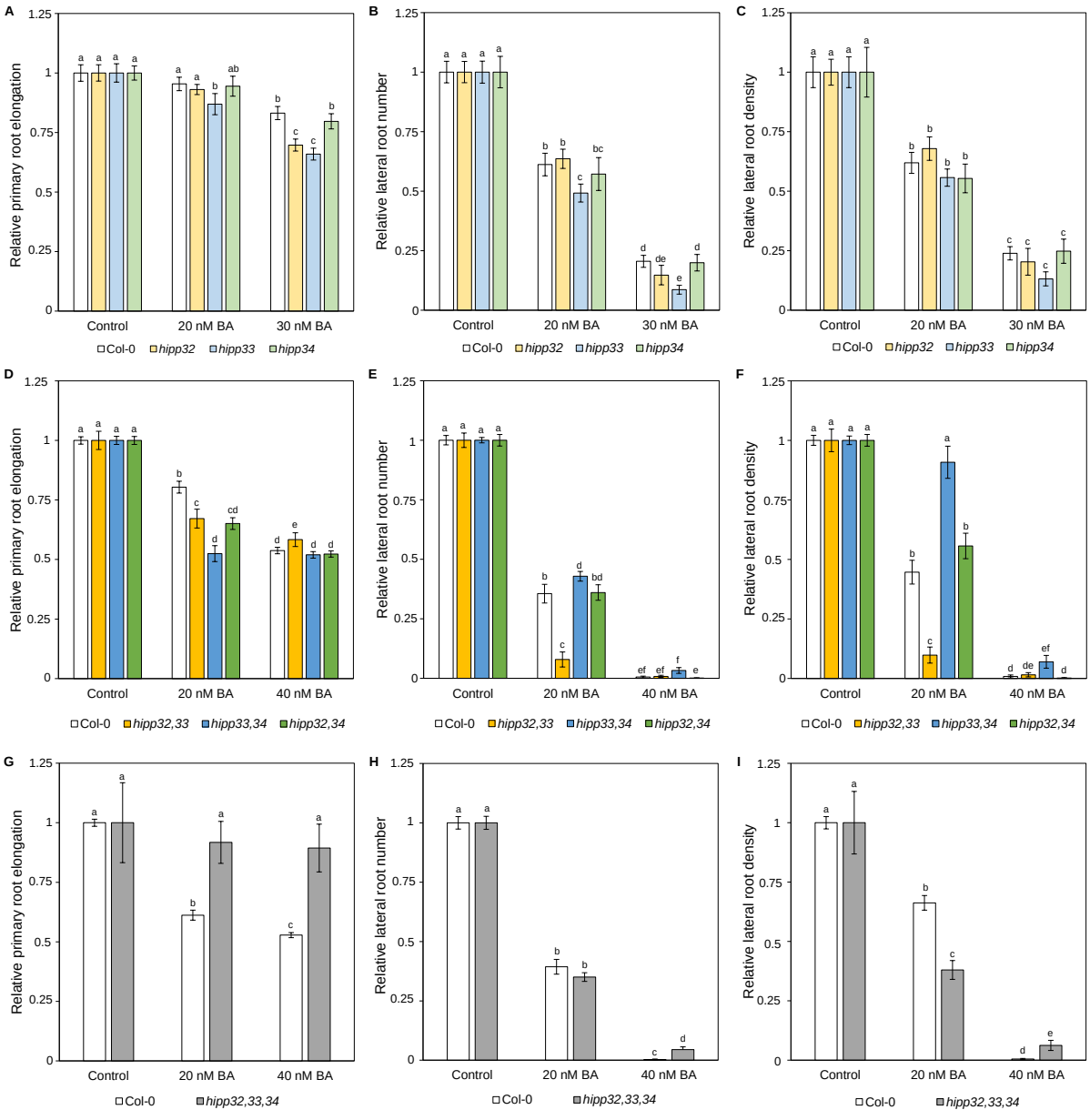

Figure 47. Analysis of *hipp* root growth responses to exogenous cytokinin.

Figure 47. Continued.
(A-C) Root growth of *hipp* single mutants. **(D-F)** Root growth of double mutants. **(G-I)** Root growth of triple mutant. The root growth was evaluated on DMSO (control) or BA-supplemented plates. **(A, D, G)** Average root elongation, determined between 3 and 12 days after germination. **(B, E, H)** Average lateral root formation, determined at 12 dpg. **(C, F, I)** Average lateral root density as lateral roots cm^{-1} primary root. Values represent means ± SE (n = 15 - 55). Statistical differences were evaluated using the Steel-Dwass pairwise ranking test ($p < 0.05$). Different letters indicate significant differences between groups.

3.7.2 The cytokinin content is subtly changed in *hipp* mutants

To analyze whether the lack of *HIPP* genes alters the endogenous cytokinin content, the cytokinin profiles of *hipp* single, *hipp32,33* and *hipp33,34* mutant seedlings was compared with that of wild-type seedlings (Figure 48). The total cytokinin content remained unchanged in *hipp* mutants in comparison to wild type. However, several changes in the content of different cytokinin metabolites were observed. The short-root *hipp32,33* mutant showed decreased levels of free cytokinin bases, cytokinin ribosides and increased levels of cytokinin *O*-glycosides (Figure 48). Increased levels of cytokinin *O*-glycosides were measured also in *hipp32* but not in *hipp33,* indicating that *HIPP32* and *HIPP33* are redundantly involved in regulating the levels of different active cytokinin types.

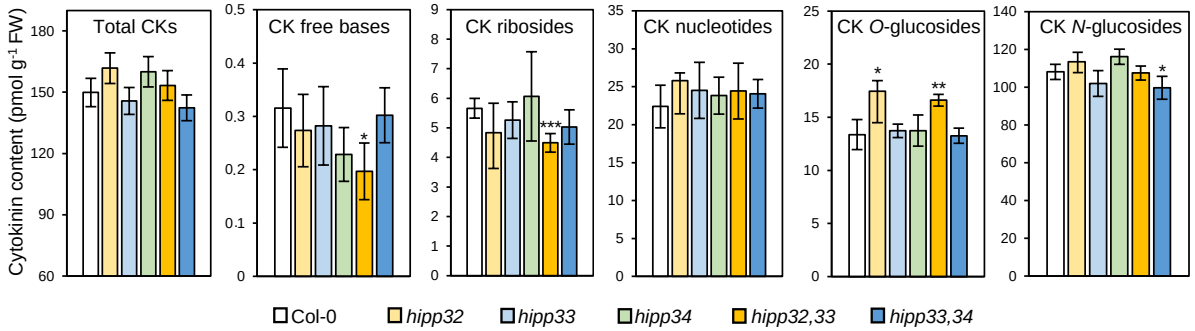

Figure 48. Cytokinin content in *hipp* single and double mutant plants.
Total content of different cytokinin (CK) types in 11-day-old seedlings grown under standard conditions *in vitro*. Significant differences to Col-0 were evaluated by one-way ANOVA followed by Dunnett post hoc test (*0.01 < p < 0.05, **0.00 < p < 0.01 and ***p < 0 .001. Values represent means ± SD (n = 5).

The content of individual cytokinin metabolites was mostly unchanged in the *hipp* mutant seedlings analyzed (Table 24). Interestingly, the free cytokinin bases, iP, *t*Z and *c*Z, were overall tendentially decreased *hipp* mutants. However, the *t*Z-level was diminished by ~50% in *hipp32,33* compared to wild type, whereas it was increased by ~42% in *hipp32* and it remained unchanged in *hipp33*. The levels of biologically inactive *t*Z glucosides, such as *t*Z 7-glucoside (*t*Z7G) and *t*Z 9-glucoside (*t*Z9G), were also decreased in *hipp32,33* mutants as compared to wild type. In *hipp33,34* mutants only the level of *t*Z riboside 5'-monophosphate (*t*ZRMP) was elevated compared to wild type. Both *hipp32* and *hipp33* single mutants exhibited

elevated levels of inactive *cZ* riboside *O*-glucoside (*c*ZROG) and increased by about twofold in *hipp32,33*, suggesting an additive effect of these genes.

Altogether, these results indicate that the lack of *HIPP* genes influences at least to some extent the endogenous cytokinin concentration, mostly by modulating the *tZ*-type cytokinin levels.

Table 24. Contents of individual cytokinin metabolites in *hipp* mutants.

Genotype	iP	iPR	iPRMP	iP7G	iP9G
Col-0	0.27 ± 0.07	2.28 ± 0.32	12.55 ± 1.11	58.24 ± 3.31	2.40 ± 0.25
hipp32	0.23 ± 0.07	2.11 ± 0.82	14.32 ± 2.57	65.76 ± 9.05	2.69 ± 0.31
hipp33	0.24 ± 0.07	2.37 ± 0.38	13.72 ± 1.65	58.22 ± 5.40	2.43 ± 0.26
hipp34	0.19 ± 0.04	2.50 ± 1.21	13.41 ± 1.38	65.54 ± 3.09*	2.72 ± 0.20
hipp32,33	0.18 ± 0.05	1.93 ± 0.46	13.55 ± 1.79	62.62 ± 3.21	2.37 ± 0.15
hipp33,34	0.26 ± 0.05	1.92 ± 0.45	13.09 ± 0.85	53.25 ± 5.19	2.10 ± 0.20

Genotype	*t*Z	*t*ZR	*t*ZRMP	*t*Z7G	*t*Z9G	*t*ZOG	*t*ZROG
Col-0	0.015 ± 0.005	2.38 ± 0.24	4.42 ± 0.29	23.35 ± 0.96	6.27 ± 0.29	7.33 ± 0.85	0.44 ± 0.06
hipp32	0.026 ± 0.007*	1.89 ± 0.39*	4.78 ± 0.63	21.35 ± 0.77**	5.21 ± 0.32**	9.07 ± 1.67	0.52 ± 0.02*
hipp33	0.011 ± 0.003	2.09 ± 0.30	4.91 ± 0.80	20.24 ± 1.85*	5.45 ± 0.28**	5.92 ± 0.44*	0.52 ± 0.07
hipp34	0.013 ± 0.004	2.70 ± 0.49	4.48 ± 0.58	24.04 ± 0.90	6.49 ± 0.21	7.90 ± 1.25	0.48 ± 0.03
hipp32,33	0.007 ± 0.001*	1.77 ± 0.23**	4.99 ± 0.40*	20.93 ± 1.26**	5.44 ± 0.41**	7.34 ± 0.88	0.58 ± 0.03**
hipp33,34	0.016 ± 0.004	2.27 ± 0.14	5.30 ± 0.71*	23.11 ± 0.96	6.15 ± 0.20	7.28 ± 0.75	0.46 ± 0.04

Genotype	*c*Z	*c*ZR	*c*ZRMP	*c*Z7G	*c*Z9G	*c*ZOG	*c*ZROG
Col-0	0.04 ± 0.01	0.89 ± 0.20	5.42 ± 1.75	17.45 ± 1.61	0.18 ± 0.03	2.24 ± 0.33	2.82 ± 0.52
hipp32	0.03 ± 0.01	0.73 ± 0.15	6.72 ± 2.01	18.02 ± 1.72	0.16 ± 0.02	2.68 ± 0.49	4.66 ± 1.04**
hipp33	0.03 ± 0.01	0.70 ± 0.12	5.91 ± 1.49	15.20 ± 1.61	0.16 ± 0.02	2.44 ± 0.17	4.29 ± 0.52**
hipp34	0.03 ± 0.01	0.77 ± 0.12	5.94 ± 1.38	16.94 ± 1.30	0.18 ± 0.02	2.08 ± 0.30	2.75 ± 0.49
hipp32,33	0.02 ± 0.01	0.69 ± 0.08	5.91 ± 1.82	15.74 ± 1.56	0.19 ± 0.05	2.51 ± 0.43	5.62 ± 0.64***
hipp33,34	0.03 ± 0.01	0.73 ± 0.09	5.69 ± 1.49	14.72 ± 1.20*	0.14 ± 0.04	2.09 ± 0.20	2.87 ± 0.14

Cytokinin metabolite content in 11-day-old seedlings (pmol g^{-1} fresh weight). iP, N^6-(Δ^2-isopentenyl)adenine; iPR, N^6-(Δ^2-isopentenyl)adenosine; iPRMP, N^6-(Δ^2-isopentenyl)adenosine 5'-monophosphate; iP7G, N^6-(Δ^2-isopentenyl)adenine 7-glucoside; iP9G, N^6-(Δ^2-isopentenyl)adenine 9-glucoside; *t*Z, *trans*-zeatin; *t*ZR, *trans*-zeatin riboside; *t*ZRMP, *trans*-zeatin riboside 5'-monophosphate; *t*ZOG, *trans*-zeatin *O*-glucoside; *t*ZROG, *trans*-zeatin riboside *O*-glucoside; *t*Z7G, *trans*-zeatin 7-glucoside; *t*Z9G, *trans*-zeatin 9-glucoside; *c*Z, *cis*-zeatin; *c*ZR, *cis*-zeatin riboside; *c*ZRMP, *cis*-zeatin riboside 5'-monophosphate; ***c***ZOG, *cis*-zeatin *O*-glucoside; *c*ZROG, *cis*-zeatin riboside *O*-glucoside; *c*Z7G, *cis*-zeatin 7-glucoside; *c*Z9G, *cis*-zeatin 9-glucoside. Significant differences to Col-0 were evaluated by one-way ANOVA followed by the Dunnett post hoc test (*0.01 < p < 0.05, **0.001 < p < 0.01 and ***p < 0.001. Values represent means ± SD (n = 5).

3.7.3 *HIPP* gene expression is not regulated by cytokinin

To investigate whether cytokinin affects the expression of *HIPP* genes, *Arabidopsis* seedlings cultivated in liquid medium for ten days and treated with 1 µM BA for 0.5, 2 and 6 hours. The *HIPP* gene expression was analyzed by qRT-PCR. The cytokinin response regulator *ARR5* was used as control (Figure 49).

The *ARR5* expression was upregulated more than 75-fold 30 min after cytokinin treatment and it dropped 50-fold after 2 hours of cytokinin treatment in plants grown under long day conditions (Figure 49A). Under short day conditions, *ARR5* expression was elevated 13-fold 1 hour after cytokinin treatment and declined gradually to 9-fold upregulation after 6 hours (Figure 49B). These results confirmed the efficiency of the treatment (Brenner *et al.*, 2005). However,

cytokinin did not affect the expression of *HIPP* genes. A slight increase was observed for *HIPP33* transcript levels upon cytokinin treatment for 0.5 h and 2 h, yet the increase was not statistically significant. A similarly slight increase was observed for *HIPP34* transcript levels in plants grown in standard conditions 2 h after cytokinin treatment (Figure 49A). *HIPP34* transcript levels were tendentially, but not significantly, increased 1 h and 6 h after cytokinin treatment of seedlings grown under short day conditions (Figure 49B).

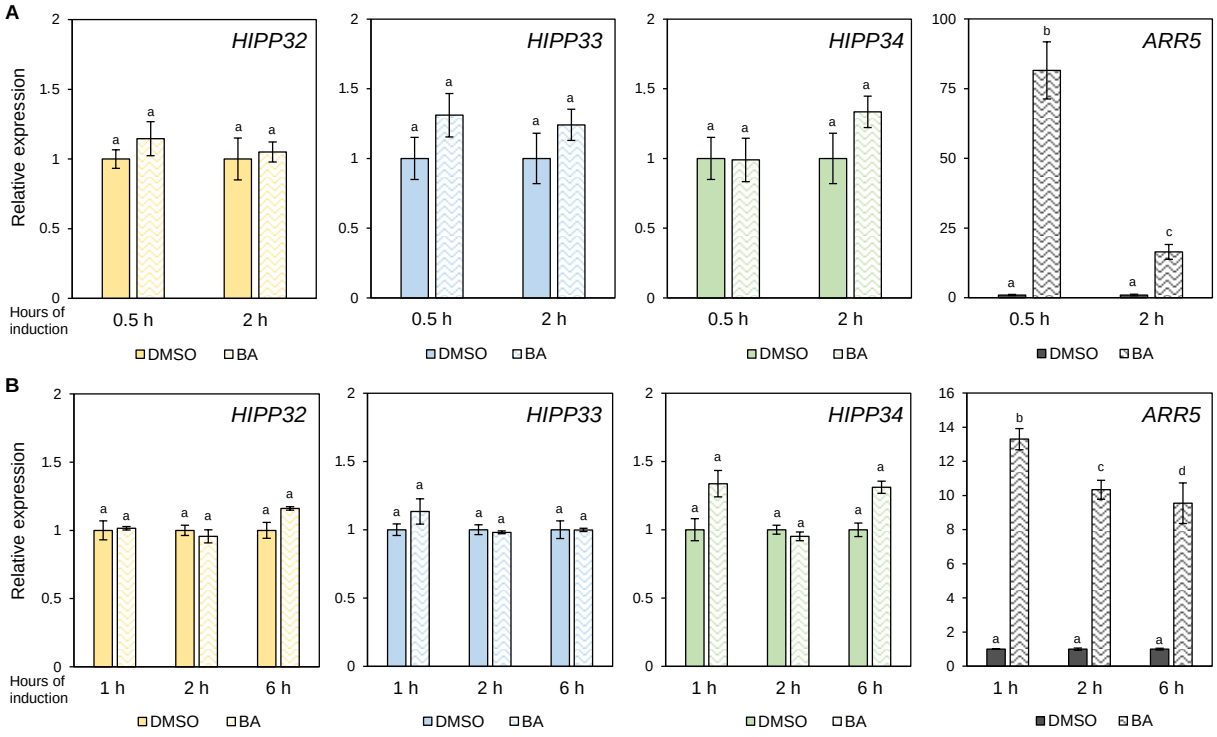

Figure 49. Expression of cluster-III *HIPP* genes in response to cytokinin.
Relative expression levels of *HIPP32*, *HIPP33* and *HIPP34* in 10-day-old *Arabidopsis* wild-type plants grown *in vitro* in standard long-day conditions **(A)** and in short-day conditions **(B)**. Quantitative RT-PCR analysis was performed using whole seedlings treated either with DMSO (control) or with 1 µM BA for 0.5 and 2 h **(A)** and 1 h, 2 h and 6 h **(B)**. The cytokinin reporter *ARR5* was used as induction control. Values are averages of three biological replicates ± SD. Significant differences were evaluated by analysis of variance (ANOVA) followed by Tukey HSD post hoc test ($p < 0.05$). Different letters indicate significant differences between groups.

3.7.4 Loss of *HIPP* genes impacts the cytokinin signaling and sensitivity in roots

To investigate whether the lack of *HIPP* genes causes changes in the cytokinin status, the expression level of several type-A *ARR* genes encoding downstream components of the cytokinin signaling pathway was analyzed (To *et al.*, 2004). The qRT-PCR analysis performed in *hipp* single mutants and selected *hipp32,33* and *hipp33,34* double mutants revealed partially strong changes in the expression of type-A *ARR* genes (Figure 50). The steady-state transcript levels of *ARR5*, *ARR6*, *ARR15* and *ARR16* genes were strongly upregulated in *hipp32* and *hipp33*. In contrast, except of *ARR5*, the transcript levels of all tested *ARRs* were

downregulated in *hipp34*. Intriguingly, the *ARR* transcript levels found to be increased in *hipp32* and *hipp33* were slightly decreased in *hipp32,33* (Figure 50). *ARR5*, *ARR6* and *ARR15* transcript levels were also elevated in *hipp33,34* (Figure 50). *ARR16* transcript level, which was upregulated in *hipp33* and downregulated in *hipp34,* was restored at the wild type level in *hipp33,34*, suggesting that *HIPP33 and HIPP34* antagonistically function to regulate *ARR16* activity.

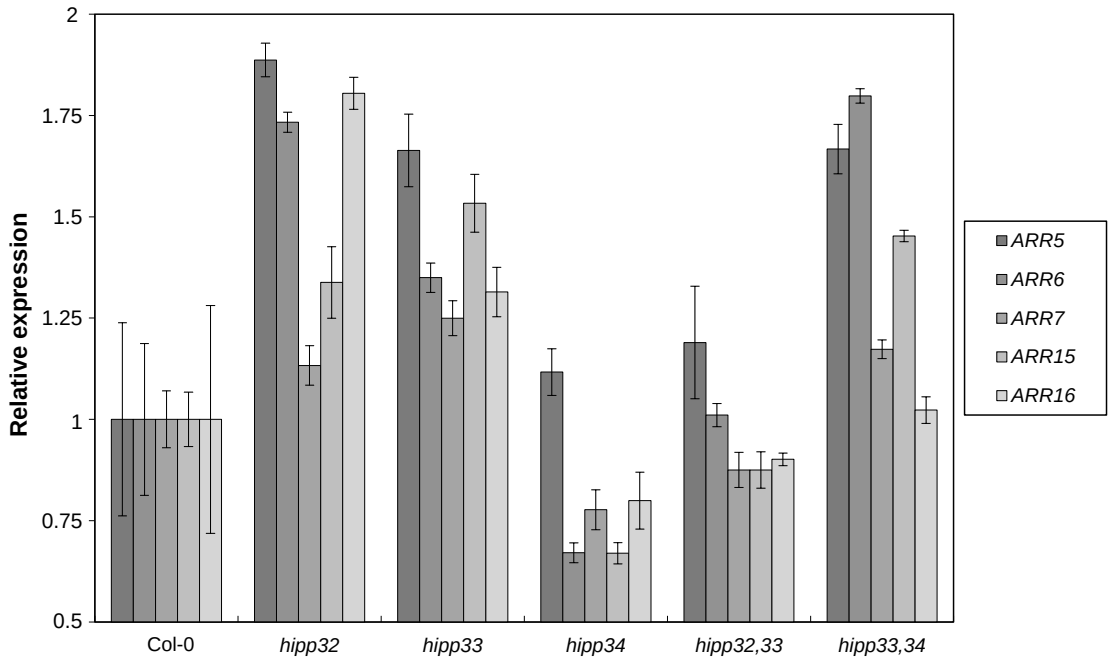

Figure 50. Expression of type-A *ARR* genes in *hipp* mutants.
Relative expression levels of *ARR5, ARR6, ARR7, ARR15* and *ARR16* in 12-day-old *hipp* plants in comparison to wild type (Col-0). Quantitative RT-PCR analysis was performed using whole seedlings. Values are averages of two or three biological replicates ± SD.

Both the altered root phenotypes and the enhanced cytokinin responsiveness suggest that the cytokinin activity in *hipp* mutants might differ from that of wild type. In order to particularly monitor the cytokinin activity in roots, the synthetic cytokinin reporter *TCSn:GFP* was introgressed in *hipp* single, double and triple mutants. *TCSn:GFP* reflects the transcriptional activity of type-B response regulators and allows the visualization of cytokinin-response in a tissue-specific manner (Zürcher *et al.*, 2013; Liu and Müller, 2017). Figure 51A illustrates representative confocal images of wild-type and *hipp* RAM expressing *TCSn:GFP*.

The general *TCSn:GFP* distribution in *hipp* single and double mutants was similar to that of wild type and it was consistent with previously described *TCSn:GFP* expression patterns (Zürcher *et al.*, 2013). The strongest expression was observed in the lateral root cap cells, followed by the columella cells and the procambial cells. However, the *TCSn:GFP* expression pattern in *hipp* triple mutants slightly differed from that of wild type and the other *hipp* mutants respectively (Figure 51A). *TCSn:GFP* intensity distribution appeared weaker and broader

within the columella cells. Moreover, unlike in wild type, in *hipp32,33,34 TCSn:GFP* was also detected in the epidermis cells and in the presumably distal stem cells, underneath the putative QC (Figure 51A).

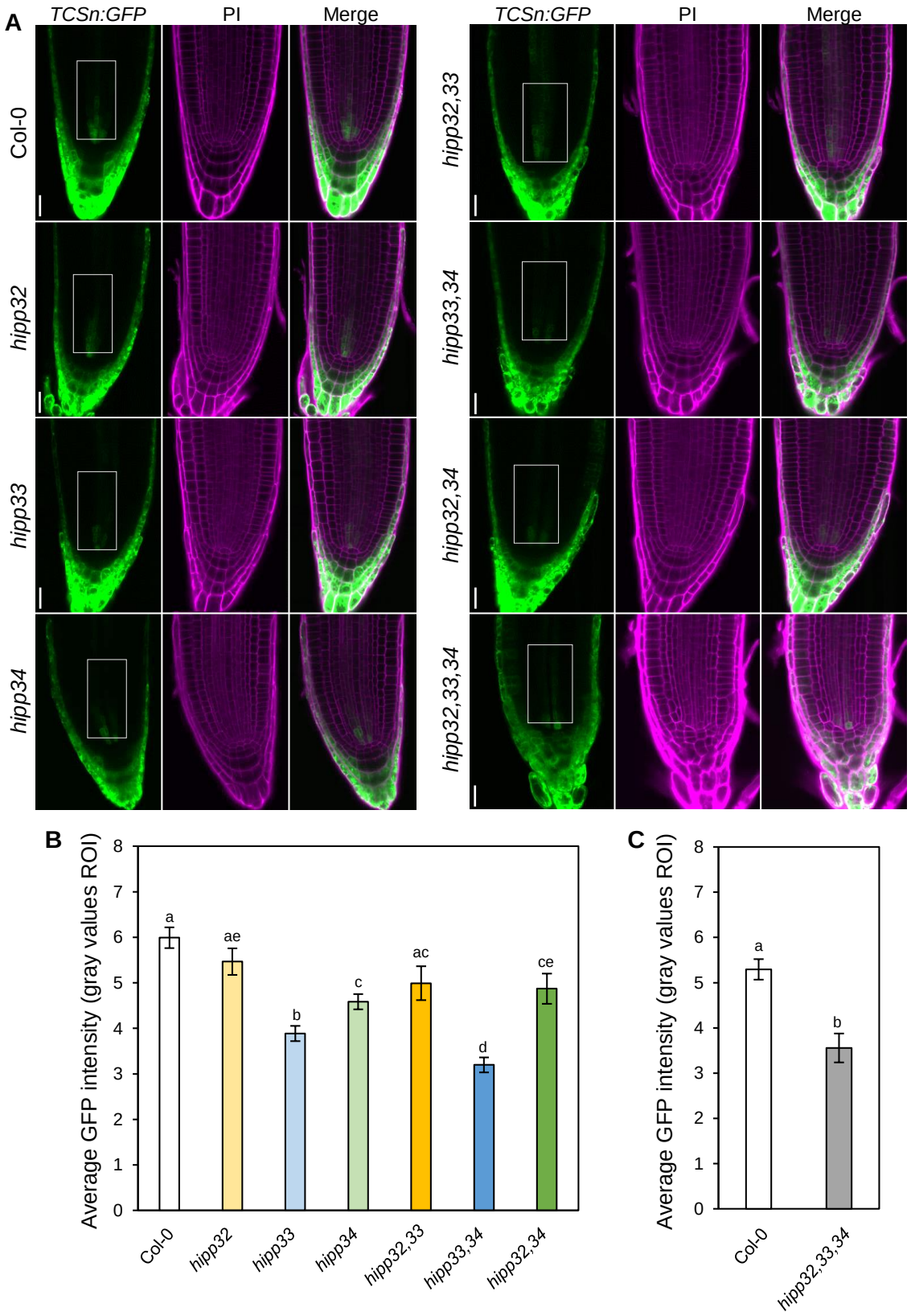

Figure 51. Cytokinin activity during root development is distinctly altered in *hipp* root meristems.

Figure 51. Continued.
(A) Expression of *TCSn:GFP* cytokinin synthetic sensor in the root apex of 5-day-old wild-type and *hipp* mutant seedlings stained with propidium iodide (PI, magenta). The boxes represent the regions used for GFP signal quantification. **(B, C)** GFP intensity in the selected region of interest (ROI). Scale bars = 25 µm. Values represent means ± SE (n=10-15). Wilcoxon test was performed to assess the significant differences between groups ($p < 0.05$). Different letters label groups of different statistical significance.

In order to quantify the *TCSn:GFP* intensity a defined region comprising procambial cells was selected directly above the quiescent center, and the mean gray value of the region was determined (Figure 51A). In comparison to wild type, the single mutants *hipp33* and *hipp34* exhibited ~30% lower *TCSn:GFP* intensity (Figure 51B). This was further reduced by ~50% in *hipp33,34* double mutant (Figure 51B). A diminished *TCSn:GFP* intensity was also measured in *hipp32,34*, but to a lesser extent than in *hipp33,34* (Figure 51B). Although not statistically significant, the cytokinin status was tendentially reduced also in *hipp32* and *hipp32,33* (Figure 51B). In the triple mutants, *TCSn:GFP* intensity was reduces as compared to wild type and exhibited similar intensity as that of *hipp33,34* (Figure 51C). These results suggest that mainly *HIPP33* and *HIPP34* contribute to positively regulate the cytokinin activity in the root.
The single mutant *hipp33* and all *hipp* double mutants showed an increased sensitivity towards exogenous cytokinin in root assays (see 3.7.1). To verify these results, cytokinin sensitivity assays were performed using *hipp* plants expressing *TCSn:GFP*. Figure 52A illustrates representative images of root apices exposed to 1 µM BA for 16 hours. A defined region above the quiescent center was selected to quantify the *TCSn:GFP* intensity in control and respectively BA-treated seedlings. The relative mean values are shown in Figure 52 (B to D). Consistent with published data (Liu and Müller, 2017), 1 µM BA was sufficient to induce *TCSn:GFP* expression in roots and the average fluorescent intensity of *GFP* increased approximately six fold in wild type (Figure 52B,C,D). The increase was significantly higher in *hipp32* and *hipp33* (Figure 52B). In *hipp34*, the change in *TSCn:GFP* intensity upon BA treatment was similar to that of wild type (Figure 52B). The double mutants *hipp32,33* and *hipp33,34* reacted more sensitively than wild-type and *hipp32,34* (Figure 52C). However, the fold change of *TCSn:GFP* expression in these double mutant did not exceed those of *hipp* single mutants. The triple mutant *hipp32,33,34* reacted more sensitively to cytokinin than wild type (Figure 52D). However, the change in *TCSn:GFP* expression in *hipp32,33,34* upon BA-treatment was tendentially higher, but not statistically significant, than that of *hipp* single and respectively double mutants. Taken together, the lack of *HIPP* genes altered the steady-state cytokinin activity in the roots and led to an elevated responsiveness to exogenous cytokinin.

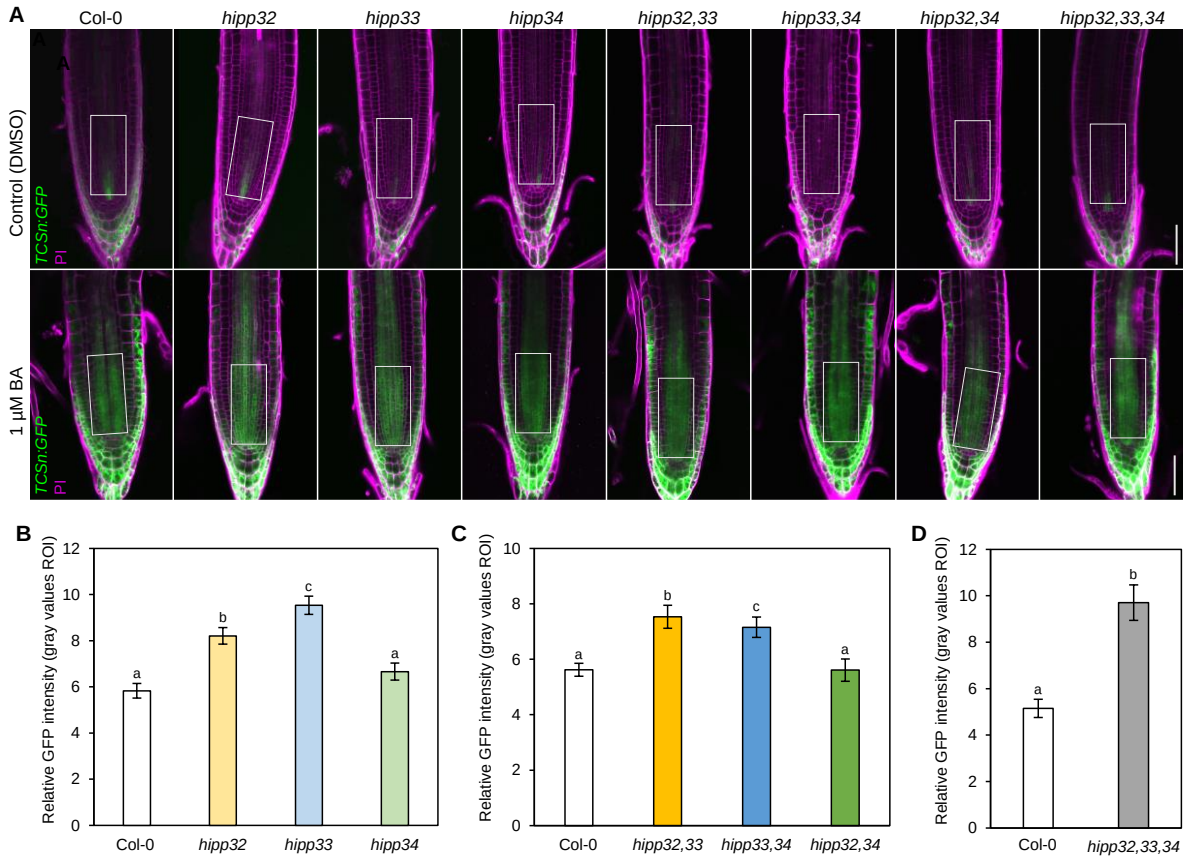

Figure 52. Lack of *HIPP32 and HIPP33* leads to an increased sensitivity towards exogenous cytokinin.
(A) Expression of *TCSn:GFP* cytokinin synthetic sensor in the primary root apex of wild-type and *hipp* mutant plants stained with propidium iodide (PI, magenta). Seedlings were grown on plates for 5 days and transferred to liquid ½ MS medium containing either DMSO (control) or 1 µM BA. Confocal images were taken 16 hours later. The boxes represent the regions used for GFP quantification. **(B, C, D)** Relative GFP intensity in the selected region of interest (ROI) in BA-treated samples normalized to control. Scale bars = 25 µm. ROI: region of interest. Values represent means ± SE (n = 5-31). Statistical differences were evaluated using the Steel-Dwass pairwise ranking test ($p < 0.05$). Different letters indicate significant differences between groups.

3.7.5 Role of cluster-III *HIPP*s in the global transcriptional response to cytokinin

To investigate whether HIPPs play a role in the transcriptional response to cytokinin, an RNA-Seq analysis was conducted in wild-type, *hipp33* and *hipp32,33,34* seedlings treated with exogenous cytokinin. A threshold for a false discovery rate (FDR) adjusted p-value < 0.05 was used to determine significant differences in gene expression between *hipp* mutants and wild type upon cytokinin treatment.

3.7.5.1 *HIPP* genes are required for transcriptional response to cytokinin

The screening for differentially expressed genes (DEGs) in response to cytokinin resulted in 2,634 DEGs in wild type, from which 1,413 genes were upregulated and 1,221 downregulated (Figure 53A). In comparison to wild type, the number of cytokinin-deregulated genes was

slightly reduced in *hipp33* mutant, where 2,493 genes (1,241 up- and 1,252 downregulated) were transcriptionally affected by cytokinin (Figure 53B). Moreover, in *hipp* triple mutant the number of cytokinin-deregulated genes was reduced by 849 genes, approximately 33% less than in wild type. 1,785 genes were thus identified to be differently expressed in *hipp32,33,34* in response to exogenous cytokinin, from which 799 genes were up- and 986 downregulated (Figure 53C). These results strongly indicate that the *HIPP* genes are functionally relevant for the transcriptional responses to cytokinin.

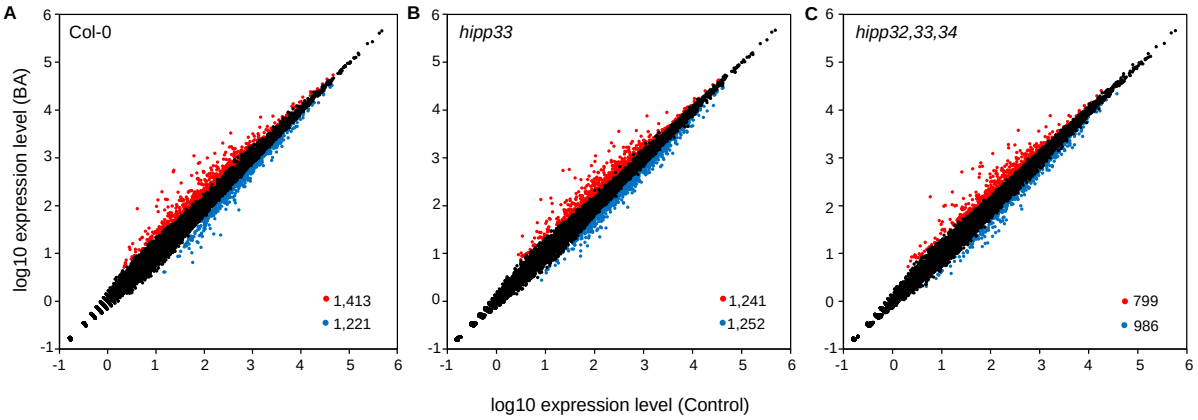

Figure 53. Differential gene expression in wild type and *hipp* mutants in response to cytokinin. Scatter plots showing differentially expressed genes (DEGs) in wild type **(A)**, *hipp33* **(B)** *and hipp32,33,34* **(C)** 5-day-old seedlings treated for 1 h with 5 µM BA. Fold change was compared with average transcript levels after BA treatment relative to control (DMSO) values in each genotype. Colors indicate statistically significant expressed gene with an adjusted p-value < 0.05 that were either upregulated (red) or downregulated (blue). Black dots represent genes which were not differentially expressed (p-value > 0.05). Numbers indicate the number of up- and downregulated DEGs.

In order to further investigate the transcriptomic changes caused by the cytokinin treatment, pairwise comparisons of the cytokinin responsive genes differently expressed in wild type and *hipp* mutants were performed. There was an overlap of approximately 60% between cytokinin responsive genes in wild type and *hipp*33 (Figure 54A). Wild-type and *hipp32,33,*34 seedlings shared 1,223 DEGs, representing approximately 45% and 70% of DEGs in wild type and *hipp32,33,34*, respectively (Figure 54B). In both cases, a large proportion of the overlapping genes between wild type and *hipp* mutants exhibited comparable fold change levels and only few genes differed in their fold change levels or were identified to be deregulated in opposite direction in *hipp* mutants compared to wild type (Figure 54C, D).

Interestingly, 1,102 cytokinin responsive genes that were no longer differentially expressed in response to cytokinin in *hipp33* (Figure 54A). Among these genes, 624 (57%) up- and 478 (43%) downregulated (data not shown). Lack of all cluster-III *HIPP* genes strongly increased the number of genes that failed to respond to cytokinin as there now were 1411 genes, equaling 54% of DEGs, exclusively deregulated in wild type (Figure 54B). In this case, the

proportion of genes induced and repressed by cytokinin was 55% (772 genes) and 45% (639 genes), respectively (data not shown). Furthermore, there were 961 and 562 DEGs that were not significantly differentially expressed in response to cytokinin in wild-type seedlings and were exclusive to *hipp33* and *hipp32,33,34*, respectively (Figure 54A, B).

Collectively, these results suggest that 42% and 54% of genes differentially expressed in response to cytokinin in wild type failed to respond to cytokinin in *hipp33* and *hipp32,33,34*, respectively. Genes from these two groups exhibiting a log2 fold change greater than 1.5 and smaller than -1.5 are listed in Table A1 and A2, respectively (Appendix).

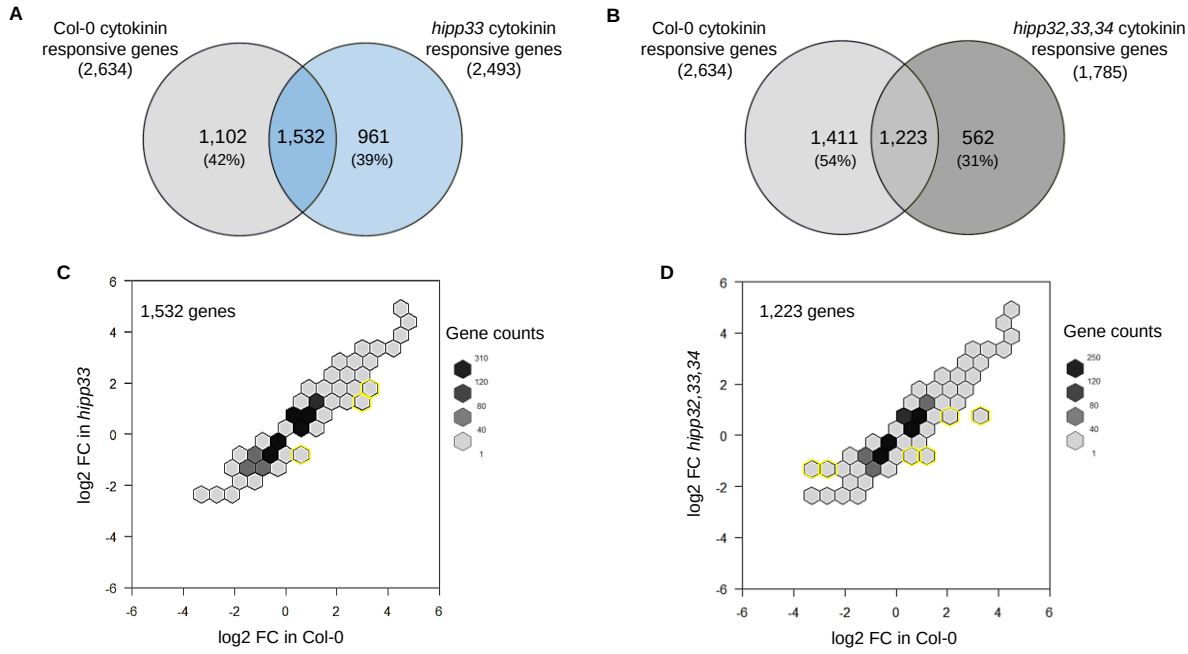

Figure 54. Comparison of differentially expressed genes in response to cytokinin.
(A, B) Venn diagrams showing the number of exclusive and overlapping DEGs in response to exogenous cytokinin in wild type and *hipp33* **(A)** and wild type and *hipp32,33,34* **(B)**. The percentages of the exclusive cytokinin responsive genes are indicated in brackets. Cytokinin responsive genes were determined relative to control. No cut off for the log2 fold change (log2 FC) was applied. FDR < 0.05. The total number of DEGs is indicated in brackets. **(C, D)** Density plots of the overlapping genes deregulated after cytokinin treatment in wild type and *hipp33* **(C)** and wild type and *hipp32,33,34* **(D)**. Hexagons comprising genes with different and/or opposite log2 FC levels are highlighted in yellow.

The hierarchical cluster analysis applied to all genes that showed a differential expression after BA treatment also demonstrates the loss of cytokinin transcriptional response in *hipp* mutants (Figure 55). The complete set of 3,995 cytokinin-deregulated genes were clustered in five major hierarchical groups, with overall different expression patterns between wild type and *hipp* mutants (Figure 55). For instance, cluster 1 contained genes that showed a strong downregulation in wild type and a gradual decrease of the expression fold change in *hipp33* and *hipp32,33,34* (Figure 55). Similarly, cluster 5 contained many strongly upregulated genes in wild type which exhibited a gradual decrease in their expression in *hipp33* and *hipp32,33,34*

(Figure 55). Cluster 2 and 3 comprised a large number of cytokinin-deregulated genes with inhomogeneous expression patterns among the genotypes. Several subgroups within these clusters contained genes that were either no longer responsive to cytokinin or showed a different response in *hipp* mutants (Figure 55; highlighted in rectangles).

To summarize, both the pairwise comparisons and the hierarchical clustering analysis revealed that a number of genes regulated by cytokinin in wild type lost or showed altered transcriptional response in *hipp33* and particularly in *hipp32,33,34*, indicating that *HIPP* gene activity is required for the cytokinin responses.

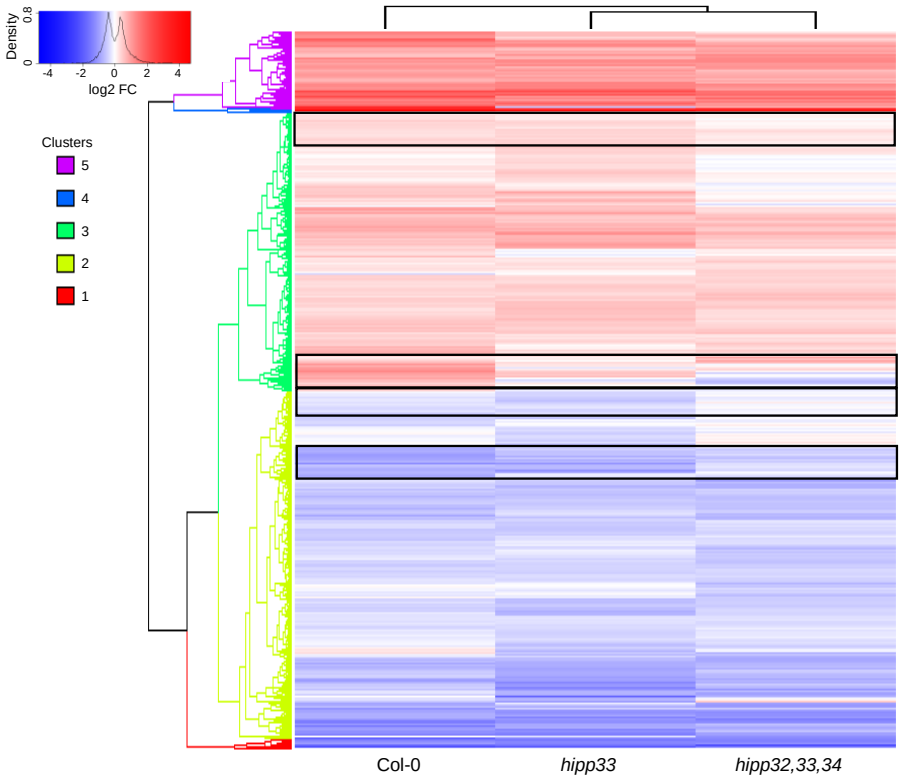

Figure 55. Clustered heat map of genes differentially expressed in response to cytokinin.
Heat map shows the expression patterns of DEGs and dendrograms representing hierarchical clustering generated from the log2 fold change (FC) values of BA-treated wild type, *hipp33* and *hipp32,33,34* samples as compared to their respective control. Black rectangles highlight gene groups with lost or altered cytokinin response in *hipp* mutants compared to wild type. Genes for which at least one genotype showed a differential expression (p-value < 0.05) were included in the analysis.

In order to gain a deeper insight into the nature of the cytokinin-responsive genes, a subset of known cytokinin-responsive genes, which exhibited an altered expression upon cytokinin treatment in various microarray and RNA-Seq analyses, was analyzed (Bhargava *et al.*, 2013). Approximately 75% of the 'golden list' cytokinin-responsive genes were also identified as up- or downregulated in wild-type samples within this RNA-Seq experiment, thus confirming that the BA treatment was successful, as prior tested by qRT-PCR (data not shown). The expression levels of the canonical cytokinin response genes in *hipp* mutants were identified

after BA treatment. Although the number of cytokinin response genes was slightly reduced in *hipp33* and *hipp32,33,34* as compared to wild type, their expression pattern was largely comparable among them and highly similar to wild type (Table A3; Appendix).

Given that the 'golden list' genes are only a small subset of cytokinin responsive genes which can vary in individual experiments, the most cytokinin-deregulated genes were identified in wild type and their response to cytokinin in *hipp* mutants was analyzed (Figure 56).

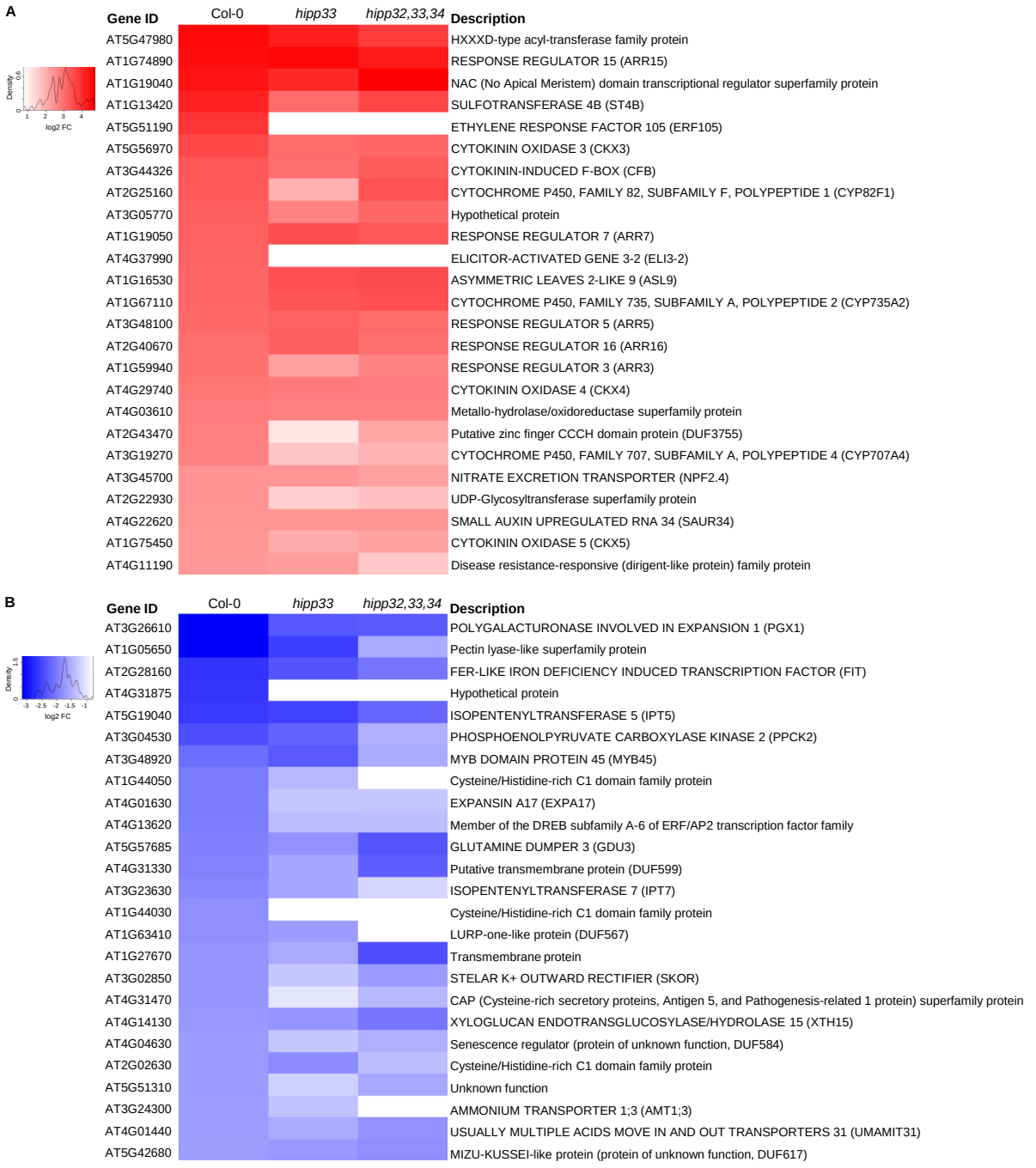

Figure 56. Expression pattern of the top 25 cytokinin-induced genes.
The heat map shows the expression pattern of top 25 induced **(A)** and repressed **(B)** genes by cytokinin in wild type in comparison with *hipp33* and *hipp32,33,34*. No cut off for the log2 fold change (FC) was applied. FDR < 0.05.

Several of the top 25 cytokinin-induced genes in wild type exhibited partially altered expression pattern in *hipp* mutants (Figure 56A). Interestingly, the most transcriptional changes compared to wild type were observed in *hipp33*. Among the top 25 cytokinin-induced genes, two genes belonged to the *HIPP*-dependent genes, *i.e.* genes that did not respond to cytokinin in *hipp* mutants (Figure 56A). These are the *ETHYLENE RESPONSE FACTOR 105* (*ERF105*), encoding a transcription factor from the ethylene signaling and response pathway, known to be induced by cytokinin (Müller and Munné-Bosch, 2015; Brenner *et al.*, 2005), and the *ELICITOR-ACTIVATED GENE 3-2* (*ELI3-2*), encoding an aromatic alcohol dehydrogenase, which has been shown to pe upregulated under biotic stress conditions (Somssich *et al.*, 1996; Iizasa *et al.*, 2017).

Many genes among the top 25 most downregulated genes after cytokinin treatment in wild type were less pronounced in *hipp* mutants (Figure 56B). For instance, *PGX1* and *EXPA17* genes, which were also identified to be downregulated by cytokinin and encode proteins involved in cell expansion processes (Xiao *et al.*, 2014; Lee *et al.*, 2001; Lee *et al.*, 2007). Several genes encoding transmembrane proteins and transporter were moderately repressed by cytokinin in wild type and *hipp33*, whereas were strongly downregulated in *hipp32,33,34* (Figure 56B). Furthermore, a few genes of biological function were highly downregulated by cytokinin in wild type but lost the response *hipp* mutants (Figure 56B).

Taken together, these results revealed that several *HIPP*-dependent cytokinin responsive genes belong to the most deregulated genes by cytokinin in wild type. Further detailed studies will be required in order to investigate the molecular links between these genes and *HIPP*-dependent cytokinin response regulation.

3.7.5.2 Exploratory analysis of *HIPP*-dependent cytokinin responsive genes

To gain insight into the molecular nature of *HIPP*-dependent cytokinin-deregulated genes, GO term analysis was performed. Genes that were differently expressed in wild type but failed to respond to cytokinin in *hipp33* mutant (Figure 54A) were annotated in 34 enriched GO terms in the ‘biological process’ (BP), 16 in the ‘molecular function’ (MF) and 5 in the ‘cellular component’ (CC) category (Figure 57). GO terms with particularly high fold enrichment within the BP category were those involved in ‘cell-cell junction assembly’, ‘negative regulation of nucleic acid-templated transcription’ and ‘calcium ion homeostasis’ (Figure 57). Four genes were associated to the GO term ‘cell-cell junction assembly’. This GO includes 5 genes which encode members of a novel protein family, Casparian strip membrane domain proteins, and have been described to mediate Casparian strip formation in the endodermis (Roppolo *et al.*, 2011). Interestingly, the majority of genes associated to the GO term ‘negative regulation of nucleic acid-templated transcription’ encode JAZ proteins with key roles in jasmonate signaling

(Pauwels and Goossens, 2011). The GO term 'regulation of jasmonic acid mediated signaling pathway' was also enriched in this set of DEGs (GO:2000022; Figure 57).

HIPP33-dependent cytokinin responsive genes were also associated to GO terms involved in 'indole-3-acetaldehyde oxidase activity' and 'auxin binding' within the MF category (Figure 57). Genes included in these terms encode aldehyde oxidases, involved in the abscisic acid biosynthesis, and an isoform of the auxin oxidase DAO1, responsible for the root-specific oxidative inactivation of auxin in *Arabidopsis* (Zhang *et al.*, 2016). The GO term 'ferric-chelate reductase activity', including genes which encode different FERRIC REDUCTION OXIDASEs, was also markedly enriched in this DEG set (GO:0000293, Figure 57). Within the CC category, 'Casparian strip' was the highest enriched GO term, containing most of the genes associated with the GO term 'cell-cell junction assembly' (see text above). GO terms involved in 'cell wall' and 'integral component of plasma membrane' were also enriched (Figure 57).

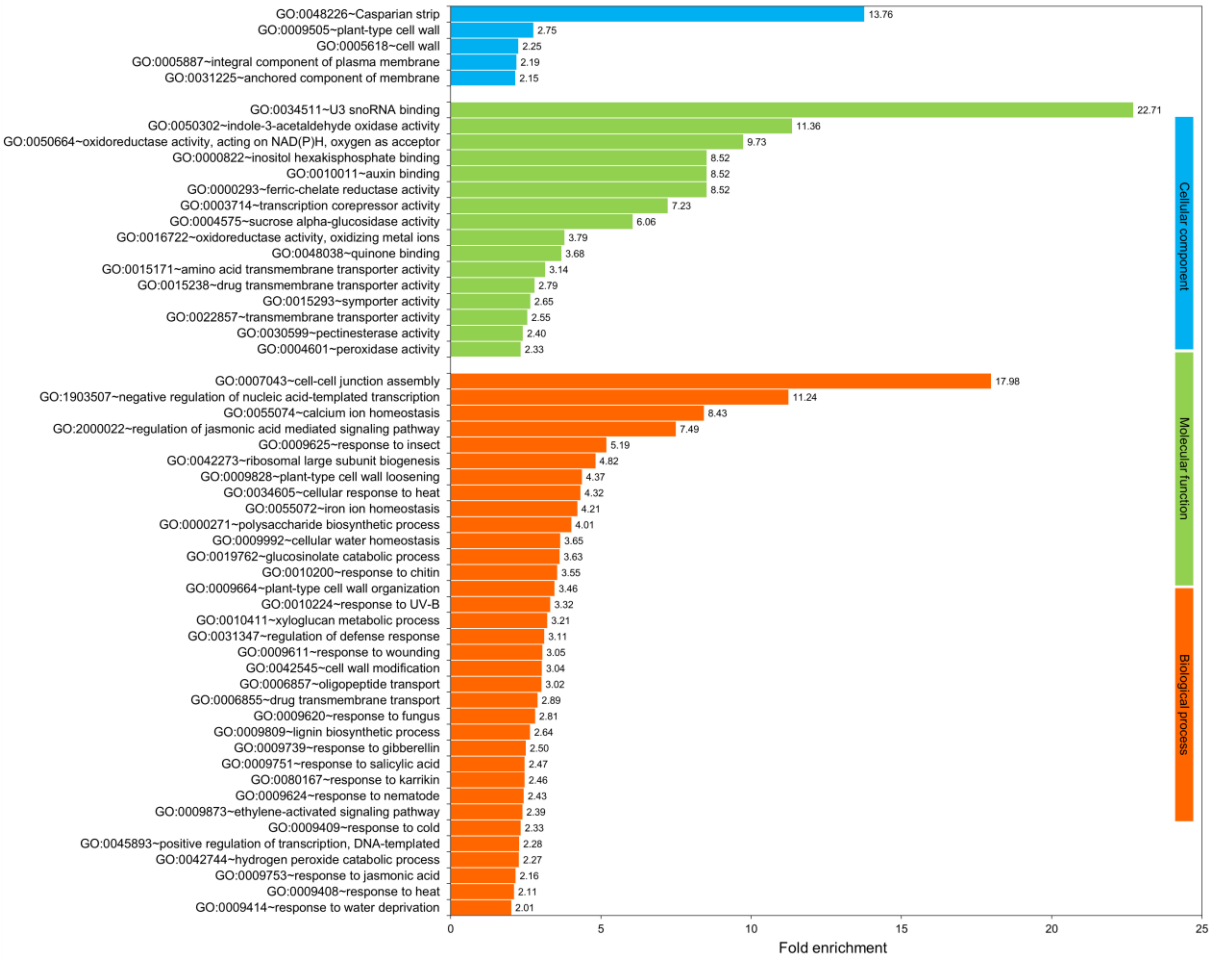

Figure 57. GO term enrichment analysis of DEGs unaffected by cytokinin in *hipp33*.
Enrichment of 'biological process', 'molecular function' and 'cellular component' GO terms for genes that were differently expressed in wild type, but not differently expressed in *hipp33* after cytokinin treatment. Fold enrichment ≥ 2. Fisher Exact modified p-value < 0.05.

Genes that did not respond to cytokinin in *hipp32,33,34* (Figure 54B) were annotated to 26 GO terms in the BP, 10 terms in MF and 5 in the CC category (Figure 58). A high number of GO terms identified for the genes unaffected by cytokinin in *hipp33* (Figure 57) were also overrepresented in this set of genes, although their fold enrichment levels were slightly lower (Figure 58). However, several GO terms were exclusively identified in each of the analyzed gene sets. For example, the GO terms 'indole-3-acetaldehyde oxidase activity' or 'auxin binding' were no longer enriched in the cytokinin-unaffected genes in *hipp32,33,34.* In contrast, the GO terms related to 'glutamate biosynthetic process' (GO:0006537) or 'growth factor activity' (GO:0008083) were identified for the cytokinin-unaffected genes in *hipp32,33,34*, but not in *hipp33* (Figure 57, 58). GO:0006537 includes mainly genes encoding GLUTAMATE SYNTHASEs and GO:0008083 contains several genes which encode proteins from the root meristem growth factor (RGF) family.

Taken together, the identified GO categories indicate that specific GO terms were considerably enriched, suggesting that *HIPP* may mediate cytokinin responses related to specific physiological or developmental processes.

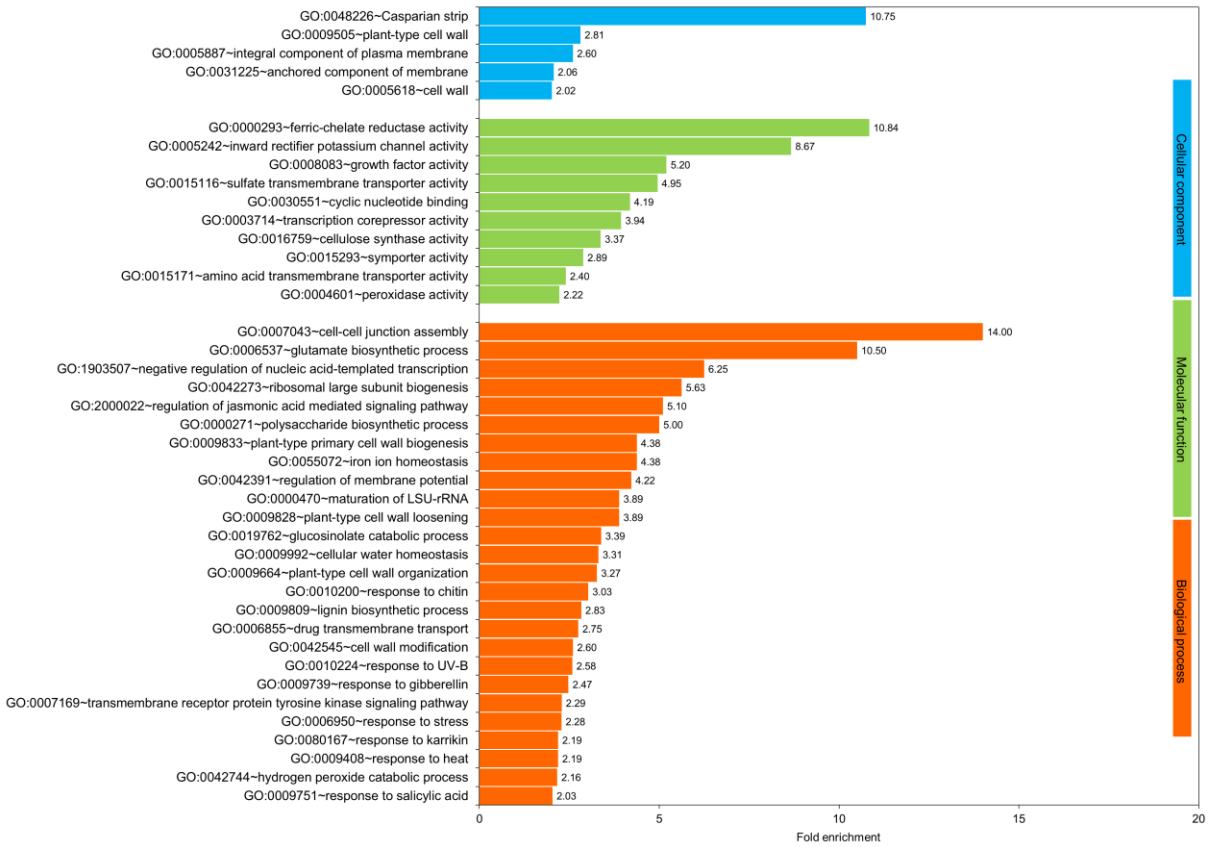

Figure 58. GO term enrichment analysis of DEGs unaffected by cytokinin in *hipp32,33,34*.
Enrichment of 'biological process', 'molecular function' and 'cellular component' GO terms for genes that were differently expressed in wild type, but not differently expressed in *hipp32,33,34* after cytokinin treatment. Fold enrichment ≥ 2. Fisher Exact modified p-value < 0.05.

3.7.5.3 *HIPP* expression in RNA-Seq remains unchanged in response to cytokinin

qRT-PCR analysis (section 3.7.3) demonstrated that cluster-III *HIPP* gene expression was not regulated by cytokinin. However, it was interesting to investigate whether cytokinin affects the expression of *HIPP* genes in RNA-Seq by comparing their transcript levels in wild-type seedlings treated with DMSO (control) and cytokinin (BA). For this purpose, the sequencing coverage and the fragments per kilobase per million mapped reads (FPKM) associated with *HIPP* genes were extracted and analyzed from the raw RNA-Seq data. However, there was no difference in the transcript level of the individual *HIPP* genes, as both the read coverage (Figure 49A) and the transcript counts (Figure 59B) were comparable between the BA-treated samples and control, thus confirming the qRT-PCR results.

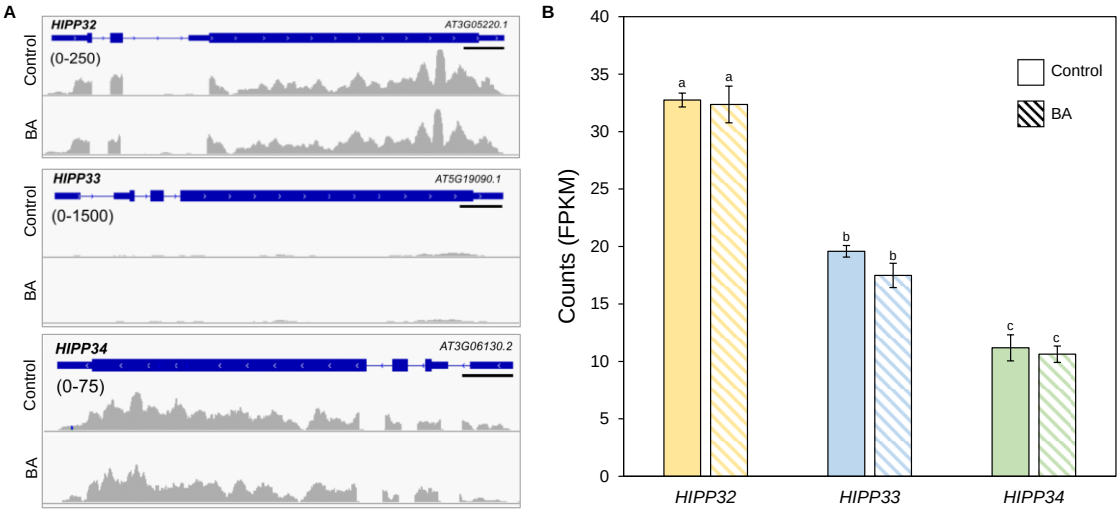

Figure 59. **Expression of cluster-III *HIPP* genes in response to cytokinin in RNA-Seq experiment. (A)** Visualization of transcript levels of *HIPP* genes in the wild-type seedlings treated with DMSO (control) and cytokinin (BA). Bed graphs were generated with the Integrated Genome Viewer (IGV). Numbers in brackets represent the coverage data range. Scale bars = 250 bp. **(B)** Counts for the expression of the *HIPP* genes in wild type, with and without cytokinin. FPKM: fragments per kilobase per million mapped reads. Values represent means ± SD (n=3). Different letters indicate significant differences between groups as evaluated by the Steel-Dwass pairwise ranking test ($p < 0.05$).

3.8 HIPPs are relevant for the symplasmic transport through PD

PD are intercellular channels across the plant cell walls that mediate and facilitate the symplasmic molecular transport between neighboring cells, which is required for plant growth and development (Benitez-Alfonso, 2014). The symplasmic transport relies on the permeability of PD and it is highly regulated throughout development in a dynamic manner (Sevilem *et al.*, 2013). Several PD-localized proteins have been found to regulate the plasmodesmal permeability (Sager and Lee, 2018). To investigate whether the lack of *HIPP* genes affects the PD permeability and thus to explore the possible functions of HIPP proteins at PD, a series of

symplasmic transport assays were performed in *hipp* mutant plants. Furthermore, the perturbations observed in the root development of *hipp* mutants, particularly *hipp32,33* and *hipp32,33,34,* might be the result of an altered symplasmic intercellular connectivity.

3.8.1 Assessing the symplasmic transport through PD using CFDA

The symplasmic tracer 5(6)-carboxyfluorescein diacetate (CFDA) has been widely used to assess the phloem transport in living plants (Zhu *et al.*, 1998). CFDA is non-fluorescent, but when applied to source leaves it is subsequently cleaved by endogenous esterases to produce the fluorescent, membrane-impermeant carboxyfluorescein (CF) (Knoblauch *et al.*, 2015), which is then translocated via phloem into the sink tissues (Oparka *et al.*, 1994). The unloading of the CF dye in root tips occurs through PD and it directly indicates the PD-mediated symplasmic diffusion (Oparka *et al.*, 1994; Ross-Elliott *et al.*, 2017).

To investigate whether HIPPs regulate PD permeability the CFDA loading assays were performed. The short-root double mutant *hipp32,33* and double mutant *hipp33,34* with enhanced roots were tested. CFDA was loaded onto single cotyledons of 6-day old seedlings and the efficacy of phloem unloading was monitored at the primary root tips after one hour (Oparka *et al.*, 1994; Knoblauch *et al.*, 2015). CLSM images exemplifying the CF unloading into the root are shown in Figure 60A.

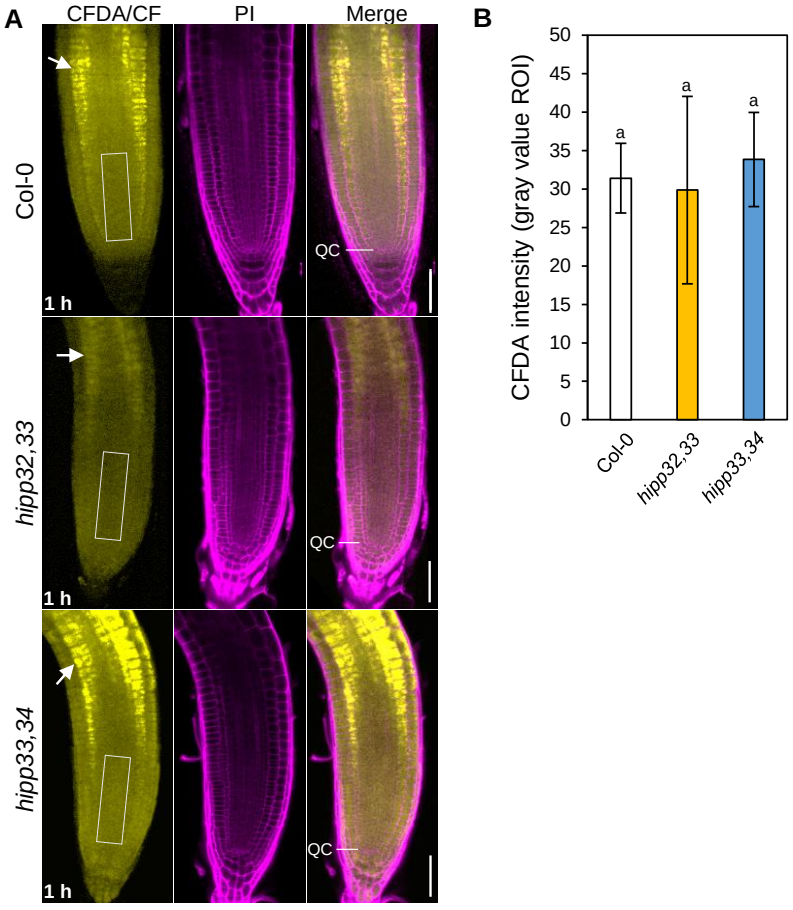

Figure 60. Symplasmic unloading of the phloem mobile probe CF into the root meristem.

Figure 60. Continued.
(A) Confocal microscopy of carboxyfluorescein (CF) unloading in the root meristem of 6-day-old wild-type (Col-0), *hipp32,33* and *hipp33,34* plants stained with propidium iodide (PI, magenta). 0.3 µl of CFDA (1 mM) was applied to cotyledons and the CF unloading was analyzed after 1 h. The arrows indicate the sequestration of CF into the vacuoles. The boxes represent the regions used for the quantification of the CF intensity. **(B)** Average CF intensity in the selected region of interest (ROI)**.** Scale bars = 50 µm. represent means ± SD (n = 8). Wilcoxon test was performed to assess the significant differences between groups ($p < 0.05$). Different letters label groups of different statistical significance.

Considerable amounts of CFDA dye accumulation were observed in the vacuoles of the cortex cells, nevertheless fluorescent CF could successfully be detected in the RAM (Figure 60A). Visual inspection suggested that the patterns of CF unloading in both double mutants differed from that in wild type. In *hipp32,33* the CF intensity in the RAM appeared lower than in wild-type and less CF accumulation in vacuoles of the cortex cells was observed. An opposite CF diffusion pattern was observed in *hipp33,34* (Figure 60A). However, the quantification of CF intensity in defined regions within the meristem showed equal CF intensities among the genotypes (Figure 60B).

To further investigate whether there is a link between HIPP-function and the PD permeability, a modified CDFA assay was used to assess the symplasmic transport specifically in the roots, independently of CF translocation through phloem. For this purpose, the root tips were briefly dipped into CFDA and the CF diffusion was monitored by imaging the roots 5, 20 and 60 min after CFDA exposure. Figure 61A illustrates representative images of CF diffusion 20 minutes after exposure to CFDA. Compared to wild type, *hipp32,33* showed a tendentially, yet statistically insignificant, increase in CF diffusion 5 minutes after CFDA exposure (Figure 61B). An exposure of 20 minutes led to a statistically significant increase in *hipp33,34*. However, this significance was lost when the exposure time was prolonged to 60 minutes (Figure 61B). Repetition of this assay revealed results with similar tendencies, but with low statistical reliability mostly due to a high standard deviation of the sample sizes.

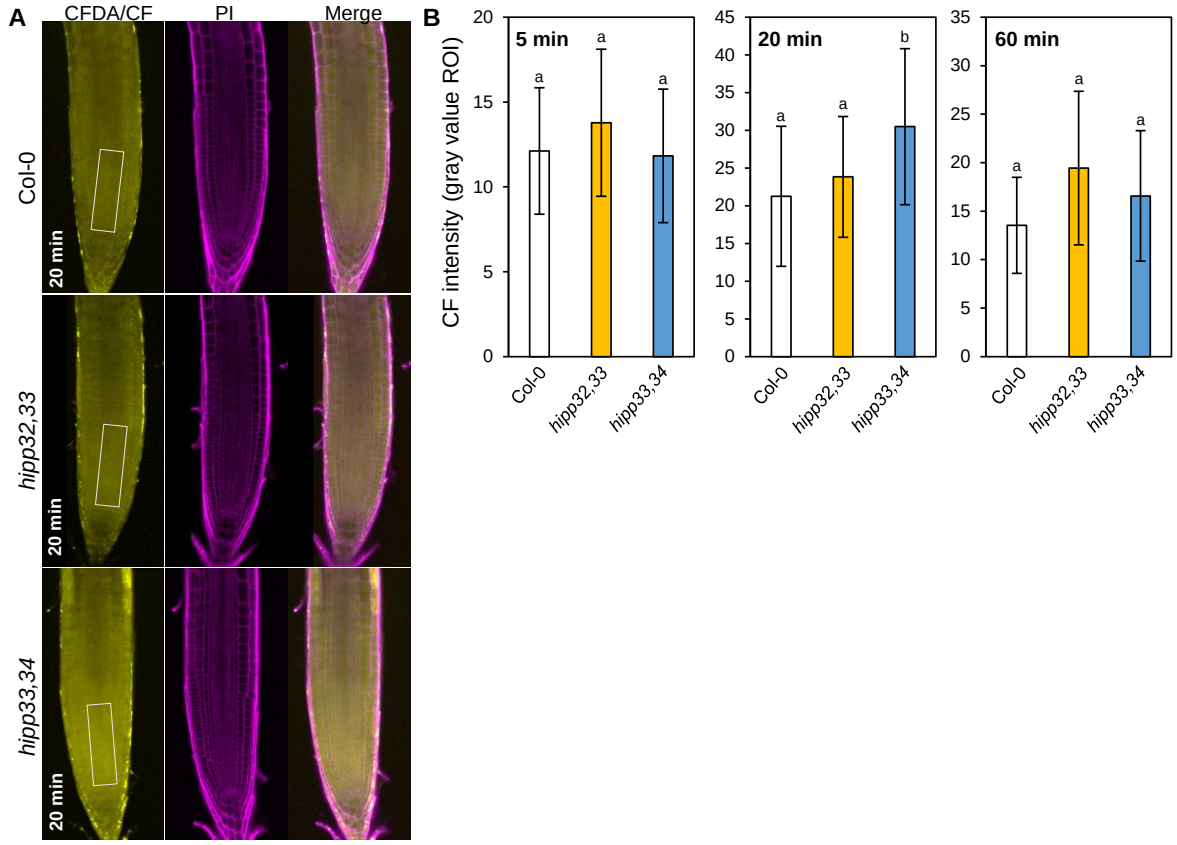

Figure 61. CF symplasmic transport in the root meristem.
(A) Confocal microscopy of carboxyfluorescein (CF) transported into the root meristem of 5-day-old wild-type (Col-0), *hipp32,33* and *hipp33,34* plants stained with propidium iodide (PI, magenta). The primary root tips were exposed to CFDA (1 mM) for 15 s. The CF diffusion was analyzed by 5, 20 and 60 min after CFDA exposure. Representative images of roots after 20 min diffusion are shown. The boxes represent the regions used for the quantification of the CF diffusion. **(B)** Average CF intensity in the selected region of interest (ROI)**.** Scale bars = 50 µm. Values represent means ± SD (n = 8-20). Wilcoxon test was performed to assess the significant differences between groups ($p < 0.05$). Different letters label groups of different statistical significance.

3.8.2 Symplasmic trafficking is enhanced in distinct *hipp* mutants

The CFDA assays indicated that the symplasmic permeability might be altered in *hipp33,34* mutants. To further explore this hypothesis, the mobile phloem marker *pSUC2:GFP* was employed to measure the PD permeability in *hipp* roots (Imlau *et al.*, 1999). The *Arabidopsis SUC2* gene encodes a companion cell-specific *SUCROSE-H$^+$ SYMPORTER 2* essential for the loading of sucrose into phloem sieve elements and its long-distance transport. The free GFP expressed under the control of *pSUC2* promoter can traffic through PD from companion cells into sieve elements and migrate within the phloem to reach different sink tissues. For instance in roots, the free GFP is symplasmically unloaded in the pericycle and diffuses via PD throughout the entire root meristem (Truernit and Sauer, 1995; Imlau *et al.*, 1999; Ross-Elliott

et al., 2017). The movement of the *SUC2*-driven GFP into the root meristem was impaired in mutants with defective symplasmic trafficking (Benitez-Alfonso *et al.*, 2009; Vatén *et al.*, 2011). Therefore, the *pSUC2:GFP* was introgressed in *hipp* mutants and the GFP movement was assessed (Figure 62).

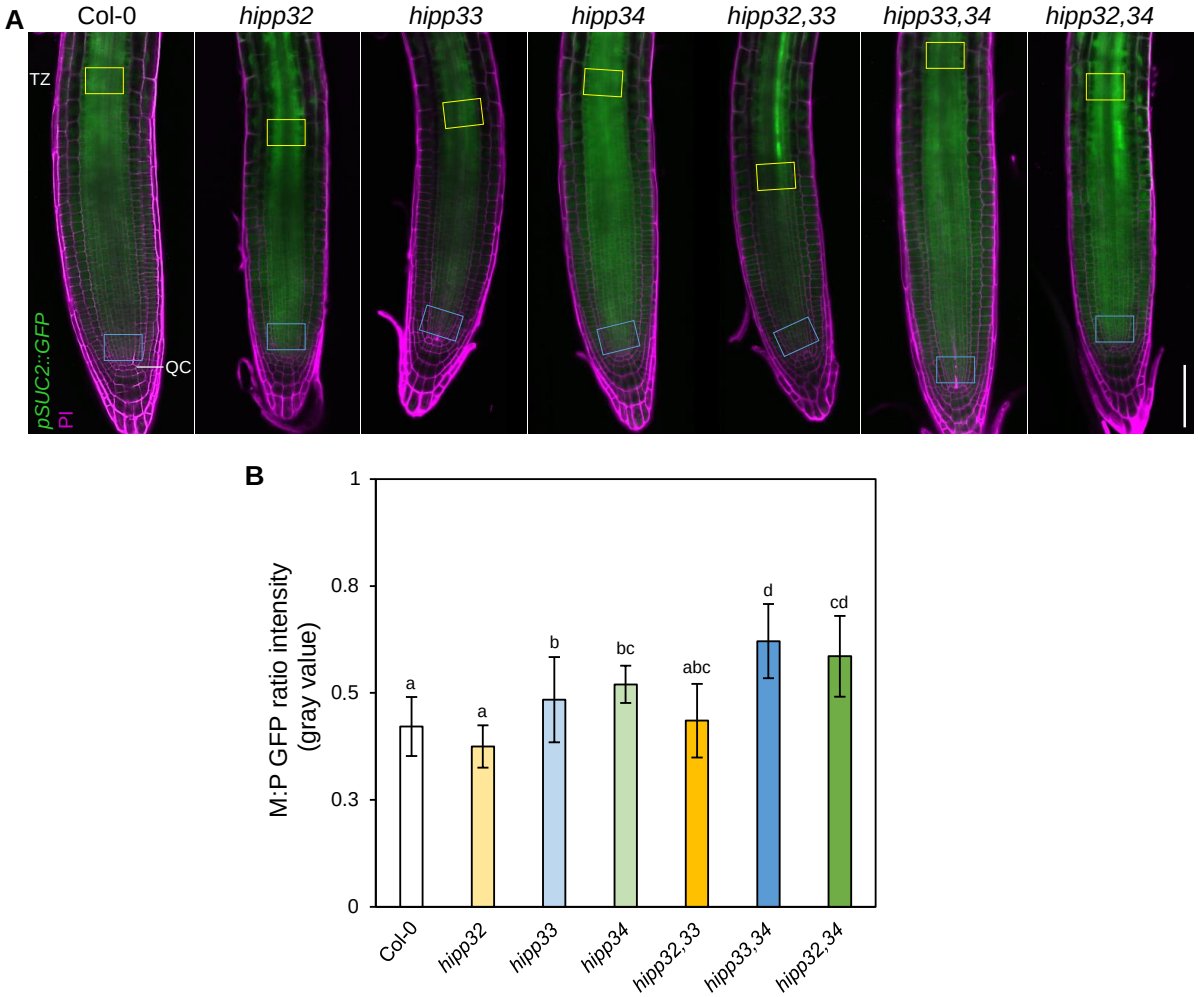

Figure 62. *HIPP33* and *HIPP34* regulate phloem unloading into the root meristem.
(A) Optical sections of 5-day-old primary root of wild-type (Col-0), *hipp* single and double mutant plants expressing the mobile phloem marker *pSUC2:GFP*. Propidium iodide (PI, magenta) was used for cell visualization. **(B)** GFP movement was determined as the ratio of GFP mean fluorescence intensity in the root meristem above the QC (M; blue box) relative to the phloem above the TZ (P; yellow box). Scale bar = 50 µm. QC: quiescent center. TZ: transition zone. DZ: differentiation zone. Values represent means ± SD (n =6-24). Wilcoxon test was performed to assess the significant differences between groups ($p < 0.05$). Different letters label groups of different statistical significance.

From the confocal imaging analysis, it was apparent that the GFP intensity was enhanced particularly in the *hipp34*, *hipp33,34* and *hipp32,34* root meristems (Figure 62A). In order to quantify the GFP movement from the phloem into the meristematic region, the ratio of GFP fluorescence was determined in a defined region within the proximal meristem, above the quiescent center (Figure 62A; blue box), relative to a defined region in the vascular bundle above the transition zone (Figure 62A; yellow box). The average of the M:P ratios were

increased in *hipp33* and *hipp34*, suggesting an enhanced GFP movement (Figure 62B). The additive effects of lacking both *HIPP33* and *HIPP34* genes was apparent in the double mutant *hipp33,34*, where the GFP movement ratio was increased by 25% relative to wild type (Figure 62B). *hipp32,34* exhibited a M:P ratio higher than that of *hipp32* and tendentially higher, yet not statically significant, than that of *hipp34* alone. No differences to wild type were determined in M:P ratios of *hipp32* and *hipp32,33* (Figure 62B). Taken together, these results suggest that HIPP33 and HIPP34 are redundantly involved in the negative regulation of plasmodesmal permeability in the roots.

3.9 Involvement of cluster-III HIPP proteins in heavy metal-associated stress

Excess of both essential and non-essential heavy metal ions such as iron (Fe), copper (Cu), zinc (Zn) and cadmium (Cd) can be toxic to plants and can have hazardous effects on plant growth (Ghori *et al.*, 2019). Most of the few HIPP proteins studied so far have been shown to be directly involved in heavy metal homeostasis, mediated by the conserved CXXC core motif of the HMA domain (Dykema *et al.*, 1999; Suzuki *et al.*, 2002; Gao *et al.*, 2009). Furthermore, it has been shown that the *hipp20,21,22* mutant is more sensitive to Cd and accumulates less Cd than the wild type, suggesting that cluster-IV HIPPs have a role in Cd-detoxification (Tehseen *et al.*, 2010). Hence the question arose whether these HIPPs might also be involved in heavy metal-associated stress.

3.9.1 Exposure to heavy metals does not affect *hipp32,33* root growth

In order to investigate whether the HIPP proteins are involved in heavy metal homeostasis, the root growth in *hipp* mutants was assessed in response to heavy metal stress. For this purpose, the primary root elongation and the lateral root development on media containing Cd or excessive micronutrients, were experimentally determined (Figure 63).

The addition of 25 µM Cd suppressed the primary root elongation in wild type to a similar extent as in *hipp33,34* and *hipp32,34* (Figure 63B). In contrast, the *hipp32,33* double mutant was insensitive to the toxic Cd concentration (Figure 63B). A similar response pattern was observed in the presence of excessive Zn. The primary root elongation was reduced by ca. 20% in wild type, *hipp33,34* and *hipp32,34*, whereas it remained unchanged in *hipp32,33* (Figure 63B). The presence of excessive Fe strongly suppressed the primary root elongation in all genotypes, however the *hipp32,33* double mutant reacted less sensitively than wild type and the two double mutants (Figure 63B). With respect to the lateral root formation, wild type as well as the *hipp* double mutants strongly reacted to the excessive metal ions and developed considerably fewer lateral roots in the presence of Cd and excessive Zn, as compared to control (Figure 63D). However, *hipp32,33* and *hipp33,34* responses were less severe than those of wild type, whereas *hipp32,34* responded similarly to wild type (Figure 63D). The

excessive iron equally affected the lateral root formation regardless of the genotype (Figure 63D).

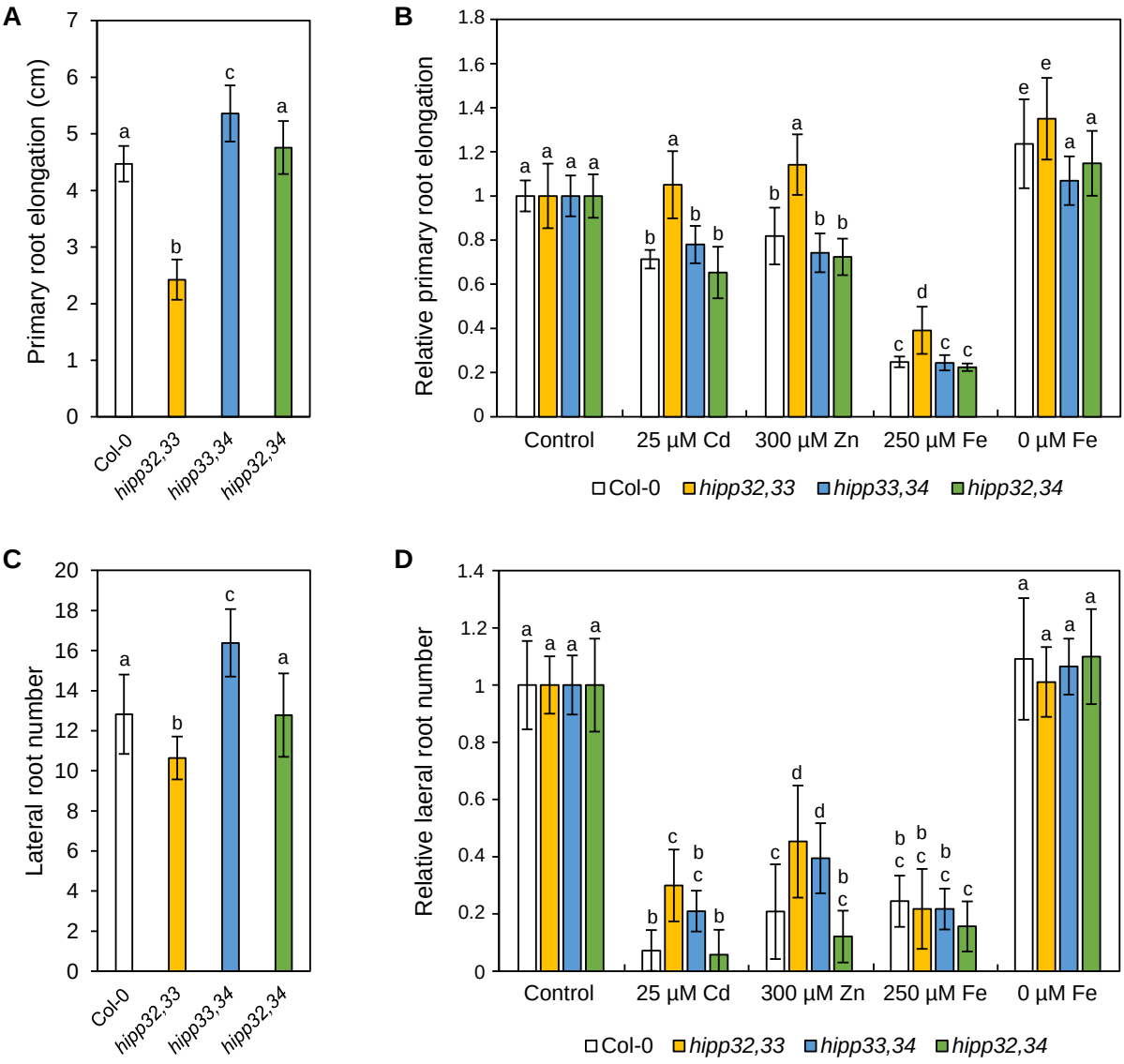

Figure 63. Root growth of *hipp* double mutants in response to heavy metal stress.
(A) Primary root elongation of wild-type (Col-0) and *hipp* double mutants grown on standard ½ MS medium for 10 days. **(B)** Primary root elongation in response to heavy metal stress, relative to control. **(C)** Lateral root formation on standard ½ MS medium for 10 days. **(D)** Lateral root number in response to heavy metal stress, relative to control. Values represent means ± SD (n =10-18). Statistical differences were evaluated with the Steel-Dwass pairwise ranking test ($p < 0.05$). Different letters indicate significant differences between groups.

Besides assessing the root growth in response to excessive iron, the root growth parameters were determined in response to Fe deficiency. Iron, as an essential micronutrient, is used in various processes from photosynthesis to metabolism and it has been shown that iron deprivation causes strong transcriptional responses in *Arabidopsis* roots (Dinneny *et al.*, 2008). The addition of ferrozine, a potent Fe(II) chelator, to the growth medium resulted in an

enhanced primary root elongation in wild type and *hipp32,*33, whereas the root elongation of both *hipp33,34* and *hipp32,34* remained unaltered (Figure 63B). In contrast, the lateral root formation was not affected by iron-deficiency (Figure 63D), suggesting that this root trait is less sensitive to iron limitation.

Taken together, these results indicate that the lack of HIPP32 and HIPP33 proteins prevents the inhibitory effects of toxic Cd, Zn and Fe on the root growth and suggest that these HIPPs redundantly act to mediate heavy metal tolerance in roots.

3.9.2 Symplasmic trafficking remains unchanged in *hipp* double mutants under Fe-stress conditions

A recent study using the mobile phloem marker *pSUC2:GFP* demonstrated that exposure to heavy metal stress triggers changes in plasmodesmal permeability (O'Lexy *et al.*, 2018). It has been shown that treating the roots for 24 hours with excessive heavy metal, such as Fe, Zn and Cd, limited the GFP movement from the phloem into root meristem (O'Lexy *et al.*, 2018). Symplasmic trafficking was particularly enhanced mutants lacking the *HIPP34* gene (see section 3.8.2) and *hipp32,33* was insensitive to exposure to heavy metals in root growth assays (section 3.9.1). Given these findings, it was intriguing to investigate whether the exposure to heavy metal stress effects the GFP movement in *hipp* mutants. Several experiments were conducting using the *pSUC2:GFP* line as described by (O'Lexy *et al.*, 2018). However, no difference in the GFP movement was detected after 24 hours of heavy metal treatment (data not shown). Increasing both heavy metal concentration and treatment time led to altered GFP movement in Fe-treated roots. Experiments with increased exposure time and Zn and Cd concentrations have not been conducted so far. Figure 64A illustrates representative confocal images of wild type and *hipp* double mutant roots expressing *pSUC2:GFP* under excessive iron conditions. The M:P ratio was significantly diminished under Fe-stress conditions in the wild-type roots, whereas in *hipp* mutants the M:P ratios were similar to control (Figure 64C). In wild-type roots, intensive GFP signal was observed in the vascular cells above the TZ (Figure 64A; white arrow), suggesting that GFP is retained in the phloem.

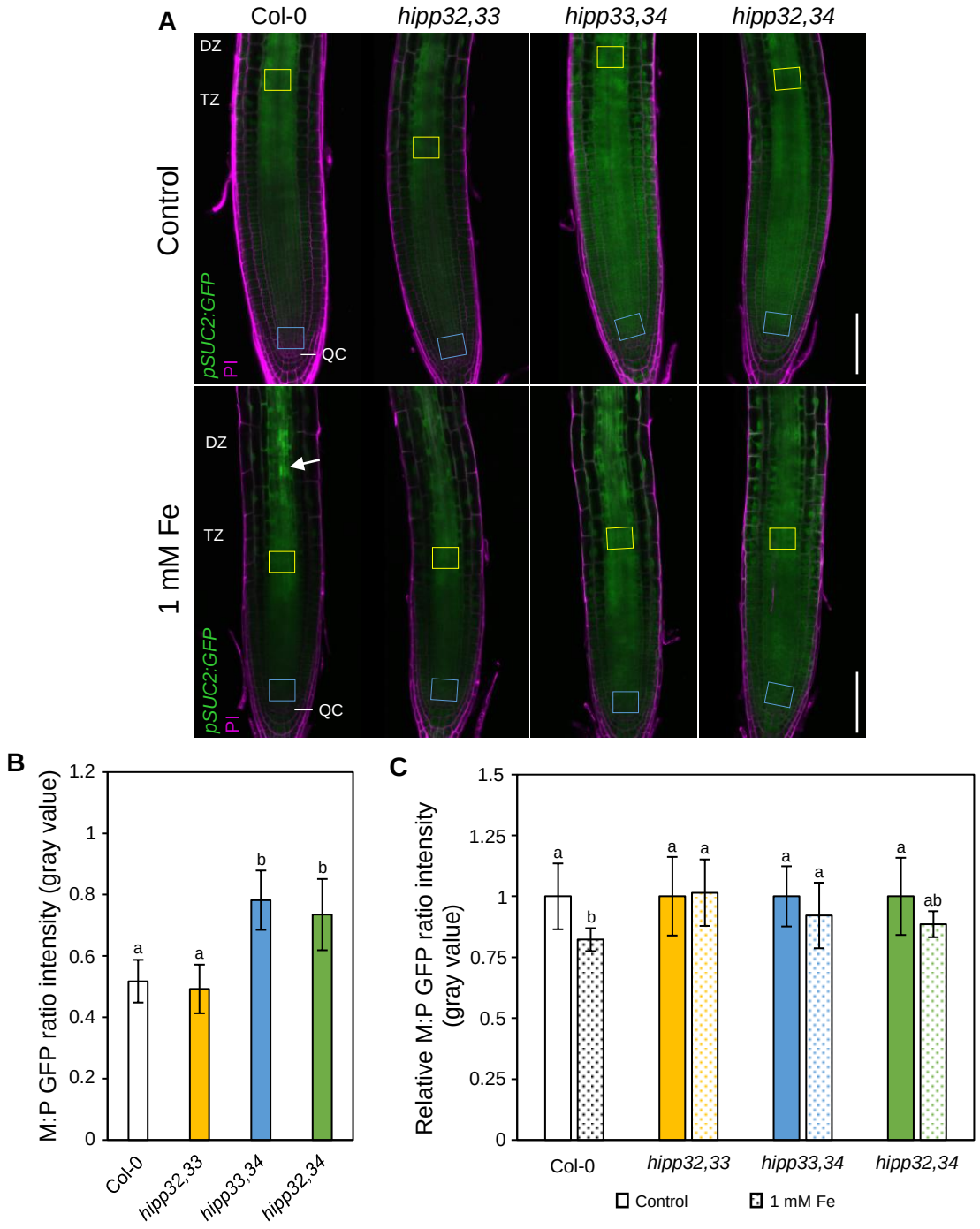

Figure 64. GFP movement is not affected by iron treatment in *hipp* mutants.
(A) *pSUC2:GFP*-expressing 7-day-old wild-type and *hipp* mutant roots imaged 48 hours after transfer to standard ½ MS medium (control) and ½ MS medium supplemented with 1 mM Fe. Propidium iodide (PI, magenta) was used for cell visualization. White arrow indicates increased GFP intensity in the vascular cells. **(B)** Ratio GFP movement under standard conditions, determined as the ratio between the mean GFP fluorescence intensity in the root meristem above the QC (M; blue box) relative to the phloem above the TZ (P; yellow box). **(C)** Ratio GFP movement under Fe stress conditions, showed relative to control. Scale bar = 75 µm. QC: quiescent center. TZ: transition zone. DZ: differentiation zone. Values represent means ± SD (n = 8-14). Significant differences between groups were assessed using the Wilcoxon test in **B)** ($p < 0.05$) and the Steel-Dwass pairwise ranking test in **C)** ($p < 0.05$). Different letters label groups of different statistical significance.

To investigate whether there is a correlation between the PD conductivity and the primary root growth, the root meristem length of wild-type and *hipp* seedlings treated for 48 hours with 1 mM Fe was determined. In the presence of excessive iron, the absolute root meristem length was significantly reduced regardless of the genotype (Figure 65A), suggesting that the Fe treatment negatively affected root growth. However, the relative change was significantly greater in wild type than in *hipp* mutants with enhanced PD trafficking *hipp33,34* and *hipp32,34*. The exposure to excessive Fe caused a reduction in RAM length of 31% in wild type and *hipp32,33*, whereas the root meristem length of *hipp33,34* and *hipp32,34* was reduced only by approximately 23% relative to control (Figure 65B). These results and the fact that only *hipp32,33* reacted insensitively to excessive iron in root growth assay (see section 3.9.1), suggest that HIPP proteins are differently involved in iron homeostasis, partially through HIPPs' involvement in general PD regulation (see section 3.8.2).

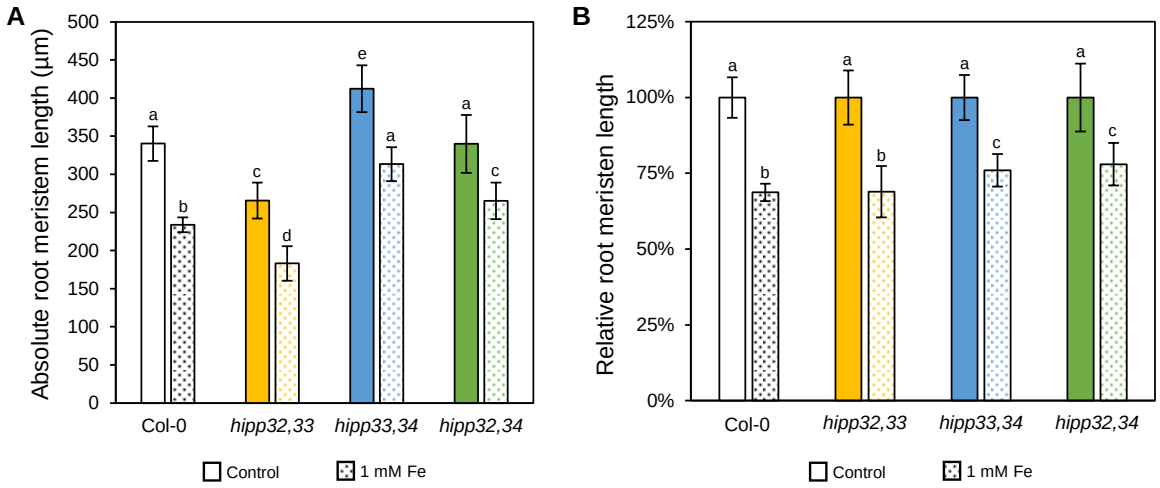

Figure 65. Effect of iron on the root meristem size.
The root meristem length was determined in 7-day-old wild-type and *hipp* double mutant seedlings 48 hours after transfer to standard ½ MS (control) and ½ MS supplemented with 1 mM Fe. **(A)** Absolute root meristem length. **(B)** Root meristem length in response to excessive iron, shown relative to control. Values represent means ± SD (n = 8-14). Significant differences between groups were assessed using the Steel-Dwass pairwise ranking test ($p < 0.05$). Different letters label groups of different statistical significance.

4. Discussion

4.1 PD-localized HIPP proteins have the potential to regulate the intercellular trafficking under standard and stress conditions

4.1.1 Cluster-III *HIPP* genes encode PD-targeted proteins

Deciphering the subcellular localization is an important aspect when investigating the biological function of unknown proteins. The cellular localization of several members of the HIPP protein family has been elucidated so far. HIPP proteins from the cluster I have been shown to exhibit multiple diverse cellular locations, *e.g.* HIPP1 localizes at PD, in the nucleus and in the cytoplasm; HIPP3 resides in the cytoplasm and nucleus; HIPP5 is a cytosolic protein and HIPP7 resides at PD and adjacent to the ER network and in the cytosol (Zschiesche *et al.*, 2015; Guo, 2019). Many HIPP proteins from cluster IV contain a nuclear localization signal predicting their nuclear residency (Barth *et al.*, 2009).

Confocal microscopy analysis of GFP-HIPP fusion proteins of cluster III transiently overexpressed in *N. benthamiana* leaves revealed dot-like fluorescence signals detected along the periphery of epidermal cells or as paired fluorescence foci spanning the cell walls, as expected for a PD-associated protein (Levy *et al.*, 2007). Furthermore, HIPP33 was previously identified during a proteomic analysis of PD-enriched fractions isolated from the cell walls of *Arabidopsis* suspension cells (Fernandez-Calvino *et al.*, 2011). Co-localization studies using the PD marker protein PDLP1 demonstrated that all cluster III members, GFP-HIPP32, GFP-HIPP33 and GFP-HIPP34, reside at PD (Figure 14). PDLP1 is a type I membrane receptor-like protein which belongs to a small family of eight proteins that are trafficked along the secretory pathway to PD, where they are incorporated into the plasma membrane that lines the PD (Thomas *et al.*, 2008; Amari *et al.*, 2010). The subcellular localization at PD was confirmed in *Arabidopsis* plants stably expressing the *35S:GFP-HIPP34* transgene (Figure 15). GFP-HIPP34 associated with PD pit fields, a form of simple PD grouped together that has been found to predominate in immature plant tissues, such as young leaves (Oparka *et al.*, 1999). In roots, GFP-HIPP34 was strongly detected at the sieve plates of the protophloem (Figure 15B), resembling the fluorescent pattern observed when staining the PD-associated callose with aniline blue (Zavaliev and Epel, 2015). Due to the overlapping spectral properties between aniline blue fluorochrome and GFP, the co-localization of GFP-HIPP34 with callose at PD was unsuitable. Alternative approaches will be required to further investigate to which structural subdomain of PD GFP-HIPP34 localizes, such as immunogold labeling coupled with transmission electron microscopy or super resolution three-dimensional structured illumination microscopy (Dahiya and Brewin, 2000; Fitzgibbon *et al.*, 2010).

Crucial for the cellular localization of many prenylated proteins is the lipid modification occurring at the CaaX prenylation motif, which endows proteins with a hydrophobic carboxyl terminus serving to increase its affinity for membranes or membrane microdomains (Hemsley, 2015). Prenyl groups appear to serve as a targeting signal and mediate specific protein functions (Hemsley, 2015). For instance, Barth *et al.* (2009) showed that prenylation acts to change the nuclear localization of the HIPP26 protein, since the prenyl-mutated HIPP26 was identified exclusively in the nucleoli. Furthermore, farnesylation of IPT3 has been shown to dictate both the cellular localization and its catalytic activity (Galichet *et al.*, 2008).

The membrane-association of HIPP34 was investigated by means of microsomal fractionation and protein analysis using the *35S:GFP-HIPP34 Arabidopsis* line. This assay revealed that GFP-HIPP34 predominantly associated with microsomal membranes, as no GFP signal was detected in the supernatant fraction of soluble proteins (Figure 17C). Examination of the effects of prenylation loss on the cellular localization of GFP-HIPP34 in *N. benthamiana* showed that the PD-associated signals were strongly reduced in HIPP34 mutants lacking the prenylation site (Figure 17E), consistent with the increased GFP-HIPP34^{prenyl} accumulation in the soluble protein fraction (Figure 17D). These results indicate that the prenylation is required for the localization of HIPP34 at PD. However, analysis of the HIPP34 protein lacking the prenylation site stably expressed in *Arabidopsis* under the control of its native promoter revealed a strong PD-association of the mutated protein (Tschuden, 2019). Recent studies revealed that the *N. benthamiana* homologue of the *Arabidopsis* protein HIPP26 is modified by both S-acylation and CaaX-prenylation. Both lipid modifications are important for HIPP26 residency at PD and plasma membrane. Interestingly, the S-acylation provided a stronger membrane association than that provided by the prenyl group (Cowan *et al.*, 2018). Protein S-acylation, historically known as palmitoylation, involves the covalent attachment of a fatty acid to a cysteine residue, usually palmitate or stearate (Hemsley, 2015). Unlike prenylation, S-acylation is a reversible process and does not require specific target sequences – the prenylated cysteine can be localized anywhere in the protein (Resh, 2006). Frequently, S-acylation also requires prior membrane anchoring of the protein, for instance through a transmembrane domain, another lipid modification or protein-protein interactions (Hemsley, 2015). Around 600 putative S-acylated proteins affecting diverse cellular processes have been identified in a proteomic approach in *Arabidopsis*, including also two HIPP proteins, HIPP4 and HIPP25 (Hemsley *et al.*, 2013). Although cluster-III HIPP proteins were not detected in this study, S-acylation prediction analysis revealed an additional cysteine residue, apart from the three cysteine residues within the HMA domain and prenylation motif, which might serve as a putative S-acylation site. An additional lipidation by S-acylation of HIPP34 might explain the observed discrepancy between *N. benthamiana* and *Arabidopsis* regarding the PD-association of GFP-HIPP34^{prenyl} mutant variant. The possible S-acylation occurring in *Arabidopsis* but not in *N.*

benthamiana might account for HIPP34 association with PD despite the missing prenylation (Figure 17B). This could be due to an impaired S-acylation process of *Arabidopsis* HIPP proteins transiently expressed in *N. benthamiana* leaf epidermal cells, possibly caused by functional differences in their S-acylation machineries, including S-acyl transferases that might not recognize *Arabidopsis* HIPP proteins as substrate (Hemsley, 2015; Guo, 2019). Interestingly, subcellular localization studies performed in *Arabidopsis* plants expressing HIPP7, a HIPP protein from cluster I that also resides at PD, revealed that the association of GFP-HIPP7 to PD was strongly impaired in the GFP-HIPP7 mutant form lacking the prenylation site (Guo, 2019). One possible explanation for this might be that HIPP34 and HIPP7 proteins are differently targeted to PD. The general knowledge and the molecular details of how proteins are specifically targeted to PD-associating membranes are still limited and no consensus PD-targeting signal has been described so far. Several PD-associated proteins carrying diverse PD-targeting sequences have been reported to use the secretory pathway for their delivery to PD (Thomas *et al.*, 2008; Simpson *et al.*, 2009; Ham *et al.*, 2012; Zavaliev *et al.*, 2016). For instance, the trafficking and accumulation of PD-localized type-I membrane protein PDLP1 relies on its transmembrane domain that contains all the information necessary for intracellular targeting to PD via the ER-Golgi secretory pathway. Inhibition of the ER-Golgi secretory pathway results in the retention of PDLP1 at the ER and abolishes the PD localization pattern of PDLP1 (Thomas *et al.*, 2008). In contrast, the PLASMODESMAL GERMIN-LIKE PROTEIN 1 (PDGLP1) and PDGLP2 delivery to PD occurs also via the ER-Golgi secretory pathway, but it is mediated by their N-terminal signal peptide (Ham *et al.*, 2012). Another PD sorting sequence has been reported for the GPI-anchored PdBG proteins and PDCB1, and it is represented by the GPI modification signal at the C-terminus, which functions as a primary signal in targeting proteins to the PD-enriched plasma membrane domain (Zavaliev *et al.*, 2016). The secretory pathway might be particularly involved in the delivery of HIPP32 to PD, since HIPP32, unlike HIPP33 and HIPP34, was shown to also localize to the Golgi apparatus, as revealed by GFP-HIPP32 co-localization with the *cis*-Golgi marker CGL1 in *N. benthamiana* (Frank *et al.*, 2008; Figure 16). No isoprenylated plant proteins have so far been identified to reside at Golgi. However, the mammalian Ras GTPases are among a class of proteins that are temporarily targeted to the ER and Golgi via the CaaX motif (Choy *et al.*, 1999). This might also be plausible for GFP-HIPP32, since no specific Golgi retention signals were predicted based on HIPP32 protein sequence (Chou *et al.*, 2010; Schoberer *et al.*, 2019). The dual subcellular localization of HIPP32 supports the hypothesis that HIPP proteins, even from the same phylogenetic cluster, might be differently targeted to reach their subcellular localization. In addition to the prenylation, the HMA domain might also play a role in determining HIPP cellular localization. Although GFP-HIPP34^{hma} showed a lower frequency of plasmodesmal localization when transiently expressed in *N. benthamiana*, it was not possible to determine

the relevance of the HMA domain in this regard due to the low GFP-HIPP34^{hma} protein expression (Figure 17D, E). However, mutating the HMA domain did not appear to influence the localization of the mutated HIPP34 protein expressed under its native promoter in *Arabidopsis* (Tschuden, 2019).

Further experiments are required to investigate the molecular mechanism underlying PD-association of HIPP34. As previously mentioned, GFP-HIPP34 was shown to associate with microsomal membrane. Therefore, it is plausible that HIPP34 might anchor via the prenyl moiety to the plasma membrane or ER at PD. BiFC assays revealed that CKX1/HIPP34 heterocomplexes exhibited a PD-specific punctuate expression pattern (Figure 18C). Given that CKX1 is an ER-associated type-II integral membrane protein, the BiFC signals probably designate the ER around PD (Niemann *et al.*, 2018; Tilsner *et al.*, 2016). Furthermore, the ER-plasma membrane contact sites around PD are highly specialized microdomains enriched in specific lipids, such as sterols and very-long-chain saturated sphingolipids (Grison *et al.*, 2015). It has been shown that lipid composition also influences the recruitment and targeting of proteins to PD (Petit *et al.*, 2019; Iswanto *et al.*, 2020). For instance, modulation of the overall sterol composition of the plasma membrane around PD resulted in the mislocalization of GPI-anchored proteins PDCB1 and β-1,3-glucanase PdBG2 and, subsequently, altered the cell-to-cell permeability (Grison *et al.*, 2015).

4.1.2 Toward the understanding of HIPPs' function at PD

Although the mechanism underlying HIPPs' association with PD was not entirely clarified, it was intriguing to explore the possible function of HIPP proteins at PD. PD enable molecules to move from cell to cell through the cytoplasmic sleeve, the space between the desmotubule and plasma membrane (Figure 9; Lucas *et al.*, 2009). Many proteins that are located within the cytoplasmic sleeve or anchored to the plasma membrane around PD have been shown to selectively regulate the molecular trafficking through PD, mainly by protein-protein interaction, the involvement of cytoskeletal components or partial unfolding of mobile proteins (Kim, 2018). Following the hypothesis that HIPP proteins might be linked to PD function, several techniques were employed in this study to investigate the symplasmic cell-to-cell movement in *hipp* mutants. Experiments using the molecular tracer CFDA were performed in order to investigate the phloem unloading and symplasmic connectivity in sink tissues of *hipp32,33* and *hipp33,34* mutants, with either impaired or enhanced root growth, respectively (section 3.8.1). Although CFDA has been extensively used for live imaging of phloem unloading in the roots to assess the symplasmic connectivity (Oparka *et al.*, 1994; Zhu *et al.*, 1998; Knoblauch *et al.*, 2015; Ross-Elliott *et al.*, 2017). However, it proved to be less suitable for monitoring the CF translocation in *hipp* mutants, as the experimental results obtained were not solid enough, mainly due to low statistical reliability (Figure 60, 61). There are several drawbacks to using

CF as symplasmic tracer. For instance, consistent with published results by Ross-Elliott *et al.* (2017) it was observed that after translocation through phloem, CF diffuses outwards into the cortex layers relative to the stele where it accumulates in the vacuole (Figure 60A), thus affecting the CF quantification in the unloading zone. This impediment did not occur when monitoring the CF transport in the root upon CFDA exposure (Figure 61A). The drawback in this case is that CF can also pass PD with very small size exclusion limits (SEL), the size of the largest molecule capable of moving from cell to cell (Oparka *et al.*, 1999). With an estimated Stokes radius of only 0.61 nm, the CF molecule is approximately five times as small as the GFP protein, which is used as mobile marker under the control of the phloem-specific promoter *SUC2* (Wang and Fisher, 1994; Terry *et al.*, 1995; Imlau *et al.*, 1999). Therefore, it is possible that the passive movement of protein provided by the CFDA assay is not accurate enough, particularly when the cell-to-cell trafficking is moderately affected, as it might be assumed for *hipp* double mutants. CF translocation assays can provide a clear answer in plants with severely impaired symplasmic trafficking, such as the *cals3-d* gain-of-function mutant (Vatén *et al.*, 2011) or the callose-accumulating *gfp arrested trafficking 1* mutant (*gat1*; Benitez-Alfonso *et al.*, 2009). *GAT1* encodes a thioredoxin that affects symplasmic permeability by controlling redox regulation of callose deposition in the root meristem (Benitez-Alfonso *et al.*, 2009). The symplasmic trafficking of these mutants was shown to be severely affected also by using the phloem mobile marker *pSUC2:GFP* (Truernit and Sauer, 1995; Imlau *et al.*, 1999). The transport of GFP expressed from the *SUC2* promoter was dramatically impaired in *gat1* and *cals3-d*, accompanied by completely impaired unloading of *pSUC2:GFP* into the root meristem (Vatén *et al.*, 2011; Benitez-Alfonso *et al.*, 2009).

Since the symplasmic trafficking was slightly increased in *hipp33,34* roots in CF transport assays (Figure 61), *pSUC2:GFP* was employed to further explore the PD conductivity in *hipp* mutants. CLSM analysis of GFP movement from phloem into root meristem revealed that symplasmic trafficking was enhanced in *hipp* mutants lacking either *HIPP33* or *HIPP34* genes, with a pronounced effect in *hipp33,34* and partially in *hipp32,34* (Figure 62), suggesting that HIPP33 and HIPP34 are redundantly involved in the negative regulation of PD function.

PD aperture is mainly regulated by the callose deposition in the cell wall surrounding PD, mediated by the joint action of two enzymes – PdBG and CALS – which degrade and synthesize callose, respectively (Levy *et al.*, 2007; Zavaliev *et al.*, 2011). Hence, the callose turnover provides an important mechanism for controlling the PD aperture, and thus the symplasmic trafficking. CalS10/GSL8, CalS7/GSL7 and CalS3/GSL12 are only three out of 12 callose synthases identified in *Arabidopsis* that have been found to be involved in callose synthesis and control of proper callose accumulation during plant growth and development (De Storme and Geelen, 2014). *gls8* loss-of-function mutation in *Arabidopsis* leads to reduced accumulation of callose at PD, causing dysregulation of cell-to-cell connectivity and stomatal

patterning, presumably due to the unrestricted mobility of the bHLH transcription factor SPEECHLESS, which controls asymmetric cell division in order to establish stomata cell fate (Guseman *et al.*, 2010). Gain-of-function mutations in *CALS3* (*cals3-d*) result in increased accumulation of callose at PD, leading to impaired root development and defects in tissue patterning, as the transport of key transcription factors and miRNAs (such as *SHR* and *microRNA165*) was blocked (Vatén *et al.*, 2011). Interestingly, in a Y2H screen recently performed in Dr. Werner's group using HIPP33 proteins as bait, CalS9/GSL10 has been identified to interact with HIPP33 (personal communication). Although CalS9/GSL10 is not known to be directly involved in callose-mediated PD-regulation, there are studies speculating that CalS9 forms heterodimeric complexes with CalS10 which might be part of the callose synthase complex (Saatian *et al.*, 2018; Töller *et al.*, 2008). It is plausible that HIPP proteins participate in the PD regulation by interacting and modulating the activity of PD-localized proteins. Acting antagonistically to callose synthases, two out of 12 *Arabidopsis* annotated PdBG proteins, PdBG1 and PdBG2, have been found to play a role in callose degradation at the PD (Levy *et al.*, 2007; Benitez-Alfonso *et al.*, 2013). A third PdBG1/2-related protein, PdBG3, was also found to localize at PD, but its role in callose degradation is still uncertain (Benitez-Alfonso *et al.*, 2013). Double *pdbg1,2* mutants show an increased accumulation of callose at PD during lateral root formation, accompanied by reduced cell-to-cell macromolecular trafficking, with critical consequences for lateral root patterning (Benitez-Alfonso *et al.*, 2013). The transcript levels of *PdBG* and *CALS* genes were investigated by qRT-PCR, but no differences were observed in transcript accumulation in *hipp* double mutants compared to wild-type seedlings (results not shown). Based on the negative correlation between PD conductivity and callose accumulation, the callose-specific aniline blue dye can be used as an indirect tool to assess the plasmodesmal gating (Zavaliev and Epel, 2015). However, no visual differences were detected in PD-associated callose in *hipp* mutants compared to wild type stained with aniline blue (results not shown). However, a quantitative analysis of the aniline blue staining was not possible within the context of this thesis and needs to be addressed in the future.

In addition to callose-dependent regulation of general PD aperture, specific macromolecules like RNA or other proteins can also alter PD function and thus PD conductivity. For instance, PDGLP1 has been shown to interact with a subset of proteins in the PD-enriched cell wall protein fractions, such as actin, PdBG, PDGLP2 or PHOSPHATE RESPONSIVE 1, a putative ABC transporter, and might be involved in transferring specific non-cell-autonomous proteins from the cytoplasmic phase into the orifice of the PD microchannel (Ham *et al.*, 2012). Another example are remorin proteins, which associate to plasma membrane rafts around PD through their myristoyl group and which have been shown to interact with the movement protein TGB1 from potato virus X and to impair the cell-to-tell movement of the viral particles by titrating

TGB1 away from PD (Raffaele *et al.*, 2009). The HIPP26 homologue from *N. benthamiana* has been shown to interact with the movement protein TGB1 from potato mop-top virus in the vicinity of PD and to promote virus long-distance movement. Interestingly, TGB1 interaction suppresses HIPP26 lipidation, thus releasing HIPP26 from PD and redirecting it via microtubules to the nucleus, thereby activating the drought stress response and facilitating virus long-distance movement (Cowan *et al.*, 2018).

Several plausible hypotheses might explain the mechanisms by which HIPP33 and HIPP34 proteins influence the molecular trafficking through PD. Given their ability to undergo protein-protein interaction by virtue of their farnesyl hydrophobic moiety, HIPP proteins might interact with various proteins, such as transcription factors, and affect their presumable PD-mediated translocation. For instance, the cell-to-cell trafficking of homeobox transcription factors KN1 and STM, and TRANSPARENT TESTA GLABROUS 1, a tryptophan-aspartic acid 40 (WD40)-repeat protein whose movement is involved in trichome spacing, requires their interaction with CHAPERONIN CONTAINING T-COMPLEX POLYPEPTIDE 8, a subunit of a type-II chaperonin complex responsible for their correct folding before and after translocation through PD (Bouyer *et al.*, 2008; Xu *et al.*, 2011). The cell-to-cell movement of the mobile transcription factor SHR has been shown to be mediated by SHR interaction with the endosome-associated protein, SHORT-ROOT INTERACTING EMBRYONIC LETHAL (SIEL; Koizumi *et al.*, 2011). SHR intercellular movement relies on intact microtubules and the correct localization of SHR and SIEL at endosomes, which serve as platforms for the assembly of a movement competent SHR protein complex (Wu and Gallagher, 2014). In the above-mentioned Y2H screen performed in Dr. Werner's group, several members of different transcription factor families were identified to interact with HIPP33 (personal communication). Among HIPP33 interactor partners, several plant-specific transcription factors from BASIC PENTACYSTEINE (BPC) family were detected. Similar to *hipp* mutants, higher order *bpc* mutants displayed severe developmental defects, highlighting the important roles played by *BPC* genes during plant development (Monfared *et al.*, 2011). The idea that HIPP might affect the intercellular trafficking of key cellular regulators can be supported by the fact that *hipp* mutants showed strong pleiotropic developmental defects, although the general symplasmic trafficking was rather moderately affected (Figure 62).

Since HIPP proteins are described as metallochaperones, acting in heavy metal binding and transport (Tehseen *et al.*, 2010; Suzuki *et al.*, 2002; Gao *et al.*, 2009; Zschiesche *et al.*, 2015), it is plausible that the function of HIPP proteins at PD is related to their putative capacity of delivering heavy metal ions to specific metalloproteins. Numerous zinc finger transcription factors, metal-containing enzymes or heavy metal transporter have been identified to associate to PD in PD proteomic studies (Fernandez-Calvino *et al.*, 2011; Kraner *et al.*, 2017).

As previously stated, specific lipids, such as sterols and sphingolipids, which are enriched in the plasma membrane nanodomain across PD cell boundaries, also play important roles in modulating the flexibility of the plasma membrane at PD (Grison *et al.*, 2015; Yan *et al.*, 2019). On a speculative note, the prenyl-anchored HIPP proteins might contribute to the maintenance of the PD membrane system required for proper intercellular trafficking.

4.1.3 HIPP-mediated PD regulation in response to iron stress

PD-mediated trafficking is not only crucial for normal plant growth and development, but it also mediates plant responses to specific environmental challenges. Several studies have shown that decreasing plasmodesmal permeability is a common response to biotic and abiotic stresses, such as pathogen infection, oxidative stress and metal toxicity (Cui and Lee, 2016; Faulkner *et al.*, 2013; Benitez-Alfonso and Jackson, 2009; O'Lexy *et al.*, 2018).

O'Lexy *et al.* (2018) have published a study in which the effects of nutrient and exposure to heavy metal stress on the plasmodesmal permeability in *Arabidopsis* root were investigated. Measuring the movement of GFP driven by the *SUC2* promoter from the phloem into the root meristem revealed that a decrease in plasmodesmal permeability is not a universal response to excessive metal ions. For instance, Fe inhibited the primary root growth and decreased PD permeability, whereas Cu generally increased movement through PD (O'Lexy *et al.*, 2018). Excessive exposure to Zn and Cd has also been shown to limit the GFP movement in roots (O'Lexy *et al.*, 2018). Although the experimental setups published by O'Lexy *et al.* (2018) were strictly followed, these findings could not be reproduced in experiments performed within the frame of this work. However, altering the Fe treatment conditions affected the GFP movement to a similar extent as described in the above-mentioned study. Explicitly, increasing the Fe concentration from 0.6 mM to 1 mM and doubling the exposure time caused in wild type a decrease in GFP movement by approximately 25%, indicating a decrease in plasmodesmal trafficking (Figure 64). Furthermore, GFP was detected to accumulate in wild type phloem (Figure 64). The decreased PD trafficking was accompanied by a reduction of the root meristem size in wild type (Figure 65A), consistent with reported callose-mediated PD closure triggered by exposure to heavy metal stress (Sivaguru *et al.*, 2000; Müller *et al.*, 2015; O'Lexy *et al.*, 2018). Interestingly, the Fe treatment did not affect the plasmodesmal trafficking in the *hipp* double mutants – the GFP movement ratios remained unchanged compared to control (Figure 64). This implies that *hipp* mutants might be less susceptible to callose deposition in response to excessive iron stress. Further analyses are necessary to support this hypothesis. For instance, staining the roots with aniline blue could provide an answer in this regard (Zavaliev and Epel, 2015). Although excessive Fe did not affect the GFP movement in *hipp* mutants, their root meristem sizes were also reduced upon Fe treatment (Figure 65A). Interestingly, in *hipp33,34* and *hipp32,34* mutants with an enhanced molecular PD trafficking

under normal conditions (Figure 62B), the iron-induced root meristem reduction was less pronounced than in wild type (Figure 65B). One explanation could provide their enhanced steady-state PD conductivity, which might counteract the inhibitory effects of excess heavy metals on root growth. In general, the biological significance of blocking the PD in response to heavy metal stress is not clear. One hypothesis is that a decrease in cell-to-cell movement serves to restrict the accumulation of toxic or excessive heavy metals in actively growing tissues, such as the root meristem (Clemens *et al.*, 2002). Transition metals taken up by the roots are transported to the apoplast of leaves in the xylem sap, from where they are scavenged and subsequently redistributed to the sink tissues via the symplasmic route (Karley *et al.*, 2000). Restricting the molecular PD flux to reduce heavy metal toxic effects on the root growth would also affect the general symplasmic trafficking which is required for proper root growth and development. Intriguingly, the root growth analysis, in terms of root elongation and LR formation, revealed that *hipp33,34* and *hipp32,34* mutants reacted similarly to wild type when grown on excessive Fe, whereas *hipp32,33* root growth remained insensitive (section 3.9.1). These results contradict the above discussed root meristem size in *hipp* mutants grown on excessive Fe, regardless of the differences in both experimental setups. Similar to *hipp32,23*, the *cals5* mutant, which have reduced basal steady-state callose levels, have been shown to be less sensitive to the inhibitory effects of excessive Fe (O'Lexy *et al.*, 2018). A plausible explanation can be that PD flux might be controlled in a dynamic fashion, and that the short-term responses to excessive Fe might not reflect longer term effects.

To sum up, HIPP proteins appear to be involved in root plasmodesmal regulation in Fe-treated plants, but there are likely other factors that modulate root growth in response to iron stress, independently of the symplasmic trafficking. Possible roles of HIPP proteins in heavy metal stress will be discussed in section 4.5).

4.2 *HIPP* gene activity affects various developmental processes in *Arabidopsis*

The histochemical analysis of transgenic *Arabidopsis* plants containing *HIPP:GUS* chimeric genes demonstrated that the spatiotemporal expression patterns directed by the *HIPP32*, *HIPP33* and *HIPP34* promoter regions are remarkably different. While the *HIPP32* and *HIPP34* promoters displayed discrete expression patterns across multiple sites throughout plant development, the *HIPP33* promoter activity was restricted to few tissues during plant growth. The differences were particularly evident in the root. Distinct reporter gene activity patterns were observed also in other tissues, such as young leaves and inflorescence. In contrast, in mature leaves *HIPP* genes exhibited partially overlapping GUS activity patterns. The multiple expression patterns for *HIPP* genes suggest variable sites of *HIPP* function *in planta*, in good agreement with the pleiotropic defects observed in the *hipp* loss-of-function mutants. Selected

developmental processes in which *HIPP* genes play a decisive role will be discussed in the following.

4.2.1 *HIPP* genes are required for pattern formation and maintenance of the apical meristems during embryonic development

Analysis of the *hipp32,33,34* mature embryos revealed that the lack of all cluster-III *HIPP* genes led to pleiotropic morphological defects, such as small cotyledons, short embryonal axis, irregular cotyledon number and fused cotyledons (Figure 29). A large number of *hipp32,33,34* embryos isolated from mature seeds appeared to resemble the morphology of an embryo at the late torpedo stage, suggesting an impaired temporal coordination during embryogenesis (Figure 29; ten Hove *et al.*, 2015).

The most prominent embryonic defects in *hipp32,33,34* mutants were the abnormal cell division, differentiation and morphogenesis observed in shoot and root apical meristems (Figure 30). Mature *hipp32,33,34* embryos had unusually enlarged SAMs, occasionally exhibiting a dome-like shape, which is characteristic of post-embryonic development, implying a premature proliferation of SAM cells occurring already at the cotyledon bent stage (Capron *et al.*, 2009). *hipp32,33,34* SAM also exhibited highly disorganized cell arrangements and unsharp cotyledon borders (Figure 30). Given the overlapping functions of *HIPP* genes in regulating the symplasmic trafficking, it is plausible that the defective SAM phenotypes observed in *hipp32,33,34* embryos may be linked to disrupted intercellular communication occurring in this mutant. Studies of cell-to-cell movement during embryogenesis have demonstrated the existence of the symplasmic connectivity within and between the individual structures of the *Arabidopsis* seed (Stadler *et al.*, 2005a). It has been shown that *Arabidopsis* embryos constitute a single symplasmic domain during the globular and heart stages and that additional symplastic domains, which correlate with the development of primary tissues, are established along the body axis by the mid-torpedo stage (Kim *et al.*, 2002; Stadler *et al.*, 2005a; Kim *et al.*, 2005). Since PD are crucial for symplasmic communication, mutants with altered PD function have severe growth defects manifested as early as embryogenesis. For instance, embryo defective *Arabidopsis* mutants *increased size exclusion limit* 1 (*ise1*) and *ise2* that fail to downregulate PD permeability at the torpedo stage, causing an increase in intercellular movement via PD, do not survive beyond this stage in homozygous state (Kim *et al.*, 2002; Stonebloom *et al.*, 2009; Kobayashi *et al.*, 2007). *ise2* mutants have a pleiotropic phenotype during embryogenesis, including alterations in cell fate, partially resembling the *hipp32,33,34* phenotype (Stonebloom *et al.*, 2009). Both *ise1 and ise2* embryos contain increased proportion of branched and secondary PD compared to wild type, which only contain simple PD (Stonebloom *et al.*, 2009; Kobayashi *et al.*, 2007). Consistent with this, *Arabidopsis* mutants *decreased size exclusion limit 1* (*dse1*) with the opposite phenotype, decreased PD

trafficking, contain fewer branched and secondary PD (Xu *et al.*, 2012). Like *ise1* and *ise2*, *dse1* null mutants are embryo-lethal (Xu *et al.*, 2012). Interestingly, none of these genes encode PD-localized proteins. *ISE1* encodes a DEAD-box RNA-helicase that localizes to mitochondria and is essential for mitochondrial function (Stonebloom *et al.*, 2009), *ISE2* encodes a chloroplast DEVH-type RNA helicase involved in posttranscriptional gene silencing and cell fate determination (Kobayashi *et al.*, 2007), and *DSE1* encodes a nuclear and cytoplasm-localized protein with putative roles in chloroplast homeostasis (Xu *et al.*, 2012). The only gene encoding a PD-localized protein described to be involved in *Arabidopsis* embryogenesis is the *GLS8*, which has been shown to be required for proper cell division starting in the early embryo (Chen *et al.*, 2009). Similarly to *hipp32,33,34*, *gsl8* embryos show a range of aberrant phenotypes, including asymmetrically shaped cotyledons, single or triple cotyledon-like organs (Chen *et al.*, 2009).

SAM function and maintenance rely on an elaborate regulatory network consisting of hormone signaling, transcriptional loops and intercellular trafficking of key regulators that are crucial for cellular differentiation and stem cell maintenance (Kitagawa and Jackson, 2017). A disrupted intercellular trafficking presumably occurring in *hipp32,33,34* embryos might affect the PD-mediated movement of important molecules known to regulate SAM maintenance, including the transcription factors WUS and STM (Daum *et al.*, 2014; Yadav *et al.*, 2011; Kim *et al.*, 2003), hormones like auxin (Jackson, 2015) or small non-coding RNAs (Hisanaga *et al.*, 2014). Regulators of the WUS/cytokinin feedback during SAM development, such as ARR7, ARR15 and AHP6, have also been shown to move within SAM layers through PD (Schuster *et al.*, 2014; Besnard *et al.*, 2014). Furthermore, since PD function as signaling hubs, where receptors and downstream signaling proteins are concentrated (Lee, 2015), it is plausible that HIPP proteins might be integrated in diverse cellular signaling pathways, *e.g.* via protein-protein interactions, and thus contribute to PD-mediated SAM regulation and embryo patterning in general. Moreover, HIPP proteins might participate in the modulation of cytokinin signaling during SAM development, since it has been shown in this study that loss of *HIPP* gene activity affects cytokinin signaling output in root (section 3.7.4). Investigating the activity of the synthetic cytokinin reporter *TCSn:GFP* in *hipp32,33,34* SAM would provide solid information in this regard. In general, it would be revealing to investigate the spatial and temporal expression of *HIPP* genes in embryos and whether their expression patterns correlate with the expression of cell identity markers, such as stem cell markers *WUS* and *CLV3*, which dynamically maintain SAM size and activity and are detectable as early as the 16-cell stage embryo or in transition stage embryo, respectively (Mayer et al., 1998; Clark et al., 1995; Schoof et al., 2000).

The RAM formation and organization were also severely affected during embryogenesis of *hipp32,33,34* (Figure 30). Ectopic starch accumulation was often observed in the presumable

QC cells of *hipp32,33,34* embryos (Figure 30D, E), implying that these mutants fail to establish the QC and/or to maintain its identity. Furthermore, the CSCs exhibited an irregular cell arrangement and an abnormal behavior of accumulating starch granules (Figure 30), a specific marker for differentiated columella cells (Barlow *et al.*, 1984). This suggests that the stem cell state of columella initials is not stably maintained in *hipp32,33,34* embryonic roots. These phenotypes resemble those of *wox5* mutant which lacks the expression of the transcription factor *WOX5* in the QC, required to promote CSC maintenance in a non-cell-autonomous manner from the early stages of embryogenesis on (Sarkar *et al.*, 2007; Forzani *et al.*, 2014; Pi *et al.*, 2015). Therefore, it would be revealing to investigate the molecular changes occurring in the QC cells of *hipp32,33,34* embryonic root meristem. For instance, well-characterized QC cell-specific markers, such as *pWOX5:erGFP* or *pQC25:GUS* could be used to investigate the QC identity *hipp32,33,34* (Blilou *et al.*, 2005; Sabatini *et al.*, 2003; Sarkar *et al.*, 2007). Crosses between *hipp* mutants and *pWOX5:erGFP* were initiated, but the analysis exceeded the timeframe of this study. Another study has elucidated a regulatory pathway of WOX5, in which the signaling peptide CLV3/ERS (CLE)-related protein 40 (CLE40) and the receptor-like kinase *ARABIDOPSIS* CRINKLY4 (ACR4) maintain the stem fate of the columella initials through the negative regulation of *WOX5* (Stahl *et al.*, 2009). CLE40 has been shown to also activate the receptor kinase CLV1 which acts in the same pathway as ACR4 to regulate distal stem cell number in *Arabidopsis* (Stahl *et al.*, 2013). Both ACR4 and CLV1 associate with PD, where they have been shown to form heteromeric complexes (Stahl *et al.*, 2013). However, the mechanism underlying ACR4/CLV1 complex formation at PD is not clear. Stahl *et al.* (2013) have proposed that PD-localized ACR4/CLV1 complexes may directly regulate or restrict the non-cell-autonomous signaling occurring between QC and stem cells and thereby confine stem cell identity to a single cell layer in direct contact with the QC (Stahl *et al.*, 2013). A recent study proposed that other, yet unknown factors, might act independently of WOX5 in the QC to control CSC fate and that the main function of the CLE40/CLV1/ACR4 module is to regulate the QC activity and position (Berckmans *et al.*, 2020). Further factors are known to be involved in the embryonic specification of stem cell organizing QC cells and in the maintenance of root stem cells. For instance, *SHR* is expressed in the stele tissue from embryogenesis onward, but the SHR protein traffics via PD to the QC cells where it promotes *SCR* expression, required for the QC identity and the activity of surrounding stem cells (Helariutta *et al.*, 2000; Sabatini *et al.*, 2003; Nakajima *et al.*, 2001). Loss of either *SHR* or *SCR* expression results in the formation of a short root that fails to maintain the QC (Helariutta *et al.*, 2000; Sabatini *et al.*, 2003). *SHR* and *SCR* also control the balance between two phytohormones, auxin and cytokinin, which is crucial for SCN specification from the early globular stage of embryogenesis (Salvi *et al.*, 2018). Since the cytokinin signaling output was strongly reduced in *hipp32,33,34* post-embryonic roots (Figure 51), it is plausible that the defects observed in the embryonic

roots may be caused by an altered interaction between auxin and cytokinin, which in turn might have led to QC and stem cell misspecification. Further experiments would be required to investigate whether *HIPP* genes are involved in the cytokinin-mediated cell lineage specification during early embryogenesis. For instance, it would be informative to monitor the activity of *TCSn:GFP* in *hipp32,33,34* during early stages of embryogenesis, as *TCSn:GFP* responses has been shown to be sensitive and specific already in the hypophysis at the early globular stage (Müller and Sheen, 2008).

In addition to the SHR/SCR pathway, the PLT pathway acts downstream of auxin to specify QC identity and to maintain stem cell fate (Aida *et al.*, 2004; Galinha *et al.*, 2007). It has been shown that loss of both *PLT1* and *PLT2* causes the loss of QC identity and premature differentiation of CSCs (Aida *et al.*, 2004).

PD-mediated intercellular trafficking in the root apex plays an important role in the auxin-dependent regulation of stem cell identity. It has been recently demonstrated that blocking the PD-mediated trafficking between QC and surrounding stem cells by expressing *icals3m* (inducible form of *cals3m*) in QC resulted in elevated local auxin maxima and the establishment of AP2-domain transcription factors PLT gradients, essential for SCN specification and maintenance (Liu *et al.*, 2017a; Aida *et al.*, 2004). On a speculative note, an altered PD conductivity in *hipp32,33,34* embryonic root apex might directly affect the PIN-mediated polar transport of auxin, disrupting thus the auxin/PLT regulatory loop required for proper patterning of the RAM (Friml *et al.*, 2003; Blilou *et al.*, 2005; Liu *et al.*, 2017a). Given the fact that numerous auxin-associated genes were deregulated in *hipp* mutant seedlings (section 3.5.2), it is plausible that the lack of *HIPP* genes alters the overall auxin signaling and activity, including the spatiotemporal distribution of auxin during embryogenesis. In would be informative to study the expression of the auxin-dependent reporter *DR5:GFP* in *hipp32,33,34* embryos, which could help to identify possible alterations occurring in auxin distribution connected to specific patterning events during embryogenesis (Friml *et al.*, 2003).

The embryonic phenotypes partially correlate with *pHIPP:GUS* expression pattern in mature embryos. *pHIPP32:GUS* was expressed in the root meristem (Figure 11) and *pHIPP34*:*GUS* showed strong expression throughout the whole embryo (Figure 13). Although the *HIPP33* promoter did not drive GUS expression in the embryo, the post-embryonical *pHIPP33:GUS* expression was restricted to the SAM and to the QC and CSC within the RAM (Figure 12).

To sum up, based on the patterning defects observed in *hipp32,33,34* embryos, it is highly likely that *HIPP* genes function in a redundant fashion to regulate shoot and root apical meristem formation during embryogenesis.

4.2.2 Roles of cluster-III *HIPP* genes in regulating root growth

The cellular organization of the RAM is essential for establishing the radial patterning of the root and promoting root growth. *hipp* mutants exhibited severe defects in their root morphology. The primary root elongation, RAM size and root patterning, as well as LR formation were altered in *hipp* mutants. While *HIPP32* and *HIPP33* appeared to have synergistic roles as positive regulators of primary root elongation, *HIPP34* acts rather antagonistically in this regard (Figure 32). Interestingly, *HIPP32* negatively affected the LR formation, whereas *HIPP34* had a positive effect (Figure 32). The partially opposite effects of *HIPP* genes in regulating root growth correlate with different expression patterns, as deduced from *pHIPP:GUS* reporter studies. For instance, *pHIPP32:GUS* exhibited its strongest activity within the meristematic region, *pHIPP33:GUS* expression was restricted to the QC and the CSC, and *pHIPP34:GUS* expression was associated with the vasculature. This suggests that cluster-III *HIPP* genes might control different aspects of root growth, despite their close phylogenetic relation.

Except for *hipp32*, *hipp* single mutants showed rather weak root phenotypic changes compared to wild type. In contrast, the higher order mutants displayed partially severe phenotypic changes. For instance, *hipp32,33* exhibited a reduction in the root meristem which correlated with a retarded rate of root growth (Figure 32). Interestingly, *hipp33,34* root phenotype was characterized by an increase of the meristem size and an enhanced primary root growth (Figure 32). *hipp32,33,34* displayed shorter roots than *hipp32,33,* accompanied by further peculiarities, including loss of the gravitropic response, premature adventitious root formation, enhanced LR density and longer LR (Figure 33).

Critical to maintaining the root meristem size is the balance between auxin and cytokinin signaling components, which ensures the continuous root growth by strictly regulating the cell transition from the meristematic state to elongation and differentiation (Di Mambro and Sabatini, 2018). Auxin promotes cell division and inhibits cell elongation in the proximal meristem, while cytokinin promotes cell elongation and differentiation in the transition zone (Blilou *et al.*, 2005; Dello Ioio *et al.*, 2007). Exogenous application of cytokinin reduces the meristem cell number, whereas endogenous reduction of cytokinin by *CKX* overexpression leads to increased primary root growth because of the increased number of dividing cells in the meristem. Cytokinin biosynthesis and signaling mutants display an increase in root meristem size and growth (Dello Ioio *et al.*, 2007; Werner *et al.*, 2003). The enhanced root growth observed in *hipp33,34* mutants correlated with reduced *TCSn:GFP* activity in the root meristem (Figure 51). Intriguingly, *TCSn:GFP* activity was tendentially or significantly reduced also in *hipp* mutants with retarded root growth – *hipp32,33* and *hipp32,33*,*34*, respectively (Figure 51). RNA-Seq data revealed a significant upregulation of *ARR15* transcript levels in *hipp32,33,34* seedlings (Figure 43), correlating with the reduced *TCSn:GFP* activity observed in *hipp32,33,34* roots, given that ARR15 acts as a negative regulator in the cytokinin-mediated

signal transduction in root (Kiba *et al.*, 2002). In the roots of *cre1-1* mutant, which is a loss-of-function mutant of *AHK4* exhibiting enhanced root growth, the expression of *ARR15* was significantly reduced (Kiba *et al.*, 2002). In addition, RNA-Seq data indicated that other factors may contribute to *hipp* root phenotype, although the RNA-Seq analysis was not conducted on roots. For instance, many genes associated with the auxin signal transduction pathway were differentially expressed in *hipp* mutants, particularly early auxin response genes from the large *SAUR* family (Ren and Gray, 2015; Figure 43). Among these, several *SAUR* genes were identified to associate with auxin signaling during root development. For instance, genes from SAUR19 subfamily (*SAUR19* to *SAUR24*), which are expressed in elongating tissues – including the root elongation zone – and which promote cell expansion (Spartz *et al.*, 2012), were downregulated in single mutants with decreased root meristem size, *hipp32* and *hipp33* (Figure 34). *SAUR* genes from SAUR10 subfamily have also been shown to positively regulate the auxin-mediated plant cell expansion (Spartz *et al.*, 2014). Among these, *SAUR9* and *SAUR10* were downregulated in *hipp32,33,34* as detected by RNA-Seq (Figure 43). Moreover, *SAUR71* and *SAUR72*, expressed in the stele of young roots and hypocotyl, have been attributed potential roles as signal molecules in ensuring the coordination of cell proliferation and cell expansion in *Arabidopsis* roots (Qiu *et al.*, 2013). Both *SAUR71* and *SAUR72* were downregulated in *hipp32,33,34* (Figure 43). Recent studies have identified a cytokinin-dependent molecular mechanism that acts in the LR cap to control auxin activity in the root meristem (Di Mambro *et al.*, 2019). ARR1 activates the expression of *GRETCHEN HAGEN 3.17* (*GH3.17*) gene, which encodes an IAA-amino synthase that mediates the irreversible auxin conjugation and catabolically controls the auxin levels at the transition zone and in the LR cap, which serves as an auxin sink, under the control of cytokinin, regulating the entire root meristem (Di Mambro *et al.*, 2017; Di Mambro *et al.*, 2019). Other genes from the *GH3* group II family, *GH3.5* and *GH3.6,* were also identified to be involved in the cytokinin-dependent regulation of auxin levels in both root meristem and vascular tissue (Pierdonati *et al.*, 2019). Interestingly, two *GH3* genes, *GH3.1* and *GH3.5*, were differentially expressed in *hipp32,33,34* as detected by RNA-Seq (Figure 43). These findings suggest that *HIPP* genes might function in auxin signaling, transport, or biosynthesis. Experiments using auxin-responsive reporters, which allow to monitor the auxin distribution in roots, would be necessary to clarify whether the *HIPP* genes are relevant for auxin activity in roots (Sabatini *et al.*, 1999; Friml *et al.*, 2003). The possible disruption of the auxin signaling in *hipp32,33,34* roots might also have caused the gravitropism defects evident in this mutant (Figure 33), as polar auxin transport and redistribution are essential for proper responses to gravity stimuli (Geisler *et al.*, 2014).

In addition to the primary root length, the lack of *HIPP* genes also affected the homeostasis and patterning of the RAM. Particularly in *hipp32,33* roots, the QC cells, columella cells, and CSCs were disorganized and misspecified (Figure 34). The extent of these defects was greater

in *hipp32,33,34* (Figure 34), suggesting that *HIPP* genes might have redundant roles of crucial significance for stem cell-fate specification and proper cell patterning in both embryonic and post-embryonic roots. *TCSn:GFP* reporter studies demonstrated that cytokinin signaling output is strongly diminished in *hipp32,33,34* roots (Figure 51), suggesting that *HIPP* genes modulate the cytokinin activity in the RAM. It would be revealing to investigate whether the reduced cytokinin signaling in *hipp32,33,34* is linked to the activity of key regulatory genes, such as *WOX5*, *SHR*, *SCR* and *PLT*, which control the stem cell niche activity and maintenance of the QC identity (Sarkar *et al.*, 2007; Sabatini *et al.*, 2003; Aida *et al.*, 2004). Since cytokinin promotes the mitotic activity in the QC by repressing the expression of *SCR* and *WOX5* (Zhang *et al.*, 2013), it is possible that the QC specification and the maintenance defects observed in *hipp* mutants might not be directly linked to cytokinin activity. Since numerous auxin-associated genes were differentially regulated in *hipp32,33,34*, it is possible that *HIPP* gene activity interferes with components of auxin pathways and thereby contribute to the regulation of the RAM development. Another hypothesis could be that HIPP-mediated symplasmic communication might be linked to either auxin distribution or PD-dependent trafficking of key regulators, both necessary to maintain root SCN activity in *Arabidopsis* (Liu *et al.*, 2017a; Sarkar *et al.*, 2007; Nakajima *et al.*, 2001; Mellor *et al.*, 2020).

Root assays revealed that *HIPP* genes act in a complex genetic fashion to regulate LR growth in *Arabidopsis*. Particularly *hipp32,33,34* displayed an increased LR number and density (Figure 33). These observations are in agreement with the diminished activity of *TCSn:GFP* in *hipp32,33,34* root meristems (Figure 51). In addition, the LRs in *hipp32,33,34* appeared longer than in wild type (results not shown). LRs in *Arabidopsis* originate from a subset of pericycle founder cells (Casimiro *et al.*, 2003). The interplay between auxin and cytokinin also regulates the LR organogenesis. While auxin promotes the LR initiation, as well as the later phases of primordium formation and emergence, cytokinin inhibits both LR initiation and development (Bielach *et al.*, 2012). The root branching phenotype of *hipp32,33,34* resembles that of *Arabidopsis* cytokinin receptor and response regulator mutants (Riefler *et al.*, 2006; To *et al.*, 2004; Mason *et al.*, 2005). A low cytokinin signaling would reduce the inhibitory effects of cytokinin on the expression of *PIN* genes, and would thus enhance the formation of an auxin gradient that is required during the early stages of LR organogenesis (Laplaze *et al.*, 2007). A recent study has provided insight into PD-auxin interactions that modulate LR emergence (Sager *et al.*, 2020). It has been demonstrated that the auxin-dependent expression of the plasmodesmal regulator PDLP5 in the cells overlying newly forming LR primordia stimulates the formation of a temporary symplasmic domain in these cells, which allows the expansion of auxin distribution, thus enhancing the LR emergence (Sager *et al.*, 2020). That symplasmic connectivity and callose are important for the emergence of LR and root patterning has been previously shown (Maule *et al.*, 2013; Benitez-Alfonso *et al.*, 2013). It is possible that the

presumably enhanced symplasmic mobility in *hipp32,33,34* might influence auxin transport and distribution, both of which are critical for LR development (Blilou *et al.*, 2005).

4.2.3 *HIPP* genes influence leaf morphology

The most obvious changes in *hipp* mutant leaf morphology were the reduced leaf size, narrowed leaf blade, as well as serrated leaf margins (Figure 21). The phenotypic changes were in good agreement with the results of the GUS staining. Particularly in young leaves, *pHIPP32:GUS* and *pHIPP33:GUS* expression was strong in the margins and the stipules of arising leaves, respectively, whereas *pHIPP34:GUS* was expressed throughout the entire leaf but not in the leaf tip (Figure 11 to 13). This suggests that the processes controlling leaf growth, whether in the form of division or expansion, are affected by *HIPP* genes' activity.

Leaves are initiated at the flanks of the SAM where leaf primordia subsequently engage in coordinated cell division, expansion, and differentiation, until the final leaf size and shape are reached (Bar and Ori, 2014). Cytokinin activity controls leaf development at distinct phases and plays an important role in determining the final leaf size and shape (Werner *et al.*, 2001; Riefler *et al.*, 2006; Skalák *et al.*, 2019). The extent to which the leaf morphology of *hipp* mutants is linked to an altered cytokinin activity is still unclear. It has been shown that CKX interaction with cluster-I HIPP proteins is involved in the regulation of leaf growth. *Arabidopsis* plants overexpressing either *HIPP6* or *HIPP7* formed smaller rosette leaves with shorter petioles and crinkly lamina (Guo, 2019). These phenotypical changes were accompanied by enhanced cytokinin responses and, intriguingly, increased CKX protein levels, implying that these HIPPs might negatively function in the degradation of CKX via the ERAD pathway (Guo, 2019). It would be revealing to investigate whether the decreased leaf blade area observed in *hipp* mutants correlates with an altered steady-state cytokinin activity in leaf primordia, as cytokinin affects, in a dose-dependent manner, both cell proliferation and leaf cell expansion (Holst *et al.*, 2011; Skalák *et al.*, 2019). Considering the numerous auxin-associated genes that were deregulated in *hipp* mutants (section 3.5.2.), it is plausible that the altered leaf morphology and particularly the leaf serration phenotype displayed by *hipp* plants may also be linked to a possibly disturbed auxin signaling and distribution (Xiong and Jiao, 2019). For instance, the leaf serration in *Arabidopsis* is mainly regulated by the feedback between auxin through the activity of the carrier PIN1 and CUP-SHAPED COTYLEDON 2 (CUC2), a growth repressor known to control leaf margin development in a *MIR164*-dependent manner (Bilsborough *et al.*, 2011; Nikovics *et al.*, 2006). Both *pin1* and *cuc2 Arabidopsis* mutants failed to initiate serrations and formed leaves with smooth margins (Hay *et al.*, 2006; Nikovics *et al.*, 2006). Polar cellular PIN1 localization creates a convergence pattern and directs the auxin flow toward the leaf margin, where the auxin maximum is required for the outgrowth of serrations (Scarpella *et al.*, 2006; Hay *et al.*, 2006). *CUC2*, expressed in the leaf sinus regions,

promotes the generation of PIN1-dependent auxin maxima and thus contributes to creating leaf margin serrations (Bilsborough *et al.*, 2011; Nikovics *et al.*, 2006). In addition, auxin treatments repressed the expression of the *CUC2:GUS* transcriptional reporter gene, suggesting that auxin negatively regulates *CUC2* during simple leaf development (Bilsborough *et al.*, 2011).

4.2.4 HIPP proteins act as negative regulators of flowering time

Flowering time experiments conducted under both long- and short-day light conditions showed that mainly *HIPP33* and *HIPP34* are involved in the repression of flowering time. Previous studies showed that HIPP34 negatively influences flowering time, as *Arabidopsis* plants overexpressing *HIPP34* under *35S* promoter (line *HIPP34ox #5-1*) flowered considerably later than wild type (Tschuden, 2019). Similarly delayed flowering phenotype was observed in transgenic plants overexpressing distinct *HIPP* genes from cluster I (Zschiesche *et al.*, 2015; Guo, 2019). In the present study, *HIPP34ox #5-1* flowered either at the same time as wild type (LD) or earlier than wild type (SD; Figure 46). Expressing *HIPP34* under the control of its native promoter did not affect flowering time regardless of the light regime (Tschuden, 2019). Despite these discrepancies, the redundant role of *HIPP* genes in negatively regulating flowering time was obvious from the early onset of flowering in *hipp32,33, hipp33,34* and *hipp32,33,34* (Figure 23).

The regulatory network of flowering time in *Arabidopsis* consists of more than 300 genes integrated in multiple, complex pathways that quantitatively control the timing and the switch of the SAM from the vegetative to the reproductive developmental phase (Simpson and Dean, 2002; Bouché *et al.*, 2016). Several lines of evidence demonstrate the biological role of cytokinin in controlling flowering time in *Arabidopsis*. For instance, increasing the endogenous cytokinin levels or exogenous cytokinin application correlate with early flowering in various *Arabidopsis* ecotypes (Chaudhury *et al.*, 1993; He and Loh, 2002; D'Aloia *et al.*, 2011). Gain-of-function mutants of cytokinin receptors AHK2 and AHK3 exhibiting elevated cytokinin activity flowered significantly earlier than wild type (Bartrina *et al.*, 2017). Conversely, reducing the cytokinin levels in transgenic plants overexpressing *CKX1* or *CKX3*, as well as cytokinin receptor mutants *ahk2,3,4*, either showed a retarded flowering phenotype or failed to flower (Werner *et al.*, 2003; Riefler *et al.*, 2006). On a speculative note, the interaction between HIPP34 and CKX1 (Figure 18; see section 4.4.1) might participate in modulating the flowering time. The early flowering phenotype of *hipp34* would imply that HIPP34, by interacting with CKX1, suppresses its activity, leading to an enhanced cytokinin concentration and thereby promotes early flowering. It would be informative to investigate whether the early flowering phenotype caused by the lack of *HIPP* genes is linked to an enhanced cytokinin activity.

Analysis of the *TCSn:GFP* activity in the SAM of *hipp* plants before and after SAM transition to reproductive development would provide insights in this regard.

Other factors might be involved in the HIPP-mediated flowering time regulation as well, including the enhanced symplasmic trafficking through PD observed in distinct *hipp* mutants, since important flowering signals are transported through phloem (Giakountis and Coupland, 2008). For instance, the primary component of the *Arabidopsis* florigenic signaling system, FT, moves long-distance through phloem from source leaves to the vegetative apex where it mediates floral induction (Corbesier *et al.*, 2007; Lin *et al.*, 2007). It has been shown that the ER-localized transmembrane protein FT INTERACTING PARTNER 1 (FTIP1) interacts with FT in companion cells of the phloem and mediates FT protein movement from companion cells to sieve elements (Liu *et al.*, 2012). Loss of *FTIP1* causes late flowering under long-day conditions, which is partly due to the compromised FT movement to the SAM (Liu *et al.*, 2012). Furthermore, it has been demonstrated that one of the *Arabidopsis* HPP proteins, NaKR1/HPP2, which is specifically expressed in companion cell-sieve element complexes of the phloem, interacts with FT and that the NaKR1-FT interaction is required for FT transport to shoot apices through sieve elements during floral transition (Tian *et al.*, 2010; Zhu *et al.*, 2016). Analysis of *pHIPP34:GUS* revealed that *HIPP34* is expressed in vascular tissues of the root, shoot and rosette leaves (Figure 13). Given the influence of HIPP33 and HIPP34 proteins on the symplasmic trafficking (Figure 62), a hypothetical role of HIPP proteins in mediating long-distance delivery of florigenic signals might be plausible. Unlike *ftip1* and *nakr1* (Liu *et al.*, 2012; Zhu *et al.*, 2016), *hipp* mutants flower earlier than wild type, implying that *HIPP*s are involved in the negative regulation of flowering time under long-day conditions.

4.2.5 Insights into the overlapping roles of *HIPP* genes during reproductive growth

The phenotypic characterization of *hipp* higher-order mutants revealed that particularly *HIPP33* and *HIPP34* play overlapping roles in regulating inflorescence meristem activity and have pleiotropic effects on the development of the reproductive organs in *Arabidopsis*. These results are in good agreement with GUS activity assays showing that cluster-III *HIPP* genes are active in various floral tissues (Figure 11 to 13). The inflorescence meristem was enhanced in *hipp32,33, hipp33,34* and particularly in *hipp32,33,34* (Figure 24). Furthermore, *hipp33,34* and particularly *hipp32,33,34* exhibited prolonged reproductive growth, accompanied by an increased number of flowers and siliques. A similar phenotype, as well as increased duration of flowering and increased total life span, were observed in the gain-of-function mutants of cytokinin receptors AHK2 and AHK3, exhibiting strong cytokinin signal transduction activities (Bartrina *et al.*, 2017). Likewise, the *ckx3,5* double mutant has been shown to form larger inflorescence and floral meristems as a result of elevated cytokinin content in the SAM (Bartrina *et al.*, 2011). However, *TCSn:GFP* expression analyses showed that cytokinin activity

was strongly reduced in the root of *hipp* mutants (Figure 51). Although it was not directly analyzed, it is probable that *hipp* mutants exhibit low cytokinin signaling activity in the SAM and inflorescence meristem, suggesting that their increased meristem activity might not be linked to cytokinin.

In *Arabidopsis* and other plants with indeterminate inflorescences, the end of flower production occurs by a regulated proliferative arrest of inflorescence meristems and it depends on seed development (Hensel *et al.*, 1994; Balanzà *et al.*, 2019). Terminal flower formation is controlled genetically by the FRUITFULL-APETALA2 (FUL-AP2) pathway, by a correlative control exerted by the seeds through a mechanism not yet elucidated (Balanzà *et al.*, 2019). In the absence of seeds, meristem proliferative arrest does not occur, and the meristem remains active and produces flowers until it becomes determinate (Balanzà *et al.*, 2019). There are several lines of evidence suggesting that mutants with strongly reduced fertility exhibit extended flowering periods (Hensel *et al.*, 1994; Wuest *et al.*, 2016). This type of relationship between low fruit development and high proliferative capacities of inflorescence meristems was also observed in *hipp33,34* and *hipp32,33,34*. The high inflorescence meristem activity correlated with the increased longevity and high number of siliques (Figure 24).

In addition to the increased inflorescence meristem activity, the lack of *HIPP* genes affected the floral organ formation, female fertility, and seed production. *hipp32,33,*34 in particular formed rudimentary flowers with misshapen petals and sepals, suggesting cell division and patterning defects (Figure 25). Furthermore, *hipp32,33,34* exhibited aberrant floral organ numbers and fused floral organs (results not shown). Congruent with the flower phenotypic severity, the self-pollination was impaired in *hipp32,33,34* plants, causing decreased plant fecundity, as inferred from the high frequency of aborted, probably unfertilized, ovules (Figure 25). Extrapolating from the silique inability to elongate after hand-pollination with wild type pollen*, hipp33,34* and, to a greater extent, *hipp32,33,34* appeared to exhibit reduced female fertility (Figure 26). Since *hipp32,33,34* produced only few pollen grains that could not properly adhere to the stigma surface (results not shown), it is possible that certain processes during male and female gametogenesis may be affected in the *hipp* triple mutant. These reproductive growth defects caused the extremely poor seed production, especially in *hipp32,33,34* mutants. Whether these defects are related to an altered cytokinin signaling in these mutants is unclear. Similar fertility problems have been reported for mutants with an impaired cytokinin response, such as plants that lack all three cytokinin receptors (Nishimura *et al.*, 2004), or plants overexpressing *UGT73C1* and *UGT85A3,* which act downstream of *CUC1* and *CUC2* to regulate cytokinin activity of the meristematic placenta tissue (Cucinotta *et al.*, 2018). Auxin is also known to act as a morphogen during gynoecium development and is required for proper formation of both male and female reproductive organs, before and after fertilization (Nemhauser *et al.*, 2000; Pagnussat *et al.*, 2009; Panoli *et al.*, 2015; Liu *et al.*, 2017b).

Interestingly, auxin homeostasis in ovules was shown to be regulated in an anther-dependent manner, presumably to synchronize reproductive organ development (Larsson *et al.*, 2017). Histochemical GUS staining of *pHIPP33:GUS* revealed that *HIPP33* is expressed in ovules at different stages (Figure 12). Several studies have shown that symplasmic communication is important for female gametophyte development before and after fertilization (Tilney *et al.*, 1990; Han *et al.*, 2000; Dresselhaus, 2006; Erdmann *et al.*, 2017). Whether HIPP proteins are present at PD during ovule development is still unclear. Assuming this to be the case and given the involvement of HIPP proteins in regulating the plasmodesmal trafficking, it might be possible that the gametogenesis defects observed in *hipp33,34* and *hipp32,33,34* are linked to a presumably disturbed PD function. It would be informative to investigate the symplasmic connectivity during ovule development in *hipp* mutants (Werner *et al.*, 2011), for instance by using the *pSUC2:GFP* lines generated in this work.

4.3 Deciphering transcriptional programs underlying the activity of *HIPP* genes

To gain a broader understanding of the genetic context of the *HIPP* genes, a transcriptional profiling in *hipp* single and triple mutants was performed using RNA-Seq. Relative to wild type, the largest number of DEGs were identified in *hipp32*, while in *hipp33* and *hipp34* the number of DEGs was three and four times lower, respectively (Figure 35). In *hipp32,33,34*, the number of DEGs was 2.5-fold lower as in *hipp32*, and comparable to DEG number in *hipp33* and *hipp34* (Figure 35). Comparison of DEGs in individual *hipp* single mutants showed a large and significant overlap (Figure 36A), indicating that the *HIPP* genes control in part similar genetic pathways and biological processes. Furthermore, *HIPP* genes appear to have a similar regulatory potential, since the overlapping DEGs were regulated in the same direction and exhibited comparable transcriptional changes (Figure 37). These findings are in good agreement with the additive phenotypic effects observed in the multiple *hipp* mutant combinations. However, the significantly higher number of DEGs in *hipp32* might also indicate that *HIPP32* has either have a stronger effect or controls in part different pathways than *HIPP33* and *HIPP34*. This would be in concordance with the slightly different expression pattern of *pHIPP32:GUS* and with the dual subcellular localization of HIPP32, which was shown to localize to the Golgi apparatus (Figure 16) in addition to its PD-localization. Moreover, HIPP32 shares only 44% sequence homology with HIPP33 and HIPP34, whereas between the latter two HIPP proteins exists a homology of 76%. However, the GO term enrichment analysis performed based on the DEGs identified in the *hipp* mutants resulted in overall similar and mostly overlapping GO term categories (Figure 38 to 41), further supporting the functional redundancy between *HIPP* genes.

A detailed analysis of the genes which were most strongly affected by the lack of *HIPP* genes revealed that many of them encode enzymes (Table 20 to 23). For instance, several members

from the large *CYTOCHROME P450* (*CYP*) gene superfamily were identified among the ten most deregulated genes in *hipp* single mutants. CYPs are monooxygenases which contain a heme with iron as catalytic center (Bak *et al.*, 2011; Schuler *et al.*, 2006). Given the metallochaperone character of HIPP proteins and their ability to bind and transport heavy metal ions (Tehseen *et al.*, 2010; Suzuki *et al.*, 2002; Gao *et al.*, 2009; Zschiesche *et al.*, 2015), it is plausible that the deregulation of *CYP* genes in *hipp* mutants might be related to the putative function of HIPP proteins in delivering iron to the cofactors of CYP oxygenases. One would expect that the lack of HIPP proteins should result in non-functional CYP enzymes, which in turn would correlate with a compensatory upregulation of *CYP* genes, as identified in *hipp32* (Table 20) and *hipp34* (Table 22). However, some *CYP* genes were downregulated in *hipp34* (Table 22), implying that other mechanisms might underlie the *HIPP*-mediated transcriptional regulation of *CYP* genes. The GO terms for molecular functions revealed overrepresentation of genes involved in heme and iron ion binding in all *hipp* mutants (Figure 38 to 41), supporting the idea of HIPP proteins functioning as metallochaperones which shuttle metal ions to specific intracellular target proteins. Furthermore, several genes encoding members of FERRITIN iron-storage protein family (Arosio *et al.*, 2009) were also associated with these GO terms.

Interestingly, the strongest upregulated gene in *hipp32,33,34* was *MATERNAL EFFECT EMBRYO ARREST 26* (*MEE26*, Table 23). *MEE26* was originally identified in a forward genetic screening as a female gametophytic factor which is essential for early embryo development (Pagnussat *et al.*, 2005). *MEE26* expression was shown to be strongly induced by ABA during germination and throughout early seedling growth and it is required to maintain cotyledon embryonic identity (Kinoshita *et al.*, 2010). Further experiments would be required to elucidate whether the embryonic patterning defects observed in *hipp32,33,34* might be linked to disruptions in the *MEE26* functional activity.

One of the most downregulated gene commonly detected in all *hipp* mutants was *QQS* (Figure 37), which was identified as a component of starch metabolism, as its mRNA showed a notably large increase in the *Arabidopsis ss3* mutant lacking the STARCH SYNTHASE 3 (SSE) encoding gene (Li *et al.*, 2009). Given the starch accumulation observed in embryonic *hipp32,33,34* mutants (Figure 30), the question arose whether the *SSE* expression was altered in *hipp* mutants in RNA-Seq analysis. However, the *SSE* expression levels in *hipp* mutant lines did not differ from wild type (data not shown). The only statistically significant DEG related to starch biosynthesis was the *CT-BMY*, which encodes a chloroplast-targeted beta-amylase (Lao *et al.*, 1999) and which was upregulated in all *hipp* mutants analyzed (Figure 37).

Several genes encoding components of auxin metabolism and signaling were identified among the top ten most downregulated genes in *hipp* mutants (Table 20 to 23). Most of those belong to the early auxin response genes from the large *SAUR* family (Ren and Gray, 2015) and were discussed as potential factors influencing the *HIPP*-dependent root growth regulation in section

4.2.2. Interestingly, the *INDOLE-3-ACETIC ACID INDUCIBLE 29* (*IAA29*) gene was identified among the most downregulated in *hipp33* (Table 21). The expression level of *IAA29* has been shown to be directly regulated by the transcription factor PHYTOCHROME INTERACTING FACTOR 4, which binds to *IAA29* promoter to repress the activity of ARF7 and thereby negatively regulates phototropism and auxin signaling (Sun *et al.*, 2013). This finding would support the hypothesis that the partial loss of the gravitropic response observed *hipp32,33,34* roots (Figure 33A) might be due to altered polar auxin transport and redistribution occurring in this mutant (Geisler *et al.*, 2014, see also section 4.2.2).

Many early auxin response genes from the families *Aux/IAA*, *GH3* and *SAUR* (Hagen and Guilfoyle, 2002) were associated with the auxin-related GO terms ‘auxin-activated signaling pathway’ and ‘response to auxin’ which were overrepresented in *hipp* mutants (Figure 38 to 41). Accordingly, numerous *SAUR* genes were significantly enriched in the ‘plant hormone signal transduction’ pathway in all *hipp* mutants in KEGG analysis (Figure 42). Although the functions of SAURs are largely unknown, several *SAUR* genes have been shown to be involved in the regulation of various aspects of plant growth and development, such as cell expansion, root meristem patterning (section 4.2.2), leaf senescence and shade avoidance (Markakis *et al.*, 2013; Kong *et al.*, 2013; Hou *et al.*, 2013; Spartz *et al.*, 2012). *SAUR* regulation does not only depend on auxin. Recent studies have shown that several *SAUR* genes are also regulated by other hormones, including cytokinin (van Mourik *et al.*, 2017). It is plausible that the differential expression of *SAUR*s in *hipp* mutants is caused by the altered cytokinin activity. Possible causes might also be an altered auxin activity (section 4.2.1) or an imbalance between cytokinin and auxin signaling output in *hipp* mutants.

Common to all *hipp* mutants was a large number of genes associated with the GO terms ‘regulation of transcription’ and ‘transcription factor activity’ (Figure 38 to 41). Among these genes, several genes encode for zinc-finger transcription factors, such as CONSTANS-LIKE 2, CYCLING DOF FACTOR 1 or TANDEM ZINC KNUCKLE PROTEIN. Hence, a putative role of HIPP34 as metallochaperone delivering zinc ions to activate these transcription factors is plausible. A similar mode of action has been discussed for the zinc-binding nuclear-localized HIPP protein, HIPP3 (Zschiesche *et al.*, 2015).

Given the HIPP localization at PD and their role in influencing the intercellular trafficking, it was compelling to investigate possible changes of PD-related gene expression in *hipp* mutants. Microarray-based gene expression analyses performed in mutants with increased PD trafficking, *ise1* and *ise2*, have revealed that several genes previously implicated in PD structure or function, including *PDCB3*, *PDLP3*, *PDLP5*, *PDLP8* and *GSL8* are differentially expressed in *ise* mutants (Burch-Smith *et al.*, 2011; see also section 4.2.1). The GO term ‘plasmodesma’ was indeed overrepresented in *hipp32* in the presented RNA-Seq analysis (Figure 38). However, no PD-related genes known to directly alter PD function were identified

to associate with this GO term or to be differentially regulated. Many DEGs associated with this GO term encode cell wall-related enzymes such as expansins, β-galactosidases, pectin methyltranseferases, and xyloglucan endotransglucosylase/hydrolases (XTHs) and signaling proteins, as for example cysteine-rich receptor-like protein kinases. Accordingly, these genes were also associated with the GO terms 'extracellular region' and 'cell wall' overrepresented in *hipp* mutants (Figure 38 to 41). *EXPANSINS* and *XLH* genes were also differentially regulated in *ise* mutants (Burch-Smith *et al.*, 2011). Both EXPANSINS and XTH enzymes function as modulators of cell wall expansion with important roles in cell wall remodeling during normal plant growth and in response to distinct stresses (Cosgrove, 2005; Pauly and Keegstra, 2016; Houston *et al.*, 2016). The cell wall microdomains surrounding PD have been attributed roles in influencing both PD biogenesis and function (Knox and Benitez-Alfonso, 2014). Therefore, it is plausible that the differential expression of *EXP* and *XTH* in *hipp* mutants might be linked to changes in the mechanics and composition of the cell wall around PD, altering in turn the PD function or influencing PD biogenesis. For instance, remodeling of the cell wall is required for the formation of secondary PD (Ehlers and Kollmann, 2001). This might explain the *EXP* upregulation, as the enhanced symplasmic trafficking in *hipp* mutants might be due to a possible increase in number of primary and/or secondary PD (section 4.1.2). However, the *XTH* downregulation in *hipp* mutants does not support this hypothesis.

So far, the knowledge about the transcriptional regulation of gene expression underlying the activity of *HIPP* genes in *Arabidopsis* is limited to *HIPP3* from cluster I (Zschiesche *et al.*, 2015; Figure 2). A microarray-based transcriptome analysis revealed that overexpression of *HIPP3* affects the regulation of more than 400 genes involved in pathogen and abiotic stress response as well as seed and flower development (Zschiesche *et al.*, 2015). The global transcript analysis presented in this work revealed that the lack of *HIPP* genes influences the expression of numerous genes involved in diverse processes of plant growth and development, in agreement with the pleotropic phenotypic alterations exhibited by the *hipp* mutants. Several DEGs might be causally linked to HIPPs' presumptive metallochaperone function, while others indicate that they mediate crosstalk factors between auxin and different developmental pathways. Furthermore, HIPP might be involved in regulation of cell wall modifications to regulate PD transport. However, further experimental analyses are necessary to clarify the putative role of *HIPP* genes in these processes.

4.4 Dissecting the relevance of HIPPs in mediating cytokinin activity

4.4.1 Open questions concerning the interaction of HIPP proteins with CKX1

The cluster-III HIPP proteins analyzed in this study were identified to interact with the cytokinin degrading enzyme CKX1 in a genome-wide Y2H screen previously performed in Dr. Werner's group. Based on the same Y2H screen, additional HIPP proteins from cluster I, HIPP5, HIPP6, and HIPP7, were described to interact with CKX1 and others CKX proteins (Guo, 2019). Two HIPP proteins, HIPP19 and HIPP35, randomly chosen from outside cluster I and III, were not able to interact with CKX1 (Guo, 2019). The fact that CKX1 interacts with HIPP proteins belonging to two phylogenetically distinct clusters suggests that the interactions are specific and not mediated through the conserved domains of the HIPP proteins. The interactions between cluster-III HIPP proteins and CKX1 was confirmed by *in vivo* Co-IP experiments (Figure 18A). Aiming to investigate the interaction between CKX1 and HIPPs at the cellular level, the CKX1/HIPP32 and CKX1/HIPP34 complex formation was analyzed in BiFC assays (Figure 18B, C), which confirmed the interaction between CKX1 and the HIPP proteins (Figure 18C). CKX1/HIPP32 complex formation appeared to occur along the cell periphery, and the BiFC signals for CKX1/HIPP34 resembled the dot-like pattern specific to PD localization. Given that CKX1 is a type II integral membrane protein that localizes at the ER (Niemann *et al.*, 2018), CKX1/HIPP34 protein heterocomplex formation might for instance occur at the ER in the proximity of PD (Tilsner *et al.*, 2016; see section 4.1.1). Guo (2019) showed that the subcellular localization of BiFC complexes formed between CKX1 and HIPP1 and HIPP7, respectively, correlated with the localization of HIPP proteins. CKX1/HIPP1 exhibited cytosolic/nuclear localization and BiFC CKX1/ HIPP7 were detected at the cytosolic side of the ER (Guo, 2019). Due to the low intensity and frequency of BiFC signals in this work, further co-localization studies, *i.e.* using different organelle markers to determine the subcellular localization of CKX1/HIPP protein complex, were not possible. However, it is likely that the interaction between CKX1 and cluster-III HIPP proteins takes place at the HIPP subcellular location sites. The BiFC technique relies on the irreversible assembly of fluorescent protein fragments (Miller *et al.*, 2015) In general, the intensity of BiFC signals might be influenced by the steric arrangement of the fluorescent protein fragments that will produce a maximal signal (Kerppola, 2008). In the BiFC analysis performed in this study, both CKX1 and HIPP proteins were N-terminally fused to the N- and C-terminal fragment of the Venus fluoroprotein, respectively (Figure 18B; Gookin and Assmann, 2014). Because a C-terminal fusion of Venus fragments to the HIPP protein would interfere with the prenylation motif, additional combinations of fusion proteins that might produce optimal signals could not be tested. Since the BiFC system used in this study allows the expression of both putative interacting proteins from the same expression vector, under identical promoters, it can be likely excluded that the weak BiFC

signals were due to different expression levels of both fusion proteins (Gookin and Assmann, 2014; Kerppola, 2008). Hence, it can be interpreted that the detected BiFC signals, although weak, represent true and specific CKX1-HIPP interactions. However, the molecular mechanisms underlying the interactions between CKX1 and HIPP proteins form cluster III could not be clarified here. Overexpression of CKX1-interacting HIPP proteins from cluster I, HIPP1, HIPP6 and HIPP7, have been shown to differentially affect CKX1 protein levels (Guo, 2019). Furthermore, it has been hypothesized that HIPP7 modulates the abundance of CKX proteins by regulating their ERAD-dependent degradation (Guo, 2019; Niemann *et al.*, 2015). ERAD is a highly conserved degradation mechanism of proteins that involves the substrate retrotranslocation through ER membrane-embedded retrotranslocons, ubiquitination and subsequently its 26S proteasome-mediated degradation in cytosol (Vembar and Brodsky, 2008). Since CKX1/HIPP7 complex formation was detected at the cytosolic site of the ER membrane, it is thought that the interaction occurs during CKX retrotranslocation, and the interaction might influence the retrotranslocation efficiency and thereby the degradation rate of the CKX1 protein in cytosol (Guo, 2019). Whether cluster-III HIPP proteins have similar roles remains an open question. To which extent these interactions are relevant for the biological activity of CKX1 and other CKX proteins must also be addressed in the future.

4.4.2 *HIPP* genes function as positive regulators of the cytokinin signaling output

Lack of cluster-III *HIPP* genes caused pleiotropic phenotypes in *Arabidopsis* plants, including altered root growth and development, in the regulation of which cytokinin plays an important role. Given the context in which HIPP proteins were identified, it was thrilling to investigate whether *HIPP* genes are involved in modulating the cytokinin response and activity. The reduced root growth in *hipp32,33* and the enhanced root growth in *hipp33,34* (Figure 33 and 34) were the most evident root phenotypic changes thought to be linked to an altered cytokinin status and activity. However, these phenotypic changes were not reflected by the content of the endogenous cytokinins, as only subtle changes were detected upon measuring the endogenous cytokinin concentration in these mutants (Table 24). Nonetheless, cytokinin response assays revealed that both mutants *hipp32,33* and *hipp33,34* exhibited enhanced sensitivity to exogenous cytokinin in root assays (Figure 47). qRT-PCR expression analysis of the type-A *ARR* genes did not entirely support this result, as their expression level remained unchanged in *hipp32,33* mutant (Figure 50). Type-A *ARR*s function as cytokinin primary response genes and their expression level reflects the transcriptional activity in response to cytokinin (D'Agostino *et al.*, 2000). Loss-of-function mutations within the type-A response regulator family has been shown to cause enhanced sensitivity to cytokinin (To *et al.*, 2004). Given the inhibitory function of the type-A *ARR* genes on cytokinin response, their expression level would have been expected to be reduced in the hypersensitive *hipp* mutants. However,

this was only partially the case in *hipp33,34* (Figure 50). These results may suggest a differential regulation of type-A *ARR* genes caused by the lack of *HIPP* genes. Unlike in *hipp32,33* and *hipp33,34*, the primary root elongation in *hipp32,33,34* appeared to be insensitive to exogenous cytokinin, and the LR formation less sensitive (Figure 47). This could indicate that *HIPP* genes may play different roles in modulating cytokinin sensitivity in roots.

To specifically monitor the cytokinin signaling output in roots, the activity of the synthetic cytokinin reporter *TCSn:GFP* in *hipp* mutants was investigated. *TCSn:GFP* analysis revealed that the cytokinin steady-state activity was reduced in all *hipp* mutants, with the exception of *hipp32* and *hipp32,33* (Figure 51). This correlates with the significant upregulation of *ARR6* and *ARR15* in *hipp* mutants revealed by RNA-Seq analysis (Figure 43; To *et al.*, 2004), and attributes *HIPP* genes, mainly *HIPP33* and *HIPP34,* redundant functions in positively regulating the cytokinin signaling output. In partial agreement with the root assay results, *hipp* mutants exhibited overall enhanced sensitivity to cytokinin, as detected by *TCSn:GFP* in root meristem (Figure 52). Intriguingly, the enhanced responsiveness towards cytokinin in *hipp* mutants did not entirely correlate with the steady-state cytokinin signaling output (Figure 51 and 52). Cytokinin signaling output can also be regulated by post-translational events, such as the proteolysis of type-B ARRs (Kim and Hwang, 2012; Kim *et al.*, 2013). It has been demonstrated that a family of F-box proteins called the KISS ME DEADLY (KMD) family targets a subset of type-B ARR proteins for degradation. KMD proteins form an E3 ubiquitin ligase complex and directly interact with type-B ARR proteins (Kim *et al.*, 2013). Three out of four *KMD* genes annotated in *Arabidopsis* were associated with the GO term ‘negative regulation of cytokinin-activated signaling pathway’, which was significantly enriched in *hipp32,33,34* in RNA-Seq analysis (Figure 41). However, the *KMD* genes were identified as downregulated in *hipp32,33,34* mutant, and thus not explaining the reduced activity of type-B ARRs reflected by the reduced *TCSn:GFP* response. One explanation for this result could be that the possible regulation of the KMD proteins by the HIPPs might be root or cell type specific and accordingly not assessed by analyzing gene expression in whole seedlings. The reduced *TCSn:GFP* response in *hipp32,33,34* might be explained by the upregulation of the *CKX4* gene in this mutant in RNA-Seq analysis (result not shown). Since *CKX4* is expressed in the root cap (Werner *et al.*, 2003), one could speculate that *HIPP* genes positively regulate the cytokinin signaling output by modulating the *CKX4* activity and thus cytokinin status in roots. It would be informative to investigate whether cluster-III HIPP proteins are able to interact with CKX4, as it has been shown for cluster-I HIPP proteins (Guo, 2019).

It is currently difficult to explain the attenuated *TCSn:GFP* activity in *hipp* mutants. An interesting question is whether the severe patterning defects displayed by the *hipp32,33,34*, in both embryonic and postembryonic root meristems are somehow coupled to the reduced cytokinin activity and to the cytokinin role in modulating the activity of important root regulatory

factors, including the transcription factors WOX5, SCR, as well as auxin influx and efflux carriers (Zhang *et al.*, 2011, 2013). For instance, it would be revealing to investigate whether the reduced *TCSn:GFP* signaling output in *hipp32,33,34* correlates with the expression of *WOX5* in the putative QC in this mutant. In cytokinin deficient plants *ahk4,* the *WOX5* reporter activity negatively correlates with the intensity of cytokinin signaling (Pernisova *et al.*, 2018). Furthermore, the attenuated *TCSn:GFP* activity in *hipp* mutants might be linked to the increased plasmodesmal trafficking associated with the lack of *HIPP33* and *HIPP34* genes. The SCR transcription factor has been shown to maintain the stem cell niche and root growth by specifically suppressing the transcription of the type-B ARR, *ARR1,* and thereby cytokinin signaling in the QC (Moubayidin *et al.*, 2013). SCR requires activation by the SHR, which traffics through PD from the stele where it is expressed to the QC cells where it promotes *SCR* expression (Helariutta *et al.*, 2000; Sabatini *et al.*, 2003; Nakajima *et al.*, 2001). An increase in plasmodesmal trafficking in *hipp32,33,34* would enhance the SHR activity, which in turn would amplify the *SCR* expression, thus leading to *ARR1* repression, detectable as low *TCSn:GFP* (Figure 51). However, further experiments are necessary to prove this hypothesis.

The role of cytokinin in the QC is interlinked with its effects on auxin transport and distribution (Zhang *et al.*, 2011). For instance, disruption of multiple type-A *ARR* genes alters the level of several PIN efflux carriers and affects the auxin gradient and distribution in the root tip, which is required for proper cell patterning (Zhang *et al.*, 2011; Sabatini *et al.*, 1999). Higher-order type-A *ARR* mutants display a decrease in RAM size with aberrant pattern of cell division and differentiation, including QC division and starch-granule formation in columella stem cells (Zhang *et al.*, 2011). Although this work shows an upregulation of the cytokinin primary response genes in *hipp32,33,34* mutants (see section 3.7.5.1), it would be informative to investigate whether the reduced *TCSn:GFP* activity in *hipp32,33,34* mutants is linked to an altered auxin distribution. The fact that numerous auxin-related genes were deregulated in *hipp* mutants in RNA-Seq analysis might support this idea.

TCSn:GFP expression exhibited spatial changes in *hipp32,33,34* (Figure 51). For instance, unlike in wild type, the *TCSn:GFP* expression in *hipp32,33,34*, was not limited to the LR cap cells, stele and differentiated columella cells (Zürcher *et al.*, 2013), but was also detected in the root epidermis and in the assumingly CSCs (Figure 51). However, it is still not clear whether these observations reflect a disruption in *TCSn:GFP* expression pattern and/or or indicate loss of epidermal cell identity, as *hipp32,33,34* exhibits strong cell patterning defects within the root meristem (Figure 34).

Cytokinins are synthesized in numerous cell types in both roots and shoots, and are translocated as long-distance mobile signals via xylem and phloem (Osugi and Sakakibara, 2015; Hirose *et al.*, 2008; Kang *et al.*, 2017). Since HIPP proteins contribute to the regulation of the symplasmic trafficking through phloem (section 3.8.2), it would be intriguing to

investigate whether the long-distance transport of cytokinin is altered in *hipp* mutants. Particularly iP-type cytokinins are translocated from shoots to roots via phloem (Hirose *et al.*, 2008; Bishopp *et al.*, 2011b). By using the cytokinin reporter *TCSn:GFP* in *hipp* seedlings, it could be investigated whether exogenous iP application to the aerial parts of the plant affects cytokinin response in the root. Alternatively, the cytokinin translocation through phloem could be analyzed, for instance, using isotope-labelled iP ribosides applied to the hypocotyl, in order to assess their accumulation in the root (Bishopp *et al.*, 2011b).

4.4.3 *HIPP* genes regulate the transcriptional response to cytokinin

To explore whether *HIPP* genes play a role in the transcriptional response to cytokinin, the transcriptome of selected *hipp* mutants treated with exogenous BA was investigated. As case examples were chosen *hipp33*, the single mutant exhibiting the lowest steady-state *TCSn:GFP* signaling output, and *hipp32,33,34*. Several transcriptomics analyses using microarrays and RNA-Seq experiments have been used to explore the transcriptional response to cytokinin in *Arabidopsis* (Rashotte *et al.*, 2003; Brenner *et al.*, 2005; Argueso *et al.*, 2010; Bhargava *et al.*, 2013; Brenner and Schmülling, 2015). Moreover, Bhargava *et al.* (2013) has performed a meta-analysis to identify genes that respond to cytokinin. As expected, a large proportion of these 'golden list' cytokinin-responsive genes were identified in the presented RNA-Seq analysis, with comparable FC levels in wild type and *hipp* mutants (Table A3; Appendix).

To examine whether the *HIPP* gene activity is required for the cytokinin responses, the genes identified to be differentially expressed upon BA-treatment in *hipp* mutants were compared to those in wild type (Figure 54A, B). The pairwise comparisons revealed that 42% and 54% of genes differentially expressed in response to cytokinin in wild type failed to respond to cytokinin in *hipp33* and *hipp32,33,34*, respectively, thus strongly indicating that *HIPPs* regulate a large subset of cytokinin responses in *Arabidopsis*. Given that *HIPP* genes have no apparent or predictable functions in regulating signaling or transcriptional activity in plants, it is currently unknown how they interfere with the cytokinin signaling process. As HIPP proteins undergo protein-protein interactions, one hypothesis could be that they modulate the activity of proteins which are directly or indirectly involved in cytokinin signaling.

Several genes which might be functionally involved in the *HIPP*-regulated processes, as indicated by the *hipp* phenotypic changes, were identified among the *HIPP*-dependent cytokinin-responsive genes (Tables A1 and A2; Appendix). For instance, *GH3.7* encoding a synthetase from the IAA-amido synthase group II, was upregulated in wild type, but not in *hipp33*. *GH3.7* was identified as cytokinin-responsive in the microarray meta-analysis and RNA-Seq analysis published by Bhargava *et al.* (2013). The function of *GH3.7* is still unknown. Several genes from the *GH3* group II family, including *GH3.17, GH3.5* and *GH3.6*, are known to be involved in the cytokinin-dependent regulation of auxin levels during root growth (Di

Mambro *et al.*, 2017; Di Mambro *et al.*, 2019; Pierdonati *et al.*, 2019; Staswick *et al.*, 2005; see also section 4.2.2). Furthermore, the auxin early response gene *IAA5*, which has been shown to be induced by cytokinin (Bhargava *et al.*, 2013), was upregulated in wild type, but failed to respond to cytokinin in *hipp32,33,34*. These findings indicate that *HIPP*s might participate in the complex crosstalk between auxin and cytokinin that regulates, among others, the root growth and development in *Arabidopsis.* Surprisingly, the type-A *ARR17*, which has not been identified as cytokinin-responsive gene in previous studies published by Brenner *et al.* (2012) and Bhargava *et al.* (2013), was upregulated in wild type, but did not respond to cytokinin in *hipp33*. Previous study has revealed that the stability of ARR17 protein is regulated by cytokinin and the proteasome pathway (Ren *et al.*, 2009a). It has been discussed that stabilized type-A ARR proteins may interact with other targets and possibly regulate processes also beyond the cytokinin signaling circuit (To *et al.*, 2007b). However, the mechanism underlying the *HIPP33*-dependent *ARR17* induction by cytokinin is currently unclear.

In addition to the *HIPP*-dependent cytokinin responsive genes, the expression levels of the 25 most deregulated genes upon cytokinin treatment in wild type was identified and subsequently compared to *hipp33* and *hipp32,33,34* mutants (Figure 56). Most of these genes were also deregulated in *hipp* mutants, exhibiting comparable FC levels as in wild type. Few genes including the *ELICITOR-ACTIVATED GENE 3-2* (*ELI3-2)* and the *ETHYLENE RESPONSE FACTOR 105* (*ERF105*) were highly induced by BA in wild type, but failed to respond in *hipp* mutants (Figure 56A), suggesting that *HIPP* gene activity is required for their cytokinin-mediated regulation. Little is known about the biological function of *ELI3-2*, apart from its putative role in stress and defense responses (Somssich *et al.*, 1996; Müller *et al.*, 2008; Iizasa *et al.*, 2017). Several *HIPP* genes have been reported to be involved in plant defense against biotic stress (Zschiesche *et al.*, 2015; Cowan *et al.*, 2018; Radakovic *et al.*, 2018). Furthermore, microarray data analysis indicated that *HIPP32* and *HIPP33* were up- or downregulated in response to various microorganisms (de Abreu-Neto *et al.*, 2013). Hence, the *HIPP*-dependent upregulation of *ELI3-2* in response to cytokinin might indicate that cluster-III *HIPP* genes are somehow involved in the cytokinin-mediated plant responses to biotic stresses (Cortleven *et al.*, 2019). This idea can be supported by the GO term analysis revealing that numerous *HIPP*-dependent cytokinin responsive genes were associated with GO categories related to plant responses to pathogens, jasmonic acid and salicylic acid (Figure 57 and 58). *ERF105* is rapidly induced by cytokinin (Brenner *et al.*, 2005) and encodes a AP2/ERF transcription factor required for freezing tolerance and cold acclimatization in *Arabidopsis* (Müller and Munné-Bosch, 2015; Bolt *et al.*, 2017). Furthermore, *erf105* mutants show impaired primary root elongation and LR formation (Illgen *et al.*, 2020). Detailed investigations are necessary to explore whether *ERF105* and *HIPP* genes operate in the same pathway and to understand the mechanisms underlying the *HIPP*-dependent upregulation of *ERF105* in response to cytokinin.

Summing up, the activity of cluster-III *HIPP* genes alters the global transcriptional response to cytokinin in *Arabidopsis*. Based on the findings presented, several *HIPP*-dependent cytokinin responsive genes belong to the most deregulated genes by cytokinin in wild type. Distinct genes associated with various GO categories might represent a functional link between HIPP proteins and cytokinin response regulation.

4.5 The role of HIPP proteins in heavy metal stress

Isoprenylated proteins capable to bind transition metal ions such as Cu^{2+}, Ni^{2+} and Zn^{2+} were first described by Dykema *et al.* (1999). Since then, several of the few HIPP proteins studied so far have been shown to be involved in heavy metal homeostasis. For instance, CdI19 (also annotated as HIPP6) has been reported to bind Cd^{2+}, Hg^{2+} and Cu^{2+} via the CXXC core motif of the HMA domain (Figure 1), while *CdI19* overexpression conferred Cd tolerance in transgenic *Arabidopsis* (Suzuki *et al.*, 2002). Similar binding properties have been identified for FP6 (also annotated as HIPP26), which interacts with the plasma membrane-localized protein ACYL-CoA-BINDING PROTEIN 2 to mediate the transport of heavy metal ions in *Arabidopsis* roots (Gao *et al.*, 2009). Further studies have reported that HIPP20, HIPP21 and HIPP22 play an important role in Cd-detoxification, as the *hipp20,21,22 Arabidopsis* triple mutant was more sensitive to Cd and accumulated less Cd than wild type; the probable mechanism involved being Cd sequestration (Tehseen *et al.*, 2010). Zschiesche *et al.* (2015) reported that the nuclear HIPP3 is capable of binding zinc ions via the central cysteines of the conserved HMA domains. To test whether the cluster-III HIPP proteins are involved in heavy metal-associated stress, the root response was assessed in *hipp* double mutants, grown under Cd, Zn and Fe excessive conditions, as well as under Fe deficient conditions (Figure 63). Root elongation assays revealed that *hipp32,33* was insensitive to the toxic concentration of Cd, Zn and Fe (Figure 63A). Formation of LRs was also less affected by excessive Cd and Zn in *hipp32,33* than in wild type and other two *hipp* double mutants (Figure 63B). It would be revealing to investigate whether *hipp32,33* accumulates reduced levels of heavy metals, *e.g.* by measuring Cd content in roots and shoots. However, the present findings suggest that HIPP32 and HIPP33 are involved in mediating heavy metal homeostasis in roots, in line with the fact that several GO terms in ‘heme’ and ‘iron ion binding’ were overrepresented in *hipp* mutants in RNA-Seq analysis (Figure 38 to 41; see section 4.3). However, the increased tolerance in *hipp32,33* – in contrast to other *hipp* mutants – suggests that heavy metal sequestration by binding through the HMA domain might not be the universal mechanism among HIPP proteins. *HIPP32* and *HIPP33* have been identified in a microarray analysis to be downregulated in the roots and shoots of plants treated with Cd; and also downregulated in leaves under Fe deficiency conditions (de Abreu-Neto *et al.*, 2013). Intriguingly, both wild type and *hipp32,33* performed better on growth media without Fe (Figure 63), although Fe

deficiency is known to inhibit primary growth (Bouain *et al.*, 2019). How exactly HIPP might function in heavy metal homeostasis is currently unknown. HIPP proteins appear to be involved in the regulation of PD function in the root, as Fe treatment did not affect the plasmodesmal trafficking in the *hipp* double mutants (Figure 64; see section 4.1.3). The scenario that HIPP proteins interact with other proteins, *e.g.* at plasma membrane or PD, and are involved in their function is highly likely (section 4.1.2). HIPP27 has been for instance reported to interact with the UBIQUITIN-SPECIFIC PROTEASE16 and their interaction might modulate Cd tolerance in *Arabidopsis* (Zhao *et al.*, 2013). The main hypothesis for the mechanism of Cd homeostasis is that HIPPs protect the plant from Cd toxicity by partitioning Cd into vacuoles or trapping free Cd^{2+} in the cytosol (Tehseen *et al.*, 2010; Clemens and Ma, 2016). However, HIPP32 and HIPP33 appear to negatively influence these processes, supporting the idea that heavy metal sequestration by HIPP proteins might not be the universal response. Their role could be linked to the action of other factors, known to modulate heavy metal accumulation and tolerance, including TFs and certain hormones (Wu *et al.*, 2012; Zhang *et al.*, 2015; Hindt and Guerinot, 2012). For instance, it has been shown that Cd-induced ABA upregulates the expression of *ABSCISIC ACID-INSENSITIVE 5* (*ABI5*), encoding a basic region/Leu zipper TF able to interact with the Cd-induced R2R3-MYB TF MYB49. ABI5 interaction with MYB49 prevents MYB49 binding to the promoters of downstream genes, resulting in their downregulation and thereby reducing Cd uptake and accumulation (Zhang *et al.*, 2019). *HIPP22* and *HIPP44* have been identified among the target genes of MYB49 (Zhang *et al.*, 2019). Cluster-III *HIPP* genes might also be part of a similar and complex regulation, which might also include cytokinin activity, as the GO term ‘iron ion homeostasis’ was enriched in the GO analysis performed based on the *HIPP*-dependent cytokinin-responsive genes (section 3.7.5).

4.6 Future perspectives

In this work, the biological function of three plant-specific HIPP proteins constituting one distinct phylogenetic cluster was investigated. Subcellular localization studies of GFP-HIPP fusion proteins revealed that these proteins associate with PD. However, it is still unclear to which structural subdomains of PD HIPP proteins localize. Further experiments involving immunoelectron or super resolution microscopy should be performed to address this aspect. How HIPP proteins are targeted to PD is also an open question. Confocal microscopy and the protein analysis performed in this study indicated that prenylation is required for HIPP34 association with PD. However, this result was not supported by similar analysis performed in Dr. Werner’s group using transgenic *Arabidopsis* lines expressing *HIPP34* under the control of its native promoter. An additional lipidation of HIPP34 by S-acylation occurring in *Arabidopsis*, but not in *N. benthamiana*, which might account for HIPP34 PD-association despite the missing

prenylation, has been discussed. Mutagenesis studies of predicted amino acid residues which might serve as S-acylation sites in HIPP34 should be performed to explore this hypothesis.

CFDA and GFP translocation assays performed in this work revealed that the cell-to-cell trafficking was enhanced in distinct *hipp* mutants. Further research should investigate the mechanisms possibly causing the enhanced symplasmic trafficking, such as PD abundance, structure, and morphology. The possibility that HIPP proteins participate in the PD-mediated intercellular signaling hub could also be explored.

The pleiotropic defects in *hipp32,33,34* plants indicated that the respective genes are involved in the regulation of different aspects of plant growth. Particularly interesting were the defects in pattern formation and maintenance of the RAM observed in *hipp32,33,34*. Further research should aim to investigate the molecular mechanisms underlying these developmental changes. For instance, experiments aiming to investigate the expression of cell-specific markers in *hipp* knockouts have been initiated and are currently being performed in Dr. Werner's group. The RNA-Seq analysis revealed different genetic pathways, which are connected to *HIPP* gene activity. The molecular basis of this regulatory crosstalk remains to be elucidated in future investigations.

Following the hypothesis that HIPP-CKX interaction might be physiologically relevant for the cytokinin activity, a series of experiments were conducted in this work to explore the possible link between HIPP proteins and cytokinin signaling in plants. qRT-PCR and RNA-Seq analysis showed that the cluster-III *HIPP* gene expression is not regulated by cytokinin. At the same time, the cytokinin content in *hipp* seedlings was only subtly changed. Nevertheless, analysis of the synthetic cytokinin reporter *TCSn:GFP* in the *hipp* mutant background revealed changes in cytokinin signaling output, suggesting that the loss of *HIPP* genes impacts the cytokinin activity. A possible link between the attenuated steady-state *TCSn:GFP* activity in *hipp* mutants and the increased plasmodesmal trafficking in the root has been discussed.

Several HIPP proteins have been reported to be involved in plant responses to biotic and abiotic stresses, including heavy metal-associated stress. Experiments performed in this work revealed that HIPP proteins are involved in mediating heavy metal homeostasis in roots. Their mechanism of action in this regard is still unclear, and it should be addressed in the future.

5. References

Abas, L., and Luschnig, C. (2010). Maximum yields of microsomal-type membranes from small amounts of plant material without requiring ultracentrifugation. *Anal Biochem*. **401**:217-227.

Abdel-Ghany, S. E., Muller-Moule, P., Niyogi, K. K., Pilon, M., and Shikanai, T. (2005). Two P-type ATPases are required for copper delivery in *Arabidopsis thaliana* chloroplasts. *Plant Cell*. **17**:1233-1251.

Abràmoff, M. D., Magalhães, P. J., and Ram, S. J. (2004). Image processing with *ImageJ*. *Biophotonics Int*. **11**:36-42.

Acheampong, A. K., Shanks, C., Chang, C.-Y., Schaller, G. E., Dagdas, Y., and Kieber, J. J. (2020). EXO70D isoforms mediate selective autophagic degradation of Type-A ARR proteins to regulate cytokinin sensitivity. *bioRxiv*. **938712**:2020.2002.2007.938712.

Aguilar-Martinez, J. A., Poza-Carrion, C., and Cubas, P. (2007). *Arabidopsis* BRANCHED1 acts as an integrator of branching signals within axillary buds. *Plant Cell*. **19**:458-472.

Aida, M., Beis, D., Heidstra, R., Willemsen, V., Blilou, I., Galinha, C., Nussaume, L., Noh, Y. S., Amasino, R., and Scheres, B. (2004). The *PLETHORA* genes mediate patterning of the *Arabidopsis* root stem cell niche. *Cell*. **119**:109-120.

Alonso, J. M., Stepanova, A. N., Leisse, T. J., Kim, C. J., Chen, H., Shinn, P., Stevenson, D. K., Zimmerman, J., Barajas, P., Cheuk, R., Gadrinab, C., Heller, C., Jeske, A., Koesema, E., Meyers, C. C., Parker, H., Prednis, L., Ansari, Y., Choy, N., Deen, H., Geralt, M., Hazari, N., Hom, E., Karnes, M., Mulholland, C., Ndubaku, R., Schmidt, I., Guzman, P., Aguilar-Henonin, L., Schmid, M., Weigel, D., Carter, D. E., Marchand, T., Risseeuw, E., Brogden, D., Zeko, A., Crosby, W. L., Berry, C. C., and Ecker, J. R. (2003). Genome-wide insertional mutagenesis of *Arabidopsis thaliana*. *Science*. **301**:653-657.

Amari, K., Boutant, E., Hofmann, C., Schmitt-Keichinger, C., Fernandez-Calvino, L., Didier, P., Lerich, A., Mutterer, J., Thomas, C. L., Heinlein, M., Mely, Y., Maule, A. J., and Ritzenthaler, C. (2010). A family of plasmodesmal proteins with receptor-like properties for plant viral movement proteins. *PLOS Pathog*. **6**:e1001119.

Amari, K., Lerich, A., Schmitt-Keichinger, C., Dolja, V. V., and Ritzenthaler, C. (2011). Tubule-guided cell-to-cell movement of a plant virus requires class XI myosin motors. *PLOS Pathog*. **7**:e1002327.

Anderson, C. T., Carroll, A., Akhmetova, L., and Somerville, C. (2010). Real-time imaging of cellulose reorientation during cell wall expansion in *Arabidopsis* roots. *Plant Physiol*. **152**:787-796.

Andres-Colas, N., Sancenon, V., Rodriguez-Navarro, S., Mayo, S., Thiele, D. J., Ecker, J. R., Puig, S., and Penarrubia, L. (2006). The *Arabidopsis* heavy metal P-type ATPase HMA5 interacts with metallochaperones and functions in copper detoxification of roots. *Plant J*. **45**:225-236.

Argueso, C. T., Ferreira, F. J., and Kieber, J. J. (2009). Environmental perception avenues: the interaction of cytokinin and environmental response pathways. *Plant Cell Environ*. **32**:1147-1160.

Argueso, C. T., Raines, T., and Kieber, J. J. (2010). Cytokinin signaling and transcriptional networks. *Curr Opin Plant Biol*. **13**:533-539.

Armstrong, D. J. (1994). Cytokinin oxidase and the regulation of cytokinin degradation. *Cytokinins: chemistry, activity and function DWS Mok MC Mok, eds (Boca Raton)*.

Arosio, P., Ingrassia, R., and Cavadini, P. (2009). Ferritins: a family of molecules for iron storage, antioxidation and more. *Biochim Biophys Acta*. **1790**:589-599.

Arvidsson, S., Kwasniewski, M., Riano-Pachon, D. M., and Mueller-Roeber, B. (2008). *QuantPrime*: a flexible tool for reliable high-throughput primer design for quantitative PCR. *BMC Bioinformatics*. **9**:465.

Bak, S., Beisson, F., Bishop, G., Hamberger, B., Höfer, R., Paquette, S., and Werck-Reichhart, D. (2011). Cytochromes P450. *The Arabidopsis Book*. **9**:e0144.

Balanzà, V., Martínez-Fernández, I., Sato, S., Yanofsky, M. F., and Ferrándiz, C. (2019). Inflorescence meristem fate is dependent on seed development and F*RUITFULL* in *Arabidopsis thaliana*. *Front Plant Sci*. **10**.

Bar, M., and Ori, N. (2014). Leaf development and morphogenesis. *Development*. **141**:4219-4230.

Barlow, P. W., Hawes, C. R., and Horne, J. C. (1984). Structure of amyloplasts and endoplasmic reticulum in the root caps of *Lepidium sativum* and *Zea mays* observed after selective membrane staining and by high-voltage electron microscopy. *Planta*. **160**:363-371.

Barnes, N., Tsivkovskii, R., Tsivkovskaia, N., and Lutsenko, S. (2005). The copper-transporting ATPases, menkes and wilson disease proteins, have distinct roles in adult and developing cerebellum. *J Biol Chem*. **280**:9640-9645.

Barnett, J. R. (1987). Changes in the distribution of plasmodesmata in developing fibre-tracheid pit membranes of *Sorbus aucuparia L. Ann Bot*. **59**.

Barth, O., Vogt, S., Uhlemann, R., Zschiesche, W., and Humbeck, K. (2009). Stress induced and nuclear localized HIPP26 from *Arabidopsis thaliana* interacts via its heavy metal associated domain with the drought stress related zinc finger transcription factor ATHB29. *Plant Mol Biol*. **69**:213-226.

Barton, D. A., Cole, L., Collings, D. A., Liu, D. Y., Smith, P. M., Day, D. A., and Overall, R. L. (2011). Cell-to-cell transport via the lumen of the endoplasmic reticulum. *Plant J*. **66**:806-817.

Barton, M. K. (2010). Twenty years on: the inner workings of the shoot apical meristem, a developmental dynamo. *Dev Biol*. **341**:95-113.

Barton, M. K., and Poethig, R. S. (1993). Formation of the shoot apical meristem in Arabidopsis thaliana: an analysis of development in the wild type and in the shoot meristemless mutant. *Development*. **119**:823-831.

Bartrina, I., Jensen, H., Novak, O., Strnad, M., Werner, T., and Schmülling, T. (2017). Gain-of-function mutants of the cytokinin receptors *AHK2* and *AHK3* regulate plant organ size, flowering time and plant longevity. *Plant Physiol*. **173**:1783-1797.

Bartrina, I., Otto, E., Strnad, M., Werner, T., and Schmülling, T. (2011). Cytokinin regulates the activity of reproductive meristems, flower organ size, ovule formation, and thus seed yield in *Arabidopsis thaliana*. *Plant Cell*. **23**:69-80.

Bashir, K., Rasheed, S., Kobayashi, T., Seki, M., and Nishizawa, N. K. (2016). Regulating subcellular metal homeostasis: the key to crop improvement. *Front Plant Sci*. **7**:1192.

Bashir, K., Takahashi, R., Akhtar, S., Ishimaru, Y., Nakanishi, H., and Nishizawa, N. K. (2013). The knockdown of *OsVIT2* and *MIT* affects iron localization in rice seed. *Rice*. **6**:31.

Bassel, G. W., Stamm, P., Mosca, G., Barbier de Reuille, P., Gibbs, D. J., Winter, R., Janka, A., Holdsworth, M. J., and Smith, R. S. (2014). Mechanical constraints imposed by 3D cellular geometry and arrangement modulate growth patterns in the *Arabidopsis* embryo. *PNAS*. **111**:8685-8690.

Becher, M., Talke, I. N., Krall, L., and Krämer, U. (2004). Cross-species microarray transcript profiling reveals high constitutive expression of metal homeostasis genes in shoots of the zinc hyperaccumulator *Arabidopsis halleri*. *Plant J*. **37**:251-268.

Belhaj, K., Chaparro-Garcia, A., Kamoun, S., Patron, N. J., and Nekrasov, V. (2015). Editing plant genomes with CRISPR/Cas9. *Curr Opin Biotechnol*. **32**:76-84.

Bencivenga, S., Simonini, S., Benkova, E., and Colombo, L. (2012). The transcription factors BEL1 and SPL are required for cytokinin and auxin signaling during ovule development in *Arabidopsis*. *Plant Cell*. **24**:2886-2897.

Benitez-Alfonso, Y. (2014). Symplastic intercellular transport from a developmental perspective. *J Exp Bot*. **65**:1857-1863.

Benitez-Alfonso, Y., Cilia, M., Roman, A. S., Thomas, C., Maule, A., Hearn, S., and Jackson, D. (2009). Control of *Arabidopsis* meristem development by thioredoxin-dependent regulation of intercellular transport. *PNAS*. **106**:3615-3620.

Benitez-Alfonso, Y., Faulkner, C., Pendle, A., Miyashima, S., Helariutta, Y., and Maule, A. (2013). Symplastic intercellular connectivity regulates lateral root patterning. *Dev Cell*. **26**:136-147.

Benitez-Alfonso, Y., and Jackson, D. (2009). Redox homeostasis regulates plasmodesmal communication in *Arabidopsis* meristems. *Plant Signal Behav*. **4**:655-659.

Benjamini, Y., and Hochberg, Y. (1995). Controlling the false discovery rate: a practical and powerful approach to multiple testing. *Journal of the Royal Statistical Society Series B (Methodological)*. **57**:289-300.

Benlloch, R., Berbel, A., Serrano-Mislata, A., and Madueno, F. (2007). Floral initiation and inflorescence architecture: a comparative view. *Ann Bot*. **100**:659-676.

Berckmans, B., Kirschner, G., Gerlitz, N., Stadler, R., and Simon, R. (2020). CLE40 signaling regulates root stem cell fate. *Plant Physiol*. **182**:1776-1792.

Berger, F., and Twell, D. (2011). Germline specification and function in plants. *Annu Rev Plant Biol*. **62**:461-484.

Bernard, P., and Couturier, M. (1992). Cell killing by the F plasmid CcdB protein involves poisoning of DNA-topoisomerase II complexes. *J Mol Biol*. **226**:735-745.

Berndt, N., Hamilton, A. D., and Sebti, S. M. (2011). Targeting protein prenylation for cancer therapy. *Nat Rev Cancer*. **11**:775-791.

Bertani, G. (1951). Studies on lysogenesis. I. The mode of phage liberation by lysogenic *Escherichia coli*. *J Bacteriol*. **62**:293-300.

Besnard, F., Rozier, F., and Vernoux, T. (2014). The AHP6 cytokinin signaling inhibitor mediates an auxin-cytokinin crosstalk that regulates the timing of organ initiation at the shoot apical meristem. *Plant Signal Behav*. **9**:6.

Bhargava, A., Clabaugh, I., To, J. P., Maxwell, B. B., Chiang, Y. H., Schaller, G. E., Loraine, A., and Kieber, J. J. (2013). Identification of cytokinin-responsive genes using microarray meta-analysis and RNA-Seq in *Arabidopsis*. *Plant Physiol*. **162**:272-294.

Bielach, A., Podlesakova, K., Marhavy, P., Duclercq, J., Cuesta, C., Muller, B., Grunewald, W., Tarkowski, P., and Benkova, E. (2012). Spatiotemporal regulation of lateral root organogenesis in *Arabidopsis* by cytokinin. *Plant Cell*. **24**:3967-3381.

Bilsborough, G. D., Runions, A., Barkoulas, M., Jenkins, H. W., Hasson, A., Galinha, C., Laufs, P., Hay, A., Prusinkiewicz, P., and Tsiantis, M. (2011). Model for the regulation of *Arabidopsis thaliana* leaf margin development. *PNAS*. **108**:3424-3429.

Bilska, A., and Sowinski, P. (2010). Closure of plasmodesmata in maize (*Zea mays*) at low temperature: a new mechanism for inhibition of photosynthesis. *Ann Bot*. **106**:675-686.

Bishopp, A., Help, H., El-Showk, S., Weijers, D., Scheres, B., Friml, J., Benkova, E., Mahonen, A. P., and Helariutta, Y. (2011a). A mutually inhibitory interaction between auxin and cytokinin specifies vascular pattern in roots. *Curr Biol*. **21**:917-926.

Bishopp, A., Lehesranta, S., Vaten, A., Help, H., El-Showk, S., Scheres, B., Helariutta, K., Mahonen, A. P., Sakakibara, H., and Helariutta, Y. (2011b). Phloem-transported cytokinin regulates polar auxin transport and maintains vascular pattern in the root meristem. *Curr Biol*. **21**:927-932.

Blilou, I., Xu, J., Wildwater, M., Willemsen, V., Paponov, I., Friml, J., Heidstra, R., Aida, M., Palme, K., and Scheres, B. (2005). The PIN auxin efflux facilitator network controls growth and patterning in *Arabidopsis* roots. *Nature*. **433**:39-44.

Bolt, S., Zuther, E., Zintl, S., Hincha, D. K., and Schmülling, T. (2017). *ERF105* is a transcription factor gene of *Arabidopsis thaliana* required for freezing tolerance and cold acclimation. *Plant Cell Environ*. **40**:108-120.

Bouain, N., Krouk, G., Lacombe, B., and Rouached, H. (2019). Getting to the root of plant mineral nutrition: combinatorial nutrient stresses reveal emergent properties. *Trends Plant Sci*. **24**:542-552.

Bouché, F., Lobet, G., Tocquin, P., and Périlleux, C. (2016). FLOR-ID: an interactive database of flowering-time gene networks in *Arabidopsis thaliana*. *Nucleic Acids Res*. **44**:D1167-1171.

Bouyer, D., Geier, F., Kragler, F., Schnittger, A., Pesch, M., Wester, K., Balkunde, R., Timmer, J., Fleck, C., and Hülskamp, M. (2008). Two-dimensional patterning by a trapping/depletion mechanism: the role of TTG1 and GL3 in *Arabidopsis* trichome formation. *PLOS Biol*. **6**:e141.

Bowman, J. L., Smyth, D. R., and Meyerowitz, E. M. (2012). The ABC model of flower development: then and now. *Development*. **139**:4095-4098.

Bracha-Drori, K., Shichrur, K., Lubetzky, T. C., and Yalovsky, S. (2008). Functional analysis of *Arabidopsis* postprenylation CaaX processing enzymes and their function in subcellular protein targeting. *Plant Physiol*. **148**:119-131.

Bracha, K., Lavy, M., and Yalovsky, S. (2002). The *Arabidopsis* AtSTE24 is a CAAX protease with broad substrate specificity. *J Biol Chem*. **277**:29856-29864.

Brenner, W. G., Ramireddy, E., Heyl, A., and Schmülling, T. (2012). Gene regulation by cytokinin in *Arabidopsis*. *Front Plant Sci*. **3**:8.

Brenner, W. G., Romanov, G. A., Köllmer, I., Burkle, L., and Schmülling, T. (2005). Immediate-early and delayed cytokinin response genes of *Arabidopsis thaliana* identified by genome-wide expression profiling reveal novel cytokinin-sensitive processes and suggest cytokinin action through transcriptional cascades. *Plant J*. **44**:314-333.

Brenner, W. G., and Schmülling, T. (2015). Summarizing and exploring data of a decade of cytokinin-related transcriptomics. *Front Plant Sci*. **6**:29.

Brunetti, P., Zanella, L., Proia, A., De Paolis, A., Falasca, G., Altamura, M. M., Sanita di Toppi, L., Costantino, P., and Cardarelli, M. (2011). Cadmium tolerance and phytochelatin content of *Arabidopsis* seedlings over-expressing the phytochelatin synthase gene *AtPCS1*. *J Exp Bot*. **62**:5509-5519.

Brunkard, J. O., Runkel, A. M., and Zambryski, P. C. (2013). Plasmodesmata dynamics are coordinated by intracellular signaling pathways. *Curr Opin Plant Biol*. **16**:614-620.

Brunkard, J. O., and Zambryski, P. C. (2017). Plasmodesmata enable multicellularity: new insights into their evolution, biogenesis, and functions in development and immunity. *Curr Opin Plant Biol*. **35**:76-83.

Brunkard, J. O., and Zambryski, P. C. (2019). Plant cell-cell transport via plasmodesmata is regulated by light and the circadian clock. *Plant Physiol*. **181**:1459-1467.

Bruno, L., Pacenza, M., Forgione, I., Lamerton, L. R., Greco, M., Chiappetta, A., and Bitonti, M. B. (2017). In *Arabidopsis thaliana* cadmium impact on the growth of primary root by altering *SCR* expression and auxin-cytokinin cross-talk. *Front Plant Sci*. **8**:1323.

Burch-Smith, T. M., Brunkard, J. O., Choi, Y. G., and Zambryski, P. C. (2011). Organelle–nucleus cross-talk regulates plant intercellular communication via plasmodesmata. *PNAS*. **108**:1451-1460.

Caesar, K., Thamm, A. M., Witthoft, J., Elgass, K., Huppenberger, P., Grefen, C., Horak, J., and Harter, K. (2011). Evidence for the localization of the *Arabidopsis* cytokinin receptors AHK3 and AHK4 in the endoplasmic reticulum. *J Exp Bot*. **62**:5571-5580.

Caillaud, M. C., Wirthmueller, L., Sklenar, J., Findlay, K., Piquerez, S. J., Jones, A. M., Robatzek, S., Jones, J. D., and Faulkner, C. (2014). The plasmodesmal protein PDLP1 localises to haustoria-associated membranes during downy mildew infection and regulates callose deposition. *PLOS Pathog*. **10**:e1004496.

Cailliatte, R., Schikora, A., Briat, J. F., Mari, S., and Curie, C. (2010). High-affinity manganese uptake by the metal transporter NRAMP1 is essential for *Arabidopsis* growth in low manganese conditions. *Plant Cell*. **22**:904-917.

Capron, A., Chatfield, S., Provart, N., and Berleth, T. (2009). Embryogenesis: pattern formation from a single cell. *The Arabidopsis Book*. **7**:e0126.

Cary, A. J., Liu, W., and Howell, S. H. (1995). Cytokinin action is coupled to ethylene in its effects on the inhibition of root and hypocotyl elongation in *Arabidopsis thaliana* seedlings. *Plant Physiol*. **107**:1075-1082.

Casimiro, I., Beeckman, T., Graham, N., Bhalerao, R., Zhang, H., Casero, P., Sandberg, G., and Bennett, M. J. (2003). Dissecting *Arabidopsis* lateral root development. *Trends Plant Sci*. **8**:165-171.

Chaudhury, A. M., Letham, S., Craig, S., and Dennis, E. S. (1993). *amp1* - a mutant with high cytokinin levels and altered embryonic pattern, faster vegetative growth, constitutive photomorphogenesis and precocious flowering. *Plant J*. **4**:907-916.

Chen, L. Q., Qu, X. Q., Hou, B. H., Sosso, D., Osorio, S., Fernie, A. R., and Frommer, W. B. (2012). Sucrose efflux mediated by SWEET proteins as a key step for phloem transport. *Science*. **335**:207-211.

Chen, X. Y., Liu, L., Lee, E., Han, X., Rim, Y., Chu, H., Kim, S. W., Sack, F., and Kim, J. Y. (2009). The *Arabidopsis* callose synthase gene *GSL8* is required for cytokinesis and cell patterning. *Plant Physiol*. **150**:105-113.

Cheng, C. Y., Mathews, D. E., Schaller, G. E., and Kieber, J. J. (2013). Cytokinin-dependent specification of the functional megaspore in the *Arabidopsis* female gametophyte. *Plant J*. **73**:929-940.

Chiang, Y. H., Zubo, Y. O., Tapken, W., Kim, H. J., Lavanway, A. M., Howard, L., Pilon, M., Kieber, J. J., and Schaller, G. E. (2012). Functional characterization of the GATA transcription factors GNC and CGA1 reveals their key role in chloroplast development, growth, and division in *Arabidopsis*. *Plant Physiol*. **160**:332-348.

Choi, J., Huh, S. U., Kojima, M., Sakakibara, H., Paek, K. H., and Hwang, I. (2010). The cytokinin-activated transcription factor ARR2 promotes plant immunity via TGA3/NPR1-dependent salicylic acid signaling in *Arabidopsis*. *Dev Cell*. **19**:284-295.

Chomczynski, P., and Sacchi, N. (1987). Single-step method of RNA isolation by acid guanidinium thiocyanate-phenol-chloroform extraction. *Anal Biochem*. **162**:156-159.

Chou, W.-C., Yin, Y., and Xu, Y. (2010). GolgiP: prediction of Golgi-resident proteins in plants. *Bioinformatics*. **26**:2464-2465.

Choy, E., Chiu, V. K., Silletti, J., Feoktistov, M., Morimoto, T., Michaelson, D., Ivanov, I. E., and Philips, M. R. (1999). Endomembrane trafficking of ras: the CAAX motif targets proteins to the ER and Golgi. *Cell*. **98**:69-80.

Clemens, S. (2001). Molecular mechanisms of plant metal tolerance and homeostasis. *Planta*. **212**:475-486.

Clemens, S., and Ma, J. F. (2016). Toxic heavy metal and metalloid accumulation in crop plants and foods. *Annu Rev Plant Biol*. **67**:489-512.

Clemens, S., Palmgren, M. G., and Krämer, U. (2002). A long way ahead: understanding and engineering plant metal accumulation. *Trends Plant Sci*. **7**:309-315.

Clough, S. J., and Bent, A. F. (1998). Floral dip: a simplified method for *Agrobacterium*-mediated transformation of *Arabidopsis thaliana*. *Plant J*. **16**:735-743.

Corbesier, L., Vincent, C., Jang, S., Fornara, F., Fan, Q., Searle, I., Giakountis, A., Farrona, S., Gissot, L., Turnbull, C., and Coupland, G. (2007). FT protein movement contributes to long-distance signaling in floral induction of *Arabidopsis*. *Science*. **316**:1030-1033.

Cortleven, A., Leuendorf, J. E., Frank, M., Pezzetta, D., Bolt, S., and Schmülling, T. (2019). Cytokinin action in response to abiotic and biotic stresses in plants. *Plant Cell Environ*. **42**:998-1018.

Cosgrove, D. J. (2005). Growth of the plant cell wall. *Nat Rev Mol Cell Biol*. **6**:850-861.

Cowan, G. H., Roberts, A. G., Jones, S., Kumar, P., Kalyandurg, P. B., Gil, J. F., Savenkov, E. I., Hemsley, P. A., and Torrance, L. (2018). Potato mop-top virus co-opts the stress sensor HIPP26 for long-distance movement. *Plant Physiol*. **176**:2052-2070.

Crawford, K. M., and Zambryski, P. C. (2001). Non-targeted and targeted protein movement through plasmodesmata in leaves in different developmental and physiological states. *Plant Physiol*. **125**:1802-1812.

Crowell, D. N. (2000). Functional implications of protein isoprenylation in plants. *Prog Lipid Res*. **39**:393-408.

Crowell, D. N., and Huizinga, D. H. (2009). Protein isoprenylation: the fat of the matter. *Trends Plant Sci*. **14**:163-170.

Cucinotta, M., Manrique, S., Cuesta, C., Benkova, E., Novak, O., and Colombo, L. (2018). *CUP-SHAPED COTYLEDON1 (CUC1)* and *CUC2* regulate cytokinin homeostasis to determine ovule number in Arabidopsis. *J Exp Bot*. **69**:5169-5176.

Cui, W., and Lee, J. Y. (2016). *Arabidopsis* callose synthases CalS1/8 regulate plasmodesmal permeability during stress. *Nat Plants*. **2**:16034.

Curie, C., and Briat, J. F. (2003). Iron transport and signaling in plants. *Annu Rev Plant Biol*. **54**:183-206.

D'Agostino, I. B., Deruère, J., and Kieber, J. J. (2000). Characterization of the response of the *ARABIDOPSIS RESPONSE REGULATOR* gene family to cytokinin. *Plant Physiol*. **124**:1706-1717.

D'Aloia, M., Bonhomme, D., Bouché, F., Tamseddak, K., Ormenese, S., Torti, S., Coupland, G., and Périlleux, C. (2011). Cytokinin promotes flowering of *Arabidopsis* via transcriptional activation of the *FT* paralogue *TSF*. *Plant J*. **65**:972-979.

Dahiya, P., and Brewin, N. (2000). Immunogold localization of callose and other cell wall components in pea nodule transfer cells. *Protoplasma*. **214**:210-218.

DalCorso, G., Manara, A., and Furini, A. (2013). An overview of heavy metal challenge in plants: from roots to shoots. *Metallomics*. **5**:1117-1132.

Dance, A. (2015). Core Concept: CRISPR gene editing. *PNAS*. **112**:6245-6246.

Daum, G., Medzihradszky, A., Suzaki, T., and Lohmann, J. U. (2014). A mechanistic framework for noncell autonomous stem cell induction in *Arabidopsis*. *PNAS*. **111**:14619-14624.

Daviere, J. M., and Achard, P. (2017). Organ communication: cytokinins on the move. *Nat Plants*. **3**:17116.

Davis, A. M., Hall, A., Millar, A. J., Darrah, C., and Davis, S. J. (2009). Protocol: Streamlined sub-protocols for floral-dip transformation and selection of transformants in *Arabidopsis thaliana*. *Plant Methods*. **5**:3.

de Abreu-Neto, J. B., Turchetto-Zolet, A. C., de Oliveira, L. F., Zanettini, M. H., and Margis-Pinheiro, M. (2013). Heavy metal-associated isoprenylated plant protein (HIPP): characterization of a family of proteins exclusive to plants. *FEBS J*. **280**:1604-1616.

De Storme, N., and Geelen, D. (2014). Callose homeostasis at plasmodesmata: molecular regulators and developmental relevance. *Front Plant Sci*. **5**:138.

Degtyarenko, K. (2000). Bioinorganic motifs: towards functional classification of metalloproteins. *Bioinformatics*. **16**:851-864.

Del Bianco, M., Giustini, L., and Sabatini, S. (2013). Spatiotemporal changes in the role of cytokinin during root development. *New Phytol*. **199**:324-338.

Dello Ioio, R., Linhares, F. S., Scacchi, E., Casamitjana-Martinez, E., Heidstra, R., Costantino, P., and Sabatini, S. (2007). Cytokinins determine *Arabidopsis* root-meristem size by controlling cell differentiation. *Curr Biol*. **17**:678-682.

Dello Ioio, R., Nakamura, K., Moubayidin, L., Perilli, S., Taniguchi, M., Morita, M. T., Aoyama, T., Costantino, P., and Sabatini, S. (2008). A genetic framework for the control of cell division and differentiation in the root meristem. *Science*. **322**:1380-1384.

Deng, Y., Dong, H., Mu, J., Ren, B., Zheng, B., Ji, Z., Yang, W. C., Liang, Y., and Zuo, J. (2010). *Arabidopsis* histidine kinase CKI1 acts upstream of histidine phosphotransfer proteins to regulate female gametophyte development and vegetative growth. *Plant Cell*. **22**:1232-1248.

Di Mambro, R., De Ruvo, M., Pacifici, E., Salvi, E., Sozzani, R., Benfey, P. N., Busch, W., Novak, O., Ljung, K., and Di Paola, L. (2017). Auxin minimum triggers the developmental switch from cell division to cell differentiation in the *Arabidopsis* root. *PNAS*. **114**:7641-7649.

Di Mambro, R., and Sabatini, S. (2018). Developmental analysis of *Arabidopsis* root meristem. *Methods Mol Biol*. **1761**:33-45.

Di Mambro, R., Svolacchia, N., Dello Ioio, R., Pierdonati, E., Salvi, E., Pedrazzini, E., Vitale, A., Perilli, S., Sozzani, R., Benfey, P. N., Busch, W., Costantino, P., and Sabatini, S. (2019). The lateral root cap acts as an auxin sink that controls meristem size. *Curr Biol*. **29**:1199-1205

Di Marzo, M., Herrera-Ubaldo, H., Caporali, E., Novak, O., Strnad, M., Balanza, V., Ezquer, I., Mendes, M. A., de Folter, S., and Colombo, L. (2020). SEEDSTICK controls *Arabidopsis* fruit size by regulating cytokinin levels and *FRUITFULL*. *Cell Rep*. **30**:2846-2857.

Dinneny, J. R., Long, T. A., Wang, J. Y., Jung, J. W., Mace, D., Pointer, S., Barron, C., Brady, S. M., Schiefelbein, J., and Benfey, P. N. (2008). Cell identity mediates the response of *Arabidopsis* roots to abiotic stress. *Science*. **320**:942-945.

Dolan, L., Janmaat, K., Willemsen, V., Linstead, P., Poethig, S., Roberts, K., and Scheres, B. (1993). Cellular organisation of the *Arabidopsis thaliana* root. *Development*. **119**:71-84.

Dresselhaus, T. (2006). Cell-cell communication during double fertilization. *Curr Opin Plant Biol*. **9**:41-47.

Dutta, S., Mitra, M., Agarwal, P., Mahapatra, K., De, S., Sett, U., and Roy, S. (2018). Oxidative and genotoxic damages in plants in response to heavy metal stress and maintenance of genome stability. *Plant Signal Behav*. **13**:e1460048.

Dykema, P. E., Sipes, P. R., Marie, A., Biermann, B. J., Crowell, D. N., and Randall, S. K. (1999). A new class of proteins capable of binding transition metals. *Plant Mol Biol*. **41**:139-150.

Eckardt, N. A. (2009). A high-resolution map of auxin distribution in the *Arabidopsis* root apex. *Plant Cell*. **21**:1621.

Ehlers, K., and Kollmann, R. (2001). Primary and secondary plasmodesmata: structure, origin, and functioning. *Protoplasma*. **216**:1-30.

El-Gebali, S., Mistry, J., Bateman, A., Eddy, S. R., Luciani, A., Potter, S. C., Qureshi, M., Richardson, L. J., Salazar, G. A., Smart, A., Sonnhammer, E. L L., Hirsh, L., Paladin, L., Piovesan, D., Tosatto, S. C E., and Finn, R. D. (2018). The Pfam protein families database in 2019. *Nucleic Acids Res*. **47**:D427-D432.

El-Showk, S., Ruonala, R., and Helariutta, Y. (2013). Crossing paths: cytokinin signaling and crosstalk. *Development*. **140**:1373-1383.

Epel, B. L. (2009). Plant viruses spread by diffusion on ER-associated movement-protein-rafts through plasmodesmata gated by viral induced host beta-1,3-glucanases. *Semin Cell Dev Biol*. **20**:1074-1081.

Erdmann, R. M., Hoffmann, A., Walter, H.-K., Wagenknecht, H.-A., Groß-Hardt, R., and Gehring, M. (2017). Molecular movement in the *Arabidopsis thaliana* female gametophyte. *Plant Reproduction*. **30**:141-146.

Faulkner, C., Akman, O. E., Bell, K., Jeffree, C., and Oparka, K. (2008). Peeking into pit fields: a multiple twinning model of secondary plasmodesmata formation in *tobacco*. *Plant Cell*. **20**:1504-1518.

Faulkner, C., Petutschnig, E., Benitez-Alfonso, Y., Beck, M., Robatzek, S., Lipka, V., and Maule, A. J. (2013). LYM2-dependent chitin perception limits molecular flux via plasmodesmata. *PNAS*. **110**:9166-9170.

Feng, Z., Mao, Y., Xu, N., Zhang, B., Wei, P., Yang, D. L., Wang, Z., Zhang, Z., Zheng, R., Yang, L., Zeng, L., Liu, X., and Zhu, J. K. (2014). Multigeneration analysis reveals the inheritance, specificity, and patterns of CRISPR/Cas-induced gene modifications in *Arabidopsis*. *PNAS*. **111**:4632-4637.

Fernandez-Calvino, L., Faulkner, C., Walshaw, J., Saalbach, G., Bayer, E., Benitez-Alfonso, Y., and Maule, A. (2011). *Arabidopsis* plasmodesmal proteome. *PLOS One*. **6**:e18880.

Ferrandiz, C., Pelaz, S., and Yanofsky, M. F. (1999). Control of carpel and fruit development in *Arabidopsis*. *Annu Rev Biochem*. **68**:321-354.

Fitzgibbon, J., Bell, K., King, E., and Oparka, K. (2010). Super-resolution imaging of plasmodesmata using three-dimensional structured illumination microscopy. *Plant Physiol*. **153**:1453-1463.

Fletcher, J. C., Brand, U., Running, M. P., Simon, R., and Meyerowitz, E. M. (1999). Signaling of cell fate decisions by CLAVATA3 in *Arabidopsis* shoot meristems. *Science*. **283**:1911-1914.

Forzani, C., Aichinger, E., Sornay, E., Willemsen, V., Laux, T., Dewitte, W., and Murray, J. A. (2014). WOX5 suppresses *CYCLIN D* activity to establish quiescence at the center of the root stem cell niche. *Curr Biol*. **24**:1939-1944.

Frank, J., Kaulfurst-Soboll, H., Rips, S., Koiwa, H., and von Schaewen, A. (2008). Comparative analyses of *Arabidopsis complex glycan 1* mutants and genetic interaction with staurosporin and temperature sensitive. *Plant Physiol*. **148**:1354-1367.

Frébort, I., Kowalska, M., Hluska, T., Frebortova, J., and Galuszka, P. (2011). Evolution of cytokinin biosynthesis and degradation. *J Exp Bot*. **62**:2431-2452.

Friml, J., Vieten, A., Sauer, M., Weijers, D., Schwarz, H., Hamann, T., Offringa, R., and Jürgens, G. (2003). Efflux-dependent auxin gradients establish the apical-basal axis of *Arabidopsis*. *Nature*. **426**:147-153.

Gaillochet, C., and Lohmann, J. U. (2015). The never-ending story: from pluripotency to plant developmental plasticity. *Development*. **142**:2237-2249.

Galichet, A., and Gruissem, W. (2003). Protein farnesylation in plants - conserved mechanisms but different targets. *Curr Opin Plant Biol*. **6**:530-535.

Galichet, A., Hoyerova, K., Kaminek, M., and Gruissem, W. (2008). Farnesylation directs AtIPT3 subcellular localization and modulates cytokinin biosynthesis in *Arabidopsis*. *Plant Physiol*. **146**:1155-1164.

Galinha, C., Hofhuis, H., Luijten, M., Willemsen, V., Blilou, I., Heidstra, R., and Scheres, B. (2007). PLETHORA proteins as dose-dependent master regulators of *Arabidopsis* root development. *Nature*. **449**:1053-1057.

Galuszka, P., Popelková, H., Werner, T., Frébortová, J., Pospíšilová, H., Mik, V., Köllmer, I., Schmülling, T., and Frébort, I. (2007). Biochemical characterization of cytokinin oxidases/dehydrogenases from *Arabidopsis thaliana* expressed in *Nicotiana tabacum L*. *Plant Growth Regul*. **26**:255-267.

Gao, W., Xiao, S., Li, H. Y., Tsao, S. W., and Chye, M. L. (2009). *Arabidopsis thaliana* acyl-CoA-binding protein ACBP2 interacts with heavy-metal-binding farnesylated protein AtFP6. *New Phytol*. **181**:89-102.

Geisler, M., Wang, B., and Zhu, J. (2014). Auxin transport during root gravitropism: transporters and techniques. *Plant Biol*. **16**:50-57.

Gerdes, H. H., and Carvalho, R. N. (2008). Intercellular transfer mediated by tunneling nanotubes. *Curr Opin Cell Biol*. **20**:470-475.

Ghori, N. H., Ghori, T., Hayat, M. Q., Imadi, S. R., Gul, A., Altay, V., and Ozturk, M. (2019). Heavy metal stress and responses in plants. *Int J Environ Sci Te*. **16**:1807-1828.

Giakountis, A., and Coupland, G. (2008). Phloem transport of flowering signals. *Curr Opin Plant Biol*. **11**:687-694.

Gookin, T. E., and Assmann, S. M. (2014). Significant reduction of BiFC non-specific assembly facilitates in planta assessment of heterotrimeric G-protein interactors. *Plant J*. **80**:553-567.

Grant, S. G., Jessee, J., Bloom, F. R., and Hanahan, D. (1990). Differential plasmid rescue from transgenic mouse DNAs into *Escherichia coli* methylation-restriction mutants. *PNAS*. **87**:4645-4649.

Greb, T., and Lohmann, J. U. (2016). Plant stem cells. *Curr Biol*. **26**:816-821.

Grison, M. S., Brocard, L., Fouillen, L., Nicolas, W., Wewer, V., Dormann, P., Nacir, H., Benitez-Alfonso, Y., Claverol, S., Germain, V., Boutte, Y., Mongrand, S., and Bayer, E. M. (2015). Specific membrane lipid composition is important for plasmodesmata function in *Arabidopsis*. *Plant Cell*. **27**:1228-1250.

Guo, T. (2019). Functional characterization of clade-I HIPP proteins from *Arabidopsis thaliana* interacting with cytokinin-catabolizing CKX enzymes. *Doctoral thesis*.

Guseman, J. M., Lee, J. S., Bogenschutz, N. L., Peterson, K. M., Virata, R. E., Xie, B., Kanaoka, M. M., Hong, Z., and Torii, K. U. (2010). Dysregulation of cell-to-cell connectivity and stomatal patterning by loss-of-function mutation in *Arabidopsis CHORUS (GLUCAN SYNTHASE-LIKE 8)*. *Development*. **137**:1731-1741.

Gzyl, J., Chmielowska-Bak, J., Przymusinski, R., and Gwozdz, E. A. (2015). Cadmium affects microtubule organization and post-translational modifications of tubulin in seedlings of soybean (*Glycine max L*.). *Front Plant Sci*. **6**:937.

Ha, C. M., Jun, J. H., and Fletcher, J. C. (2010). Shoot apical meristem form and function. *Curr Top Dev Biol*. **91**:103-140.

Hagen, G., and Guilfoyle, T. (2002). Auxin-responsive gene expression: genes, promoters and regulatory factors. *Plant Mol Biol*. **49**:373-385.

Hala, M., and Zarsky, V. (2019). Protein prenylation in plant stress responses. *Molecules*. **24**.

Hall, J. L. (2002). Cellular mechanisms for heavy metal detoxification and tolerance. *J Exp Bot*. **53**:1-11.

Ham, B. K., Li, G., Kang, B. H., Zeng, F., and Lucas, W. J. (2012). Overexpression of *Arabidopsis* plasmodesmata germin-like proteins disrupts root growth and development. *Plant Cell*. **24**:3630-3648.

Hamim, H., Miftahudin, M., and Setyaningsih, L. (2018). Cellular and ultrastructure alteration of plant roots in response to metal stress. *In Plant growth and regulation - Alterations to sustain unfavorable conditions*.

Han, X., Huang, L. J., Feng, D., Jiang, W., Miu, W., and Li, N. (2019). Plasmodesmata-related structural and functional proteins: the long sought-after secrets of a cytoplasmic channel in plant cell walls. *Int J Mol Sci*. **20**.

Han, X., and Kim, J. Y. (2016). Integrating hormone- and micromolecule-mediated signaling with plasmodesmal communication. *Mol Plant*. **9**:46-56.

Han, Y., Huang, B., Zee, S. Y., and Yuan, M. (2000). Symplastic communication between the central cell and the egg apparatus cells in the embryo sac of *Torenia fournie***r i** Lind. before and during fertilization. *Planta*. **211**:158-162.

Hay, A., Barkoulas, M., and Tsiantis, M. (2006). ASYMMETRIC LEAVES1 and auxin activities converge to repress *BREVIPEDICELLUS* expression and promote leaf development in *Arabidopsis*. *Development*. **133**:3955-3961.

He, Y. W., and Loh, C. S. (2002). Induction of early bolting in *Arabidopsis thaliana* by triacontanol, cerium and lanthanum is correlated with increased endogenous concentration of isopentenyl adenosine (iPAdos). *J Exp Bot*. **53**:505-512.

Heinlein, M. (2015). Plant virus replication and movement. *Virology*. **479-480**:657-671.

Helariutta, Y., Fukaki, H., Wysocka-Diller, J., Nakajima, K., Jung, J., Sena, G., Hauser, M. T., and Benfey, P. N. (2000). The *SHORT-ROOT* gene controls radial patterning of the *Arabidopsis* root through radial signaling. *Cell*. **101**:555-567.

Hemsley, P. A. (2015). The importance of lipid modified proteins in plants. *New Phytol*. **205**:476-489.

Hemsley, P. A., Weimar, T., Lilley, K. S., Dupree, P., and Grierson, C. S. (2013). A proteomic approach identifies many novel palmitoylated proteins in *Arabidopsis*. *New Phytol*. **197**:805-814.

Hensel, L. L., Nelson, M. A., Richmond, T. A., and Bleecker, A. B. (1994). The fate of inflorescence meristems is controlled by developing fruits in *Arabidopsis*. *Plant Physiol*. **106**:863-876.

Heyl, A., and Schmülling, T. (2003). Cytokinin signal perception and transduction. *Curr Opin Plant Biol*. **6**:480-488.

Hindt, M. N., and Guerinot, M. L. (2012). Getting a sense for signals: regulation of the plant iron deficiency response. *BBA Mol Cell Res*. **1823**:1521-1530.

Hirose, N., Takei, K., Kuroha, T., Kamada-Nobusada, T., Hayashi, H., and Sakakibara, H. (2008). Regulation of cytokinin biosynthesis, compartmentalization and translocation. *J Exp Bot*. **59**:75-83.

Hisanaga, T., Miyashima, S., and Nakajima, K. (2014). Small RNAs as positional signal for pattern formation. *Curr Opin Plant Biol*. **21**:37-42.

Holst, K., Schmülling, T., and Werner, T. (2011). Enhanced cytokinin degradation in leaf primordia of transgenic *Arabidopsis* plants reduces leaf size and shoot organ primordia formation. *Plant Physiol*. **168**:1328-1334.

Hou, K., Wu, W., and Gan, S.-S. (2013). *SAUR36*, a small auxin up RNA gene, is involved in the promotion of leaf senescence in *Arabidopsis*. *Plant Physiol*. **161**:1002-1009.

Houston, K., Tucker, M. R., Chowdhury, J., Shirley, N., and Little, A. (2016). The plant cell wall: A complex and dynamic structure as revealed by the responses of genes under stress conditions. *Front Plant Sci*. **7**.

Huang, D., W., Sherman, B. T., and Lempicki, R. A. (2009). Bioinformatics enrichment tools: paths toward the comprehensive functional analysis of large gene lists. *Nucleic Acids Res*. **37**:1-13.

Huang, S., Cerny, R. E., Qi, Y., Bhat, D., Aydt, C. M., Hanson, D. D., Malloy, K. P., and Ness, L. A. (2003). Transgenic studies on the involvement of cytokinin and gibberellin in male development. *Plant Physiol*. **131**:1270-1282.

Huffman, D. L., and O'Halloran, T. V. (2001). Function, structure, and mechanism of intracellular copper trafficking proteins. *Annu Rev Biochem*. **70**:677-701.

Huijser, P., and Schmid, M. (2011). The control of developmental phase transitions in plants. *Development*. **138**:4117-4129.

Hussain, A., Mun, B. G., Imran, Q. M., Lee, S. U., Adamu, T. A., Shahid, M., Kim, K. M., and Yun, B. W. (2016). Nitric oxide mediated transcriptome profiling reveals activation of multiple regulatory pathways in *Arabidopsis thaliana*. *Front Plant Sci*. **7**:975.

Hussain, D., Haydon, M. J., Wang, Y., Wong, E., Sherson, S. M., Young, J., Camakaris, J., Harper, J. F., and Cobbett, C. S. (2004). P-type ATPase heavy metal transporters with roles in essential zinc homeostasis in *Arabidopsis*. *Plant Cell*. **16**:1327-1339.

Hutchison, C. E., Li, J., Argueso, C., Gonzalez, M., Lee, E., Lewis, M. W., Maxwell, B. B., Perdue, T. D., Schaller, G. E., Alonso, J. M., Ecker, J. R., and Kieber, J. J. (2006). The *Arabidopsis* histidine phosphotransfer proteins are redundant positive regulators of cytokinin signaling. *Plant Cell*. **18**:3073-3087.

Hwang, I., Sheen, J., and Muller, B. (2012). Cytokinin signaling networks. *Annu Rev Plant Biol*. **63**:353-380.

Iizasa, S., Iizasa, E., Watanabe, K., and Nagano, Y. (2017). Transcriptome analysis reveals key roles of AtLBR-2 in LPS-induced defense responses in plants. *BMC Genomics*. **18**:995.

Illgen, S., Zintl, S., Zuther, E., Hincha, D. K., and Schmülling, T. (2020). Characterisation of the *ERF102* to *ERF105* genes of *Arabidopsis thaliana* and their role in the response to cold stress. *Plant Molecular Biology*. **103**:303-320.

Imlau, A., Truernit, E., and Sauer, N. (1999). Cell-to-cell and long-distance trafficking of the green fluorescent protein in the phloem and symplastic unloading of the protein into sink tissues. *Plant Cell*. **11**:309-322.

Ishikawa, K., Tamura, K., Fukao, Y., and Shimada, T. (2019). Structural and functional relationships between plasmodesmata and plant endoplasmic reticulum-plasma membrane contact sites consisting of three synaptotagmins. *New Phytol*. **226**:798-808.

Iswanto, A. B. B., Shon, J. C., Vu, M. H., Kumar, R., Liu, K. H., and Kim, J.-Y. (2020). Sphingolipids modulate secretion of GPI-anchored plasmodesmata proteins and callose deposition. *Plant Physiol*:pp.00401.02020.

Jackson, D. (2015). Plasmodesmata spread their influence. *F1000Prime Rep*. **7**:25.

Jamshed, M., Liang, S., M. N. Hickerson, N., and Samuel, M. A. (2017). Farnesylation-mediated subcellular localization is required for CYP85A2 function. *Plant Signal Behav*. **12**:e1382795.

Jefferson, R. A., Kavanagh, T. A., and Bevan, M. W. (1987). GUS fusions: beta-glucuronidase as a sensitive and versatile gene fusion marker in higher plants. *EMBO J*. **6**:3901-3907.

Jordan, I. K., Natale, D. A., Koonin, E. V., and Galperin, M. Y. (2001). Independent evolution of heavy metal-associated domains in copper chaperones and copper-transporting atpases. *J Mol Evol*. **53**:622-633.

Kang, J., Lee, Y., Sakakibara, H., and Martinoia, E. (2017). Cytokinin transporters: GO and STOP in signaling. *Trends Plant Sci*. **22**:455-461.

Karimi, M., Inze, D., and Depicker, A. (2002). GATEWAY vectors for *Agrobacterium*-mediated plant transformation. *Trends Plant Sci*. **7**:193-195.

Karley, A. J., Leigh, R. A., and Sanders, D. (2000). Where do all the ions go? The cellular basis of differential ion accumulation in leaf cells. *Trends Plant Sci*. **5**:465-470.

Kasahara, H., Takei, K., Ueda, N., Hishiyama, S., Yamaya, T., Kamiya, Y., Yamaguchi, S., and Sakakibara, H. (2004). Distinct isoprenoid origins aof *cis*- and *trans*-zeatin biosyntheses in *Arabidopsis*. *J Biol Chem*. **279**:14049-14054.

Kerppola, T. K. (2008). Bimolecular fluorescence complementation (BiFC) analysis as a probe of protein interactions in living cells. *Annu Rev Biophys*. **37**:465-487.

Kiba, T., Yamada, H., and Mizuno, T. (2002). Characterization of the ARR15 and ARR16 response regulators with special reference to the cytokinin signaling pathway mediated by the AHK4 histidine kinase in roots of *Arabidopsis thaliana*. *Plant Cell Physiol*. **43**:1059-1066.

Kieber, J. J., and Schaller, G. E. (2014). Cytokinins. *The Arabidopsis Book*. **12**:e0168.

Kieber, J. J., and Schaller, G. E. (2018). Cytokinin signaling in plant development. *Development*. **145**.

Kim, D., Langmead, B., and Salzberg, S. L. (2015). HISAT: a fast spliced aligner with low memory requirements. *Nat Methods*. **12**:357-360.

Kim, H. J., Chiang, Y. H., Kieber, J. J., and Schaller, G. E. (2013). SCF(KMD) controls cytokinin signaling by regulating the degradation of type-B response regulators. *PNAS*. **110**:10028-10033.

Kim, H. J., Ryu, H., Hong, S. H., Woo, H. R., Lim, P. O., Lee, I. C., Sheen, J., Nam, H. G., and Hwang, I. (2006). Cytokinin-mediated control of leaf longevity by AHK3 through phosphorylation of ARR2 in *Arabidopsis*. *PNAS*. **103**:814-819.

Kim, I., Cho, E., Crawford, K., Hempel, F. D., and Zambryski, P. C. (2005). Cell-to-cell movement of GFP during embryogenesis and early seedling development in *Arabidopsis*. *PNAS*. **102**:2227-2231.

Kim, I., Hempel, F. D., Sha, K., Pfluger, J., and Zambryski, P. C. (2002). Identification of a developmental transition in plasmodesmatal function during embryogenesis in *Arabidopsis thaliana*. *Development*. **129**:1261-1272.

Kim, J. Y. (2018). Symplasmic intercellular communication through plasmodesmata. *Plants*. **7**.

Kim, J. Y., Yuan, Z., and Jackson, D. (2003). Developmental regulation and significance of KNOX protein trafficking in *Arabidopsis*. *Development*. **130**:4351-4362.

Kim, K., and Hwang, I. (2012). Attenuation of cytokinin signaling via proteolysis of a type-B response regulator. *Plant signaling & behavior*. **7**:756-759.

Kinoshita-Tsujimura, K., and Kakimoto, T. (2011). Cytokinin receptors in sporophytes are essential for male and female functions in *Arabidopsis thaliana*. *Plant Signal Behav*. **6**:66-71.

Kinoshita, N., Berr, A., Belin, C., Chappuis, R., Nishizawa, N. K., and Lopez-Molina, L. (2010). Identification of *growth insensitive to ABA3* (*gia3*), a recessive mutation affecting ABA signaling for the control of early post-germination growth in *Arabidopsis thaliana*. *Plant Cell Physiol*. **51**:239-251.

Kitagawa, M., and Jackson, D. (2017). Plasmodesmata-mediated cell-to-cell communication in the shoot apical meristem: how stem cells talk. *Plants*. **6**.

Knoblauch, M., Vendrell, M., de Leau, E., Paterlini, A., Knox, K., Ross-Elliot, T., Reinders, A., Brockman, S. A., Ward, J., and Oparka, K. (2015). Multispectral phloem-mobile probes: properties and applications. *Plant Physiol*. **167**:1211-1220.

Knox, J. P., and Benitez-Alfonso, Y. (2014). Roles and regulation of plant cell walls surrounding plasmodesmata. *Curr Op Plant Biol*. **22**:93-100.

Ko, D., Kang, J., Kiba, T., Park, J., Kojima, M., Do, J., Kim, K. Y., Kwon, M., Endler, A., Song, W. Y., Martinoia, E., Sakakibara, H., and Lee, Y. (2014). *Arabidopsis* ABCG14 is essential for the root-to-shoot translocation of cytokinin. *PNAS*. **111**:7150-7155.

Kobayashi, K., Otegui, M. S., Krishnakumar, S., Mindrinos, M., and Zambryski, P. (2007). *INCREASED SIZE EXCLUSION LIMIT2* encodes a putative DEVH box RNA helicase involved in plasmodesmata function during *Arabidopsis* embryogenesis. *Plant Cell*. **19**:1885-1897.

Koizumi, K., Wu, S., MacRae-Crerar, A., and Gallagher, K. L. (2011). An essential protein that interacts with endosomes and promotes movement of the SHORT-ROOT transcription factor. *Curr Biol*. **21**:1559-1564.

Köllmer, I., Novak, O., Strnad, M., Schmülling, T., and Werner, T. (2014). Overexpression of the cytosolic cytokinin oxidase/dehydrogenase *(*CKX7) from *Arabidopsis* causes specific changes in root growth and xylem differentiation. *Plant J*. **78**:359-371.

Koncz, C., and Schell, J. (1986). The promoter of *T L-DNA GENE 5* controls the tissue-specific expression of chimaeric genes carried by a novel type of *Agrobacterium* binary vector. *Molecular and General Genetics*. **204**:383-396.

Kong, Y., Zhu, Y., Gao, C., She, W., Lin, W., Chen, Y., Han, N., Bian, H., Zhu, M., and Wang, J. (2013). Tissue-specific expression of *SMALL AUXIN UP RNA41* differentially regulates cell expansion and root meristem patterning in *Arabidopsis*. *Plant Cell Physiol*. **54**:609-621.

Krämer, U. (2010). Metal hyperaccumulation in plants. *Annu Rev Plant Biol*. **61**:517-534.

Krämer, U., Talke, I. N., and Hanikenne, M. (2007). Transition metal transport. *FEBS Lett*. **581**:2263-2272.

Kraner, M. E., Müller, C., and Sonnewald, U. (2017). Comparative proteomic profiling of the *choline transporter-like1* (*cher1*) mutant provides insights into plasmodesmata composition of fully developed *Arabidopsis thaliana* leaves. *Plant J*. **92**:696-709.

Krysan, P. J., Young, J. C., and Sussman, M. R. (1990). T-DNA as an Insertional Mutagen in Arabidopsis. *The Plant Cell*. **11**.

Kumar, D., Kumar, R., Hyun, T. K., and Kim, J. Y. (2015). Cell-to-cell movement of viruses via plasmodesmata. *J Plant Res*. **128**:37-47.

Kurakawa, T., Ueda, N., Maekawa, M., Kobayashi, K., Kojima, M., Nagato, Y., Sakakibara, H., and Kyozuka, J. (2007). Direct control of shoot meristem activity by a cytokinin-activating enzyme. *Nature*. **445**:652-655.

Kurihara, D., Mizuta, Y., Sato, Y., and Higashiyama, T. (2015). *ClearSee:* a rapid optical clearing reagent for whole-plant fluorescence imaging. *Development*. **142**:4168-4179.

Kuroha, T., Tokunaga, H., Kojima, M., Ueda, N., Ishida, T., Nagawa, S., Fukuda, H., Sugimoto, K., and Sakakibara, H. (2009). Functional analyses of LONELY GUY cytokinin-activating enzymes reveal the importance of the direct activation pathway in *Arabidopsis*. *Plant Cell*. **21**:3152-3169.

Laemmli, U. K. (1970). Cleavage of structural proteins during the assembly of the head of bacteriophage T4. *Nature*. **227**:680-685.

Lao, N. T., Schoneveld, O., Mould, R. M., Hibberd, J. M., Gray, J. C., and Kavanagh, T. A. (1999). An *Arabidopsis* gene encoding a chloroplast-targeted β-amylase. *Plant J*. **20**:519-527.

Laplaze, L., Benkova, E., Casimiro, I., Maes, L., Vanneste, S., Swarup, R., Weijers, D., Calvo, V., Parizot, B., Herrera-Rodriguez, M. B., Offringa, R., Graham, N., Doumas, P., Friml, J., Bogusz, D., Beeckman, T., and Bennett, M. (2007). Cytokinins act directly on lateral root founder cells to inhibit root initiation. *Plant Cell*. **19**:3889-3900.

Larsson, E., Vivian-Smith, A., Offringa, R., and Sundberg, E. (2017). Auxin homeostasis in *Arabidopsis* ovules is anther-dependent at maturation and changes dynamically upon fertilization. *Front Plant Sci*. **8**.

Lee, D. J., Park, J. Y., Ku, S. J., Ha, Y. M., Kim, S., Kim, M. D., Oh, M. H., and Kim, J. (2007). Genome-wide expression profiling of *ARABIDOPSIS RESPONSE REGULATOR7* (*ARR7*) overexpression in cytokinin response. *Mol Genet Genomics*. **277**:115-137.

Lee, J. Y. (2015). Plasmodesmata: a signaling hub at the cellular boundary. *Curr Opin Plant Biol*. **27**:133-140.

Lee, J. Y., and Frank, M. (2018). Plasmodesmata in phloem: different gateways for different cargoes. *Curr Opin Plant Biol*. **43**:119-124.

Lee, Y., Choi, D., and Kende, H. (2001). Expansins: ever-expanding numbers and functions. *Curr Opin Plant Biol*. **4**:527-532.

Lee, Z. H., Hirakawa, T., Yamaguchi, N., and Ito, T. (2019). The roles of plant hormones and their interactions with regulatory genes in determining meristem activity. *Int J Mol Sci*. **20**.

Lei, Y., Lu, L., Liu, H. Y., Li, S., Xing, F., and Chen, L. L. (2014). CRISPR-P: a web tool for synthetic single-guide RNA design of CRISPR-system in plants. *Mol Plant*. **7**:1494-1496.

Leibfried, A., To, J. P., Busch, W., Stehling, S., Kehle, A., Demar, M., Kieber, J. J., and Lohmann, J. U. (2005). WUSCHEL controls meristem function by direct regulation of cytokinin-inducible response regulators. *Nature*. **438**:1172-1175.

Lequeux, H., Hermans, C., Lutts, S., and Verbruggen, N. (2010). Response to copper excess in *Arabidopsis thaliana*: impact on the root system architecture, hormone distribution, lignin accumulation and mineral profile. *Plant Physiol Biochem*. **48**:673-682.

Levy, A., Erlanger, M., Rosenthal, M., and Epel, B. L. (2007). A PLASMODESMATA-ASSOCIATED BETA-1,3-GLUCANASE in *Arabidopsis*. *Plant J*. **49**:669-682.

Li, L., Foster, C. M., Gan, Q., Nettleton, D., James, M. G., Myers, A. M., and Wurtele, E. S. (2009). Identification of the novel protein QQS as a component of the starch metabolic network in *Arabidopsis* leaves. *Plant J*. **58**:485-498.

Li, X. G., Su, Y. H., Zhao, X. Y., Li, W., Gao, X. Q., and Zhang, X. S. (2010). Cytokinin overproduction-caused alteration of flower development is partially mediated by *CUC2* and *CUC3* in *Arabidopsis*. *Gene*. **450**:109-120.

Lin, M.-K., Belanger, H., Lee, Y.-J., Varkonyi-Gasic, E., Taoka, K.-I., Miura, E., Xoconostle-Cázares, B., Gendler, K., Jorgensen, R. A., Phinney, B., Lough, T. J., and Lucas, W. J. (2007). FLOWERING LOCUS T protein may act as the long-distance florigenic signal in the cucurbits. *Plant Cell*. **19**:1488-1506.

Liu, C., Zhou, J., Bracha-Drori, K., Yalovsky, S., Ito, T., and Yu, H. (2007). Specification of *Arabidopsis* floral meristem identity by repression of flowering time genes. *Development*. **134**:1901-1910.

Liu, J., and Müller, B. (2017). Imaging TCSn::GFP, a synthetic cytokinin reporter, in *Arabidopsis thaliana*. *Methods Mol Biol*. **1497**:81-90.

Liu, J. J., Wei, Z., and Li, J. H. (2014). Effects of copper on leaf membrane structure and root activity of maize seedling. *Bot Stud*. **55**:47.

Liu, L., Liu, C., Hou, X., Xi, W., Shen, L., Tao, Z., Wang, Y., and Yu, H. (2012). FTIP1 is an essential regulator required for florigen transport. *PLOS Biol*. **10**:e1001313.

Liu, Y., Xu, M., Liang, N., Zheng, Y., Yu, Q., and Wu, S. (2017a). Symplastic communication spatially directs local auxin biosynthesis to maintain root stem cell niche in *Arabidopsis*. *PNAS*. **114**:4005-4010.

Liu, Z., Miao, L., Huo, R., Song, X., Johnson, C., Kong, L., Sundaresan, V., and Yu, X. (2017b). ARF2–ARF4 and ARF5 are essential for female and male gametophyte development in *Arabidopsis*. *Plant Cell Physiol*. **59**:179-189.

Liu, Z., Yuan, L., Song, X., Yu, X., and Sundaresan, V. (2017c). AHP2, AHP3, and AHP5 act downstream of CKI1 in *Arabidopsis* female gametophyte development. *J Exp Bot*. **68**:3365-3373.

Long, J. A., Moan, E. I., Medford, J. I., and Barton, M. K. (1996). A member of the KNOTTED class of homeodomain proteins encoded by the *STM* gene of *Arabidopsis*. *Nature*. **379**:66-69.

Love, M. I., Huber, W., and Anders, S. (2014). Moderated estimation of fold change and dispersion for RNA-seq data with DESeq2. *Genome Biol*. **15**:550.

Lucas, W. J., Bouche-Pillon, S., Jackson, D. P., Nguyen, L., Baker, L., Ding, B., and Hake, S. (1995). Selective trafficking of KNOTTED1 homeodomain protein and its mRNA through plasmodesmata. *Science*. **270**:1980-1983.

Lucas, W. J., Ham, B. K., and Kim, J. Y. (2009). Plasmodesmata - bridging the gap between neighboring plant cells. *Trends Cell Biol*. **19**:495-503.

Lux, A., Martinka, M., Vaculik, M., and White, P. J. (2011). Root responses to cadmium in the rhizosphere: a review. *J Exp Bot*. **62**:21-37.

Mähönen, A. P., Bishopp, A., Higuchi, M., Nieminen, K. M., Kinoshita, K., Tormakangas, K., Ikeda, Y., Oka, A., Kakimoto, T., and Helariutta, Y. (2006). Cytokinin signaling and its inhibitor AHP6 regulate cell fate during vascular development. *Science*. **311**:94-98.

Malamy, J. E., and Benfey, P. N. (1997). Organization and cell differentiation in lateral roots of *Arabidopsis thaliana*. *Development*. **124**:33-44.

Marín-de la Rosa, N., Pfeiffer, A., Hill, K., Locascio, A., Bhalerao, R. P., Miskolczi, P., Gronlund, A. L., Wanchoo-Kohli, A., Thomas, S. G., Bennett, M. J., Lohmann, J. U., Blazquez, M. A., and Alabadi, D. (2015). Genome wide binding site analysis reveals transcriptional coactivation of cytokinin-responsive genes by DELLA proteins. *PLOS Genet*. **11**:e1005337.

Markakis, M. N., Boron, A. K., Van Loock, B., Saini, K., Cirera, S., Verbelen, J.-P., and Vissenberg, K. (2013). Characterization of a *SMALL AUXIN-UP RNA* (*SAUR*)-like gene involved in *Arabidopsis thaliana* development. *PLOS One*. **8**:e82596.

Marsch-Martínez, N., Ramos-Cruz, D., Irepan Reyes-Olalde, J., Lozano-Sotomayor, P., Zuniga-Mayo, V. M., and de Folter, S. (2012). The role of cytokinin during *Arabidopsis* gynoecia and fruit morphogenesis and patterning. *Plant J*. **72**:222-234.

Mary, V., Schnell Ramos, M., Gillet, C., Socha, A. L., Giraudat, J., Agorio, A., Merlot, S., Clairet, C., Kim, S. A., Punshon, T., Guerinot, M. L., and Thomine, S. (2015). Bypassing iron storage in endodermal vacuoles rescues the iron mobilization defect in the *natural resistance associated-macrophage protein3natural resistance associated-macrophage protein4* double mutant. *Plant Physiol*. **169**:748-759.

Mashiguchi, K., Tanaka, K., Sakai, T., Sugawara, S., Kawaide, H., Natsume, M., Hanada, A., Yaeno, T., Shirasu, K., Yao, H., McSteen, P., Zhao, Y., Hayashi, K., Kamiya, Y., and Kasahara, H. (2011). The main auxin biosynthesis pathway in *Arabidopsis*. *PNAS*. **108**:18512-18517.

Mason, M. G., Mathews, D. E., Argyros, D. A., Maxwell, B. B., Kieber, J. J., Alonso, J. M., Ecker, J. R., and Schaller, G. E. (2005). Multiple type-B response regulators mediate cytokinin signal transduction in *Arabidopsis*. *Plant Cell*. **17**:3007-3018.

Maule, A., Faulkner, C., and Benitez-Alfonso, Y. (2012). Plasmodesmata "in communicado". *Front Plant Sci*. **3**:30.

Maule, A., Gaudioso-Pedraza, R., and Benitez-Alfonso, Y. (2013). Callose deposition and symplastic connectivity are regulated prior to lateral root emergence. *Commun Integr Biol*. **6**:e26531.

Mayer, K. F., Schoof, H., Haecker, A., Lenhard, M., Jurgens, G., and Laux, T. (1998). Role of *WUSCHEL* in regulating stem cell fate in the *Arabidopsis* shoot meristem. *Cell*. **95**:805-815.

McGaw, B. A., and Horgan, R. (1983). Cytokinin metabolism and cytokinin oxidase. *Phytochemistry*. **22**:1103-1105.

Mellor, N. L., Voß, U., Janes, G., Bennett, M. J., Wells, D. M., and Band, L. R. (2020). Auxin fluxes through plasmodesmata modify root-tip auxin distribution. *Development*. **147**.

Meng, W. J., Cheng, Z. J., Sang, Y. L., Zhang, M. M., Rong, X. F., Wang, Z. W., Tang, Y. Y., and Zhang, X. S. (2017). Type-B ARABIDOPSIS RESPONSE REGULATORs specify the shoot stem cell niche by dual regulation of *WUSCHEL*. *Plant Cell*. **29**:1357-1372.

Meyerowitz, E. M. (1997). Genetic control of cell division patterns in developing plants. *Cell*. **88**:299-308.

Miller, C. O., Skoog, F., von Saltza, M. H., and Strong, F. M. (1955). Kinetin, a cell division factor from deoxyribonucleic acid. *Journal of the American Chemical Society*. **77**:1329-1334.

Miller, K. E., Kim, Y., Huh, W. K., and Park, H. O. (2015). Bimolecular fluorescence complementation (BiFC) analysis: advances and recent applications for genome-wide interaction studies. *J Mol Biol*. **427**:2039-2055.

Mizzotti, C., Mendes, M. A., Caporali, E., Schnittger, A., Kater, M. M., Battaglia, R., and Colombo, L. (2012). The MADS box genes *SEEDSTICK* and *ARABIDOPSIS* Bsister play a maternal role in fertilization and seed development. *Plant J*. **70**:409-420.

Monfared, M. M., Simon, M. K., Meister, R. J., Roig-Villanova, I., Kooiker, M., Colombo, L., Fletcher, J. C., and Gasser, C. S. (2011). Overlapping and antagonistic activities of *BASIC PENTACYSTEINE* genes affect a range of developmental processes in *Arabidopsis*. *Plant J*. **66**:1020-1031.

Moubayidin, L., Di Mambro, R., Sozzani, R., Pacifici, E., Salvi, E., Terpstra, I., Bao, D., van Dijken, A., Dello Ioio, R., Perilli, S., Ljung, K., Benfey, P. N., Heidstra, R., Costantino, P., and Sabatini, S. (2013). Spatial coordination between stem cell activity and cell differentiation in the root meristem. *Dev Cell*. **26**:405-415.

Moubayidin, L., Salvi, E., Giustini, L., Terpstra, I., Heidstra, R., Costantino, P., and Sabatini, S. (2016). A SCARECROW-based regulatory circuit controls *Arabidopsis thaliana* meristem size from the root endodermis. *Planta*. **243**:1159-1168.

Müller, B., and Sheen, J. (2008). Cytokinin and auxin interaction in root stem-cell specification during early embryogenesis. *Nature*. **453**:1094-2007.

Müller, J., Toev, T., Heisters, M., Teller, J., Moore, K. L., Hause, G., Dinesh, D. C., Burstenbinder, K., and Abel, S. (2015). Iron-dependent callose deposition adjusts root meristem maintenance to phosphate availability. *Dev Cell*. **33**:216-230.

Müller, M., and Munné-Bosch, S. (2015). ETHYLENE RESPONSE FACTORS: a key regulatory hub in hormone and stress signaling. *Plant Physiol*. **169**:32-41.

Müller, S., Hilbert, B., Dückershoff, K., Roitsch, T., Krischke, M., Müller, M. J., and Berger, S. (2008). General detoxification and stress responses are mediated by oxidized lipids through tga transcription factors in *Arabidopsis*. *Plant Cell*. **20**:768-785.

Mullis, K. B., and Faloona, F. A. (1987). Specific synthesis of DNA in vitro via a polymerase-catalyzed chain reaction. *Methods Enzymol*. **155**:335-350.

Murashige, T., and Skoog, F. (1962). A revised medium for rapid growth and bio assays with tobacco tissue cultures. *Physiologia Plantarum*. **15**:473-497.

Nakajima, K., Sena, G., Nawy, T., and Benfey, P. N. (2001). Intercellular movement of the putative transcription factor SHR in root patterning. *Nature*. **413**:307-411.

Nelson, B. K., Cai, X., and Nebenfuhr, A. (2007). A multicolored set of in vivo organelle markers for co-localization studies in *Arabidopsis* and other plants. *Plant J*. **51**:1126-1136.

Nemhauser, J. L., Feldman, L. J., and Zambryski, P. C. (2000). Auxin and ETTIN in *Arabidopsis* gynoecium morphogenesis. *Development*. **127**:3877-3888.

Niemann, M. C., Bartrina, I., Ashikov, A., Weber, H., Novak, O., Spichal, L., Strnad, M., Strasser, R., Bakker, H., Schmülling, T., and Werner, T. (2015). *Arabidopsis* ROCK1 transports UDP-GlcNAc/UDP-GalNAc and regulates ER protein quality control and cytokinin activity. *PNAS*. **112**:291-396.

Niemann, M. C. E., Weber, H., Hluska, T., Leonte, G., Anderson, S. M., Novak, O., Senes, A., and Werner, T. (2018). The CYTOKININ OXIDASE/DEHYDROGENASE CKX1 is a membrane-bound protein requiring homooligomerization in the endoplasmic reticulum for its cellular activity. *Plant Physiol*. **176**:2024-2039.

Nikovics, K., Blein, T., Peaucelle, A., Ishida, T., Morin, H., Aida, M., and Laufs, P. (2006). The balance between the *MIR164A* and *CUC2* genes controls leaf margin serration in *Arabidopsis*. *Plant Cell*. **18**:2929-2945.

Nishimura, C., Ohashi, Y., Sato, S., Kato, T., Tabata, S., and Ueguchi, C. (2004). Histidine kinase homologs that act as cytokinin receptors possess overlapping functions in the regulation of shoot and root growth in *Arabidopsis*. *Plant Cell*. **16**:1365-1377.

O'Lexy, R., Kasai, K., Clark, N., Fujiwara, T., Sozzani, R., and Gallagher, K. L. (2018). Exposure to heavy metal stress triggers changes in plasmodesmatal permeability via deposition and breakdown of callose. *J Exp Bot*. **69**:3715-3728.

Oparka, K. J., Duckett, C. M., Prior, D. A. M., and Fisher, D. B. (1994). Real-time imaging of phloem unloading in the root tip of *Arabidopsis*. *Plant J*. **6**:759-766.

Oparka, K. J., Roberts, A. G., Boevink, P., Santa Cruz, S., Roberts, I., Pradel, K. S., Imlau, A., Kotlizky, G., Sauer, N., and Epel, B. (1999). Simple, but not branched, plasmodesmata allow the nonspecific trafficking of proteins in developing tobacco leaves. *Cell*. **97**:743-754.

Orozco-Arroyo, G., Paolo, D., Ezquer, I., and Colombo, L. (2015). Networks controlling seed size in *Arabidopsis*. *Plant Reprod*. **28**:17-32.

Osugi, A., and Sakakibara, H. (2015). Q&A: How do plants respond to cytokinins and what is their importance? *BMC Biol*. **13**:102.

Pagnussat, G. C., Alandete-Saez, M., Bowman, J. L., and Sundaresan, V. (2009). Auxin-dependent patterning and gamete specification in the *Arabidopsis* female gametophyte. *Science*. **324**:1684-1689.

Pagnussat, G. C., Yu, H. J., Ngo, Q. A., Rajani, S., Mayalagu, S., Johnson, C. S., Capron, A., Xie, L. F., Ye, D., and Sundaresan, V. (2005). Genetic and molecular identification of genes required for female gametophyte development and function in *Arabidopsis*. *Development*. **132**:603-614.

Panoli, A., Martin, M. V., Alandete-Saez, M., Simon, M., Neff, C., Swarup, R., Bellido, A., Yuan, L., Pagnussat, G. C., and Sundaresan, V. (2015). Auxin Import and local auxin biosynthesis are required for mitotic divisions, cell expansion and cell specification during female gametophyte development in *Arabidopsis thaliana*. *PLOS One*. **10**:e0126164.

Pauly, M., and Keegstra, K. (2016). Biosynthesis of the plant cell wall matrix polysaccharide xyloglucan. *Ann Rev Plant Biol*. **67**:235-259.

Pauwels, L., and Goossens, A. (2011). The JAZ proteins: a crucial interface in the jasmonate signaling cascade. *Plant Cell*. **23**:3089-3100.

Pavlů, J., Novak, J., Koukalova, V., Luklova, M., Brzobohaty, B., and Cerny, M. (2018). Cytokinin at the crossroads of abiotic stress signaling pathways. *Int J Mol Sci*. **19**.

Perilli, S., and Sabatini, S. (2010). Analysis of root meristem size development. *Methods Mol Biol*. **655**:177-187.

Pernisova, M., Grochova, M., Konecny, T., Plackova, L., Harustiakova, D., Kakimoto, T., Heisler, M. G., Novak, O., and Hejatko, J. (2018). Cytokinin signaling regulates organ identity via the AHK4 receptor in *Arabidopsis*. *Development*. **145**.

Petit, J. D., Immel, F., Lins, L., and Bayer, E. M. (2019). Lipids or proteins: Who is leading the dance at membrane contact sites? *Front Plant Sci*. **10**:198.

Pi, L., Aichinger, E., van der Graaff, E., Llavata-Peris, C. I., Weijers, D., Hennig, L., Groot, E., and Laux, T. (2015). Organizer-derived WOX5 signal maintains root columella stem cells through chromatin-mediated repression of *CDF4* expression. *Dev Cell*. **33**:576-588.

Pierdonati, E., Unterholzner, S. J., Salvi, E., Svolacchia, N., Bertolotti, G., Dello Ioio, R., Sabatini, S., and Di Mambro, R. (2019). Cytokinin-dependent control of *GH3* group II family genes in the *Arabidopsis* root. *Plants*. **8**.

Pischke, M. S., Jones, L. G., Otsuga, D., Fernandez, D. E., Drews, G. N., and Sussman, M. R. (2002). An *Arabidopsis* histidine kinase is essential for megagametogenesis. *PNAS*. **99**:15800-15805.

Potter, K. C., Wang, J., Schaller, G. E., and Kieber, J. J. (2018). Cytokinin modulates context-dependent chromatin accessibility through the type-B response regulators. *Nat Plants*. **4**:1102-1111.

Qiu, T., Chen, Y., Li, M., Kong, Y., Zhu, Y., Han, N., Bian, H., Zhu, M., and Wang, J. (2013). The tissue-specific and developmentally regulated expression patterns of the *SAUR41* subfamily of small auxin up RNA genes: potential implications. *Plant Signal Behav*. **8**.

Radakovic, Z. S., Anjam, M. S., Escobar, E., Chopra, D., Cabrera, J., Silva, A. C., Escobar, C., Sobczak, M., Grundler, F. M. W., and Siddique, S. (2018). *Arabidopsis HIPP27* is a host susceptibility gene for the beet cyst nematode *Heterodera schachtii*. *Mol Plant Pathol*:1917-1928.

Raffaele, S., Bayer, E., Lafarge, D., Cluzet, S., German Retana, S., Boubekeur, T., Leborgne-Castel, N., Carde, J. P., Lherminier, J., Noirot, E., Satiat-Jeunemaitre, B., Laroche-Traineau, J., Moreau, P., Ott, T., Maule, A. J., Reymond, P., Simon-Plas, F., Farmer, E. E., Bessoule, J. J., and Mongrand, S. (2009). Remorin, a solanaceae protein resident in membrane rafts and plasmodesmata, impairs potato virus X movement. *Plant Cell*. **21**:1541-1555.

Rashotte, A. M., Carson, S. D., To, J. P., and Kieber, J. J. (2003). Expression profiling of cytokinin action in *Arabidopsis*. *Plant Physiol*. **132**:1998-2011.

Rashotte, A. M., Mason, M. G., Hutchison, C. E., Ferreira, F. J., Schaller, G. E., and Kieber, J. J. (2006). A subset of *Arabidopsis* AP2 transcription factors mediates cytokinin responses in concert with a two-component pathway. *PNAS*. **103**:11081-11085.

Reddy, G. V., Heisler, M. G., Ehrhardt, D. W., and Meyerowitz, E. M. (2004). Real-time lineage analysis reveals oriented cell divisions associated with morphogenesis at the shoot apex of *Arabidopsis thaliana*. *Development*. **131**:4225-4237.

Reimand, J., Kull, M., Peterson, H., Hansen, J., and Vilo, J. (2007). *g:Profiler*: a web-based toolset for functional profiling of gene lists from large-scale experiments. *Nucleic Acids Res*. **35**:193-200.

Remy, E., and Duque, P. (2016). Assessing tolerance to heavy-metal stress in *Arabidopsis thaliana* seedlings. *Methods Mol Biol*. **1398**:197-208.

Ren, B., Liang, Y., Deng, Y., Chen, Q., Zhang, J., Yang, X., and Zuo, J. (2009a). Genome-wide comparative analysis of type-A Arabidopsis response regulator genes by overexpression studies reveals their diverse roles and regulatory mechanisms in cytokinin signaling. *Cell Research*. **19**:1178-1190.

Ren, H., and Gray, W. M. (2015). SAUR proteins as effectors of hormonal and environmental signals in plant growth. *Mol Plant*. **8**:1153-1164.

Ren, J., Wen, L., Gao, X., Jin, C., Xue, Y., and Yao, X. (2009b). *DOG 1.0*: illustrator of protein domain structures. *Cell Res*. **19**:271-273.

Resh, M. D. (2006). Trafficking and signaling by fatty-acylated and prenylated proteins. *Nat Chem Biol*. **2**:584-590.

Riefler, M., Novak, O., Strnad, M., and Schmülling, T. (2006). *Arabidopsis* cytokinin receptor mutants reveal functions in shoot growth, leaf senescence, seed size, germination, root development, and cytokinin metabolism. *Plant Cell*. **18**:40-54.

Robert, C., Noriega, A., Tocino, A., and Cervantes, E. (2008). Morphological analysis of seed shape in *Arabidopsis thaliana* reveals altered polarity in mutants of the ethylene signaling pathway. *J Plant Physiol*. **165**:911-919.

Robinson, N. J., and Winge, D. R. (2010). Copper metallochaperones. *Annu Rev Biochem*. **79**:537-562.

Romanov, G. A., Lomin, S. N., and Schmülling, T. (2018). Cytokinin signaling: from the ER or from the PM? That is the question! *New Phytol*. **218**:41-53.

Rong, X. F., Sang, Y. L., Wang, L., Meng, W. J., Zou, C. H., Dong, Y. X., Bie, X. M., Cheng, Z. J., and Zhang, X. S. (2018). Type-B ARRs control carpel regeneration through mediating *AGAMOUS* expression in *Arabidopsis*. *Plant Cell Physiol*. **59**:756-764.

Roppolo, D., De Rybel, B., Denervaud Tendon, V., Pfister, A., Alassimone, J., Vermeer, J. E., Yamazaki, M., Stierhof, Y. D., Beeckman, T., and Geldner, N. (2011). A novel protein family mediates Casparian strip formation in the endodermis. *Nature*. **473**:380-383.

Rosenzweig, A. C. (2002). Metallochaperones: bind and deliver. *Chem Biol*. **9**:673-677.

Ross-Elliott, T. J., Jensen, K. H., Haaning, K. S., Wager, B. M., Knoblauch, J., Howell, A. H., Mullendore, D. L., Monteith, A. G., Paultre, D., Yan, D., Otero, S., Bourdon, M., Sager, R., Lee, J.-Y., Helariutta, Y., Knoblauch, M., and Oparka, K. J. (2017). Phloem unloading in *Arabidopsis* roots is convective and regulated by the phloem-pole pericycle. *eLife*. **6**.

Running, M. P. (2014). The role of lipid post-translational modification in plant developmental processes. *Front Plant Sci*. **5**:50.

Saatian, B., Austin, R. S., Tian, G., Chen, C., Nguyen, V., Kohalmi, S. E., Geelen, D., and Cui, Y. (2018). Analysis of a novel mutant allele of GSL8 reveals its key roles in cytokinesis and symplastic trafficking in Arabidopsis. *BMC Plant Biol*. **18**:295.

Sabatini, S., Beis, D., Wolkenfelt, H., Murfett, J., Guilfoyle, T., Malamy, J., Benfey, P., Leyser, O., Bechtold, N., Weisbeek, P., and Scheres, B. (1999). An auxin-dependent distal organizer of pattern and polarity in the *Arabidopsis* root. *Cell*. **99**:463-472.

Sabatini, S., Heidstra, R., Wildwater, M., and Scheres, B. (2003). *SCARECROW* is involved in positioning the stem cell niche in the *Arabidopsis* root meristem. *Genes Dev*. **17**:354-358.

Sablowski, R. (2007). Flowering and determinacy in *Arabidopsis*. *J Exp Bot*. **58**:899-907.

Sager, R., and Lee, J. Y. (2014). Plasmodesmata in integrated cell signaling: insights from development and environmental signals and stresses. *J Exp Bot*. **65**:6337-6358.

Sager, R., Wang, X., Hill, K., Yoo, B.-C., Caplan, J., Nedo, A., Tran, T., Bennett, M. J., and Lee, J.-Y. (2020). Auxin-dependent control of a plasmodesmal regulator creates a negative feedback loop modulating lateral root emergence. *Nature Commun*. **11**:364.

Sager, R. E., and Lee, J. Y. (2018). Plasmodesmata at a glance. *J Cell Sci*. **131**.

Sakakibara, H. (2006). Cytokinins: activity, biosynthesis, and translocation. *Annu Rev Plant Biol*. **57**:431-449.

Salvi, E., Di Mambro, R., Pacifici, E., Dello Ioio, R., Costantino, P., Moubayidin, L., and Sabatini, S. (2018). *SCARECROW* and *SHORTROOT* control the auxin/cytokinin balance necessary for embryonic stem cell niche specification. *Plant Signal Behav*. **13**:e1507402.

Sancenón, V., Puig, S., Mateu-Andres, I., Dorcey, E., Thiele, D. J., and Penarrubia, L. (2004). The *Arabidopsis* copper transporter COPT1 functions in root elongation and pollen development. *J Biol Chem*. **279**:15348-15355.

Santuari, L., Sanchez-Perez, G. F., Luijten, M., Rutjens, B., Terpstra, I., Berke, L., Gorte, M., Prasad, K., Bao, D., Timmermans-Hereijgers, J. L., Maeo, K., Nakamura, K., Shimotohno, A.,

Pencik, A., Novak, O., Ljung, K., van Heesch, S., de Bruijn, E., Cuppen, E., Willemsen, V., Mahonen, A. P., Lukowitz, W., Snel, B., de Ridder, D., Scheres, B., and Heidstra, R. (2016). The *PLETHORA* gene regulatory network guides growth and cell differentiation in *Arabidopsis* roots. *Plant Cell*. **28**:2937-2951.

Sarkar, A. K., Luijten, M., Miyashima, S., Lenhard, M., Hashimoto, T., Nakajima, K., Scheres, B., Heidstra, R., and Laux, T. (2007). Conserved factors regulate signaling in *Arabidopsis thaliana* shoot and root stem cell organizers. *Nature*. **446**:811-814.

Scarpella, E., Marcos, D., Friml, J., and Berleth, T. (2006). Control of leaf vascular patterning by polar auxin transport. *Genes Dev* **20**:1015-1027.

Schaller, G. E., Bishopp, A., and Kieber, J. J. (2015). The yin-yang of hormones: cytokinin and auxin interactions in plant development. *Plant Cell*. **27**:44-63.

Schoberer, J., König, J., Veit, C., Vavra, U., Liebminger, E., Botchway, S. W., Altmann, F., Kriechbaumer, V., Hawes, C., and Strasser, R. (2019). A signal motif retains Arabidopsis ER-α-mannosidase I in the *cis*-Golgi and prevents enhanced glycoprotein ERAD. *Nat Commun*. **10**:3701.

Schoof, H., Lenhard, M., Haecker, A., Mayer, K. F., Jurgens, G., and Laux, T. (2000). The stem cell population of *Arabidopsis* shoot meristems in maintained by a regulatory loop between the *CLAVATA* and *WUSCHEL* genes. *Cell*. **100**:635-644.

Schuler, M., and Bauer, P. (2011). Heavy metals need assistance: the contribution of nicotianamine to metal circulation throughout the plant and the *Arabidopsis NAS* gene family. *Front Plant Sci*. **2**:69.

Schuler, M. A., Duan, H., Bilgin, M., and Ali, S. (2006). *Arabidopsis* cytochrome P450s through the looking glass: a window on plant biochemistry. *Phytochem Rev*. **5**:205-237.

Schuster, C., Gaillochet, C., Medzihradszky, A., Busch, W., Daum, G., Krebs, M., Kehle, A., and Lohmann, J. U. (2014). A regulatory framework for shoot stem cell control integrating metabolic, transcriptional, and phytohormone signals. *Dev Cell*. **28**:438-449.

Schutzendübel, A., and Polle, A. (2002). Plant responses to abiotic stresses: heavy metal-induced oxidative stress and protection by mycorrhization. *J Exp Bot*. **53**:1351-1365.

Sevilem, I., Miyashima, S., and Helariutta, Y. (2013). Cell-to-cell communication via plasmodesmata in vascular plants. *Cell Adh Migr*. **7**:27-32.

Sevilem, I., Yadav, S. R., and Helariutta, Y. (2015). Plasmodesmata: channels for intercellular signaling during plant growth and development. *Methods Mol Biol*. **1217**:3-24.

Simpson, C., Thomas, C., Findlay, K., Bayer, E., and Maule, A. J. (2009). An *Arabidopsis* GPI-anchor plasmodesmal neck protein with callose binding activity and potential to regulate cell-to-cell trafficking. *Plant Cell*. **21**:581-594.

Simpson, G. G., and Dean, C. (2002). *Arabidopsis*, the Rosetta stone of flowering time? *Science*. **296**:285-289.

Sivaguru, M., Fujiwara, T., Samaj, J., Baluska, F., Yang, Z., Osawa, H., Maeda, T., Mori, T., Volkmann, D., and Matsumoto, H. (2000). Aluminum-induced 1→3-β-D-glucan inhibits cell-to-cell trafficking of molecules through plasmodesmata. A new mechanism of aluminum toxicity in plants. *Plant Physiol*. **124**:991-1006.

Skalák, J., Vercruyssen, L., Claeys, H., Hradilova, J., Cerny, M., Novak, O., Plackova, L., Saiz-Fernandez, I., Skalakova, P., Coppens, F., Dhondt, S., Koukalova, S., Zouhar, J., Inze, D., and Brzobohaty, B. (2019). Multifaceted activity of cytokinin in leaf development shapes its size and structure in *Arabidopsis*. *Plant J*. **97**:805-824.

Skoog, F., and Miller, C. O. (1957). Chemical regulation of growth and organ formation in plant tissues cultured *in vitro*. *Symp Soc Exp Biol*. **11**:118-130.

Smehilova, M., Galuszka, P., Bilyeu, K. D., Jaworek, P., Kowalska, M., Sebela, M., Sedlarova, M., English, J. T., and Frebort, I. (2009). Subcellular localization and biochemical comparison of cytosolic and secreted cytokinin dehydrogenase enzymes from maize. *J Exp Bot*. **60**:2701-2712.

Smith, P. K., Krohn, R. I., Hermanson, G. T., Mallia, A. K., Gartner, F. H., Provenzano, M. D., Fujimoto, E. K., Goeke, N. M., Olson, B. J., and Klenk, D. C. (1985). Measurement of protein using bicinchoninic acid. *Anal Biochem*. **150**:76-85.

Smyth, D. R., Bowman, J. L., and Meyerowitz, E. M. (1990). Early flower development in *Arabidopsis*. *Plant Cell*. **2**:755-767.

Solioz, M., and Vulpe, C. (1996). CPx-type ATPases: a class of P-type ATPases that pump heavy metals. *Trends Biochem Sci*. **21**:237-241.

Somssich, I. E., Wernert, P., Kiedrowski, S., and Hahlbrock, K. (1996). *Arabidopsis thaliana* defense-related protein ELI3 is an aromatic alcohol:$NADP^+$ oxidoreductase. *PNAS*. **93**:14199-14203.

Sorek, N., Bloch, D., and Yalovsky, S. (2009). Protein lipid modifications in signaling and subcellular targeting. *Curr Opin Plant Biol*. **12**:714-720.

Spallek, T., Gan, P., Kadota, Y., and Shirasu, K. (2018). Same tune, different song-cytokinins as virulence factors in plant-pathogen interactions? *Curr Opin Plant Biol*. **44**:82-87.

Sparkes, I. A., Runions, J., Kearns, A., and Hawes, C. (2006). Rapid, transient expression of fluorescent fusion proteins in tobacco plants and generation of stably transformed plants. *Nat Protoc*. **1**:2019-2025.

Spartz, A. K., Lee, S. H., Wenger, J. P., Gonzalez, N., Itoh, H., Inzé, D., Peer, W. A., Murphy, A. S., Overvoorde, P. J., and Gray, W. M. (2012). The *SAUR19* subfamily of *SMALL AUXIN UP RNA* genes promote cell expansion. *Plant J*. **70**:978-990.

Spartz, A. K., Ren, H., Park, M. Y., Grandt, K. N., Lee, S. H., Murphy, A. S., Sussman, M. R., Overvoorde, P. J., and Gray, W. M. (2014). SAUR inhibition of PP2C-D phosphatases activates plasma membrane H^+-ATPases to promote cell expansion in *Arabidopsis*. *Plant Cell*. **26**:2129-2142.

Stadler, R., Lauterbach, C., and Sauer, N. (2005a). Cell-to-cell movement of green fluorescent protein reveals post-phloem transport in the outer integument and identifies symplastic domains in *Arabidopsis* seeds and embryos. *Plant Physiol*. **139**:701-712.

Stadler, R., Wright, K. M., Lauterbach, C., Amon, G., Gahrtz, M., Feuerstein, A., Oparka, K. J., and Sauer, N. (2005b). Expression of GFP-fusions in *Arabidopsis* companion cells reveals non-specific protein trafficking into sieve elements and identifies a novel post-phloem domain in roots. *Plant J*. **41**:319-331.

Stahl, Y., Grabowski, S., Bleckmann, A., Kuhnemuth, R., Weidtkamp-Peters, S., Pinto, K. G., Kirschner, G. K., Schmid, J. B., Wink, R. H., Hulsewede, A., Felekyan, S., Seidel, C. A., and Simon, R. (2013). Moderation of *Arabidopsis* root stemness by CLAVATA1 and ARABIDOPSIS CRINKLY4 receptor kinase complexes. *Curr Biol*. **23**:362-371.

Stahl, Y., Wink, R. H., Ingram, G. C., and Simon, R. (2009). A signaling module controlling the stem cell niche in *Arabidopsis* root meristems. *Curr Biol*. **19**:909-914.

Staswick, P. E., Serban, B., Rowe, M., Tiryaki, I., Maldonado, M. T., Maldonado, M. C., and Suza, W. (2005). Characterization of an *Arabidopsis* enzyme family that conjugates amino acids to indole-3-acetic acid. *Plant Cell*. **17**:616-627.

Sternberg, S. H., Redding, S., Jinek, M., Greene, E. C., and Doudna, J. A. (2014). DNA interrogation by the CRISPR RNA-guided endonuclease Cas9. *Nature*. **507**:62-67.

Stonebloom, S., Burch-Smith, T., Kim, I., Meinke, D., Mindrinos, M., and Zambryski, P. (2009). Loss of the plant DEAD-box protein ISE1 leads to defective mitochondria and increased cell-to-cell transport via plasmodesmata. *PNAS*. **106**:17229-17234.

Stortenbeker, N., and Bemer, M. (2019). The SAUR gene family: the plant's toolbox for adaptation of growth and development. *J Exp Bot*. **70**:17-27.

Sturtz, L. A., Diekert, K., Jensen, L. T., Lill, R., and Culotta, V. C. (2001). A fraction of yeast Cu,Zn-superoxide dismutase and its metallochaperone, CCS, localize to the intermembrane space of mitochondria. A physiological role for SOD1 in guarding against mitochondrial oxidative damage. *J Biol Chem*. **276**:38084-38089.

Su, Y. H., Liu, Y. B., and Zhang, X. S. (2011). Auxin-cytokinin interaction regulates meristem development. *Mol Plant*. **4**:616-625.

Sun, J., Qi, L., Li, Y., Zhai, Q., and Li, C. (2013). PIF4 and PIF5 transcription factors link blue light and auxin to regulate the phototropic response in *Arabidopsis*. *Plant Cell*. **25**:2102-2014.

Suzuki, N., Yamaguchi, Y., Koizumi, N., and Sano, H. (2002). Functional characterization of a heavy metal binding protein CdI19 from *Arabidopsis*. *Plant J*. **32**:165.

Takei, K., Yamaya, T., and Sakakibara, H. (2004). *Arabidopsis CYP735A1* and *CYP735A2* encode cytokinin hydroxylases that catalyze the biosynthesis of *trans*-Zeatin. *J Biol Chem*. **279**:41866-41872.

Taniguchi, M., Sasaki, N., Tsuge, T., Aoyama, T., and Oka, A. (2007). ARR1 directly activates cytokinin response genes that encode proteins with diverse regulatory functions. *Plant Cell Physiol*. **48**:263-277.

Tehseen, M., Cairns, N., Sherson, S., and Cobbett, C. S. (2010). Metallochaperone-like genes in *Arabidopsis thaliana*. *Metallomics*. **2**:556-564.

ten Hove, C. A., Lu, K. J., and Weijers, D. (2015). Building a plant: cell fate specification in the early *Arabidopsis* embryo. *Development*. **142**:420-430.

Terry, B. R., Matthews, E. K., and Haseloff, J. (1995). Molecular characterization of recombinant GREEN FLUORESCENT PROTEIN by fluorescence correlation microscopy. *Biochem Bioph Res Co*. **217**:21-27.

Thomas, C. L., Bayer, E. M., Ritzenthaler, C., Fernandez-Calvino, L., and Maule, A. J. (2008). Specific targeting of a plasmodesmal protein affecting cell-to-cell communication. *PLOS Biol*. **6**:e7.

Tian, H., Baxter, I. R., Lahner, B., Reinders, A., Salt, D. E., and Ward, J. M. (2010). *Arabidopsis* NPCC6/NaKR1 is a phloem mobile metal binding protein necessary for phloem function and root meristem maintenance. *Plant Cell*. **22**:3963-3979.

Tian, Q., and Reed, J. W. (1999). Control of auxin-regulated root development by the *Arabidopsis thaliana SHY2/IAA3* gene. *Development*. **126**:711-721.

Tilney, L. G., Cooke, T. J., Connelly, P. S., and Tilney, M. S. (1990). The distribution of plasmodesmata and its relationship to morphogenesis in fern gametophytes. *Development*. **110**:1209-1221.

Tilsner, J., Nicolas, W., Rosado, A., and Bayer, E. M. (2016). Staying tight: plasmodesmal membrane contact sites and the control of cell-to-cell connectivity in plants. *Annu Rev Plant Biol*. **67**:337-364.

To, J. P., Deruère, J., Maxwell, B. B., Morris, V. F., Hutchison, C. E., Ferreira, F. J., Schaller, G. E., and Kieber, J. J. (2007a). Cytokinin regulates type-A *Arabidopsis* response regulator activity and protein stability via two-component phosphorelay. *Plant Cell*. **19**:3901-3914.

To, J. P., Haberer, G., Ferreira, F. J., Deruère, J., Mason, M. G., Schaller, G. E., Alonso, J. M., Ecker, J. R., and Kieber, J. J. (2004). Type-A *Arabidopsis* RESPONSE REGULATORs are partially redundant negative regulators of cytokinin signaling. *Plant Cell*. **16**:658-671.

To, J. P. C., Deruère, J., Maxwell, B. B., Morris, V. F., Hutchison, C. E., Ferreira, F. J., Schaller, G. E., and Kieber, J. J. (2007b). Cytokinin regulates type-A *ARABIDOPSIS RESPONSE REGULATOR* activity and protein stability via two-component phosphorelay. *Plant Cell*. **19**:3901-3914.

Töller, A., Brownfield, L., Neu, C., Twell, D., and Schulze-Lefert, P. (2008). Dual function of *Arabidopsis GLUCAN SYNTHASE-LIKE* genes *GSL8* and *GSL10* in male gametophyte development and plant growth. *Plant J*. **54**:911-923.

Trueblood, C. E., Boyartchuk, V. L., Picologlou, E. A., Rozema, D., Poulter, C. D., and Rine, J. (2000). The CaaX proteases, Afc1p and Rce1p, have overlapping but distinct substrate specificities. *Mol Cell Biol*. **20**:4381-4392.

Truernit, E., Bauby, H., Dubreucq, B., Grandjean, O., Runions, J., Barthelemy, J., and Palauqui, J. C. (2008). High-resolution whole-mount imaging of three-dimensional tissue organization and gene expression enables the study of phloem development and structure in *Arabidopsis*. *Plant Cell*. **20**:1494-1503.

Truernit, E., and Sauer, N. (1995). The promoter of the *Arabidopsis thaliana SUC2 SUCROSE-H+ SYMPORTER* gene directs expression of beta-glucuronidase to the phloem: evidence for phloem loading and unloading by SUC2. *Planta*. **196**:564-570.

Truskina, J., and Vernoux, T. (2018). The growth of a stable stationary structure: coordinating cell behavior and patterning at the shoot apical meristem. *Curr Opin Plant Biol*. **41**:83-88.

Tschuden, P. J. (2019). Molecular characterization of the HEAVY METAL-ASSOCIATED ISOPRENYLATED PLANT PROTEIN 34 (HIPP34) in *Arabidopsis thaliana*. *Master thesis*.

Turgeon, R., and Wolf, S. (2009). Phloem transport: cellular pathways and molecular trafficking. *Annu Rev Plant Biol*. **60**:207-221.

Untergasser, A., Nijveen, H., Rao, X., Bisseling, T., Geurts, R., and Leunissen, J. A. M. (2007). Primer3Plus, an enhanced web interface to Primer3. *Nucleic Acids Research*. **35**:W71-W74.

Ursache, R., Andersen, T. G., Marhavy, P., and Geldner, N. (2018). A protocol for combining fluorescent proteins with histological stains for diverse cell wall components. *Plant J*. **93**:399-412.

van Mourik, H., van Dijk, A. D. J., Stortenbeker, N., Angenent, G. C., and Bemer, M. (2017). Divergent regulation of *Arabidopsis SAUR* genes: a focus on the SAUR10-clade. *BMC Plant Biol*. **17**:245.

Van Norman, J. M., Breakfield, N. W., and Benfey, P. N. (2011). Intercellular communication during plant development. *Plant Cell*. **23**:855-864.

Vandesompele, J., De Preter, K., Pattyn, F., Poppe, B., Van Roy, N., De Paepe, A., and Speleman, F. (2002). Accurate normalization of real-time quantitative RT-PCR data by geometric averaging of multiple internal control genes. *Genome Biol*. **3**.

Vatén, A., Dettmer, J., Wu, S., Stierhof, Y. D., Miyashima, S., Yadav, S. R., Roberts, C. J., Campilho, A., Bulone, V., Lichtenberger, R., Lehesranta, S., Mahonen, A. P., Kim, J. Y., Jokitalo, E., Sauer, N., Scheres, B., Nakajima, K., Carlsbecker, A., Gallagher, K. L., and Helariutta, Y. (2011). Callose biosynthesis regulates symplastic trafficking during root development. *Dev Cell*. **21**:1144-1155.

Vembar, S. S., and Brodsky, J. L. (2008). One step at a time: endoplasmic reticulum-associated degradation. *Nat Rev Mol*. **9**:944-957.

Viehweger, K. (2014). How plants cope with heavy metals. *Bot Stud*. **55**:35.

Vilaine, F., Kerchev, P., Clement, G., Batailler, B., Cayla, T., Bill, L., Gissot, L., and Dinant, S. (2013). Increased expression of a phloem membrane protein encoded by *NHL26* alters phloem export and sugar partitioning in *Arabidopsis*. *Plant Cell*. **25**:1689-1708.

Voinnet, O., Rivas, S., Mestre, P., and Baulcombe, D. (2003). An enhanced transient expression system in plants based on suppression of gene silencing by the p19 protein of tomato bushy stunt virus. *Plant J*. **33**:949-956.

Voytas, D. F. (2013). Plant genome engineering with sequence-specific nucleases. *Annu Rev Plant Biol*. **64**:327-350.

Wagner, D., Sablowski, R. W. M., and Meyerowitz, E. M. (1999). Transcriptional activation of *APETALA1* by LEAFY. *Science*. **285**:582-584.

Waidmann, S., Ruiz Rosquete, M., Scholler, M., Sarkel, E., Lindner, H., LaRue, T., Petrik, I., Dunser, K., Martopawiro, S., Sasidharan, R., Novak, O., Wabnik, K., Dinneny, J. R., and Kleine-Vehn, J. (2019). Cytokinin functions as an asymmetric and anti-gravitropic signal in lateral roots. *Nat Commun*. **10**:3540.

Waldie, T., and Leyser, O. (2018). Cytokinin targets auxin transport to promote shoot branching. *Plant Physiol*. **177**:803-818.

Wang, M., and Casey, P. J. (2016). Protein prenylation: unique fats make their mark on biology. *Nat Rev Mol Cell Biol*. **17**:110-122.

Wang, N., and Fisher, D. B. (1994). The use of fluorescent tracers to characterize the post-phloem transport pathway in maternal tissues of developing wheat grains. *Plant Physiol*. **104**:17-27.

Wang, Y., Li, L., Ye, T., Zhao, S., Liu, Z., Feng, Y. Q., and Wu, Y. (2011). Cytokinin antagonizes ABA suppression to seed germination of *Arabidopsis* by downregulating *ABI5* expression. *Plant J*. **68**:249-261.

Wang, Y. H. (2008). How effective is T-DNA insertional mutagenesis? *J BiochemTechnol*. **1**:11-20.

Wang, Z. P., Xing, H. L., Dong, L., Zhang, H. Y., Han, C. Y., Wang, X. C., and Chen, Q. J. (2015). Egg cell-specific promoter-controlled CRISPR/Cas9 efficiently generates homozygous mutants for multiple target genes in *Arabidopsis* in a single generation. *Genome Biol*. **16**:144.

Wani, W., Masoodi, K. Z., Zaid, A., Wani, S. H., Shah, F., Meena, V. S., Wani, S. A., and Mosa, K. A. (2018). Engineering plants for heavy metal stress tolerance. *Rendiconti Lincei Scienze Fisiche e Naturali*. **29**:709-723.

Werner, D., Gerlitz, N., and Stadler, R. (2011). A dual switch in phloem unloading during ovule development in *Arabidopsis*. *Protoplasma*. **248**:225-235.

Werner, T., Köllmer, I., Bartrina, I., Holst, K., and Schmülling, T. (2006). New insights into the biology of cytokinin degradation. *Plant Biol*. **8**:371-381.

Werner, T., Motyka, V., Laucou, V., Smets, R., Van Onckelen, H., and Schmülling, T. (2003). Cytokinin-deficient transgenic *Arabidopsis* plants show multiple developmental alterations indicating opposite functions of cytokinins in the regulation of shoot and root meristem activity. *Plant Cell*. **15**:2532-3550.

Werner, T., Motyka, V., Strnad, M., and Schmülling, T. (2001). Regulation of plant growth by cytokinin. *PNAS*. **98**:10487-10492.

Werner, T., and Schmülling, T. (2009). Cytokinin action in plant development. *Curr Opin Plant Biol*. **12**:527-538.

White, R. G., and Barton, D. A. (2011). The cytoskeleton in plasmodesmata: a role in intercellular transport? *J Exp Bot*. **62**:5249-5266.

Winter, D., Vinegar, B., Nahal, H., Ammar, R., Wilson, G. V., and Provart, N. J. (2007). An "Electronic Fluorescent Pictograph" browser for exploring and analyzing large-scale biological data sets. *PLOS One*. **2**:e718.

Wintz, H., and Vulpe, C. (2002). Plant copper chaperones. *Biochem Soc Trans*. **30**:732-735.

Wolf, S., Deom, C. M., Beachy, R. N., and Lucas, W. J. (1989). Movement protein of tobacco mosaic virus modifies plasmodesmatal size exclusion limit. *Science*. **246**:377-379.

Wu, H., Chen, C., Du, J., Liu, H., Cui, Y., Zhang, Y., He, Y., Wang, Y., Chu, C., and Feng, Z. (2012). Co-overexpression *FIT* with *AtbHLH38* or *AtbHLH39* in *Arabidopsis* - enhanced cadmium tolerance via increased cadmium sequestration in roots and improved iron homeostasis of shoots. *Plant Physiol*. **158**:790-800.

Wu, S., and Gallagher, K. L. (2014). The movement of the non-cell-autonomous transcription factor, SHORT-ROOT relies on the endomembrane system. *Plant J*. **80**:396-409.

Wu, S. W., Kumar, R., Iswanto, A. B. B., and Kim, J. Y. (2018). Callose balancing at plasmodesmata. *J Exp Bot*. **69**:5325-5339.

Wu, X., Dinneny, J. R., Crawford, K. M., Rhee, Y., Citovsky, V., Zambryski, P. C., and Weigel, D. (2003). Modes of intercellular transcription factor movement in the *Arabidopsis* apex. *Development*. **130**:3735-3745.

Wuest, S. E., Philipp, M. A., Guthörl, D., Schmid, B., and Grossniklaus, U. (2016). Seed production affects maternal growth and senescence in *Arabidopsis*. *Plant Physiol*. **171**:392-404.

Wulfetange, K., Lomin, S. N., Romanov, G. A., Stolz, A., Heyl, A., and Schmülling, T. (2011). The cytokinin receptors of *Arabidopsis* are located mainly to the endoplasmic reticulum. *Plant Physiol*. **156**:1808-1818.

Wycisk, K., Kim, E. J., Schroeder, J. I., and Kramer, U. (2004). Enhancing the first enzymatic step in the histidine biosynthesis pathway increases the free histidine pool and nickel tolerance in *Arabidopsis thaliana*. *FEBS Lett*. **578**:128-134.

Xiao, C., Somerville, C., and Anderson, C. T. (2014). *POLYGALACTURONASE INVOLVED IN EXPANSION1* functions in cell elongation and flower development in *Arabidopsis*. *Plant Cell*. **26**:1018-1035.

Xiong, Y., and Jiao, Y. (2019). The diverse roles of auxin in regulating leaf development. *Plants*. **8**:243.

Xu, D., Miao, J., Yumoto, E., Yokota, T., Asahina, M., and Watahiki, M. (2017). *YUCCA9*-mediated auxin biosynthesis and polar auxin transport synergistically regulate regeneration of root systems following root cutting. *Plant Cell Physiol*. **58**:1710-1723.

Xu, M., Cho, E., Burch-Smith, T. M., and Zambryski, P. C. (2012). Plasmodesmata formation and cell-to-cell transport are reduced in decreased *size exclusion limit 1* during embryogenesis in *Arabidopsis*. *PNAS*. **109**:5098-5103.

Xu, N., Shen, N., Wang, X., Jiang, S., Xue, B., and Li, C. (2015). Protein prenylation and human diseases: a balance of protein farnesylation and geranylgeranylation. *Sci China Life Sci*. **58**:328-335.

Xu, X. M., Wang, J., Xuan, Z., Goldshmidt, A., Borrill, P. G., Hariharan, N., Kim, J. Y., and Jackson, D. (2011). Chaperonins facilitate KNOTTED1 cell-to-cell trafficking and stem cell function. *Science*. **333**:1141-1144.

Yadav, R. K., Perales, M., Gruel, J., Girke, T., Jonsson, H., and Reddy, G. V. (2011). WUSCHEL protein movement mediates stem cell homeostasis in the *Arabidopsis* shoot apex. *Genes Dev*. **25**:2025-2030.

Yadav, S. K. (2010). Heavy metals toxicity in plants: an overview on the role of glutathione and phytochelatins in heavy metal stress tolerance of plants. *S Afr J Bot*. **76**:167-179.

Yadav, S. R., Yan, D., Sevilem, I., and Helariutta, Y. (2014). Plasmodesmata-mediated intercellular signaling during plant growth and development. *Front Plant Sci*. **5**:44.

Yalovsky, S., Rodriguez-Concepcion, M., Bracha, K., Toledo-Ortiz, G., and Gruissem, W. (2000). Prenylation of the floral transcription factor APETALA1 modulates its function. *Plant Cell*. **12**:1257-1266.

Yan, D., Yadav, S. R., Paterlini, A., Nicolas, W. J., Petit, J. D., Brocard, L., Belevich, I., Grison, M. S., Vaten, A., Karami, L., El-Showk, S., Lee, J. Y., Murawska, G. M., Mortimer, J., Knoblauch, M., Jokitalo, E., Markham, J. E., Bayer, E. M., and Helariutta, Y. (2019). Sphingolipid biosynthesis modulates plasmodesmal ultrastructure and phloem unloading. *Nat Plants*. **5**:604-615.

Yanai, O., Shani, E., Dolezal, K., Tarkowski, P., Sablowski, R., Sandberg, G., Samach, A., and Ori, N. (2005). *Arabidopsis* KNOXI proteins activate cytokinin biosynthesis. *Curr Biol*. **15**:1566-1571.

Yuan, L., Liu, Z., Song, X., Johnson, C., Yu, X., and Sundaresan, V. (2016). The CKI1 histidine kinase specifies the female gametic precursor of the endosperm. *Dev Cell*. **37**:34-46.

Zavaliev, R., Dong, X., and Epel, B. L. (2016). Glycosylphosphatidylinositol (GPI) modification serves as a primary plasmodesmal sorting signal. *Plant Physiol*. **172**:1061-1073.

Zavaliev, R., and Epel, B. L. (2015). Imaging callose at plasmodesmata using aniline blue: quantitative confocal microscopy. *Methods Mol Biol*. **1217**:105-119.

Zavaliev, R., Ueki, S., Epel, B. L., and Citovsky, V. (2011). Biology of callose (β-1,3-glucan) turnover at plasmodesmata. *Protoplasma*. **248**:117-130.

Zhang, B., Liu, H., Ding, X., Qiu, J., Zhang, M., and Chu, Z. (2018). *Arabidopsis thaliana ACS8* plays a crucial role in the early biosynthesis of ethylene elicited by Cu(2+) ions. *J Cell Sci*. **131**.

Zhang, F. L., and Casey, P. J. (1996). Protein prenylation: molecular mechanisms and functional consequences. *Annu Rev Biochem*. **65**:241-269.

Zhang, J., Lin, J. E., Harris, C., Campos Mastrotti Pereira, F., Wu, F., Blakeslee, J. J., and Peer, W. A. (2016). DAO1 catalyzes temporal and tissue-specific oxidative inactivation of auxin in *Arabidopsis thaliana*. *PNAS*. **113**:11010-11015.

Zhang, J., Liu, B., Li, M., Feng, D., Jin, H., Wang, P., Liu, J., Xiong, F., Wang, J., and Wang, H.-B. (2015). The bHLH transcription factor bHLH104 interacts with IAA-LEUCINE RESISTANT3 and modulates iron homeostasis in *Arabidopsis*. *Plant Cell*. **27**:787-805.

Zhang, P., Wang, R., Ju, Q., Li, W., Tran, L. P., and Xu, J. (2019). The R2R3-MYB transcription factor MYB49 regulates cadmium accumulation. *Plant Physiol*. **180**:529-542.

Zhang, W., Swarup, R., Bennett, M., Schaller, G. E., and Kieber, J. J. (2013). Cytokinin induces cell division in the quiescent center of the *Arabidopsis* root apical meristem. *Curr Biol*. **23**:1979-1989.

Zhang, W., To, J. P., Cheng, C. Y., Schaller, G. E., and Kieber, J. J. (2011). Type-A *RESPONSE REGULATORS* are required for proper root apical meristem function through post-transcriptional regulation of PIN auxin efflux carriers. *Plant J*. **68**:1-10.

Zhao, J., Zhou, H., and Li, Y. (2013). UBIQUITIN-SPECIFIC PROTEASE16 interacts with a HEAVY METAL ASSOCIATED ISOPRENYLATED PLANT PROTEIN27 and modulates cadmium tolerance. *Plant Signal Behav*. **8**.

Zhao, Y. (2010). Auxin biosynthesis and its role in plant development. *Annu Rev Plant Biol*. **61**:49-64.

Zhao, Z., Andersen, S. U., Ljung, K., Dolezal, K., Miotk, A., Schultheiss, S. J., and Lohmann, J. U. (2010). Hormonal control of the shoot stem-cell niche. *Nature*. **465**:1089-1092.

Zheng, L., Baumann, U., and Reymond, J. L. (2004). An efficient one-step site-directed and site-saturation mutagenesis protocol. *Nucleic Acids Res*. **32**:e115.

Zhou, M. L., Qi, L. P., Pang, J. F., Zhang, Q., Lei, Z., Tang, Y. X., Zhu, X. M., Shao, J. R., and Wu, Y. M. (2013). Nicotianamine synthase gene family as central components in heavy metal and phytohormone response in maize. *Funct Integr Genomics*. **13**:229-229.

Zhu, T., Lucas, W. J., and Rost, T. L. (1998). Directional cell-to-cell communication in the *Arabidopsis* root apical meristem. An ultrastructural and functional analysis. *Protoplasma*. **203**:35-47.

Zhu, Y., Liu, L., Shen, L., and Yu, H. (2016). NaKR1 regulates long-distance movement of FLOWERING LOCUS T in *Arabidopsis*. *Nat Plants*. **2**:16075.

Zschiesche, W., Barth, O., Daniel, K., Bohme, S., Rausche, J., and Humbeck, K. (2015). The zinc-binding nuclear protein HIPP3 acts as an upstream regulator of the salicylate-dependent plant immunity pathway and of flowering time in *Arabidopsis thaliana*. *New Phytol*. **207**:1084-1096.

Zubo, Y. O., Blakley, I. C., Yamburenko, M. V., Worthen, J. M., Street, I. H., Franco-Zorrilla, J. M., Zhang, W., Hill, K., Raines, T., Solano, R., Kieber, J. J., Loraine, A. E., and Schaller, G. E. (2017). Cytokinin induces genome-wide binding of the type-B response regulator ARR10 to regulate growth and development in *Arabidopsis*. *PNAS*. **114**:5995-6004.

Zubo, Y. O., and Schaller, G. E. (2020). Role of the cytokinin-activated type-B response regulators in hormone crosstalk. *Plants*. **9**.

Zürcher, E., and Müller, B. (2016). Cytokinin synthesis, signaling, and function - advances and new insights. *Int Rev Cell Mol Biol*. **324**:1-38.

Zürcher, E., Tavor-Deslex, D., Lituiev, D., Enkerli, K., Tarr, P. T., and Müller, B. (2013). A robust and sensitive synthetic sensor to monitor the transcriptional output of the cytokinin signaling network *in planta*. *Plant Physiol*. **161**:1066-1075.

Appendix

Table A1: Genes differentially regulated with a log2 FC ≥ 1.5 (FDR < 0.05) in response to cytokinin in wild type and no longer regulated either in *hipp33* or in *hipp32,33,34* (plain black). In gray are highlighted genes that failed to respond to cytokinin only in *hipp33,* and in bold genes that failed to respond only in *hipp32,33,34*.

Gene ID	log2 FC	FDR	Description
AT5G51190	3.89	2.45E-16	ETHYLENE RESPONSE FACTOR 105 (ERF105)
AT4G37990	3.17	9.72E-27	ELICITOR-ACTIVATED GENE 3-2 (ELI3-2)
AT1G23160	2.28	1.61E-05	GRETCHEN HAGEN 3.7 (GH3.7)
AT2G02990	2.26	5.36E-07	RIBONUCLEASE 1 (RNS1)
AT1G10585	2.15	2.71E-06	Basic helix-loop-helix (bHLH) DNA-binding superfamily protein
AT3G56380	2.08	1.16E-04	RESPONSE REGULATOR 17 (ARR17)
AT2G20520	**2.08**	**7.61E-05**	**FASCICLIN-LIKE ARABINOGALACTAN 6 (FLA6)**
AT1G63600	**2.06**	**3.03E-05**	**Receptor-like protein kinase-related family protein**
AT5G28510	1.99	1.09E-10	BETA GLUCOSIDASE 24 (BGLU24)
AT4G20970	1.98	3.53E-06	Bbasic helix-loop-helix (bHLH) DNA-binding superfamily protein
AT4G22214	**1.96**	**2.98E-06**	**Defensin-like (DEFL) family protein.**
AT1G45616	1.93	5.63E-10	RECEPTOR LIKE PROTEIN 6 (RLP6)
AT1G33960	1.90	1.86E-05	AVRRPT2-INDUCED GENE 1 (AIG1)
AT5G55050	1.88	1.19E-06	GDSL-motif esterase/acyltransferase/lipase
AT1G68290	1.84	3.49E-04	ENDONUCLEASE 2 (ENDO2)
AT4G15210	1.84	1.06E-06	BETA-AMYLASE 5 (BAM5)
AT1G62840	**1.77**	**2.06E-05**	**Ankyrin repeat/KH domain protein (DUF1442)**
AT1G15580	**1.76**	**1.01E-05**	**INDOLE-3-ACETIC ACID INDUCIBLE 5 (IAA5)**
AT2G38240	1.74	8.09E-04	JASMONATE-INDUCED OXYGENASE4 (JOX4)
AT2G31540	1.74	2.15E-03	GDSL-motif esterase/acyltransferase/lipase
AT3G25180	1.74	7.05E-04	CYTOCHROME P450, FAMILY 82, SUBFAMILY G, POLYPEPTIDE 1 (CYP82G1)
AT2G44840	**1.72**	**8.82E-06**	**ETHYLENE-RESPONSIVE ELEMENT BINDING FACTOR 13 (ERF13)**
AT1G15010	1.66	5.35E-05	Mediator of RNA polymerase II transcription subunit
AT4G19680	1.64	4.02E-05	IRON REGULATED TRANSPORTER 2 (IRT2)
AT2G33780	1.61	5.53E-03	MPK3/6-TARGETED VQP 2 (MVQ2)
AT2G33020	1.59	4.65E-03	RECEPTOR LIKE PROTEIN 24 (RLP24)
AT3G51680	1.58	7.31E-04	SHORT-CHAIN DEHYDROGENASE/REDUCTASE 2 (SDR2)
AT3G28007	1.58	1.36E-04	Nodulin MtN3 family protein/(SWEET4)
AT1G69880	1.56	9.43E-04	THIOREDOXIN H-TYPE 8 (TH8)

Table A1: Continued.

Gene ID	log2 FC	FDR	Description
AT4G35720	**1.56**	**1.75E-06**	**DUF241 domain protein, putative (DUF241)**
AT2G28140	**1.56**	**9.60E-06**	**Enabled-like protein (DUF1635)**
AT5G05280	1.54	8.58E-03	DEFECTIVE IN ANTHER DEHISCENCE1- (DAD1-) ACTIVATING FACTOR (DAF)
AT4G27980	1.53	1.13E-04	Trichohyalin-like protein (DUF3444)
AT5G59580	1.53	8.83E-03	UDP-GLUCOSYL TRANSFERASE 76E1 (UGT76E1)
AT5G50600	1.51	2.70E-03	Putative hydroxysteroid dehydrogenase
AT5G01380	1.50	9.16E-06	Homeodomain-like superfamily protein

Table A2: Genes differentially regulated with a log2 FC ≥ 1.5 (FDR < 0.05) in response to cytokinin in wild type and no longer regulated either in *hipp33* or in *hipp32,33,34* (plain black). In bold are highlighted genes that failed to respond to cytokinin only in *hipp32,34,33*.

Gene ID	log2 FC	FDR	Description
AT4G35720	**1.56**	**1.75E-06**	**DUF241 domain protein, putative (DUF241)**
AT4G31875	-2.66	1.22E-14	Hypothetical protein
AT1G44050	**-2.00**	**6.12E-10**	**Cysteine/Histidine-rich C1 domain family protein**
AT1G44030	-1.81	1.01E-03	Cysteine/Histidine-rich C1 domain family protein
AT1G63410	**-1.80**	**7.25E-05**	**LURP-one-like protein (DUF567)**
AT4G13420	-1.58	9.91E-05	HIGH AFFINITY K+ TRANSPORTER 5 (HAK5)
AT1G48670	-1.56	3.79E-03	Auxin-responsive GH3 family protein
AT3G29410	-1.53	5.43E-04	TERPENE SYNTHASE 25 (TPS25)
AT5G54790	**-1.53**	**9.56E-03**	**VASCULAR-RELATED UNKNOWN PROTEIN 4 (VUP4)**

Table A3. 'Golden list' cytokinin response genes differentially expressed in wild type (WT), *hipp33* and *hipp32,33,34* identified by RNA-Seq. No cut off for the log2 fold change (FC) was applied. FDR < 0.05.

Gene ID	log2 FC WT	FDR WT	log2 FC *hipp33*	FDR *hipp33*	log2 FC *hipp32,33,34*	FDR *hipp32,33,34*	Description
AT1G03850	0.71	1.11E-09	0.49	1.84E-02			GLUTAREDOXIN 13 (GRXS13)
AT1G04240	1.16	9.76E-35	1.25	1.23E-30	1.05	4.02E-10	SHORT HYPOCOTYL 2 (SHY2)
AT1G07050	0.79	1.77E-03					FITNESS (FITNESS)
AT1G10470	2.28	6.43E-91	2.68	1.26E-73	2.22	3.10E-45	RESPONSE REGULATOR 4 (ARR4)
AT1G10480	1.14	7.97E-07	1.49	5.88E-17	1.21	1.16E-07	ZINC FINGER PROTEIN 5 (ZFP5)
AT1G13420	4.19	6.61E-122	3.05	1.62E-13	3.63	6.99E-50	SULFOTRANSFERASE 4B (ST4B)
AT1G15550			0.46	3.66E-02			GIBBERELLIN 3-OXIDASE 1 (GA3OX1)
AT1G16530	3.12	2.28E-26	3.48	4.29E-27	3.54	1.03E-41	ASYMMETRIC LEAVES 2-LIKE 9 (ASL9)
AT1G19050	3.23	3.22E-153	3.51	1.11E-151	3.36	1.50E-201	RESPONSE REGULATOR 7 (ARR7)
AT1G53885	0.61	4.87E-02	1.05	3.49E-03			Linoleate 9S-lipoxygenase-4 protein (DUF581)
AT1G59940	2.98	2.26E-24	2.23	3.42E-12	2.68	3.07E-15	RESPONSE REGULATOR 3 (ARR3)
AT1G62975	1.48	8.67E-15	1.27	2.28E-09	1.33	5.23E-14	Basic helix-loop-helix (bHLH) DNA-binding superfamily protein
AT1G67110	3.12	7.12E-119	3.39	7.27E-103	3.49	3.96E-85	CYTOCHROME P450, FAMILY 735, SUBFAMILY A, POLYPEPTIDE 2 (CYP735A2)
AT1G68520	-0.67	1.95E-04	-0.57	1.07E-04	-0.83	1.62E-05	B-BOX DOMAIN PROTEIN 14 (BBX14)
AT1G69040	0.83	1.17E-14	0.93	2.68E-16	0.78	2.96E-10	ACT DOMAIN REPEAT 4 (ACR4)
AT1G69530	1.50	6.91E-67	1.58	3.13E-57	0.96	2.30E-09	EXPANSIN A1 (EXPA1)

Table A3: Continued (a).

Gene ID	log2 FC WT	FDR WT	log2 FC *hipp33*	FDR *hipp33*	log2 FC *hipp32,33,34*	FDR *hipp32,33,34*	Description
AT1G70860	1.03	1.45E-03	1.14	7.01E-04	1.28	6.65E-04	Polyketide cyclase/dehydrase and lipid transport superfamily protein
AT1G74458	1.50	1.65E-32	1.58	5.54E-26	1.65	1.38E-24	Transmembrane protein
AT1G74890	4.48	8.14E-94	4.59	9.68E-95	4.30	6.83E-90	RESPONSE REGULATOR 15 (ARR15)
AT1G75450	2.38	8.58E-60	2.07	1.07E-38	2.22	9.21E-44	CYTOKININ OXIDASE 5 (CKX5)
AT2G01830	1.44	8.85E-45	1.57	5.70E-30	1.93	1.66E-35	WOODEN LEG (WOL)
AT2G20080	2.24	1.47E-17	1.76	2.32E-09	2.35	2.00E-21	TCP INTERACTOR CONTAINING EAR MOTIF PROTEIN 2 (TIE2)
AT2G21650	0.88	8.50E-03	1.13	2.01E-04	1.32	2.19E-04	MATERNAL EFFECT EMBRYO ARREST 3 (MEE3)
AT2G22770	1.44	7.16E-44	1.57	1.07E-38	1.25	1.58E-19	(NAI1)
AT2G26695	-1.05	6.51E-05	-1.21	1.80E-07	-0.91	4.22E-05	Ran BP2/NZF zinc finger-like superfamily protein
AT2G26980	0.28	3.95E-02			0.48	1.24E-03	CBL-INTERACTING PROTEIN KINASE 3 (CIPK3)
AT2G28160	-2.67	8.33E-49	-2.36	8.78E-40	-2.05	8.32E-17	FER-LIKE IRON DEFICIENCY INDUCED TRANSCRIPTION FACTOR (FIT)
AT2G29490	0.77	1.77E-05	0.56	2.28E-04	0.91	4.38E-09	GLUTATHIONE S-TRANSFERASE TAU 1 (GSTU1)
AT2G30540	1.32	6.49E-13	1.83	1.26E-13	0.99	1.73E-03	Member of the CC-type glutaredoxin (ROXY) family/(ROXY7)
AT2G38750	1.94	4.85E-48	1.71	3.81E-12	1.32	2.27E-16	ANNEXIN 4 (ANNAT4)
AT2G38760	1.79	1.11E-27	1.56	3.23E-11	1.45	3.91E-19	ANNEXIN 3 (ANNAT3)
AT2G40230	0.88	1.26E-06	1.23	6.45E-13	1.15	1.01E-10	HXXXD-type acyl-transferase family protein

Table A3: Continued (b).

Gene ID	log2 FC WT	FDR WT	log2 FC *hipp33*	FDR *hipp33*	log2 FC *hipp32,33,34*	FDR *hipp32,33,34*	Description
AT2G40670	2.99	4.20E-64	3.25	6.45E-60	2.97	1.66E-57	RESPONSE REGULATOR 16 (ARR16)
AT2G41310	1.27	5.86E-35	1.33	6.33E-23	1.53	1.78E-37	RESPONSE REGULATOR 3 (ARR3)
AT2G46310	1.68	6.63E-26	2.03	4.16E-31	1.41	8.40E-14	CYTOKININ RESPONSE FACTOR 5 (CRF5)
AT3G14540	1.46	1.20E-10	1.52	2.11E-08	1.24	4.58E-07	TERPENE SYNTHASE 19 (TPS19)
AT3G44326	3.36	2.44E-96	2.99	1.92E-57	3.29	3.27E-93	CYTOKININ-INDUCED F-BOX (CFB)
AT3G48100	3.09	6.15E-116	3.21	8.29E-108	3.05	3.64E-117	RESPONSE REGULATOR 5 (ARR5)
AT3G48360	-0.81	1.39E-07	-1.12	2.32E-02	-1.09	9.39E-09	BTB AND TAZ DOMAIN PROTEIN 2 (bt2)
AT3G49330	0.94	5.49E-03	0.89	1.25E-02	1.13	3.31E-04	Plant invertase/pectin methylesterase inhibitor superfamily protein
AT3G49670	0.42	1.09E-03	0.73	2.47E-13			BARELY ANY MERISTEM 2 (BAM2)
AT3G57040	0.85	2.31E-15	1.21	8.45E-20	1.27	1.05E-23	RESPONSE REGULATOR 9 (ARR9)
AT3G61630	0.94	1.01E-11	0.91	1.23E-05	0.66	6.33E-03	CYTOKININ RESPONSE FACTOR 6 (CRF6)
AT3G62930	0.81	4.60E-07	0.71	9.40E-04	0.78	1.07E-04	Member of the CC-type glutaredoxin (ROXY) family/(GRXS6)
AT4G11190	2.36	3.68E-28	2.28	4.99E-22	1.64	1.93E-22	Disease resistance-responsive (dirigent-like protein) family protein
AT4G11210	1.50	1.40E-08	1.89	1.76E-13	1.11	2.59E-04	Disease resistance-responsive (dirigent-like protein) family protein
AT4G22214	1.96	2.98E-06	2.06	7.76E-06			Encodes a defensin-like (DEFL) family protein.
AT4G23750	1.49	4.57E-39	1.84	1.06E-44	1.32	2.68E-38	CYTOKININ RESPONSE FACTOR 2 (CRF2)
AT4G25400	1.12	1.26E-08	1.15	6.58E-08	1.35	9.45E-10	Basic helix-loop-helix (bHLH) DNA-binding superfamily protein

Table A3: Continued (c).

Gene ID	log2 FC WT	FDR WT	log2 FC *hipp33*	FDR *hipp33*	log2 FC *hipp32,33,34*	FDR *hipp32,33,34*	Description
AT4G26150	2.11	3.26E-50	2.13	2.50E-38	1.87	1.51E-19	CYTOKININ-RESPONSIVE GATA FACTOR 1 (CGA1)
AT4G27410			0.59	6.01E-03			RESPONSIVE TO DESICCATION 26 (RD26)
AT4G29740	2.92	2.23E-79	2.82	1.15E-56	2.80	4.77E-88	CYTOKININ OXIDASE 4 (CKX4)
AT4G37790					0.45	1.23E-02	Homeobox protein HAT22, member of the HD-Zip II family/(HAT22)
AT4G39070	1.27	1.49E-14	1.27	6.76E-25	1.14	1.19E-08	BZS1 (BZS1)
AT5G21482	1.72	1.26E-22	1.90	8.55E-19	1.23	2.87E-07	CYTOKININ OXIDASE 7 (CKX7)
AT5G26290	1.91	1.61E-57	1.86	4.69E-25	1.78	3.19E-15	TRAF MEDIATED GAMETOGENESIS PROGRESSION (RAMGAP)
AT5G50915	2.14	9.89E-19	1.50	3.95E-12	1.97	2.80E-18	Basic helix-loop-helix (bHLH) DNA-binding superfamily protein
AT5G51780	1.63	6.54E-34	1.65	1.69E-26	1.88	1.12E-28	Basic helix-loop-helix (bHLH) DNA-binding superfamily protein
AT5G56860	0.80	6.72E-14	0.93	2.64E-15	0.77	5.88E-07	GATA, NITRATE-INDUCIBLE, CARBON METABOLISM-INVOLVED (GNC)
AT5G57685	-1.94	6.73E-29	-1.78	1.21E-23	-2.34	1.70E-45	GLUTAMINE DUMPER 3 (GDU3)
AT5G62920	2.35	7.30E-76	2.82	3.99E-97	2.58	1.76E-126	RESPONSE REGULATOR 6 (ARR6)

Acknowledgements

I want to express my sincere gratitude to Prof. Dr. Tomáš Werner for providing me with the opportunity to take on the HIPP project and to work in his lab. Your trust, patient guidance, stimulating suggestions and constant encouragement were the pillars of this thesis.

I am deeply grateful to Prof. Dr. Thomas Schmülling for reviewing this work and especially for giving me the great chance to be part of the Applied Genetics team.

Many thanks to Dr. Henriette Weber for sharing her preliminary results with me and for her kind guidance during the initial lab work. For a while I also had the luck to have Dr. Michael Niemann in the 107 crew, who kindly offered his help in numerous situations. Quite often your bold ideas were the best, thank you!

My thanks extend to all current and former members of the Applied Genetics group for their readiness to help, for all the bother with the ordering and not least for the friendly atmosphere at the institute. I am indebted to Frau Thiel for her kindness and willingness to help with the renewing of the stipend documents every couple of months. I am tremendously grateful to Sören, Louisa, Jenny, and Kathi for their professional and emotional support. Our spontaneous Aperol spritz o'clock was awesome.

I highly appreciate the kind help offered by the gardener team in the greenhouse. It was great to rely on you taking care of my *Arabidopsis* and tobacco plants.

I would like to thank to Dahlem Research School for the financial support, to the 'BCP Frauenförderung' for covering the costs of many conferences and extracurricular activities, and to the Krollow Foundation for supporting my scientific stay at the SLCU in Cambridge.

Finally, I am greatly thankful to my family and friends. A special 'mulţumesc' goes to my dear family back home in Suceava (via Bucharest obviously), and to my crazy and awesome friends in Berlin, Montpellier, and Siegen: Margherita & Mauro, Arunima, Iza, Ivana and Ana. You are so precious to me! Even if it is quite hard to put it into words, a thousand thanks to my supportive, lovely, and amazing husband who gave me strength, resilience and constantly made me laugh, even after a hard, maybe not very successful day at the confocal, waiting to cheer me up in Eierschale. This thesis would not have been possible without you!

Freie Universität Berlin

SELBSTSTÄNDIGKEITSERKLÄRUNG

gem. § 7 Abs. 4 der Promotionsordnung des Fachbereiches Biologie, Chemie, Pharmazie
basierend auf den Mitteilungen im Amtsblatt der Freien Universität Berlin
Nr. 52/2007 vom 04.09.2007, Nr. 04/2008 vom 07.02.2008 und Nr. 02/2012 vom 18.02.2012

Leonte	Georgeta
Nachname Promovend*in	Vorname Promovend*in

Hierdurch versichere ich, dass ich meine Dissertation mit dem Titel

Characterization of cluster-III HIPP proteins targeted to plasmodesmata in Arabidopsis thaliana

selbstständig und ohne unerlaubte Hilfe angefertigt habe.

☒ Hierdurch versichere ich, dass meine Dissertation nicht auf meiner Diplom- oder Masterarbeit aufbaut bzw. nicht daraus erwachsen ist.

☐ Hierdurch versichere ich, dass meine Dissertation auf meiner Diplom- oder Masterarbeit mit folgendem Titel aufbaut bzw. daraus erwachsen ist:

☒ Hierdurch versichere ich, dass ich meine Dissertation (ganz oder in Teilen) nicht veröffentlicht habe.

☐ Hierdurch versichere ich, dass ich meine Dissertation im Einvernehmen mit meinem/meiner Betreuer*in _____ (Name Betreuer*in) ganz oder in Teilen veröffentlicht habe.

↳ Die _____ (Anzahl eintragen) Publikation/en

☐ sind Betandteil meiner kumulativen Dissertation.

☐ werden jedem Exemplar meiner Monographie als Ausdruck beigelegt.

Hierdurch versichere ich, dass ich meine Dissertation nicht schon einmal in einem anderen Promotionsverfahren eingereicht habe.

27.01.2021
Datum

Unterschrift Promovend*in